CRANFIELD UNIVERSITY

MICHAEL MUSTER

NOVEL APPROACHES TO BREECH FORCE AND BULLET RICOCHET MEASUREMENT FOR SMALL ARMS FIRE

DEFENCE AND SECURITY

PhD Thesis
Academic Year: 2016 - 2020

Supervisors: Prof Amer Hameed and Dr David Wood
Associate Supervisor: Dr Kilian Wasmer
04 2020

CRANFIELD UNIVERSITY

DEFENCE AND SECURITY

PhD Thesis

Academic Year 2016 - 2020

MICHAEL MUSTER

NOVEL APPROACHES TO BREECH FORCE AND BULLET RICOCHET MEASUREMENT FOR SMALL ARMS FIRE

Supervisors: Prof Amer Hameed and Dr David Wood
Associate Supervisor: Dr Kilian Wasmer
04 2020

This thesis is submitted in partial fulfilment of the requirements for the degree of Doctor of Philosophy

ABSTRACT

Small arms ammunition measurements are difficult to conduct. This is especially true in the field of internal and terminal ballistics. However, accurate measurements are important for safety considerations.

Danger zones are defined as an area on shooting ranges in which there is a high risk of harm. Risk driving factor for the size of the danger zone is the ammunition used, properties and ricochet behaviour of the specific ammunition design. The danger zone is of interest because a wrong estimation may lead to unwanted damage to the shooter's far environment.

The distant environment is less affected when it comes to weapon breech damage. However, the internal ballistic breech investigation during the process of firing is of high relevance for the safety considerations of the shooter.

The purpose of this study is to show the influence of novel ballistic measurement devices on recent safety considerations. It is an experimental research study that looks at internal and terminal ballistic effects. The pushout force was investigated with a separately developed weapon breech, capable of measuring loads in a dynamic manner. The other investigated parameter was the ricochet danger which was also investigated with a device developed during the project. Both parameters lead to new safety considerations.

During this thesis it became evident that the most relevant parameter for an accurate ricochet quantification is the momentum of the fragment. This measurement is possible thanks to a novel type of accelerometer equipped sensor plates developed in this work.

The other main finding of this thesis is the fact that lubricated ammunition casings, irrespective of whether with water or oil lubrication, leads to a significant rise in pushout force. This pushout force is taken up by the breech and leads to safety-relevant rises of internal forces on the breech.

Both measurement approaches need to be taken into account when it comes to future safety considerations of small arms fire.

Keywords:

ricochet, oblique plate, flexural vibrations, metallic plate, force measurement, internal ballistics, momentum measurement, terminal ballistics

ACKNOWLEDGEMENTS

I thank Prof Amer Hameed and Dr David Wood for their help and supervision during this project. I am grateful for the valuable time they spent reading my reports, articles, and manuscripts. Since I did much of the writing work overseas, I also appreciated the excellent feedback culture by e-mail. I would also like to thank Dr Gareth Appleby-Thomas for his interest, strategic support, and helpful discussions concerning the project. Many thanks also to Bea Kingdon and all the administrative staff of the Cranfield University in Shrivenham, their support was great. In Switzerland, I had the best possible academic support from my co-supervisor Dr Kilian Wasmer, who was for some long periods, my only academic face-to-face contact. Big thanks, also, go to Sergey Shevchik, whose skills and expertise astonished me.

This thesis would not have been possible without the support of Donald Meyer, who gave me the self-confidence, freedom, and general opportunity to start the PhD. He always understood and supported me throughout the project, including the thesis. I would also like to thank Dr Peter Spatz for his interest and contribution to this work. Many thanks also to Dr Ralf Wahrenberg, who provided massive help with his network and practical ideas. The shooting-range team was crucial for all hands-on tests, thank you for the support. A big thank you also goes to Dominique Maurer who motivated me to take the risk and start such a long-term project. I would like to thank my family and friends for their moral support.

Thanks to all colleagues and friends at RUAG Ammotec and Cranfield University Centre of Defence Engineering. Especially to Markus Gruenig who is a great mechanic, with his help we developed various fancy workarounds. Sometimes we had even more fun when a created device failed miserably.

TABLE OF CONTENTS

LIST OF FIGURES

LIST OF TABLES

LIST OF ABBREVIATIONS

®	Regristered Trademark
°	Degree
µs	Microsecond
2D	Two Dimensional
3D	Three Dimensional
AIP	American Istitute of Physics
ASP	Advanced Signal Processing
AT	Arrival Time
BMG	Browning
C	Celsius
C.I.P	Commision Internationale Permanente
COTS	Commercial Off-The-Shelf
Cr	Chromium
DAQ	Data Acquisition
DCH	Casing Head Diameter
DCM	Casing Mouth Diameter
DOF	Degree Of Freedom
DWT	Discret wavelet distribution
EMPA	Eidgenoessische Material Pruefanstalt (Swiss Federal Laboratories for Materials Science and Technology)
EPVAT	Electronic Pressure Velocity and Action Time
ETH	Eidgenoessische Technische Hochschule (Swiss Federal Institute of Technology)
FEA	Finite Element Analysis
Fig.	Figure
FMJ	Full Metal Jacket
fps	frames per second
FT	Fourier Transformation
G	Acceleration
g	Gram

GP	Gewehr Patrone (German for rifle cartridge)
gr	Grain
HHT	Hilbert- Huang Transformation
ICP	Implemented Culoumb Amplifier
J	Joule (Energy)
kg	Kilo Gram
kHz	Kilo Hertz
m/s	Meters per Second
m/s^2	Acceleration
Mag.	Magnum
MCMOPI	Multi Caliber Manual of Proof and Inspection
MEMS	Micro Electro Mechanical System
mm	Milli Metres
MPa	Stress (Mega Pascal)
ms	Millisecond
N	Newton
NATO	North Atlantic Treaty Organization
NI	National Instruments
Ni	Nickel
Ns	Newton Second (Momentum)
PCB	Company (PicoCoulomB) Piezotronics
Pmax	Maximal Pressure
R&D	Research and Development
Ra	Avarage Roughness
RDA	Range Danger Area
Rem.	Remington
RMS	Root Mean Square
RUAG	Ruestungs Unternehmungs Aktien Gesellschaft (company specialising in the defense industry)
SDZ	Secure Danger Zone
SP	Signal Processing
STFT	Short Time Fourier Transformation

SX	Sintox
SXF	Sintox Forensis
TDOA	Time Difference Of Arrival
TDOF	Time Difference of Flight
TFA	Time Frequency Analysis
TOF	Time Of Flight
TR	Technische Richtlinie (technical guideline)
USA	United States of America
USB	Universal Serial Bus
V0	Muzzle Velocity
VWD	Vigner-Wille Distribution
Win.	Winchester
WLAN	Wireless Local Area Network

1 Introduction

This chapter describes the overall scope of this work. It explains why it is important to quantify small arms ammunition. This first chapter also serves to provide initial insight into both the measurement devices and technical questions which are answered within this thesis. The technical questions to be addressed are consolidated into four main objectives relevant to the overreaching project plan for this study. Finally, this chapter also lists the different parts of the thesis, connecting these with the associated journal publications which comprise the main study deliverables.

1.1 Thesis plan

The initial plan was to develop a simple, fast and accurate way to measure the terminal ballistic ricochet events. One aim was to produce data to feed the statistical tools for range danger assessments of specific projectile types.

During the path of the thesis, it became rapidly apparent that using other measurement devices would not only be very interesting but would add weight to the thesis. It was very beneficial to measure other ballistic properties using the same sensor principle. The focus was on the force produced on the head of the casing during the firing process, known as the pushout force.

Quantification of the pushout force, like ricochet quantification, is rarely described in the literature. However, both ballistic processes are safety-relevant, and both take place in the same timeframe.

The identified positive synergistic effects using two different ballistic measurement approaches had several advantages:

- Gaining of knowledge concerning short time physical measurement instruments
- Providing evidence that the acquired sensor signals are plausible
- Scientific publications focused on two safety topics concerning ballistics
- Safety recommendations for the far and near fields of the soldier
- Two novel approaches for small- arms fire measurements

The potential to profit from the synergies between both measurement approaches was so high that the fundamental research question of this thesis was modified and the anticipated thesis plan adapted. It is important to emphasis here that the modifications has not impact on the initial focus, namely the quantification of the projectile after deflection.

This thesis is presented as a series of journal papers. All papers have been submitted to a peer-reviewed journal and have already been accepted for publication. For reference, the published journal articles in their final form are included at the end of the thesis. However, to maintain thesis flow, papers are converted into chapters to fit into the thesis layout. All papers were written by the primary author and the investigator of this research, Michael Muster, and edited by Prof. Amer Hameed, Dr David Wood from Cranfield University and Dr Kilian Wasmer from Empa. All experiments were designed and completed at RUAG Ammotec AG Switzerland by Michael Muster, the author and sole investigator of this study. The author had excellent access to a Swiss shooting range to compliment facilities at Cranfield University.

During the early phase of research it became clear that the basic idea of the triangulation of accelerometer data is more complicated than assumed. The problem was that both ricochet and witness plate are a finite structure (steel plates) which have boundary effects. If the plate is too small and the impact too strong, the wave resulting from the impact does not build up nicely, and the wave which is crucial for the positioning process is randomly reflected from the plate boundaries. During a literature- review phase, a novel damping system which enhances the properties of the signal for triangulation and momentum measurement purposes, was found. This was also the starting point for chapter 4.

Thanks to the knowledge gained in Chapter 4, the research opened up so that Michael Muster was able to pursue his research and investigation to meet the newly defined objectives.

A big step with respect to ballistics was made between chapters 4 and 5. Chapter 4 investigated basically a terminal ballistic event. Chapter 5 investigated an

internal ballistic event, something not originally planned and which led to further consideration due to the safety relevance and the close relation to the measurement system.

- Sections 5.2 and 5.4 are interlinked since their prime focus is on the design and verification of the development of the pushout force measurement system.
- All algorithms developed in section 5.2 to smoothen the primary signal can be applied in section 5.4 and chapter 6.
- Section 5 describes the pushout force measurement, which is more reproducible compared to the ricochet measurement. However, both measurements are interesting for safety considerations.
- Chapter 5 was a good starting point to investigate the momentum and force production of a ballistic event. This knowledge was later used for ricochet investigations.

With the successful proof of concept (including algorithm, sensor principle and damping plates) the ricochet measurement device could be built. This was the basis for chapter 6.

Chapter 7 is the overall discussion of the topics presented in this thesis. This chapter covers a full and detailed discussion of the entire project. Besides, the conclusions and the future work constitutes a substantial part of chapter 7.

1.2 Author's contribution statement

Chapter 1 introducing the original research idea was written by Michael Muster and supervised by Amer Hameed and David Wood.

Michael Muster developed the basic idea for the ricochet measurement system during his work at RUAG and then proposed it to Gareth Appleby-Thomas for approval. Donald Meyer and Peter Spatz approved this collaboration between Cranfield University and RUAG. Michael Muster designed and planned the project.

Michael Muster wrote the PhD project proposal with the support of Amer Hameed.

Gareth Appleby-Thomas initially suggested the idea to elaborate this PhD thesis in paper format. The final decision to do so was taken by Michael Muster, as he was responsible

1.3 Fundamental research question

The reason for the fundamental research question was that some small arms fire measurements has only been rarely investigated despite evidences that it has a significant influence on the safety

The fundamental research question was: How do novel ballistic measurements affect recent safety considerations? To answer this question novel measurement systems needed to be developed and evaluated.

The strategy to answer the research question is shown in Figure 1-1. The underlying topic for answering this question is ballistics. However, this is split up into two sections:

- Internal ballistics for the pushout force measurement and,
- Terminal ballistics for ricochet measurements.

While these are entirely different aspects, they are both of interest to answer the fundamental question. Both measurement systems are interlinked and can be realised using piezoelectric sensors and are of interest for the shooter's safety and yet are rarely described in the literature.

One novel aspect of this research work is that the pushout force is strongly dependent on the lubrication of the casing. This pushout force affects the safety of the weapon’s breech, which is one of the most important parts of the weapon. Using this knowledge will result in new safety considerations.

New safety considerations are also wanted for the terminal ballistic investigation, e.g. the aforementioned ricochet measurement. One can observe a projectile dependent ricochet danger. A frangible bullet, for example, fragments in multiple pieces after hitting a target. This fragmentation behaviour reduces the danger potential of ricochets for the far field.

By answering the fundamental research question with two ballistic scenarios, research fields of relevance to safety are opened. This new knowledge influences the design of projectiles and the design of weapons to enhance the overall safety of the field.

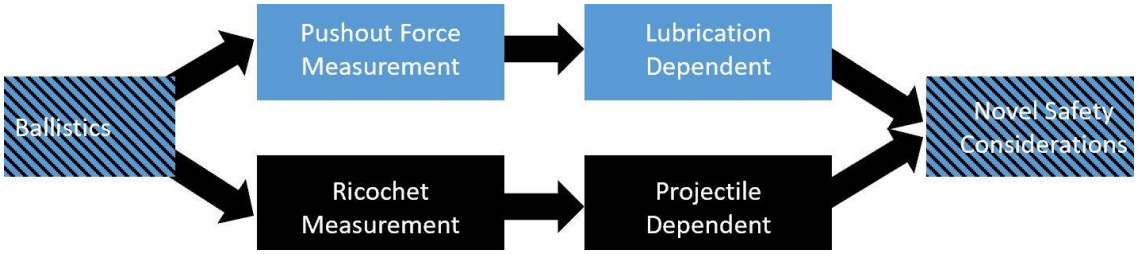

Figure 1-1: Strategy to answer the fundamental research question.

1.4 Ricochet measurement

Ricocheting is the change of direction and velocity of a projectile after hitting an oblique surface [1]. Ricochets have a significant effect on the shape of Surface Danger Zones (SDZ) [2], see Figure 1-2. The SDZ is a depiction of the mathematically predicted area of a projectile return to earth, either by direct fire or by the ricochet [3]. However, depending on the design of the projectile, these fragments may represent differing hazards dangers. This effect is often not considered during ricochet quantifications.

Due to this effect, it is necessary to know the ricochet mechanics. A regular 5.56 mm projectile requires an SDZ of approximately 3.4 kilometres, for larger small arms calibres like 12.7 mm the SDZ is over six kilometres [4].

There are several identification tools to measure the ricochet mechanics of a specific projectile type. High-speed imaging plays a vital role in state-of-the-art measurement techniques [5]. With the right choice of the frame rate and sharp shutter time, the velocity of the particles can be measured with an accuracy of +/- 30 m/s [6]. Another possibility to identify the behaviour of projectiles during impact is that of Finite Element Analysis (FEA) [7]. These software packages are used to reduce the number of costly full-scale impact experiments [8].

An additional advantage is that no heavy and bulky equipment has to be moved to shooting ranges for measurements.

Modern high-speed imaging is often used to investigate the effects of the impact. These measurements are used as a reference for FEA calculations. FEA fragmentation studies still need this reference; without it, the fragmentation behaviour cannot be calculated precisely [5], [9]. High-speed imaging techniques used to measure ricochet mechanics also have some drawbacks. The equipment is expensive compared with other measurement techniques, and the cameras are susceptible to breakage because of their optical systems.

Accelerometers are often used in the field of impact engineering to investigate severe mechanical shock, specifically ballistic shock [10]. These sensor types are widely accepted - for example, they are used for shock evaluations according to military standards [11]. By using a matrix of accelerometers placed on a well-defined witness material, it is possible to calculate the position of the impact relying on Time Difference of Arrival (TDOA) methods. The TDOA method is accepted if the speed of sound propagates homogeneously through a solid material. In this case, the impact location on a flat surface can be treated as transmitter and the accelerometers as receivers [12]. Signal Processing (SP) allows obtaining essential parameters from the acquired data. Mechanical shocks are always non-stationary signals, which can be analysed by short-time spectral analysis and wavelet transformations [13].

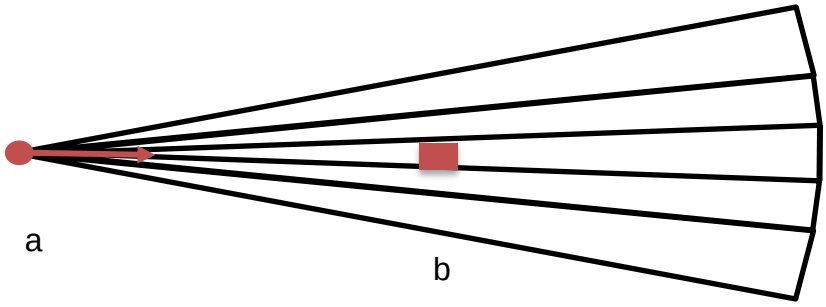

Figure 1-2: A typical example of an SDZ (a) represents the shooter, (b) the target and the length of the SDZ is around 3.4 kilometres for 5.56 mm projectiles.

In this study, the focus is on a measurement device, which can measure the ricochet mechanics quickly, and precisely after impact on well-defined oblique targets.

A conceptual approach on how to measure the ricochet using a novel device is shown in Figure 1-3. The measurement concept is as follows:

- The projectile hits under horizontal trajectory a steel plate, called the ricochet plate. The distance between the small arms barrel and the ricochet measurement device is kept the same for all tests. However, it is possible to use a different amount of propellant to adjust the impact velocity even though the distance between the barrel and ricochet plate remains the same. The reason for this procedure is to enable simulation of several real-world impact distances.
- The ricochet plate can be adjusted to different angles (angle α of Figure 1-3 is variable). With this system, it is possible to reproduce different incident angles. During the impact of the intact projectile on the ricochet plate, the position of the projectile is recorded using at least 3 accelerometers and the aforementioned triangulation technique.
- The projectile is deflected on the ricochet plate. During this process, the projectile is deformed or fragmented to one or multiple ricochets. These ricochets are thrown against a second steel plate which is also equipped with accelerometers. This second plate stops the ricochets and measures their momentum as well as the position at the same time.
- Besides knowing the momentum and position of the impact this approach also provides the time difference between the impact on the ricochet plate and the witness plate (the distance between the ricochet and witness plate is known).
- One can now calculate the velocity by dividing the distance (impact to ricochet plate) by the time difference of arrival. The weight of the ricochet can further be calculated by dividing the momentum with the velocity.

With this basic concept, a novel, fast approach for ricochet quantification is presented.

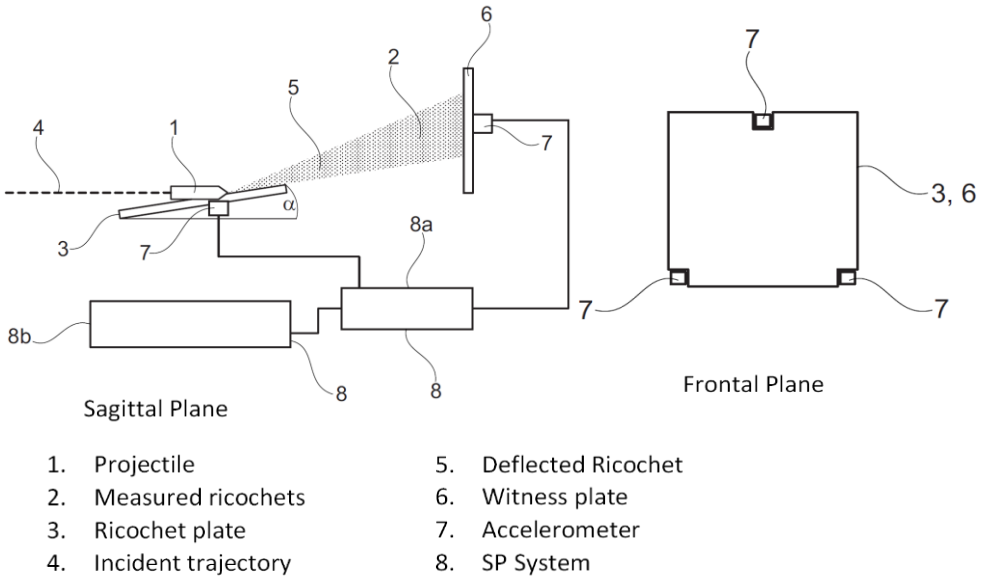

1. Projectile
2. Measured ricochets
3. Ricochet plate
4. Incident trajectory
5. Deflected Ricochet
6. Witness plate
7. Accelerometer
8. SP System

Figure 1-3: Schematic view of the ricochet measurement device.

1.5 Breech force and pushout force measurement

At present, the internal ballistic force measurement has only been rarely investigated despite evidences that it has a significant influence on the weapon safety. A typical example is shown Figure 1-4, a broken breech bolt.

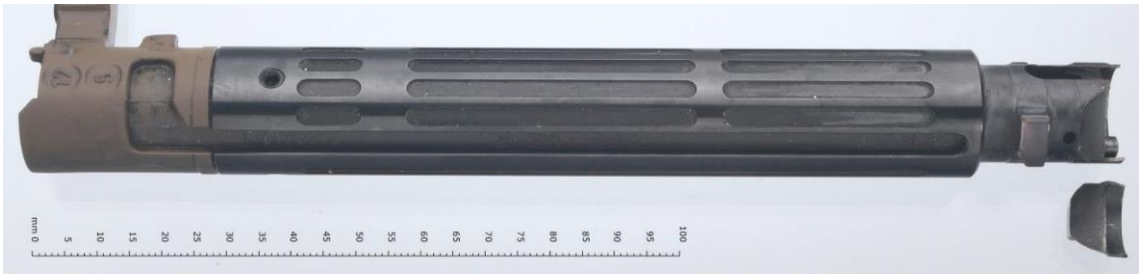

Figure 1-4: Broken breech bolt which failed due to high pushout force. This is a very safety- relevant event which may lead to severe injuries of the shooter.

As for a general introduction, it is vital to explain the relationship between the breech force and the pushout force as well as how this force is produced. The breech force and the pushout force are constraining forces which build a force equilibrium. While the pushout force is related to the ammunition the breech force is related to the weapon in question.

The pushout force is produced during the firing process and occurs when the casing is under pressure. The pushout force can be identified at the bottom of the casing. It pushes the casing against the breech, which is often a boltlike structure. Since the pushout force depends on the ammunition, this term is used for ammunition- related measurements.

The breech force holds the casing in place and acts on the breech system. Due to its direct influence on the weapon, the term is used for issues of relevance to weapon and safety

Besides the different nomenclature, the breech force and the pushout force are vectors which have the same direction and the same absolute value. However, the signs are reversed. Figure 1-5 illustrates this force equilibrium

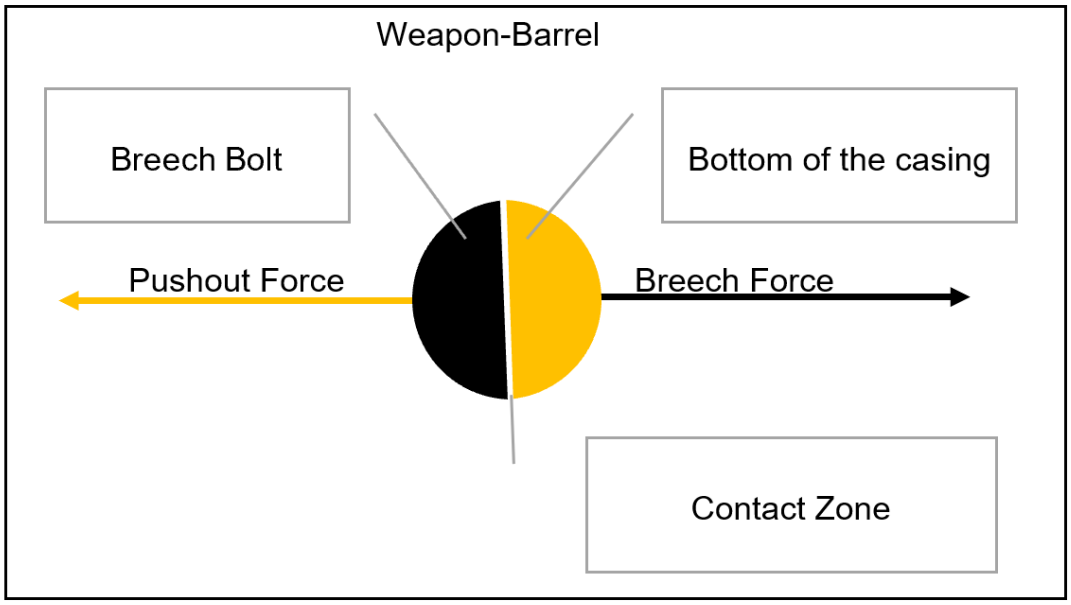

Figure 1-5: A schematic presentation of the breech force and pushout force.

The potential pushout force can be calculated by Finite Element Analysis (FEA) or analytical calculations. State- of- the- art piezoelectric force washers enable dynamic measurements which are used as a reference for FEA calculations.

A conceptual approach on how to measure the pushout force using a novel device is shown in Figure 1-6. Compared with the ricochet measurement system, the pushout force measurement method is more straightforward. The measurement concept is as follows: A special measurement breech bolt shall be developed, capable of bearing the pushout force and serving as the force measurement device at the same time.

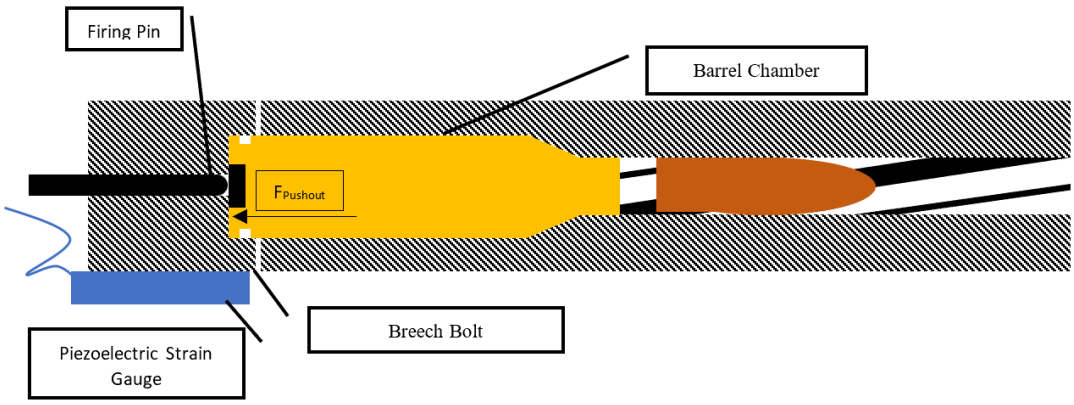

Figure 1-6: Initial concept for bolt force measurement.

1.6 Aims and objective

The main objective of this thesis was the development of a measurement system for ricochet quantification, breech force measurement and to evaluate different ammunition types concerning their ricochet and breech safety. All main measurements are performed using piezoelectric accelerometers, strain gauges and force washers.

It was hypothesised that a simple measurement system using two sensor plates with four sensors each will be enough to quantify the ricochet adequately. It was also hypothesised that a simple force washer is enough to assess the breech force. For increased accuracy, it is apparent that a signal processing method should be developed to filter the raw signal from the piezoelectric sensors. Momentum and force are in focus for the quantification. The following objectives were agreed as the core foci of this study:

1. To generate a state-of-the-art signal processing approach which enhances the measurement accuracy of piezoelectric sensors.

2. To establish an approach for momentum measurement of ballistic processes with the aid of force washers and accelerometers.
3. To undertake triangulation of the impact position using modern Time Difference of Arrival (TDOA) methods.
4. To investigate the effect of different ammunition types on the developed measurement system

A graphical presentation of the objectives can be seen in Figure 1-7 and Table 1-1.

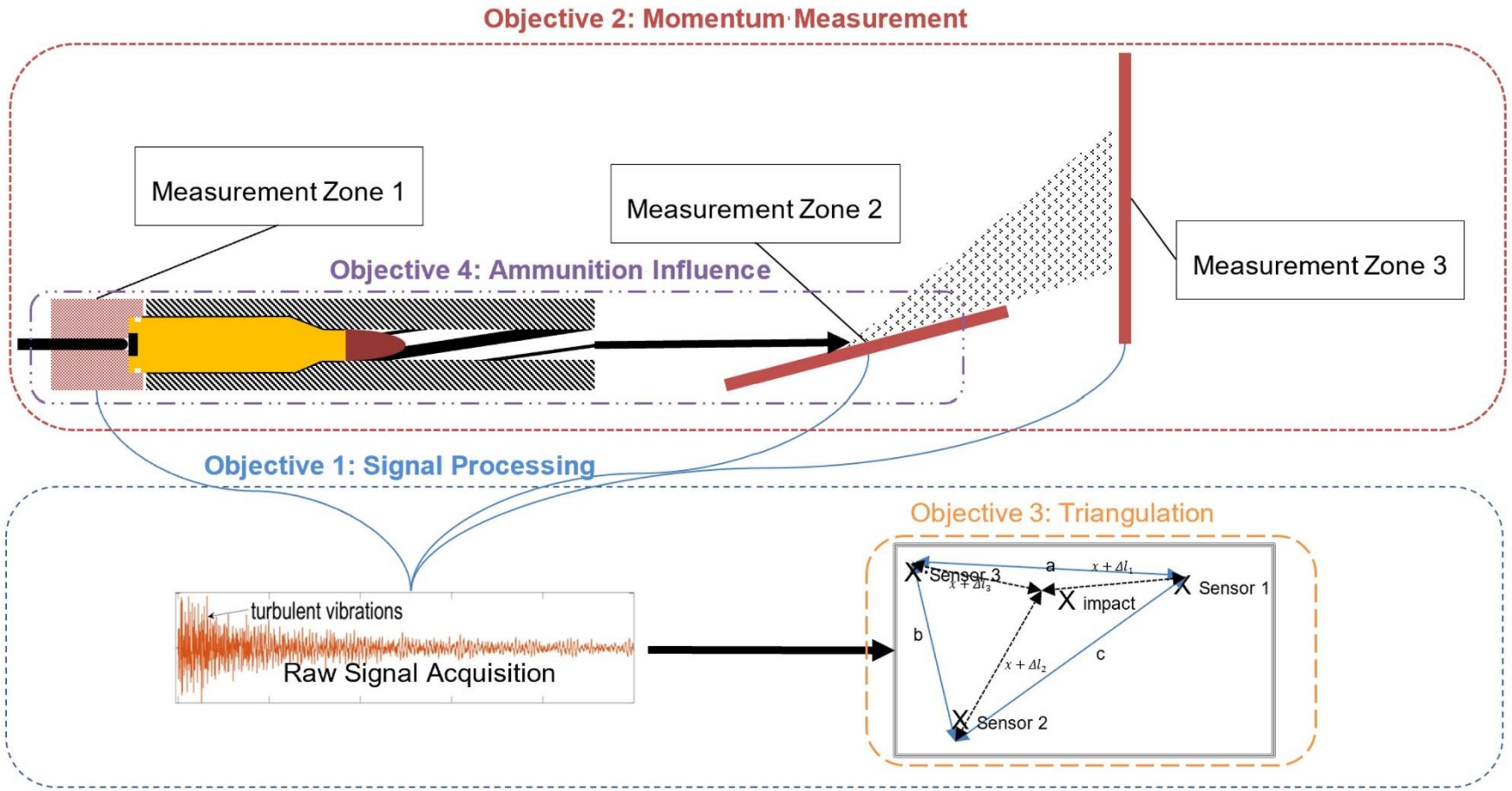

Figure 1-7: Overview of the device concerning the thesis objectives.

Table 1-1 Objectives in relation to the chapter.

Chapter/Topics	Objective Treated
4 / Measurement Plate	1, 3
5 / Pushout force measurement System - Investigation on different Ammunition	1, 2, 4
6 / Ricochet Measurement System	3, 4

1.7 List of published work

A list of the publications is shown in Table 1-2

Table 1-2 List of Published Work.

Title	Journal	Status
Damping of post-impact vibrations	Elsevier Applied Acoustics	Published
Dynamic qualitative pushout force measurements for investigating influence factors on the pushout effect of small calibre ammunition	AIP Advances	Published Open Source
Pushout force and impulse measurement of seven types of small arms ammunition with three different surface states	AIP Advances	Published Open Source
Ricochet quantification using a multiple sensor approach	Elsevier Defence Technology	Published Open Source

1.8 Conclusion

The main goal of this chapter is to provide clear guidance for the reader on the thesis structure and approach taken. In particular, it is focused on explaining that the thesis is designed to solve the fundamental research question: How do novel ballistic measurements affect recent safety considerations.

This guidance has been achieved using a graphical and tabular representation of the objectives agreed. In addition, this section has provided an insight into the importance and complexity of the question of measuring ricochets and why the intermediate step of consideration of pushout force measurement was necessary.

1.9 References

[1] MoD, *Handbook of Defence Land Ranges Safety*, 3rd ed., vol. 2. Joint Service Publication (JSP) 403, 2015.

[2] S. Hoxa and E.B. Vasquez, “Surface Danger Zone (SDZ) Methodology Study, Probability Based Surface Danger Zones,” *Piccatiny Arsenal, New Jersey*, Mar. 1995.

[3] “RTLP-MCX Range Design Guide Definition,” in Surface Danger Zone, *BUILDING STRONG®*, 2015

[4] Department of the Army, *Range Safety, Pamphlet 385–63*. 2003.

[5] V. Paris, A. Weiss, A. Vizel, E. Ran, and F. Aizik, “Fragmentation of armor piercing steel projectiles upon oblique perforation of steel plates,” in *EPJ Web of Conferences*, 2012, vol. 26.

[6] Y. Feng, J. Goree, and B. Liu, “Accurate particle position measurement from images,” *Rev. Sci. Instrum.*, vol. 78, no. 5, p. 53704, 2007.

[7] D. Yaziv, M. Mayseless, and Y. Reifen, “The penetration process of long rods into thin metall targets at high obliquity,” in *Proc. 19th Int. Symp. On Ballistics*, 2001, pp. 1257–1264.

[8] J. A. Zukas and B. Gaskill, “Ricochet of deforming projectiles from deforming plates,” *Int. J. Impact Eng.*, vol. 18, no. 6, pp. 601–610, Sep. 1996.

[9] B. Kneubuehl, R. M. Coupland, M. A. Rothschild, and M. Thali, *Wundballistik: Grundlagen und Anwendungen*. Springer Science & Business Media, 2008.

[10] A. Agnello, J. Dosch, R. Metz, R. Sill, and P. Walter, “Acceleration Sensing Technologies for Severe Mechanical Shock,” *Sound Vib.*, vol. 48, no. 2, pp. 8-19, 2014.

[11] “MIL-STD-810G Method 517.1,” Department of Defense, New York, NY, USA. 2008.

[12] F. Gustafsson and F. Gunnarsson, “Positioning using time-difference of arrival measurements,” in *IEEE International Conference on Acoustics, Speech, and Signal Processing*, vol. 6, pp. VI–553, 2003.

[13] R. Hoffmann and M. Wolff, *Intelligente Signalverarbeitung 1: Signalanalyse*. Springer-Verlag, 2014.

2 Background

2.1 Author contribution statement

Michael Muster wrote the background section with support from Amer Hameed and David Wood.

Michael Muster personally designed all measurement devices needed for the research. Michael Muster and Markus Grünig cooperated to manufacture the devices.

The ammunition used is serially produced in Thun. Some ammunition was produced by hand. Marlies Jenni carried out this manufacturing process under the guidance of Michael Muster.

2.2 Introduction

This chapter explains the fundamental aspects of the ricochet process in more detail. It also provides an in-depth background of the tested ammunition and equipment used to enable the scientific publications. Overall, this chapter provides the necessary ballistic knowledge which is essential to investigate ricochets.

2.3 About ricochets and SDZ

This section aims to show that ricochet measurement is of great importance for safety considerations. Ricochets are one factor for the design of SDZ. The investigation results, and the layout of the proposed device deal with the topic of oblique impacts on steel plates and the generation of ricochets. Furthermore, it is highlighted that the matter is worth investigating from a scientific point of view since bullets on steel produce more reproducible and comparable ricochets compared to other combinations.

2.3.1 Assessment of SDZ

Range Danger Areas (RDA), also known as SDZ, are of great importance to secure safety in a field which the systems are inherently packed with dangers. According to Greer [1], it is simultaneously both a “science and art” to create a safe environment which allows still efficient training. Due to the requirements of the different parties, the creation of a secure range danger area is necessarily a multidisciplinary task.

There are various opinions on how an SDZ should look. Planners for towns are happy if they can place buildings as close to the shooting range as possible. Other parties go further and do not want to have any shooting ranges close to other urban areas - not only because of the danger but also because of the noise. In their opinion, adequate SDZ’s need to be huge.

SDZ depends further on the country where the manoeuvre takes place. As an example, Switzerland is relatively small and packed with high mountains. Only 40 % of the space is easily accessible. These geographical circumstances lead to a high population density in the centres. Because of the restricted space, acceptable SDZ are very small compared to other countries. This leads to some interesting peculiarities – for example, in no other country is it is allowed to shoot with small arms over frequented roads which are not closed during exercises, see Figure 2-1. In addition, in Switzerland, it is also permitted to shoot large-calibre artillery shots over whole villages for training purposes.

Other countries like the USA have a considerable amount of rules which regulate all scenarios connected to SDZ. The Pamphlet 385-63 [2], which relies on chapter 4 of the DA PAM (Paragraph 4-1, b-c) [1] is one example. These regulations are in some aspects, even contrary [1], which makes it difficult to generate useful training scenarios.

According to the presentation of the U. S Army Training Support Centre (ATSC), there are two shapes used for Surface Danger Zones (SDZ’s). The Basic cone SDZ and the Basic Batwing SDZ, represented in Figure 2-2b and Figure 2-2a, respectively. The Cone Shaped SDZ is the better known and significantly easier

to be assessed, it relies on the distance X and a predefined angle, see Figure 2-2b. It is used for static training, where the stationary target is taken under fire for all cases.

The Batwing SDZ considers possible trajectories of all ricochets; it depends on computer-simulated models. It takes already rough values concerning the danger potential of a specific weapon into account. Furthermore, it also considers very rough ideas with respect to the maximal flight path of a particular type of ammunition. The pocket guide for range safety [3], which is based on the aftermentioned Pamphlet 385-63, describes the danger potential of ricochets after being deflected. This guide shows the danger area after a deflection on earth, water, steel and concrete for the whole calibre range from .22 cal Long Rifle M24 to 30 mm M788 TP-T.

Steel represents the largest danger area for all ammunition types – based on the significance of the results produced by the ricochet measurement device, which is intended to be built up with two steel plates. If projectiles fly farthest after impact on steel, one can produce with purely “impact on steel plate” measurement data a meaningful worst-case SDZ.

Comparing the Batwing SDZ with the Cone Shaped SDZ one has to recognize that the Batwing considers more factors and is adequate when it comes to safety considerations. The proposed ricochet measurement device gives with its results a contribution to the Batwing SDZ.

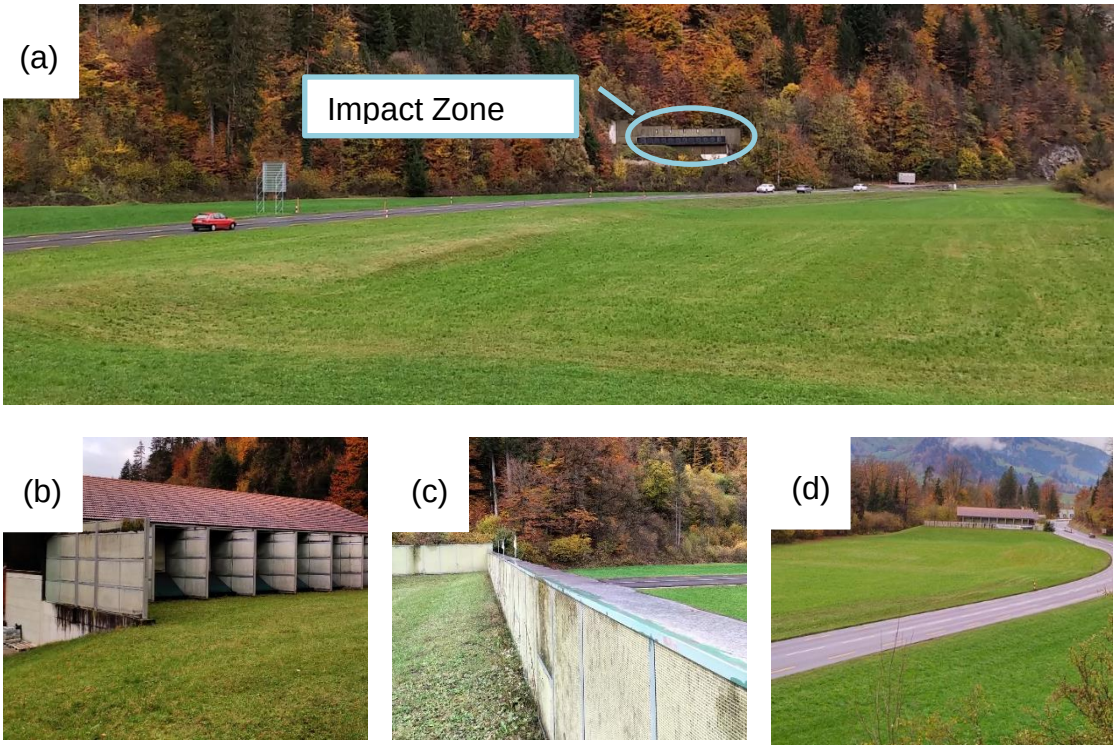

Figure 2-1: A shooting range in Switzerland, (a) shows the path of the projectile over the street. (b) shows the shooting balcony with the ricochet break (c). Picture (d) shows the view from the bullet trap to the shooting house 300 m away. Road travel is allowed also during shooting competitions. Projectiles fly over the driver's head in this case.

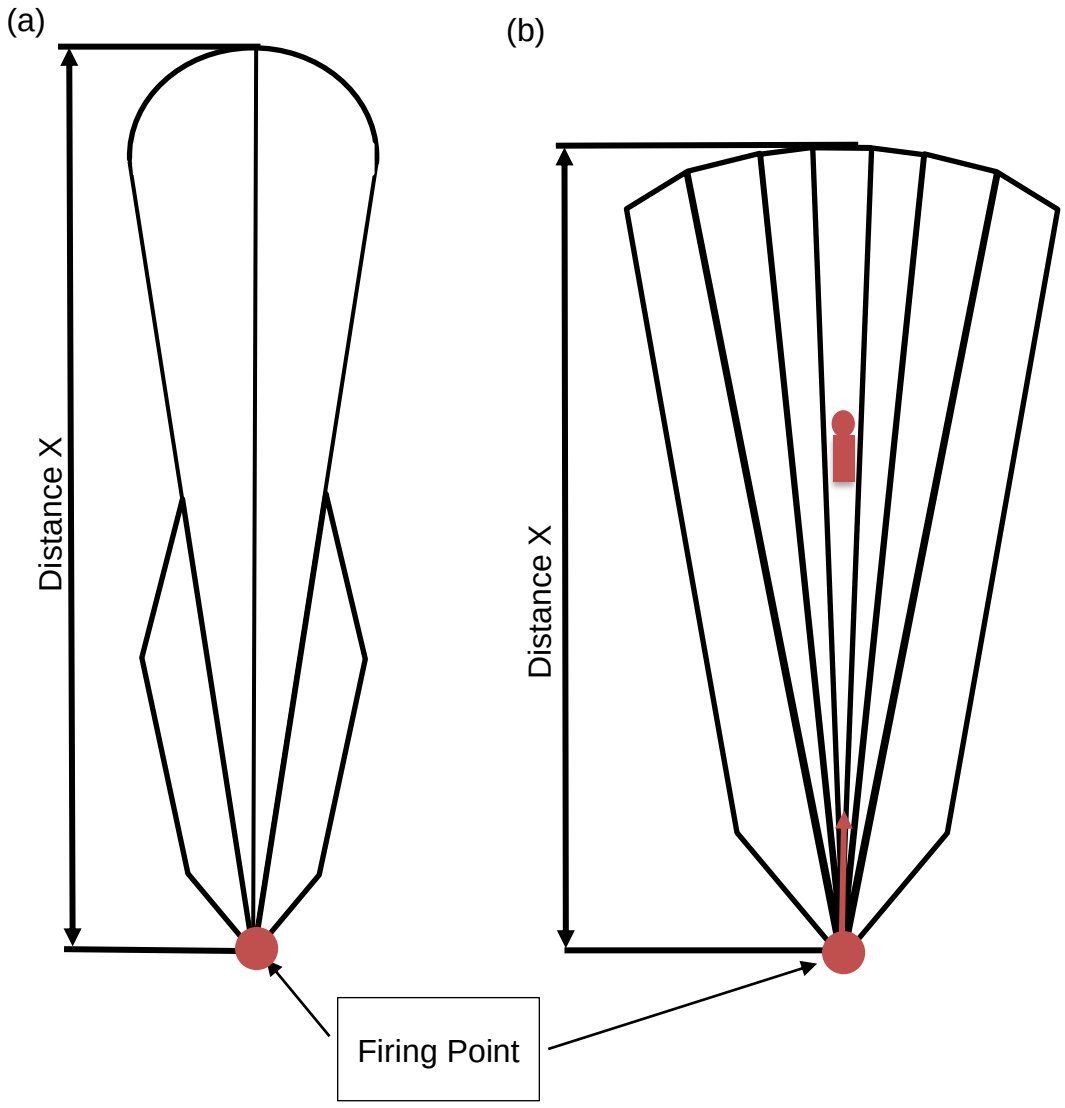

Figure 2-2: Different types of SDZ. The basic Batwing SDZ is represented in (a), whereas the basic Cone Shaped SDZ is represented in (b).

2.3.2 Ballistics of ricochets

There are three ways in which projectiles typically behave after hitting a target. A mild steel plate is assumed for better understanding. Firstly, the projectile may penetrate a target in a broken or still intact condition (depending on the projectile/-steel plate combination). The second possibility is that it may penetrate the target halfway and parts of the projectile are then stuck in the target. In this case, backscattering or bouncing back of the projectile are also possible. It may also be that the jacket of the projectile remains in the steel plate and the core penetrates it. Thirdly, with increasing obliquity of the target, the projectile starts ricocheting. During this deflection process, the projectile may stay intact or fragment. The danger potential comes especially from intact ricochets. However, small particles at slower speed still cause severe eye injuries. The relation between these parameters is well described by Backman and Goldsmith [4], see Figure 2-3. The diagram developed by Goldsmith shows the velocity/-obliquity relation for one specific target-projectile combination.

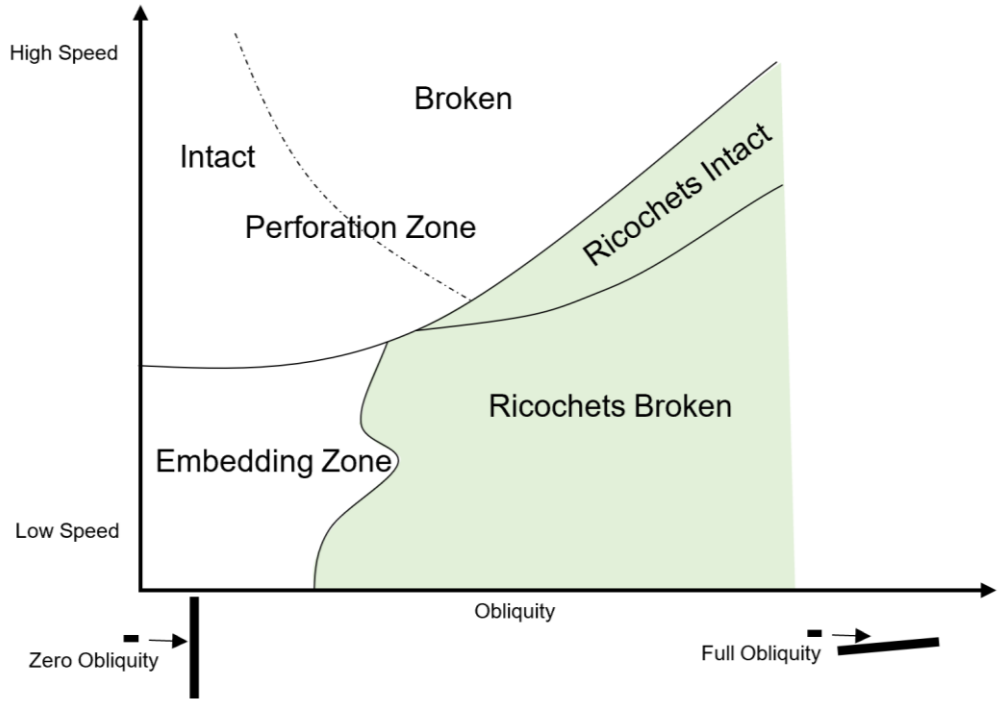

Figure 2-3: Simplified Backman Goldsmith diagram with the three zones. The interesting zone for the thesis is the green zone where the ricochets occur.

A deflection of a projectile takes place after a force acts on it. One can treat an oblique impact on a plate like a multidimensional partially elastic collision [5], [6]. Figure 2-4 represents a partially elastic collision. Basic properties of such collisions are that some of the collision energy dissipates to heat and deformation, and some lead to the velocity after deflection, see Figure 2-4. In a real-world scenario, one sphere may represent the projectile and the other a simplified pebble stone. However, typically, the soil where the bullet impacts is considered as significantly more substantial in weight compared to the projectile itself. This assumption leads to the case represented in Figure 2-5. Here, the energy of the projectile dissipates into the heavier structure. The projectile is ricocheted in the other direction, whereas the soil remains in the same position due to its greater inertia.

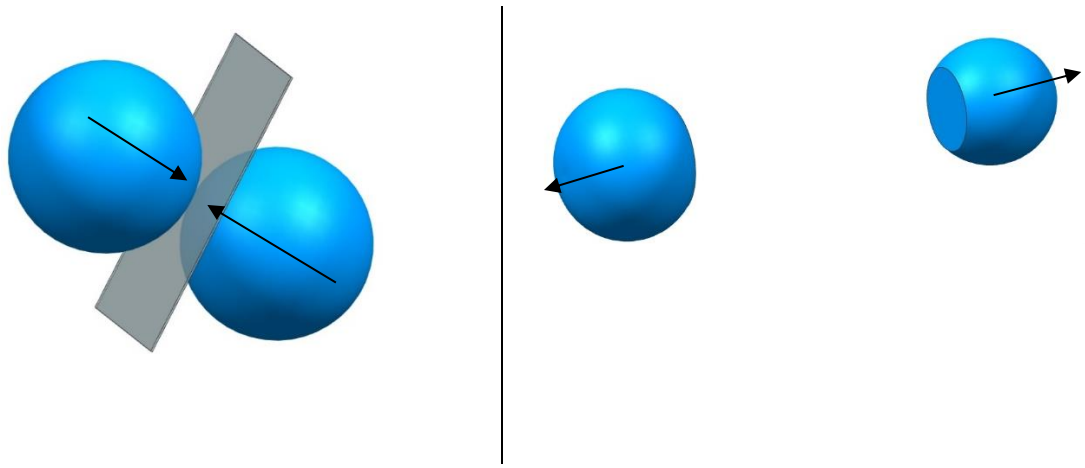

Figure 2-4: Partially elastic collision between two bodies of equivalent weight.

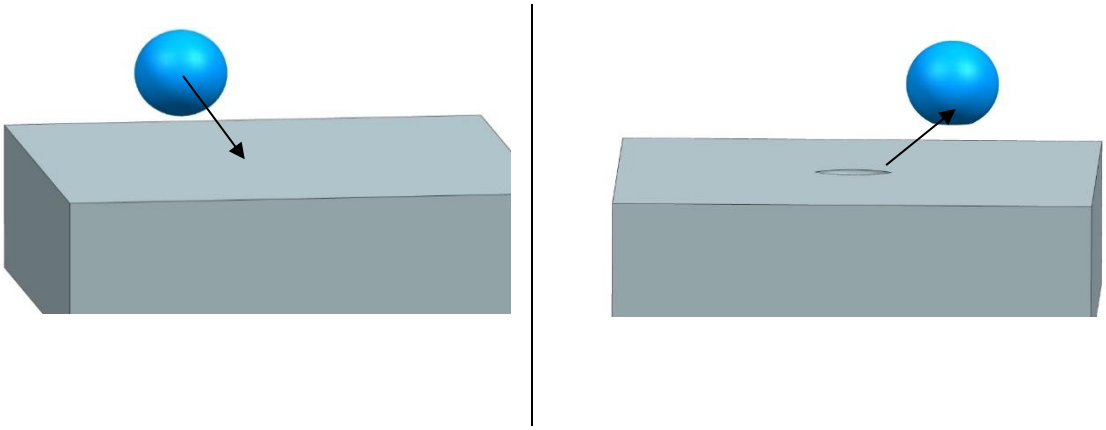

Figure 2-5: Partially elastic collision with a heavy counterpart.

Figure 2-6 represents a typical process of how ricochets are generated. A projectile may fragment or stay intact after bouncing off the impact surface during this process, independent on the fragment, the residual piece is called ricochet. The path of the ricochet is represented by the blue tube in Figure 2-6. After hitting the ricochet plate under the incident angle (α), the rotation of the projectile remains persistent. Because of this rotation, the ricochet is deflected in a horizontal and vertical direction [7].

Depending on the right or left twist, the projectile gets deflected to the left or right respectively. This second deflection angle is represented in Figure 2-6 as the angle γ. In the case of an impact without rotation, this ballistic property would not exist.

Another ballistic property of ricochet generation is the distance between the points of impact and departure. The distance between these points depends on the hardness of the projectile, the hardness of the ricocheting surface and the incident angle. The more inelastic the collision, the longer the distance between the arrival and departure points. In turn, the more oblique the plate is in relation to the incident trajectory, the shorter the distance between the arrival and departure points.

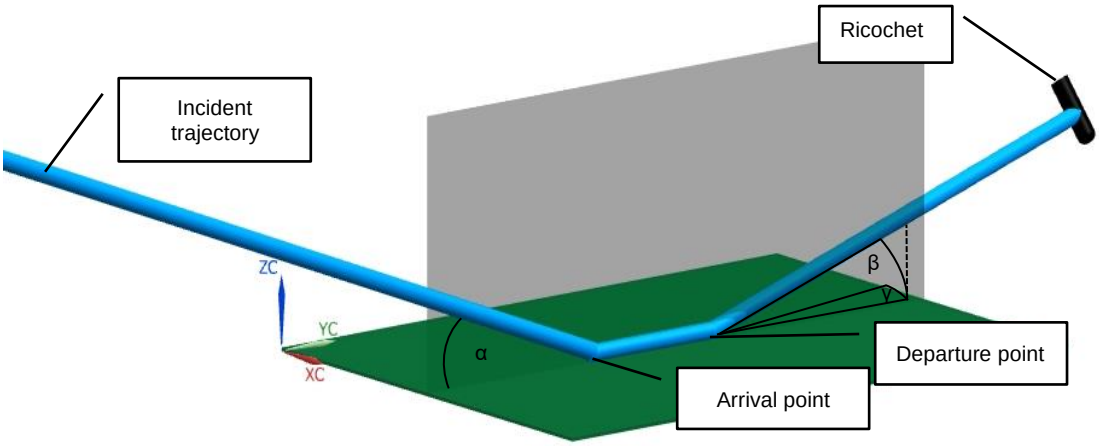

Figure 2-6: Generation of ricochets, under the incident angle (α), impacts of a projectile on a steel plate. The arrival and the leaving point is not necessarily the same. After the deflection, the projectile or its fragments are called ricochets. They are also deflected under a different angle (β). It might be that there is also a side bias compared to the incident plane, (γ) represents this bias.

2.3.3 Ricochets and their danger potential

A projectile ricochets after hitting a surface. The ricochet behaviour depends strongly on the angle and the mechanical parameters of the surface hit. The impact velocity and the mechanical parameters of the projectile are also of relevance. All these factors make it impossible to predict the trajectory of a ricochet in the field, which is why probabilistic models are used to estimate an SDZ which holds a danger potential of almost zero.

As explained above, it is the unpredictable trajectory, which poses the main danger potential of a ricochet. This statement is especially true for urban conflicts or close- combat scenarios. For such situations it is impossible to precisely follow the guidelines for an SDZ.

Besides the unpredictable trajectory of ricochets, the intrinsic wound ballistic property of ricochets represents a significant danger. A generic military small calibre projectile is spin stabilised and does not fragment if it hits a wound ballistic medium. In Figure 2-7, one can see a typical wound ballistic channel of a projectile which does not fragment. The energy dissipation is almost equal over the whole wound ballistic path; the rotation remains persistent. Ricochets, on the other hand, change the rotation speed significantly after fragmentation, and the impacts cause large wounds [8]. This effect results in severe injuries [9]. Figure 2-8a shows the destructive effect of ricochets in terms of wound ballistics.

Similar to fragments of a bomb or shrapnel, all the energy dissipates within a short distance into the wound track. Figure 2-8b shows a block of wound ballistic material penetrated by fragments. The area of the wound ballistics affected by the particles is substantial in comparison with one single intact projectile impact. The the penetration keyholes are oval or round, depending on the deformity of the fragments. This behaviour in terms of the spread of projectile fragments is a third reason for the dramatic danger potential of ricochets.

The danger potential of ricochets, especially the related increase in the spread was used to increase the probability of hitting enemies in the first wars where machine guns were used. Ricochet fire also served to increase the distance which a projectile can travel on a flat surface [10]. All these notes impressively demonstrate the importance of ricochets and their danger potential.

Figure 2-7: Typical wound ballistic picture of an unfragmented spin- stabilised projectile.

Figure 2-8: (a) represents a typical wound ballistic channel of a fragment, (b) shows ricochets impacted into wound ballistic soap.

2.3.4 Quantification of ricochets

Up until now, the quantification of ricochets has been a time-consuming process. There are two main reasons to investigate ricochets. Reason one is for criminal investigations. Ricocheting projectiles may give evidence of what happened at a crime scene. For example, if one knows the projectile type and the weapon used for the crime, this might enable statements about the possible positions where the offender was standing. It would be possible to state the velocity of the projectile and the lethality or the weapon used. A second reason to investigate a ricochet is the construction of a suitable and bullet specific SDZ.

Criminal investigations often consider surfaces like glass windows, concrete plates, timber boards or dirt hit under a certain incident angle, and the deflection angle is measured with a simple witness measurement device like cardboard. This technique provides evidence for a particular crime scene. However, such investigations are not suitable for the generation of an overall fragmentation model of a projectile type.

Experimentally the projectile or its ricochets may also be trapped with ballistic soap to measure the danger potential. The penetration depth and the shape of the resultant wound channel give evidence about the energy dissipation of the projectile in the wound ballistic medium. Another advantage is that the trapped projectile can be analysed under a microscope.

As already mentioned, the above ricochet measuring approaches are suitable to answer specific questions. Feeding into this area, extensive work was conducted by Karl Sellier [5]. Sellier investigated the ricocheting behaviour of different projectiles on metal plates (steel, aluminium, brass) of different thicknesses and under different angles. This work was extended to for wood, glass, sand and concrete. The results of this study showed that there is always a big spread of ricochet behaviour, especially when sand and concrete are concerned. These major differences of ricochet spread were clearly demonstrated by the tests of Kneubühl [11] and Rottenberger [12]. Besides the incident and deflection angles, the side angle and the residual energy are also measured to enable an estimation of the maximum possible trajectory which determines the safety zone. The trajectory spread for projectiles containing lead is found to be between 114 m and 1470 m, whilst the general spread for lead-free projectiles is between 79 m and 1521 m.

Another way of investigating ricochets was studied by Nishshanka [13] and Liddell [14]. They used a Doppler radar to investigate the impact velocity. A high-speed camera served to record the fragmentation speed and a fragments capture box allowed them to investigate the size, weight and shape of the fragments or bullet after a deflection.

2.3.5 Pushout force measurements

The quantification of the pushout force is less time consuming than the ricochet quantification. However, these measurements are rarely conducted up to now. One reason might be the lack of suitable measurement equipment because it is a closed system which is not directly accessible. Another reason might be a lack of interest. However, with the increased availability of new casing materials, a quantification of the pushout force seems a very important and timely endeavour.

Like ricochet measurements, pushout force measurements are important for safety reasons. A significant rise in the pushout force may lead to weapon breakage and severe harm to the shooter or bystanders. Essentially, ricochet measurement contributes to the safety of the far environment, whereas the pushout force measurement contributes to the close environment.

Apart from the safety aspect, the pushout force measurement is a defined dynamic system and measurements are repeatable.

2.4 Scientific software

The scientific software used in this study comprised of LabVIEW [15], MATLAB® [16] and Spyder [17]. LabVIEW is a software package from National Instruments (NI) which is ideal for acquiring data from all kind of sensor signals. It can further be used for complex control engineering tasks. Another strength of LabVIEW is the fast and direct generation of User Interfaces (UI). MATLAB® and Spyder are suitable for the manipulation of multimillions of data points. Usefully, all software used is the implemented toolboxes, especially the statistics toolboxes.

LabVIEW is a graphical programming language. The focus is on the data stream. The dataflow is represented with lines between boxes, called Virtual Instruments (VIs). The data manipulation takes place in these VIs. In LabVIEW, one has two main panels which are connected. The front panel is the UI which contains the instruments. The block diagram panel contains the full graphical code. This system enables fast switching between the connected panels, and this makes the software suitable for rapid prototyping UI and simple interface measurement devices.

The UI of LabVIEW is essential for this thesis because using a UI gives a good opportunity to train the ballistics test team in using the measurement device. The person who acquires the raw data is not necessary the person who processes the data afterwards.

The company NI is not a pure software developer. Besides LabVIEW, which can be used for measurement technique, control engineering and automation purposes. It produces different kinds of devices for measuring signals or controlling actuators. These devices are called NI-DAQ devices. The advantage of the raw data acquisition using a combination of LabVIEW and NI-DAQ is that all interfaces are plug and play. Further, all functionalities of the device are enabled using LabVIEW.

The NI-DAQ device used is equipped with a pre-trigger which can be initiated by the LabVIEW software. The advantage of the pre-trigger is that the ballistic event itself can trigger the acquisition without loss of any data points. It is possible to define a set of data points which is acquired before the ballistic trigger event took place. Despite the fact that there are a lot of signal processing is possible with LabVIEW like filtering or Fourier transforms, LabVIEW is in this case purely used for acquisition of the sensor signal and the automated generation of a data .txt file which can be used as an interface for other software packages.

The .txt files can be further used either by MATLAB® or by Spyder. During the first phase of this thesis the filtering and signal processing software MATLAB® was used. MATLAB® is a software package used for mathematical computations. The underlying idea of MATLAB® is to use matrixes to solve mathematical problems. The programming language is close to C. However, there are many pre implemented mathematical functions which use built-in matrix calculations. The advantage is that matrix operations are computation wise less complicated compared to classical loops, so scripts run very fast. A vast amount of data can be analysed within a short time. Data acquisition is also possible using MATLAB®. However, MATLAB® is not primarily focused on this element.

The post-processing of the acquired raw data was done in this thesis using several script files. These script files were run using one main script file. There was no User Interface implemented in the developed script. The reason for this was that the person who does the post-processing needs to modify parameters fast and knows how to work with scripts, since the person wrote the script. One reason for using MATLAB® for initial post-processing algorithm was that MATLAB® features also has a large number of already implemented algorithms, which can be used for rapid prototyping. Signal envelopes, wavelet transformations, windowed Fourier transformations, and different filter types, amongst others. Even a Time Difference of Arrival (TDOA) algorithm is realised. It was initially developed for the triangulation of Wi-Fi devices. It was postulated that this triangulation algorithm could also be used to analyse in a first test the precision of the impact measurements.

After the first measurements, a third software package called Spyder was used. This change was necessary since Spyder can be installed on multiple devices, as there are no licence restrictions. The open-source software presents benefits if one uses multiple-processor systems or cluster computers and different workstations. Spyder originates from the MIT (Massachusetts Institute of Technology) and uses Python as language. The user interface of Spyder is similar to MATLAB®. However, the basic principle is not matrix computations which means that the existing algorithms need to be changed.

The final ricochet measurement device was realised, using LabVIEW with a UI as data acquisition software. The final overall post-processing momentum measurement and triangulation algorithm are realised with Spyder software which is installed on several computers.

2.5 Devices developed during the thesis

During the path of the thesis, it was necessary to design and develop two custom measurement devices. The investigated parameters can’t be measured using COTS measurement systems. The ricochet measurement device was separately manufactured for these tests. However, the pushout force measurement system was an additional feature of an already existing device.

2.5.1 Pushout force measurement device

During the firing process, the casing of the cartridge is under significant pressure. This pressure could push the casing out of the chamber out of the weapon barrel. To prevent this, a breech bolt is needed. The quantity, i.e. the scalar of the pushout force, is equal to the breech force. The vectors, however, point in opposite directions, so that they compensate each other, thereby eventually creating a statically determined system.

One has to differentiate between the pushout and the extraction force. The extraction force describes the force needed to extract an empty casing from its chamber in the barrel. This force is relevant for reloading the weapon and applies after the projectile left the barrel. It acts in the opposite direction, i.e. rearwards. The casing sticks in the barrel chamber due to its expansion during firing. Figure 2-9 schematically shows the difference between the pushout and the extraction force.

The main structure consisting of housing, trigger device, force measurement sensor, breech bolt and igniter should remain the same for all calibres. The only exchangeable item should be the barrel of the shooting machine. Each calibre needs at least one barrel, consequently, more than seven barrels were necessary for the relevant investigations. The heavy metal housing, proof barrels and removable trigger device existed already, see Figure 2-11 and Figure 2-12. The measurement plate shown in Figure 2-10, is an entirely newly developed device (similar to the ignitor pin, which is also newly designed).

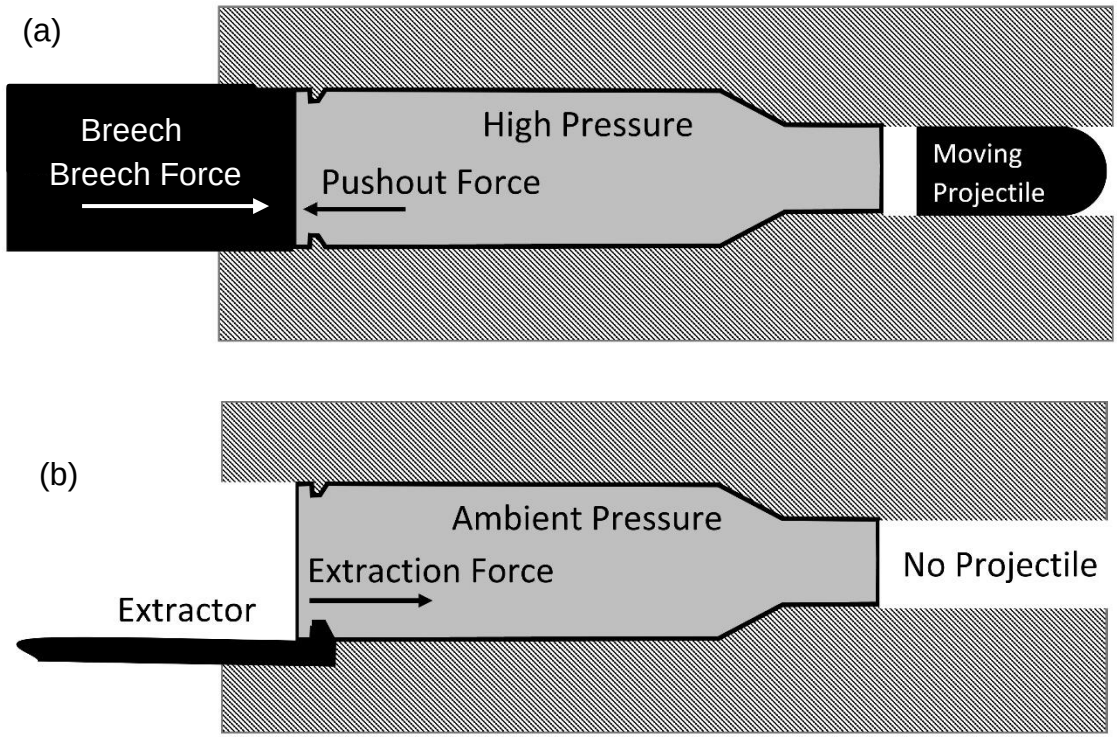

Figure 2-9: (a) represents the pushout force measured with the measurement device. (b) represents the extractor force, which occurs at a later stage.

Figure 2-10: Picture of the measurement plate, which is at the same time the breech. The round zone under the casing presses directly on the piezoelectric force measurement ring.

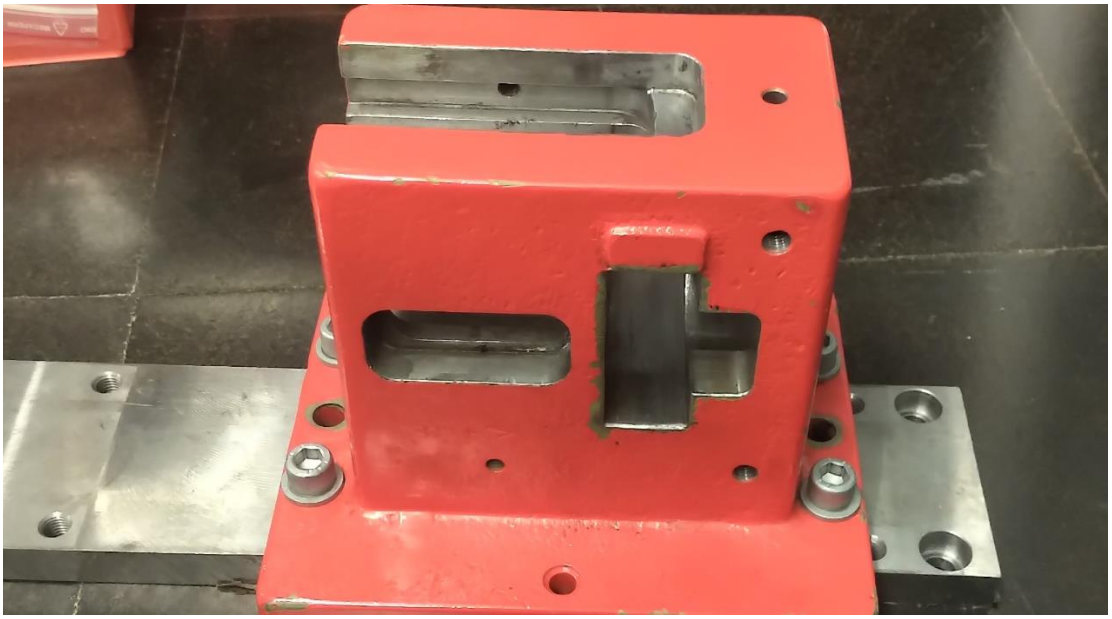

Figure 2-11: Housing of the barrel and the measurement plate.

Figure 2-12: Interchangeable barrels used for ballistic investigations the largest barrel is a standard .50 Browning test barrel, and the smallest is a 9 mm Luger barrel.

2.5.2 Ricochet measurement device

The ricochet measurement device has two main parts, a ricochet plate and a witness plate. Both plates are equipped with sensors. The plates need to be mounted on a suitable system, a heavy metal frame is needed to bear the massive (100 kg) witness plate (Figure 2-13).

The frame forms a tunnel in which dangerous fragments are kept. This reduces the possibility of damaging the measurement equipment significantly. The heavyweight metal frame (900 kg) is also important to provide good stability against overturning, i.e. essential for the measurement accuracy of the witness plate.

The ricochet plate is smaller compared to the witness plate and is mounted on a pushcart. With this system, the cart can move up and down. Further, the impact angle can be adjusted using a linear drive, while the pushcart provides enough ballistically protected space for the housing of the measurement equipment.

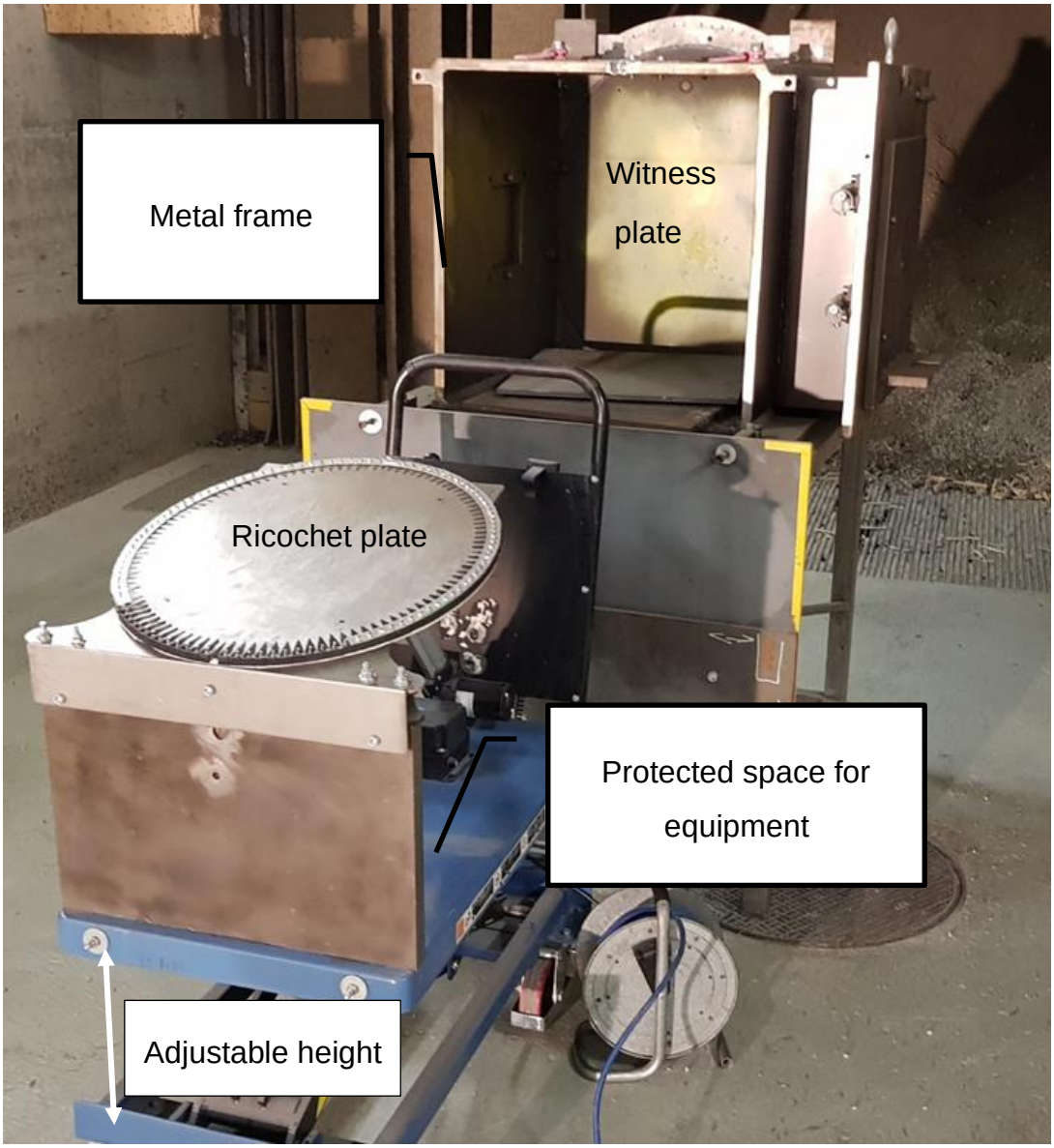

Figure 2-13: The Ricochet measurement device.

2.5.3 Design principle of the devices

It is a challenging task to state design principles of devices for ballistic investigations. Crucial aspects are that the devices can resist the huge loads which occur during very short periods. In the internal ballistic field, typical values are around. 0.5 ms for the acceleration process from 0 m/s to 1000 m/s [6], or a rise in barrel temperature from ambient to 2700 °C [18]. During the time, pressure rises from ambient to more than 350 MPa [19], [20].

To cope with these conditions, tempered steel is the preferred material. Especially during the terminal ballistic measurement, the impact transmits a considerable impulse to the measurement device which must be accordingly heavy to resist it. The most sensitive parts of a ballistic testing device are always the sensors and cabling. The mechanical properties of the device must be considered and adequate housing should be provided for each sensor.

Vibration-damping structures like rubber dampers were used to support the metal frames. As described in [21], a design capable of resisting high- energy mechanical oscillations is the principal criterion. In small-calibre ballistic investigations, different ammunition calibres are often analysed. The system should be as modular as possible to meet this requirement and facilitate a solution. One can do the calculation with the most massive possible projectile flying at the highest velocity. With this approach the measurement device will thus be suitable for every projectile type.

2.6 Ammunition

This subsection describes the ammunition used for all tests carried out during the courde of the work contributing to this thesis.

2.6.1 9 mm Parabellum

This calibre was used for initial tests because the energy produced is considerably lower compared with all other tested calibres.

2.6.1.1 9x19 FMJ 8 g/124 gr

This standard ammunition type was always used for the first test. It showed good results as regards ricochet behaviour. The projectile deforms in such a way that it does not fly a long distance after deflection. The fragmentation pattern is due to the fact that the projectile consists of a lead core and a soft steel jacket, see Table 2-1 and Figure 2-14.

Figure 2-14: Regular FMJ Projectile.

Table 2-1: 9x19 FMJ 8 g/124 gr.

Projectile Material	Cu-coated steel jacket, lead core
Term of reference	C.I.P
Mean chamber pressure	max. 2’350 bar
Muzzle velocity	380 m/s
Muzzle energy	575 J

2.6.1.2 Frangible Copper Matrix SX 6.4 g/98 gr

Frangible ammunition was used to analyse the effect of ricochet-reduced bullets. The overall momentum transferred was significantly lower because the projectile consists of copper embedded in a polymer matrix. The result is that the projectile is transformed into dust after deflection. See Figure 2-15. The frangible ammunition displayed high, but short-duration forces during the firing process. This is because the projectile mass is low compared with the other 9 mm projectiles considered. See Table 2-2.

Figure 2-15: Frangible 9 mm Ammunition.

Table 2-2: Frangible Copper Matrix 9 mm.

Projectile Material	Copper polymer matrix
Term of reference	MCMOPI
Mean chamber pressure	max. 2’850 bar
Muzzle velocity	430 m/s
Muzzle energy	590 J

2.6.1.3 9x19 Action 4 SXF

Action 4 ammunition was developed for the police. The projectile deforms in the body. For the purposes of ricochet and especially pushout force measurements, it is a different ammunition type since it has a solid and light body as evident in Figure 2-16. Furthermore, the ammunition is certified according to the TR, see Table 2-3. This makes it worth investigating since higher pressures are allowed.

Figure 2-16: Action 4.

Table 2-3: Action 4.

Projectile Material	CuZn Alloy 6.1 g/94 gr
Term of reference	TR
Mean chamber pressure	max. 2’700 bar
Muzzle velocity	420 m/s
Muzzle energy	540 J

2.6.2 5.56x45 Ammunition

The bottleneck 5.56x45 mm ammunition allows proper sealing of the casing in the chamber during the firing process. During experiments the projectile exhibited significant differences in pushout force depending on whether the casing surface was dry or lubricated. Ricochet behaviour depends on the design. Seeing that this projectile represents a standard design, and a very frequently used calibre, it was also taken as a reference for the ricochet behaviour throughout this study.

2.6.2.1 5.56x45 FMJ M193

The advantage of this projectile was that it is very well tested and known. It is a full metal jacket projectile, see Figure 2-17. The copper jacket and the lead core provide limited penetration capabilities. It displayed comparatively significant pushout force differences, between the dry and lubricated casing. The ricochet behaviour depends on the design. Since this projectile is of a standard design, it was also taken as a baseline reference for the ricochet behaviour.

Figure 2-17: M193 Cartridge.

Table 2-4: M193 Cartridge.

Projectile Material	tombac jacket, lead core 3.6 g/55 gr
Term of reference	MCMOPI
Mean chamber pressure	max. 4100 bar
Muzzle velocity	990 m/s
Muzzle energy	1764 J

2.6.2.2 5.56x45 Frangible SX

This specific ammunition type is intended for use in urban areas. The projectile is uniquely designed to decrease the danger of ricochets. However, the main threat comes from the big fragments of the polymer matrix projectile, see Figure 2-18 and the description of the projectile material in Table 2-5. This ammunition type was used for the ricochet analysis exclusively. It showed excellent performances as regards momentum reduction after hitting an oblique surface.

Figure 2-18: Frangible 5.55x45.

Table 2-5 Frangible 5.55x45.

Projectile Material	sintered Cu in tombac jacket 2.9 g/62 gr
Term of reference	MCMOPI
Mean chamber pressure	max. 4100 bar
Muzzle velocity	920 m/s
Muzzle energy	1296 J

2.6.2.3 SS109

This ammunition type was tested for two reasons: Firstly, it is widely used and suitable as a reference. Secondly, it has a soft lead and a hardened steel core for better penetration - see Figure 2-19. This double core design gives it unique properties for ricochet measurement. The heavier weight compared with the other projectile types, see Table 2-6, offers different features for the resultant impulse transmission.

Figure 2-19: SS109.

Table 2-6: SS109.

Projectile Material	tombac jacket, hardened steel and lead core 4.0 g/62 gr
Term of reference	MCMOPI
Mean chamber pressure	max. 4100 bar
Muzzle velocity	945
Muzzle energy	1785 J

2.6.3 7.5x55 GP11

This projectile type was investigated because its performance is highly comparable with that of the M80, see Table 2-7. The projectile has a steel jacket, which leads to other pushout forces compared with the M80, see Figure 2-20. Another aspect is that the projectile features almost no cylindrical parts to reduce the push through force, i.e. the force required to push the projectile through the barrel. This conical design also reduces the pushout force.

Figure 2-20: GP11.

Table 2-7: GP11.

Projectile Material	Plated steel jacket, lead core 11.3 g
Term of reference	Swiss Army
Mean chamber pressure	max. 3300 bar
Muzzle velocity	787 m/s
Muzzle energy	3500 J

2.6.4 7.62x51 FMJ (M80)

The M80 full metal jacket, see Figure 2-21, is a standard ammunition type, well known and defined. The purpose of testing this projectile type was to obtain a reference for ricochet measurements. The maximum capacity for many shooting ranges is often designed around this projectile ammunition combination. The second purpose was to crosscheck the results from the GP11 since the properties are similar. In Table 2-8, one can see that the bullet weight is slightly lower compared with the GP11. The muzzle velocity, however, is higher.

Figure 2-21: 7.62x51 FMJ (M80).

Table 2-8: 7.62x51 FMJ (M80).

Projectile Material	tombac-plated steel-jacket, lead core 9.5 g
Term of reference	MCMOPI
Mean chamber pressure	max. 4100 bar
Muzzle velocity	855 m/s
Muzzle energy	3455 J

2.6.5 .338 Lapua Mag. SWISS P BALL

This .338 ball ammunition is intended for snipers. The kinetic energy is high in comparison with smaller calibres, see Table 2-9. However, the projectile design is similar to the other FMJ types, see Figure 2-22. In the pushout force tests, a considerable dispersion between the force measurements was detected. The reason for this difference compared to the M80 ammunition is a different obturation process.

Figure 2-22: .338 Lapua Mag. SWISS P BALL.

Table 2-9: .338 Lapua Mag. SWISS P BALL.

Projectile Material	tombac jacket, lead core 16.g / 255 gr
Term of reference	CIP
Mean chamber pressure	max. 4200 bar
Muzzle velocity	855 m/s
Muzzle energy	5958 J

2.6.6 .375 SWISS P

This calibre was investigated for a cross-reference with the .338 Ball. The cartridge size and design are similar (see Figure 2-23). However, in Table 2-10, one can see that the projectile energy is high compared to the .338, even the size is similar.

Figure 2-23: .375 SWISS P.

Table 2-10 .375 SWISS P.

Projectile Material	tombac jacket, lead core 22.7 g / 350 gr
Term of reference	CIP
Mean chamber pressure	max. 4200 bar
Muzzle velocity	880 m/s
Muzzle energy	8800 J

2.6.7 .50 Browning Training SX

This projectile was the heaviest and most energetic one tested. The jacket is called a “shoe” and is wrapped around a solid core consisting of a special zinc alloy, see Figure 2-24. The centre is made of this soft metal because of the reduced penetration capabilities which are highly desirable for training. The projectile energy of 17077 joules was very high, see Table 2-11. Because of these properties, the projectile was mainly used to assess the ruggedness of the developed device. This cartridge type showed the most significant change as regards the pushout force, irrespective of whether the casing was lubricated or not.

Figure 2-24: .50 Browning Training SX.

Table 2-11: .50 Browning Training SX.

Projectile Material	tombac jacket, lead core 41.7 g / 644 gr
Term of reference	MCMOPI
Mean chamber pressure	max. 4500 bar
Muzzle velocity	905 m/s
Muzzle energy	17077 J

2.7 Conclusion

Ballistics is the overarching topic of ricochet analysis. Thus, it is important to describe ballistics and the ballistic equipment needed for the planned ricochet investigations. One main objective of this chapter is to show that ballistic processes, especially in small arms, are potentially dangerous. They take place within a short time and the delivered kinetic energy is high. These factors are demanding on the environment, the measurement equipment and the material to be tested.

2.8 References

[1] A. Greer, “The Art vs Science of Maneuver Range Planning,” Infantry Online, no. 4, 2015

[2] Department of the Army, *Range Safety, Pamphlet 385–63*. 2003.

[3] *USMC Range Safety Pocket Guide,* Version 1.7. Quantico: Training and Education Command, 2013.

[4] M. E. Backman and W. Goldsmith, “The mechanics of penetration of projectiles into targets,” *Int. J. Eng. Sci.*, vol. 16, no. 1, pp. 1–99, 1978.

[5] K. Sellier, *Schußwaffen und Schußwirkungen. 2. Forensische Ballistik, Wundballistik: mit 64 Tab.* Schmidt-Römhild, 1977.

[6] B. Kneubuehl, *Geschosse : Ballistik, Messtechnik, Wirtksamkeit, Treffsicherheit*. Stocker-Schmid, 2013.

[7] M. G. Haag and L. C. Haag, “Projectile Ricochet and Deflection,” in *Shooting Incident Reconstruction*, 2011, pp. 143–174.

[8] B. Kneubuehl, R. M. Coupland, M. A. Rothschild, and M. Thali, *Wundballistik: Grundlagen und Anwendungen*. Springer Science & Business Media, 2008.

[9] Y. E. Yong, “A systemic review on ricochet gunshot injuries,” *Leg. Med.*, vol. 26, pp. 45–51, 2017.

[10] T. W. Burke and W. F. Rowe, “Bullet Ricochet: A Comprehensive Review,” *J. Forensic Sci*., vol. 37, no. 5, pp. 1254–1260, 1992.

[11] B. P. Kneubuehl, “Das Abprallen von Geschossen aus forensischer Sicht,” Université de Lausanne, 1999.

[12] I. Rottenberger, “Abprallverhalten von Jagdmunition,” *DEVA*, Altenbeken, Germany, 2011.

[13] B. Nishshanka, “Analysis of the ricochet behaviour of Kalashnikov bullets (7.62X39 mm) on sheet metal,” Cranfield University, 2017.

[14] C. R. Liddell, “Investigating Ricochet of 9 mm Luger on Mild Steel Sheets,” Cranfield University, 2010.

[15] “LabVIEW.” National Instruments, 2015.

[16] “MATLAB®.” MATHWORKS, 2018.

[17] “Spyder.” MIT, 2019.

[18] J. Powling and W. A. W. Smith, “Measurement of Burning Surface Temperatures of Propellant Composition by Infrared Emission,” Essex, 1962.

[19] L. Elkarous, C. Robbe, M. Pirlot, and J. Golinval, “Dynamic calibration of piezoelectric transducers for ballistic high-pressure measurement,” *Int. J. Metrol. Qual. Eng.*, vol. 7, 2016.

[20] L. Elkarous, M. Pirlot, and J. C. Golinval, “Dynamic calibration of piezoelectric sensors for the ballistic high-pressure measurement / Étalonnage dynamique des capteurs piézoélectriques pour la mesure de haute pression balistique,” in *International Metrology Conference CAFMET 2012*, pp. 1–8, 2012.

[21] F. Aggogeri *et al.*, “Design of piezo-based AVC system for machine tool applications,” *Mech. Syst. Signal Process.*, pp. 1–12, 2011.

3 Sensor data and its processing

3.1 Author’s contribution statement

Michael Muster contributed the basic ideas of the sensor system to the research.

Michael Muster contributed the signal processing system for the analysis of the sensor results.

Michael Muster wrote this chapter with the inputs of David Wood.

3.2 Introduction

The focus of this chapter is on the signal processing of piezoelectric sensors. The post-processing of piezoelectric raw signals is necessary to get reliable results. This chapter discusses possible signal processing approaches and their applicability to ballistic investigations.

Measurements are always connected to errors. Due to this fact, the present chapter also elaborates on possible errors of the measurement systems presented in this thesis.

3.3 Signal processing of ballistics events

The quantification of single impact events is essential for the entire system. For the measurement and sensor system itself, it does not matter whether the impact is produced by the actual projectile or the casing pressed against a breech. Single impact events in ballistics produce strong signals during a short time (to the order of milliseconds).

Separate ways of processing the raw signal are investigated in this thesis. A signal envelope-based approach showed the best performance and the highest accuracy as far as momentum measurements and triangulation are concerned. The accurate capturing of Arrival Time (AT) and the momentum transfer are crucial to get a reasonable estimation of the properties of the ricochet. If the AT is not precise enough, one gets an imprecise positioning, which would be a hindrance to answering the main research question.

It is hypothesised that the performance of piezoelectric sensors could be increased with modern SP approaches, especially ricochet mechanics for a new device to measure ballistic events.

The next subsection is a short review of the possibilities of processing the acceleration signals. However, best practice is to work with the physical properties of the signals, especially for short-time events.

3.4 Advanced signal processing

This section concerns various signal processing approaches and evaluation. Here, modern machine and deep learning techniques to solve the triangulation problem have also been considered to improve the processing and data cleaning.

This part of the review was performed to critically appreciate the influence of the triangulation of several impacts has on accurately identifying the location of points of impacts. The approaches are rather mathematical-statistical than physical.

Knowledge about a signal processing of unsteady signals has increased significantly over the past few decades. Comparable approaches for processing the signals are those used in techniques of human speech recognition.

Starting with how the signal is acquired, it is observed that more and more micro-electro-mechanical system (MEMS) microphones are now in use for mobile devices [1], [2]. These systems convert acoustic energy (movements caused by pressure differences) into electrical energy [3]. This is comparable to accelerometers which convert larger-scale mechanical oscillations into electrical energy. Also, how these systems produce the signals are similar; both detection systems can be realized with piezoelectric crystals. The basic properties of the signals are also similar: both signals are vectors containing waves of varying frequencies and magnitudes.

However, there are also some differences between acoustic and impact signals. The period of highest importance for location triangulation is immediately after impact, while the period of free oscillation is less critical. In the case of speech recognition, the whole body of the signal is essential.

In other words, the main difference is that the signal acquired in the case of impact detection is in microseconds and the case of speech recognition in milliseconds. But the same analytical principles apply.

3.4.1 Acoustic phonetic approach

The acoustic-phonetic approach is the oldest method to be described. Liberman et al. [4], using this approach, tried to identify conditions which make speech unique. A phoneme is defined as the unit of sound, which makes it possible to distinguish a particular word from another. With the linguistic approach, it was attempted to teach machines to hear human words.

However, the main problem with this approach is the segmentation of the signal into phonetic units. Due to threshold problems, segmentation errors appear to be inevitable [5]. Further problem areas are the individuality of the speaker, time normalisation, and recording quality [5]. Several similar issues exist concerning the applicability to AT estimation. These, however, without workable solutions. For instance, impact detection can be similar to phoneme detection, but in the case of the AT detection, minimal time differences can lead to significant errors.

3.4.2 Pattern recognition approach

One of the main problems in speech recognition is the linguistic behaviour of the speaker, pronouncing words differently depending on dialect or speed, as well as the identification of separate words in a whole sentence. The pattern recognition approach considers this. It is connected to the language and requires the analysis of statistics. The basic idea is that each word is split into a set of phonemes (similar to the acoustic-phonetic approach). Such sets are then compared with a trained pattern of similar sequences of phonemes. This allows a much more precise speech recognition. The approach is mathematical and can be represented in a statistical model. Typically the “Hidden Markov” model, with which it is possible to recognise whole phrases that are not known initially. These patterns can be compared with known words or phrases, and it is possible to grade the quality of fit between the unknown and the known. This very sophisticated approach depends strongly on the trained pattern.

As the trained data sets have been greatly extended during the last few decades, this approach has given speech recognition a reliable precision. This concept has been used and accepted since the 1960s [4], [6].

3.4.3 Conclusion of advanced signal processing

Accelerometers measure the acceleration of a physical event. This physical event is directly connected to the physical property of interest. In this work, it is the position and momentum. This fact leads to the assumption that it should be possible to work with a conventional signal processing approach, as presented in this thesis. For multiple impact triangulation, it would be necessary to use approaches like pattern recognition. Nevertheless, this issue can be solved using thermography, which relies again on physical principles and is much easier to process, because in this case image-processing approaches can be used which exist already in many applications as a standard. Or already implemented vision algorithms.

3.5 Conventional signal processing

During this thesis, only traditional signal processing approaches where used. With slight modifications, the necessary signal processing approach was for all experiments the same. This makes it worth to go deeper in this thesis with respect to signal envelope, bandpass filtering and mechanical filters.

3.5.1 Mechanical filter

Mechanical filters are in this thesis used in two ways. Sensors like shock accelerometer and load cell used in in the experiments of chapter 5 have an internal mechanical filter which is related to the material properties of the sensor housing.

For load cell rings, oscillating forces over 60 kHz are damped out by the titanium or stainless steel housing. Furthermore, these ring load cells detecting forces from one direction.

Piezo crystals produce in all directions a signal if one put force on it. The piezoelectric load cell housing filters the forces in such a way that only one direction is measured. The mechanical filter is more critical for piezoelectric shock accelerometers. The shock has the intrinsic property that it produces high frequencies in the piezo crystal, which may lead to destruction. Because of these multidirectional high frequencies, it was not possible to assess the accuracy of shock sensors, without fundamental changes. Complex mechanical structures in the accelerometer itself make it possible to filter and remove noise from 5 of 6 degrees of freedom out. This makes it possible to calibrate and use these accelerometers as references when it comes to the assessment of vibrations after shock loading, which is the main topic of chapter 4.

In this thesis, chapter 4 is devoted to describing a novel way to mechanical filter noise from the original impact signal. With a spiked witness plate, it was proved the noise could be damped effectively. The basic idea behind the mechanical plate filter is to dampen all signals at the boundaries of the plate. The remaining signal is the one which comes directly from the initial impact.

How effective and direct passive mechanical filters are shown in section 5.2. This publication treated beside others the cross verification of a piezoelectric mechanically filtered load cell with a piezoelectric strain gauge. The Strain gauge itself was unfiltered, strains in all directions where recorded in high resolution. All filtering needed to be done after recording the signal. The result was that the digital signal processing approach was robust and useful. However, the overall results from the mechanical filtered load cell were superior compared to the high frequency unfiltered raw signal of the load cell.

Mechanical filtering is a significant step in the overall signal processing of ballistic events. It gives the security that the primary signal is not overloaded with mechanical noise originating from other sources than the one which is of interest.

3.5.2 Signal envelope

Internal and terminal ballistic processes are connected to large forces applied in a short timeframe. Because of the mechanical filtering described above, ballistic shocks are defined banded. These mechanical shocks lead to force and acceleration signals which oscillate.

The oscillations are wrapped to wave packages which oscillate slower. This is similar to the wave sets which one can see on the sea. These wave packages have a close connection to signal envelopes. Signal envelopes can be generated with different approaches. They are widely used in almost all fields of engineering and physics. A property of the signal envelope is that smoothed the signal out without losing the peak value. For time-sensitive events, it is furthermore essential keeping the time of the first rise repeatable.

The Hilbert-Huang Transformation (HHT) is a relatively new approach to analyse signals. Like other transformations, e.g. the windowed Fourier transform, HHT is also a time and frequency decomposition. There is no inverse function, from a mathematical point of view; it does not fulfil the requirements of an analytical tool. However, it is a robust tool for the investigation of physical processes like gravitational waves [7]. One main advantage is that it is a computationally fast transformation which can be used for investigating non-linear features. The empirical HHT is conducted within two main steps. The raw-signal is packet into an envelope which wraps the peaks of the peaks. This average envelope is then subtracted from the original signal. This subtraction marks the end of the first iteration step. With this approach, the original signal is reduced step by step until a previously set threshold is reached. The decomposition consists finally of the peak envelopes of many iteration steps. The HHT is suitable for broadband signals which does not loose spatial resolution. For momentum detection out of acceleration signals, this transformation is appropriate. However, the time resolution of the first rise when it comes to wave packages is insufficiently low. An envelope approach which represents the physical properties of the wave packages from a time perspective better is needed.

A property of the acquired ballistic force and the acceleration signal is that it can be considered as a narrowband signal. This type of envelope is produced within three steps, see Figure 3-1.

- In the first step, the absolute value of the signal is considered. This simplification makes the data array easier to handle. However, it does not reduce the meaning of the data, because just the extreme values (independent of minimal or maximal) are of interest. This manipulation does not affect the time resolution. Which is essential for the detection of the first wave package (the Arrival Time).
- In a second step runs a peak finding algorithm over the signal. Every peak of the signal is detected and gives a strength which remains persistent until the next peak arrives. This signal looks similar to steps/stairs. However, the amount of data points remains the same as in the original signal. This makes it easier to compare it with the initial signal.
- The signal from the second step looks like stairs with unequal stair length. In the final step, these stairs are smoothed out with a simple lowpass filter.

With this simple three-step RMS envelope one gets an envelope which gives a reproducible hull for the first wave package, which is necessary for the AT detection and the maximal amplitude which is required for the momentum measurement remains preserved.

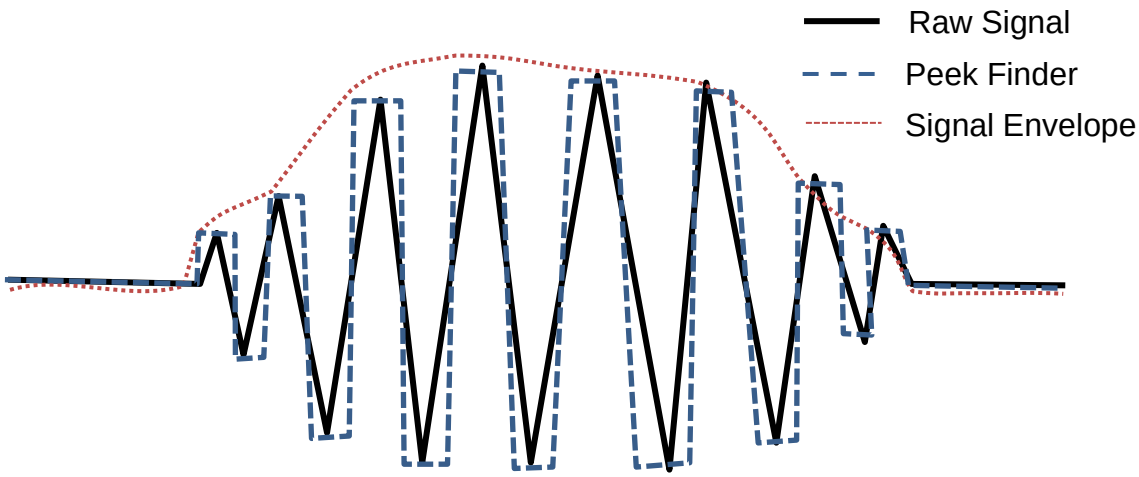

Figure 3-1: Principle of the signal envelope algorithm.

3.5.3 Bandpass filter

The use of a bandpass filter can further enhance the RMS envelope. A third-order Butterworth filter is suitable for this application. This filter makes the connection between the mechanical filter and the RMS envelope. Some unwanted high, as well as low-frequency stray signals, may be generated in the cable. These signals are eliminated using the Butterworth filter. The used filter is a digital filter, which can be easily modified or adapted. The digital filter also has the advantage that it filters the digitalised and saved signal. Thus different parameters can be tested.

3.6 Position measurement

Projectiles, which affect a solid surface, produce vibrations. During this impact, flexural waves travel circularly outwards from the point of impact. These waves are used for triangulation. The idea behind the triangulation is shown in Figure 3-2.

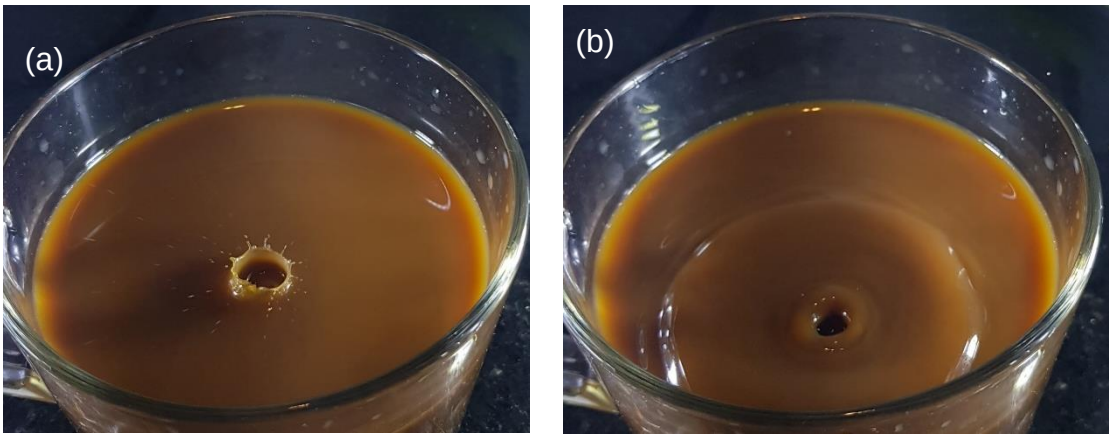

Figure 3-2: Picture (a) shows a drop falling onto a calm surface. Picture (b) also indicates a drop falling onto a smooth surface, but a few ms later in time. One can easily detect that waves are circularly emitted from the point of impact. These waves are the physical background for the detection system. The height of the wave represents the momentum, and the eccentricity relative to the circle of the coffee mug, the position.

To calculate the position, finding the correct arrival time is crucial. Sensors for positioning may rely on the principle of ultrasonic sonar and are used for applications such as autonomous driving. Other sensors like acoustic sensors serve to detect the position of failures in machines [8]. An additional application is the triangulation of mobile phone devices in an arbitrary matrix of transmission masts. There are also approaches in the defence field like simulation and training, where the position of exercising soldiers is measured in real-time. Many position systems rely on different TDOF or TDOA calculations. All these tracking approaches have demanding requirements concerning the underlying short-time physics. Due to this, sampling rates of the data acquisitions systems are more than one MHz, and the sensors have to be able to measure the physical event, preferably without latency. The accelerometer signals need to be acquired simultaneously since the correct time difference between threshold exceeding of each sensor signal is crucial. Studies concerning the application of spectral analysis for impact detection have been conducted by Doyle [9] and Park [10].

Gaul and Hurlebaus [11] conduct recent studies dealing with different concepts for the impact analysis. They assessed three different methods of Time-Frequency Analysis (TFA) in respect of their performance to detect flexural waves emitted from impacts on a steel plate. The four concepts for TFA investigated by Gaul and Hurlebaus were Short- Time Fourier Transformation (STFT), Wigner-Ville Distribution (WVD) and Discrete Wavelet Transformation (DWT). The performance of STFT and VWD are uniquely assessed in theory, whereas the DWT is assessed extensively by Gaul and Hurlebaus in both theory and practice. A significant advantage of the STFT is the direct connection to the physical world. The inverse of the STFT is easy to compute. According to Gaul and Hurlebaus [16], the major drawback of the STFT is that one needs a fixed window size, which causes problems for high resolution in the time-frequency domain. High resolution in the frequency domain is crucial if one wants to calculate the precise AT. This problem does not exist in the VWD since the system is based on a correlation function and allows an adjustable window size. However, there are also drawbacks. The interpretation of the spectrogram is difficult, i.e. very tedious computation-wise.

Focusing on the three assessed TFA, the DWT is the best way to compute the AT. DWT has a low computational effort, and the window size can be varied either in the time or frequency domain [12], which is the basis for a multiresolution analysis [13].

Gaul and Hurlebaus [11] also applied an optimisation method to find the impact location. To this end, they evaluated the expected group velocity analytically. Gaul and Hurlebaus did a great job, and some of their findings can be applied directly to other impact triangulation problems. However, it might be more suitable to choose a sensor system, which does not detect all variations of waves. Uniaxial sensors like uniaxial accelerometers are more suitable in this case. Accelerometers mounted on the surface of a plate, which predominantly recognises Rayleigh waves, are adequate. These waves propagate on the surface of the material. Uniaxial accelerometers detect also reflected waves at the boundaries of the plate. However, the strength of these reflected waves inhibits a very low amplitude in the uniaxial case, which leads to the verdict that these reflections do not need to be considered in the calculation procedure.

Furthermore, the sampling rate of 1 MHz is rather low. For high-precision measurements, a sampling rate of 2-10 MHz might be required. The estimated velocity is around 3000 m/s, which means that, if one wants to get a resolution of approximately 1 mm, the sampling rate should be at least 3 MHz.

3.7 Momentum and force measurement

There are different approaches on how to measure the momentum, each of which has its benefits. An accurate method of measuring the momentum of a ballistic impact is the ballistic pendulum. It is based on gravity, which is a well known natural constant. A ballistic pendulum contains a reference weight held in place by a pendulum arm, see Figure 3-3. By shooting a projectile in the soft reference weight, the projectile is embedded in the mass. Because of the embedding process, a perfectly inelastic collision takes place.

The oscillations of the pendulum can be measured repeatably. Major drawbacks of this system are the large measurement equipment needed for this, plus the fact that it is not possible to measure multiple impacts. However, huge advantages are the simple measurement principle and the achieved accuracy.

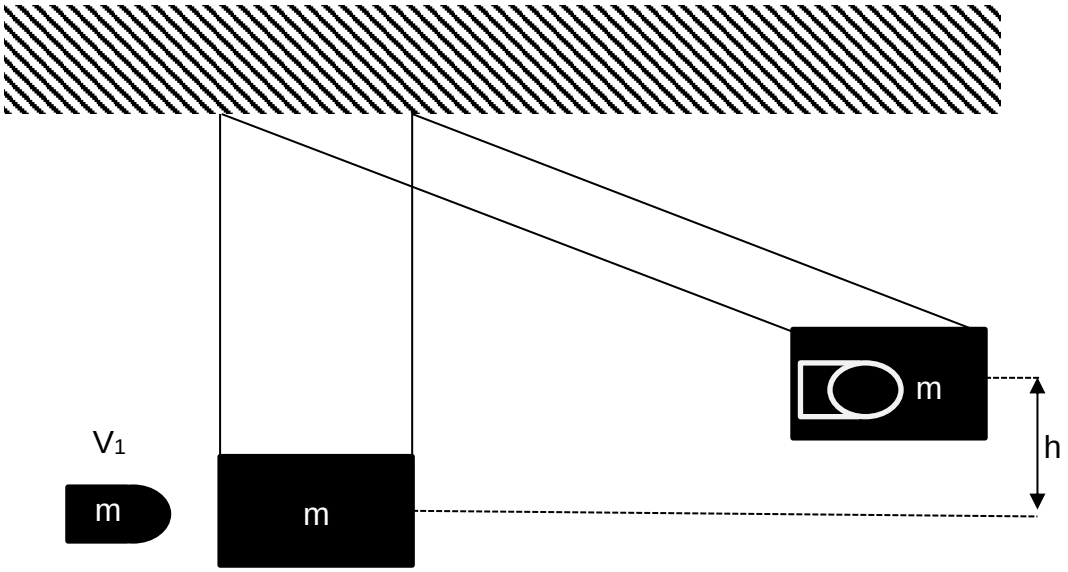

Figure 3-3: Example of a ballistic pendulum. The projectile gets embedded into a mass of a pendulum. The embedding process represents a perfectly inelastic collision. As the masses of the pendulum and the projectile are known, one can calculate the momentum with the height of the first excitation.

Another possibility to measure the momentum are strain gauges. Their advantage is that they can be placed easily on large structures. And since they acquire signals from all directions, it is possible to measure multiple Degree of Freedom (DOF) systems. The overall momentum of complex structures can be derived if one uses a matrix of all possible directional momentums. This system can measure the momentum load over time, which is crucial if one wants to measure multiple impacts.

Drawbacks of the strain gauge measurements are the filtering requirements, since unwanted multiaxial oscillations of the system - which have nothing to do with the momentum - may disturb the system.

A third possibility is to measure the momentum with accelerometers. It combines both already described approaches. With conventional uniaxial accelerometers it is not possible to measure the momentum in all directions. This measurement approach is like the measurement principle of the ballistic pendulum. By this method it is also possible to measure impacts on large plate-shaped structures.

Another similarity between the strain gauge and the accelerometer is the nature of the signal. The indirect output signal of the strain gauge is a force, the change in resistance depends on the deformation and the deformation itself depends on the applied force. The indirect output signal of the accelerometer is also a force since the mass of the system is known. With the known mass and the measured acceleration, one can compute the force by Newton's second law.

If the ballistic impact on the plate occurs in an orthogonal direction, it is advantageous to measure in the direction where the impact occurs. Here it makes sense to rely on uniaxial accelerometers. Another advantage is that the accelerometer can be used easily to measure other properties like the AT of wave packages, which enables a reliable TDOA positioning.

A reliable approach to measure the momentum is the combination of a bandpass filter and a signal envelope (Figure 3-4). The signal envelope has an integral characteristic. With this knowledge, it is possible to work with the peak of the signal to derive the momentum directly. For measuring the energy, empirical approaches are necessary and efficient since the signal depends strongly on the shape of the impact plate.

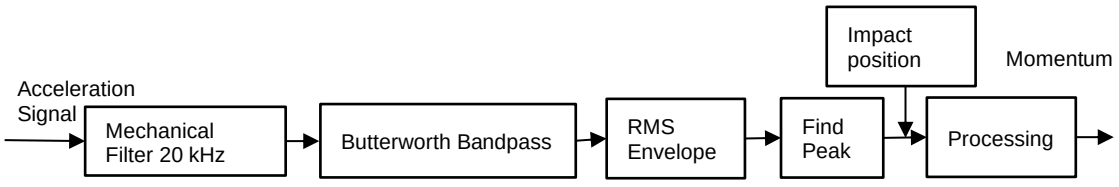

Figure 3-4: Filtering system.

3.8 Sensors used

The thermographic camera was used for a straightforward position and dispersion measurement, which did not need to acquire the signal in a range of µs. The range of seconds was sufficient. All other sensors were dynamic and relied on the same piezoelectric measurement principle, pictures of the sensor are represented in Figure 3-5. The piezoelectric sensors came mainly from manufacturer PCB, USA. The sensors used for the experiment were high-shock ICP® accelerometer [14], [15], sensors which are specifically designed for events where severe accelerations up to 50,000 G may rise and decay in 10 µs. Another sensor was a reusable piezoelectric strain sensor ICP® [16]. This sensor type is often used to support the measurements from the accelerometer. The advantage of this kind of sensor is that it may detect an event very quickly and that tiny strains may be detected. For the ballistic test, the sensor needed to be rugged and able to detect frequencies up to 100 kHz. The last sensor type used were piezoelectric force rings which are also based on a piezoelectric principle. Two different ring force sensor (also known as force washer) manufacturers were tested to underline the significance of the tests. One was Kistler Switzerland [17], and the other PCB USA [18].

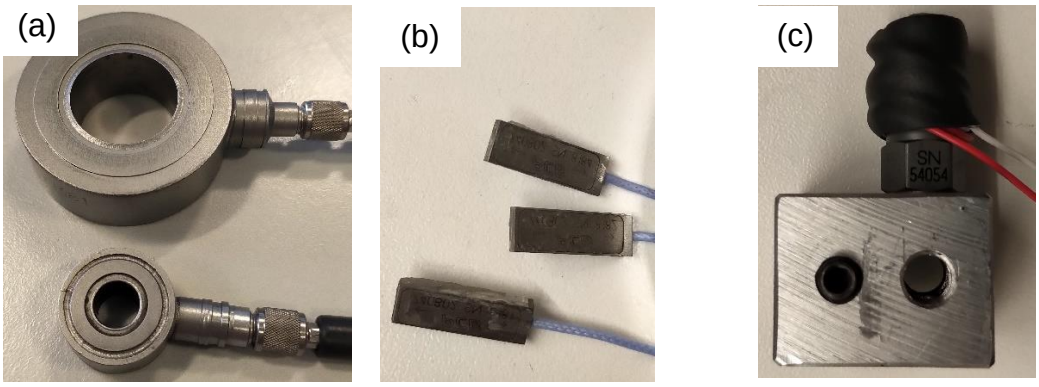

Figure 3-5: Picture of all sensors used (a) represents piezoelectric force washers, (b) represents three piezoelectric strain gauges (c) shows the filtered piezoelectric shock accelerometer.

3.8.1 Piezoelectric principle

The main characteristics of the piezoelectric sensors used are that they are active. These sensors do not need an external power source, because of a non-homogenous deformation of the piezoelectric crystal, which is often SiO_2, a charge in the lattice structure of the quartz is produced which is nearly linear to the applied force, see Figure 3-6. This charge of the signal in the range of Pico coulomb and needs to go true a signal conditioner which provides a stable sink for the source charge. The measurements performed are very demanding; other sensor approaches like MEMS sensors are less dynamic and not suitable for such a harsh environment. Most internal ballistic testing's are so demanding that they often lack a dynamic calibration test. It is possible to cross-verify between different sensors to get an estimation of the status of the sensor [19]. This is also valid for the acceleration calibration of shock sensors.

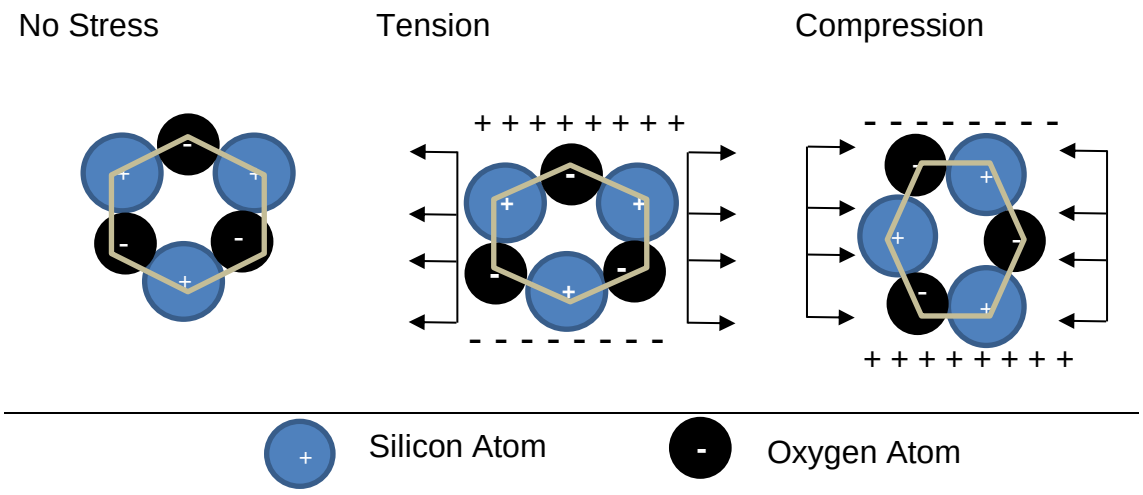

Figure 3-6: Piezoelectric effect in quartz.

3.8.2 Measurement errors

This subsection is split into two more sections, because of the complexity of the measurement system, which is the main driver for error. The overall ricochet measuring device can lead to more single errors which sum up concerning the error of the force measurement system. This was the reason due to which the impulse/momentum measurement was conducted first in the force measurement system. Internal ballistic processes are controlled and reproducible, and it is possible to do cross verification.

3.8.2.1 The error of the ricochet measurement system

To estimate the accuracy of the ricochet system, one has to define the measurement properties of interest. The fragmentation pattern is dependent on the resolution of the thermal camera and the area which is under investigation. The proposed system investigated an area of 600x400 mm, and the thermal resolution of the camera was 320x240 thermal pixel. With the setup of the measurement system, it was not possible to reach all pixels, which means that the spatial resolution of the fragmentation pattern was 2 mm. The primary source of error besides the pixel is the temperature drift, which gives blurred pictures and increases the inaccuracy because of the boundary of the fragments. The third source of error was the need for a change of the rubber layer, which was not changed after every shot. For more reliable fragmentation measurements, a replacement of the rubber layer after every shot would be required. The setup using the rubber layer is in chapter 6 described in more detail.

The momentum measurement is the second main parameter investigated. The momentum of the impact depends on the ammunition size and its design. The overall accuracy of the momentum measurement is 0.01 Ns. This was measured with different reference ammunition types. Main drivers for errors are the whole calibration process. It is very challenging to calibrate sensors for such short time events. Reference shots conducted the calibration. The strength of the momentum depends on the weight and velocity of the projectile and could be measured with an analytic scale which has a precision of +/- 0.0001 g.

Furthermore, the speed of the projectiles before impact is measured via a calibrated light gate. The accuracy of the velocity is +/- 2 m/s. These two errors might lead to an overall calibration error of $2*10^{-7}$ Ns. This is more accurate than the achieved accuracy of 0.01 Ns. This leads to the conclusion that the primary source of error is the signal processing and the short time data acquisition capabilities of the shock sensors. The quantification of a bullet itself during impact is more demanding than the inner ballistic pressure or force quantification. The primary source of error is the sensor system itself. However, 0.01 Ns is still a good result for the final aim, the ricochet measurement for RDA estimation.

The error of the velocity is driven by the distance error between the two plates, the accuracy of the impact position. Furthermore is also the time estimation of the first and the second impact of importance. The distance error between the ricochet and witness plate is +/- 3 mm. The triangulation error of the position estimation of the ricochet plate is +/- 5 mm. As already mentioned in the positioning error of the measurement error +/- 1 mm. With this approach, one is also able to calculate the time error +/- 5 mm leads to a timing error of the impact of +/- 2 µs for both plates. For a “standard” ricochet flying at 750 m/s all these errors together lead to the worst-case velocity measurement error of +/- 7.5 m/s or 1 %. This is congruent with the error measured in the tests described in chapter 6.

3.8.2.2 The error of the force measurement system

The reduced complexity of the measurement system increases the overall measurement accuracy. Errors are related to the performance of the measurement system (data acquisition, signal conditioner) and the sensor sensitivity itself.

The force measurement sensitivity of the force sensor is 27 mV/kN. The data acquisition box is capable of a resolution of 16 bit over a range of 20 V. Combining this parameter results in a measurement error of 11 Newton. Concerning the expected force of 7 kN in minimum (9 mm Luger), this factor is in the range of 2 ‰, which is an acceptable value for such dynamic measurements.

3.9 Conclusion

This chapter investigated different signal processing possibilities. It was shown that conventional signal processing approaches are sufficient for ballistic investigations. The main message of this chapter is that the measurement error in not driven by the signal processing approach, but by the design and the sensor itself

3.10 References

[1] Eric Mournier, “MEMS Markets & Applications 2011-2017,” in *Proceedings of dMEMS*, 2012.

[2] T. Heline, “Electret microphones to voice-input designs,” *Gentex Corp.*, vol. 29, no. 17, 1981.

[3] P. R. Scheeper, A. G. H. van der Donk, W. Olthuis, and P. Bergveld, “A review of silicon microphones,” *Sensors Actuators A. Phys.*, vol. 44, no. 1, pp. 1–11, 1994.

[4] A. M. Liberman, F. S. Cooper, D. P. Shankweiler, and M. Studdert-Kennedy, “Perception of the speech code,” *Psychol. Rev.*, vol. 74, no. 6, pp. 431–461, 1967.

[5] D. H. Klatt, “Speech perception: A model of acoustic-phonetic analysis and lexical access,” *Journal of Phonetics*, vol. 7. pp. 279–312, 1979.

[6] T. B. Martin, A. L. Nelson, and H. J. Zadell, “Speech Recognition by Feauture-Abstraction Techniques.,” Air Force Avionics Lab, 1964.

[7] J. B. Camp, J. K. Cannizzo, and K. Numata, “Application of the Hilbert-Huang transform to the search for gravitational waves,” *Phys. Rev. D - Part. Fields, Gravit. Cosmol.*, vol. 75, no. 6, 2007.

[8] P. Nguyen, M. Kang, J.-M. Kim, B.-H. Ahn, J.-M. Ha, and B.-K. Choi, “Robust condition monitoring of rolling element bearings using de-noising and envelope analysis with signal decomposition techniques,” *Expert Syst. Appl.*, vol. 42, no. 22, 2015.

[9] J. F. Doyle, “An experimental method for determining the location and time of initiation of an unknown dispersing pulse,” *Exp. Mech.*, vol. 27, no. 3, pp. 229–233, 1987.

[10] J.-H. Park and Y.-H. Kim, “Impact source localization on an elastic plate in a noisy environment,” *Meas. Sci. Technol.*, vol. 17, no. 10, pp. 2757–2766, 2006.

[11] L. Gaul and S. Hurlebaus, “Identification of the impact location on a plate using wavelets,” *Mech. Syst. Signal Process.*, vol. 12, pp. 783–795, 1998.

[12] F. Jurado and J. R. Saenz, “Comparison between discrete STFT and wavelets for the analysis of power quality events,” *Electr. power Syst. Res.*, vol. 62, no. 3, pp. 183–190, 2002.

[13] A. Perelli, L. De Marchi, A. Marzani, and N. Speciale, “Frequency warped cross-wavelet multiresolution analysis of guided waves for impact localization,” *Signal Processing*, vol. 96, pp. 51–62, 2014.

[14] PCB, “High Shock ICP ® Accelerometer.” 2016.

[15] A. Agnello, J. Dosch, R. Metz, R. Sill, and P. Walter, “Acceleration Sensing Technologies for Severe Mechanical Shock,” *Sound Vib.*, vol. 48, no. 2, pp. 8-19, 2014.

[16] PCB, “Reuseable Piezoelectric ICP® Strain Sensor.” 2016.

[17] Kistler Group, “Data sheet, Type 9001A, 9011A, 9021A, 9031A, 9041A, 9051A, 9061A, 9071A,” 2009.

[18] PCB, “Piezoelectric Force Rings,” 2016.

[19] L. Elkarous, M. Pirlot, J.-C. Golinval, and M. Maldague, “Investigation on gas pressure measurement inside small caliber weapons with piezoelectric transducers,” *Meas. Sci. Conf. 2012*, pp. 1–8, 2012.

4 Damping of post-impact vibrations

4.1 Introduction to chapter

This chapter covers the first publication of the thesis. Initial tests showed that the signal quality of the impact triangulation on a steel plate was not sufficient and had to be augmented. The focus of this chapter is the reduction of unwanted flexural waves which affect the impact position calculation. The proposed solution is very efficient and suitable for enhancing the triangulation signal. However, many other applications are possible.

4.2 Author's contribution statement

Michael Muster wrote this publication, the main conceptual ideas and proof outline. Michael Muster worked out almost all of the technical details and completed the design of the two test setups. Michael Muster did the research concerning strong damping systems. Michael Muster worked out the plate design with the help of Markus Grünig.

Michael Muster wrote the paper with input from all authors.

Michael Muster, first author
Centre for Defence Engineering, Cranfield University, Defence Academy of the United Kingdom
Shrivenham, SN6 8LA, UK
michael.muster@cranfield.ac.uk

Amer Hameed, second author
Centre for Defence Engineering, Cranfield University, Defence Academy of the United Kingdom
Shrivenham, SN6 8LA, UK
a.hameed@cranfield.ac.uk

David Wood, third author
Centre for Defence Engineering, Cranfield University, Defence Academy of the United Kingdom
Shrivenham, SN6 8LA, UK
d.wood@cranfield.ac.uk

Gareth Appleby-Thomas, fourth author
Centre for Defence Engineering, Cranfield University, Defence Academy of the United Kingdom
Shrivenham, SN6 8LA, UK
g.thomas@cranfield.ac.uk

Kilian Wasmer, fifth author
Laboratory for Advanced Materials Processing, EMPA, Swiss Federal Laboratories for Materials Science and Technology
3602 Thun, Switzerland, CH
kilian.wasmer@empa.ch

Keywords: flexural vibrations, damping, metallic plate, boundary reflection

Abstract

Impacts of solid bodies on rigid plates produce loud noise and strong vibrations. During this impact, flexural waves travel circularly outwards from the point of impact. These waves are used to determine the properties of the impacting body. For reliable location and momentum measurements, the set of flexural waves must pass acceleration sensors once without being disturbed by reflections.

Different plate designs are tested to evaluate the shape, which offers the best damping properties against a single strong impact.

The investigations showed that the damping properties of the plates are significantly better with a star-shaped design, which is equipped with a damping layer. The novelty presented here is that the damping properties are significantly increased using a star-shaped plate with especially power-law formed and damped edges.

The work offers a solution to get significantly better damping properties and a better signal for impact investigations. The results demonstrate that it is a promising approach for an impact detection system, which could be equally applicable to acoustic damping applications.

4.3 Introduction to publication

This study investigates the effect of different plate shapes on their damping behaviour after a single excitation burst leading from a small arms projectile. The focus is on a short-time scale from microseconds up to milliseconds.

Small arms projectiles are structures that weigh from 2 to 10 grams, which travel at supersonic speed and produce strong acceleration and acoustic signals when they impact. Due to their high speed and rotation rates, they are generally challenging to characterise during flight and impact. The impact characterisation is used for applications like the estimation of range-danger areas after deflection of the projectile on oblique plates.

For impact characterisations, one needs to know the position of impact and the momentum transmitted into the plate. With this information, one can estimate the residual energy and deflection angle of the projectile after impact. The main challenge of the impact detection is connected to huge decelerations and large deformations in a short time regime. Such projectiles are often too small to be equipped with sensors. Therefore, sensors mounted on witness plates are widely used for impact detection devices.

So-called Impact Soft-Recovery Experiments [1] are made, for example, with impact detection devices. In this case, the target under investigation is a brittle plate made of ceramic, monitored by an interferometer. The projectile impact generates strong vibrations, the characterisation of which helps to calculate the nature of the impact. Espinosa et al. [2] showed that it is possible to get a cleaner raw signal from the target plate by using a star-shaped flyer geometry. Their tests revealed that the effect of the outer layer of the plate on the impact zone itself could be minimised significantly. Besides interferometers, accelerometers are frequently used to measure properties of the impact like the impact position or the transferred momentum [3]–[5].

One of the significant sources for measurement inaccuracies is random and reflected vibrations [6]. Hammetter et al. used an array of accelerometers fixed on the plate to determine the momentum transferred. They showed that geometrical properties of the detecting plate itself might lead to inaccurate measurements.

Another source of measurement inaccuracy is electronic filtering of the acceleration data. Best practice for severe-shock investigations is to use mechanically insulated accelerometers [7]. Severe mechanical shocks such as caused by bullet impact, typically lead to six degrees of freedom accelerations represented in broadband frequencies. This makes it difficult to determine the overall momentum [6], or the position. Mechanical insulators combined with electrical filters were found to be an appropriate way to overcome this rapid excitation problem.

The impacting body excites the witness plate within a very short time in a non-linear and random vibration regime, where scattering and reflections of vibrations at boundaries will occur [8], [9]. Right after the impact is the moment when the point of interest occurs. This moment is called the Arrival Time (AT). The AT is defined as the time when the sensor detects the first set of waves, which originate from the impact position. Consequently, knowing the exact AT is necessary to recalculate the exact impact position [10] with the Time Difference of Arrival (TDOA) algorithms.

TDOA algorithms are often used nowadays and optimised for passive tracking of wireless communication systems [11]. The underlying computations for wireless-devices tracking and impact location, are the same. The main issue for the triangulation of impact remains accurate AT detection.

For flexural group waves travelling in steel at a speed of more than 2500 m/s, already minor AT detection errors lead to large positioning errors. The speed of sound in the target material and the AT difference must be known for positioning. Furthermore, by knowing the positions of the sensors, one can easily calculate the position of the impact/of the origin of the waves by numerical methods [12]. Mingzhouet al. showed the possibility of precisely detecting the AT of flexural waves using accelerometers after the impact of a test weight dropped on a large steel plate, also in noisy environments like power plants [13]. They used a sophisticated decomposition algorithm combined with the Hilbert Huang Transformation.

They found that the proposed algorithm was capable of detecting the AT with a precision of several milliseconds. The main reason for the inaccuracies was still the noise in the signal. During a ballistic impact on a plate, stochastic waves appear inevitably, which affects the precision of the AT calculation. In an idealised case, flexural and compression waves emitted from the origin of impact would not be reflected. Two approaches can realise this: Using a plate significantly larger in comparison with the investigated area (this approach is presented in [9]) or using a damping plate.

A promising approach is a plate of special shape which decreases in thickness at the edge (called a wedge shape) in a power-law profile [14]. Internal refractions eliminate different waveforms. However, the power-law shape is difficult to manufacture, which is why it is not used in practical vibration dampers [15]. Possible ways of manufacturing this wedge shape are 3D milling or casting [16], both of which are expensive.

For hardened-steel and supersonic impacts, such delicate and large structures are unsuitable to be made by industrial methods. There are some highly effective damping alternatives which are easier to manufacture, i.e. the application of a thin absorbing layer to the plate surface. Another possibility is an acoustic black hole, reduced in its space requirements as proposed by Lee [17]. This showed that a damping layer is covering and wrapping the acoustic black hole results in a reduced vibration.

However, for impact analysis purposes, other shapes are more desirable. From a manufacturing point of view, if one wants to process a hardened wear plate, just 2D shapes should be used. Such plate designs can be produced by water-jet or plasma cutting. Possible shapes that can be produced easily are polygons or any round, but two-dimensional. Star-shaped (polygonal) flyer plates are also able to trap compression waves, as used for normal impact soft-recovery experiments [2]. With the star-shaped plate, much lower level reflection is observed during impact. This enhances the quality of the raw data in ballistic experiments. The edge morphology can serve as a trap for waves and be investigated computationally in [18]. Apart from the computational investigations, the real noise-damping properties of the plates need to be quantified.

The plate experiences random vibrations after significant impulse is applied. The plate's response cannot be assessed using purely analytical models. The random-decrement method is a possible way to quantify the damping factor of a system. This approach is suitable for systems which are randomly excited, for example fluid flow against rigid structures like ships or bridges [19]. Using the logarithmic decrement to determine the damping ratio is widely used for such damped systems [20].

This random decrement method is unsuitable for the present application because the plate is just excited once with a strong burst, then recovers fully as the vibration decays down to the not-excited state. The random decrement method would be more applicable if the system were excited by many fragments impacting simultaneously. In the case of a strong excitation burst, the plate vibrates stochastically. According to the experimental results of Humbertet al. [21], all frequencies are abundant during the first 70 ms after excitation with one strong mechanical burst. All frequency bands of the broadband spectra of the free vibrational decay have different decay rates. It is not possible to calculate just one valid damping ratio [22], especially if one wants to calculate the AT, which is the case in this investigation. In this case, one can use band-pass filters to determine each specific damping ratio.

The information about the properties of the impacting mass and the AT is retained in flexural waves only for the first few post-impact milliseconds. The first 100 ms must not be disturbed by reflections, to get a meaningful result. It is possible to sort out specific reflections using wave separation [24]. This approach, however, works for ultrasonic signals because small changes in frequency may be detected with such systems. Severe shock signals need to be detected with mechanically prefiltered accelerometers. The recorded acceleration broadband signal decays exponentially after a single excitation event, which is comparable to the decay of sound in room acoustics.

In-room acoustics, the ‘‘reverberation time” is a common way of describing a signal decay pattern. The reverberation time is defined as an exponential decay fit, which has the advantage that there is just one main decay rate, which includes all frequencies. This reverberation time was introduced by Schroeder [24] in 1965. He used filtered pistol shots to produce a single excitation event comparable to the application described in this paper. Since the damping is directly related to the reverberation time [25], this is a significant quantity for the system performance in the present case.

The reverberation time is mostly measured to determine room acoustics [26], but can also be measured for any solid plates, for instance, in musical equipment [27]. This paper describes different plate shapes and their capabilities to attenuate the noise, relative to a reference plate. The increased damping properties enhance the detection of the AT. The vibrations are detected with accelerometers capable of measuring uniaxial accelerations. They are normally positioned on the plate. Only flexural waves will be measured using this accelerometer type. Because of the similarities to the acoustical reverberation of a sound burst (or filtered pistol shot), the reverberation time is chosen as quantification method. In an initial study, a drop test is performed in a small-scale experiment to determine the most efficient plate shape. This shape is produced in a larger scale model and used for ballistic impact tests.

4.4 Experimental procedures and materials tested

4.4.1 Test procedures

Two different test scenarios were chosen to estimate the scalability of the system. The goal of the two scenarios is to evaluate and assess the damping properties of plate shapes after impact. The most promising design after the first test scenario is verified on a larger scale. All shapes were produced using the water- jet cutting technique, which results in surface roughness of Ra 25 µm. This is comparable to standard sandblasting. The overall tolerances are 0.1 mm, independent of the plate thickness. Concave edges are produced with radii of 0.75 mm, convex edges with minimum radii of 0.08 mm. In the case of the shapes subject to the power law, the exponent was approx. 2.8 for both test scenarios. The surface of the plate has a Ra of 8 µm, which is relatively smooth. The surface of the plate has no disturbances except for the screwed-in accelerometers. The data acquisition system for the accelerometers was the NI USB-6366 (National Instruments, USA) in both scenarios, with simultaneous sampling, acquiring and recording data every 0.5 µs. Simultaneous sampling is necessary for such tests so that the exact time shift between the excitation events is measured.

The acceleration sensors used for both scenarios are shock sensors 350B01 (PCB, USA), mechanically isolated and electrically filtered. The signal conditioner was the 483C40 (PCB, USA).

The data acquisition time was set to 150 ms, i.e. long enough to investigate the signal decay. Each test was repeated three times. The maximum signal amplitude acquired was normalised to ± 1. With this approach, one can compare low-momentum impacts with high-momentum impacts. The time from primary wave detection until 1 % of the max amplitude is reached, was used to calculate the reverberation time of the different plates. This calculation was necessary to quantify and compare the results.

4.4.2 First test scenario

The first test scenario was a small-scale setup; plates of four different shapes were used to acquire information about their damping behaviour. All plates for the first set of experiments consisted of 5 mm thick S275J2 steel. As a reference, a simple rectangular plate was analysed. This had four additional small rectangles attached for fixation purposes, as shown in Figure 4-2. Most ballistic standard tests rely on square or rectangular plate shapes. Square plates are used in the interest of simplicity and cost savings. A second reference plate of oval shape was used to examine whether this would enhance the damping properties. The third plate was made with projections featuring a 60° angle following the findings of [2], [18], called the “star-shaped with 60° edge” plate. The height of the triangle is 35 mm. It is assumed that, with this shape, the damping rate increases significantly. The fourth shape is the combination of the power-law profile and the star-shape called “star-shape with a power-law edge”, the edges are shown in Figure 4-2c. The number of spikes of the fourth shape is the same as in the case of the star-shaped plate. The width between the corners remained the same. However, the length of the edge increased to 98 mm. As suggested in [16], the surface was treated with an absorbing surface, a magnetic polymer compound. This layer can be removed if required. The star-shaped with 60° edge plate and the star-shaped plate with power-law edges were equipped with three thread bores each to accommodate three sensors.

One of these bores is closer to the centre, while the second is near the concave edge of the spike and the third in the centre of the convex edge as shown in Figure 4-3. In this way, reflections and backscatter can be detected by monitoring and comparing the sensor data. However, sensor position and the speed of sound in a given material are parameters which can be controlled very accurately.

The plates were impacted by a falling steel roller bearing ball, its layout shown in Figure 4-3. The ball's mass was 16.84 g, representing a widely used 16 mm ball bearing. The reason for using such an object was that it consists of 100cr6 hardened steel. These drop weights can sustain several drops without any deformation. The release height was 3.8 m, the release mechanism an electromagnet switched by a transistor. The standard deviation of the overall drop accuracy was 0.1 mm. This drop height delivered kinetic energy of 0.62 Joule.

The damping layer was applied only to the last section of the power-law spikes. The size of the damping layer material (10×20×1 mm) was the same in all analysed cases as shown in Figure 4-3. The damping layer was placed on the oval plate, the star-shaped 60° edge plate and the star-shaped plate with power-law edges.

For the plates with geometries such as the ones in Figure 4-2, it was possible to add an equally distributed magnetic damping layer on the spikes or attach an equally distributed magnetic damping layer to the oval plate. This attachment is not possible in the case of the rectangular plate. The reason is that the rectangular geometry has fewer edges compared to the oval plates, and they are not equidistant.

4.4.3 Second test scenario

During the initiation phase of the second test scenario, aluminium was also tested to serve as damping plate. The applied material was AlZnMgCu1,5 which is one of the toughest aluminium alloys, often used for high-performance constructions. The plate in question was 24 mm thick to prevent penetration. Tests showed that aluminium is incapable to withstand the wear mechanism of an impacting projectile. Figure 4-1 shows impressively that, compared with other ammunition types, already a low-energy impact of 9 mm ammunition, results in a massive deformation and destruction of the aluminium surface.

Figure 4-1: Impact on aluminium of a 9 mm projectile. It is easy to see that the material is not hard to enough to resist multiple loading cycles.

Due to the low wear resistance of aluminium against impact, the second experiment was finally made using a 12 mm thick Hardox 500 tempered steel plate. This steel exhibits a yield strength of 1300 MPa [28] as a target, against an impacting supersonic projectile.

Two different plates were tested in this scenario: A rectangular reference plate (Figure 4-2a) and a star-shaped plate with a power-law edge (Figure 4-2d).

Both plates had a thickness of 12 mm, the reference plate was 700 mm wide and 800 mm long, while the star-shaped plate with a power-law edge (Figure 4-2d) had a diameter of approx. 800 mm. The reference plate was fixed in a rigid frame at the four corners as shown in Figure 4-4. The power-law edged plate was mounted between a frame consisting of two steel rings and then fixed into the rigid frame shown in Figure 4-4a. A rubber inlay (called rubber damper) was mounted between the spikes and served for both damping and fixation purposes.

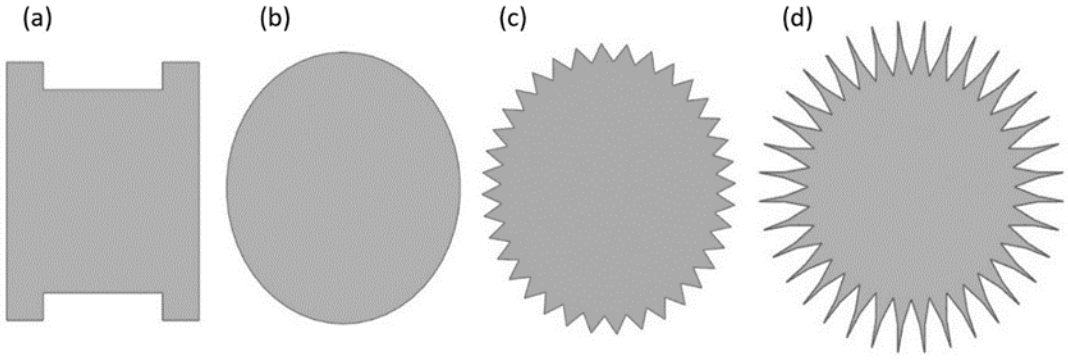

Figure 4-2: Different plate shapes: (a) reference, (b) oval (c) star shape with 60° edge (d) star shape with a power-law edge. The reference consists of five rectangles, with the large one representing the central impact zone. The four small rectangles are fixation points. The oval plate is a second reference which has, like (c) and (d), an oval central impact zone, but no spikes.

The plates were tested with a 9 mm 7.5 g Full Metal Jacket (FMJ) projectile with a velocity of 380 m/s. These projectiles were chosen because of the low occurrence of backscattering. Another reason is that they are NATO-compliant and widely available for such tests.

The velocity was measured 15 m before impact, using a BMC 31 (Kurzzeit, Germany) ballistic data processing system and an LS 260 (Kurzzeit, Germany) light gate for velocity measuring. The velocity drop within the light gate is considered, using the known drag coefficient of the specific FMJ projectile type. Knowing the velocity drop between the measurement system and impact is necessary to determine the reference impact velocity. In this case, all four sensors are equidistant from the centre, as shown in Figure 4-4b. This is easier for triangulation, which will be applied in future.

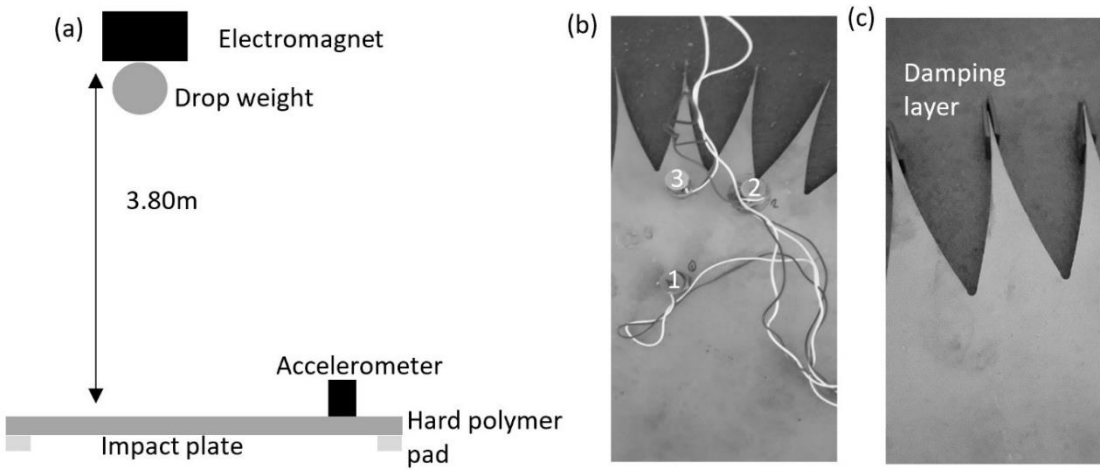

Figure 4-3: First test scenario: (a) schematic test layout, (b) accelerometer with the sensor numbers, sensor 1 is most proximal to the centre, the other two are at the same distance from the centre. Sensor 2 is exactly in front of the concave edge to see if this edge influences the signal. Sensor 3 is in line to the spike of the plate. (c) damping layer is a magnetic polymer compound which "sticks" to the contour of the plate.

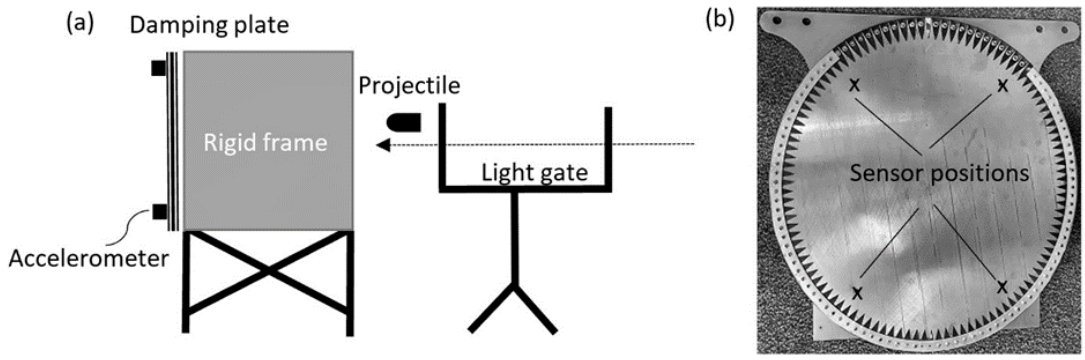

Figure 4-4: Second test scenario: (a) schematic test layout with the heavy (800 kg) metal frame and the plate attached to the back of the frame. (b) star-shaped plate with power-law edges with rubber damper. The plate is placed in an assembly of rubber pieces and a fixation plate suitable for mounting in the heavy metal frame.

4.5 Results and discussion

4.5.1 General observations

In the case of the plate with power-law edge and rubber damper, the highest excitation level occurs 10–20 µs after impact. A similar decay pattern was observed in both experimental scenarios. This, in spite of the fact that the impact energy in the second experiment was approx. 900 times higher and the plate was 30 times heavier than in the first test scenario. The results of the experiments conducted for the first and second test scenarios differ greatly in their repeatability of the impact position. In the case of the first test scenario, the radial standard deviation was less than 1 mm. The second test scenario, performed with 9 mm projectiles, showed a radial standard deviation of impacts of 40 mm. The reason for this impact distribution is the performance of the projectile acceleration system.

Interestingly, the distribution of impact positions does not affect the standard deviation between the measurements of the reverberation time shown in Table 4-1, Table 4-2. The reason for this stable reverberation time might be that, in all cases, there are some flexural waves reflected by the boundaries which keep the plate in oscillation during a few milliseconds.
One of the most demanding tasks of the damped plate is to reduce the vibrations occurring after an impact event. By dumping the plate, one ensures that the detected vibrations originate directly from the impact itself and not from the boundary reflections.

Figure 4-7 shows the acceleration signal acquired for the reference plate (shape like Figure 4-2a) and the star-shaped plate with power-law edges (shape like Figure 4-5f). In this figure, the reference plate shows a package of small flexural waves which are detected by the accelerometer 30 µs before the main wave packages arrive. These packages disturb the positioning and the momentum measurement process since it is not possible to distinguish between the small reflected flexural waves and the wave package, which is emitted directly from the impact. This is especially true if the two wave packages are overlapping more than the ones represented in Figure 4-7a.

With the proposed design, a very pure impact signal can be produced, as seen in Figure 4-7b. In this signal, no disturbances are visible before the main wave package arrives. This enhances the accuracy of the impact measurement significantly.

The magnitude of the peaks is rising steadily, and no significant disturbance in the signal can be detected before the first small excitation occurs. In the case of the star-shaped plate with power-law edges with rubber damper, the acquired signal is significantly different. The package of small waves does not occur. In both cases, the magnitude of the acceleration peak is about 20,000 m/s^2.

The best plate shape for single damping impacts is the star-shaped plate with the power-law edges with the damping layer. This shape is a combination of the shape of acoustic black holes and the star-shaped flyer plate. The damping effect of general acoustic black holes, as in the case of the power-law shapes, is strongly reduced since acoustic black holes react sensitively to truncation imperfections, material failures, surface roughness and reduced length of the last part of the spike [16]. However, with the use of rubber dampers, the damping effect is still significantly better than compared with the star-shape 60° edge with the damping layer. This can only be explained by the fact that the acoustic black hole is additional help for the star-shape geometry.

In all measurements, there is a fast-oscillating signal body followed by sharp peaks. These peaks are occurring stochastically because the plate is excited in a turbulent regime. This makes the quantification of the damping system challenging, since the peaks of the signal decay faster than the noise.

The reverberation time was chosen as the most stable value to quantify the system. It does not depend on a specific frequency, which is vital for such turbulent systems. The results reported here are promising, and a method can be developed to analyse more sophisticated impact detection systems.

4.5.2 First test scenario

The data presented in Figure 4-5 are the raw data representing typical plate vibrational signals for all plates tested in the first test scenario. One can see that the plate shape influences the signal decay pattern.

The damped and undamped power-law edged plate exhibits a steady signal decay, whereas the oval plate shows a more oscillating behaviour after the initial excitation. It is also recognised that the peak amplitude occurs shortly after impact in the case of the power-law shaped structures. In the case of other structural shapes, especially the star-shaped plate with 60° edge, however, slow rising amplitudes of the acceleration signal may occur because of internal compressive waves reflecting at the boundaries.

Compression waves travel through the plate at almost twice the velocity of flexural waves. The accelerometers detect in one direction only and therefore do not detect these initial in-plane compressive waves. At the boundary, the compressive waves are reflected and partly converted to flexural waves. These reflected flexural waves are unwanted for the triangulation process since they conflict with the arrival time of the unreflected flexural wave caused directly by the impact. Such behaviour can be seen in Figure 4-7a.

The damping layer has a significant influence, reducing or eliminating the low magnitude vibrations after 20 ms, evidence of which is observed in Figure 4-5g. This is in keeping with the experimental investigations of Kyrlov and Winward [15]. The small damping layer can absorb the energy of small magnitude vibrations. However, this effect is not recognisable in the oval damped case.

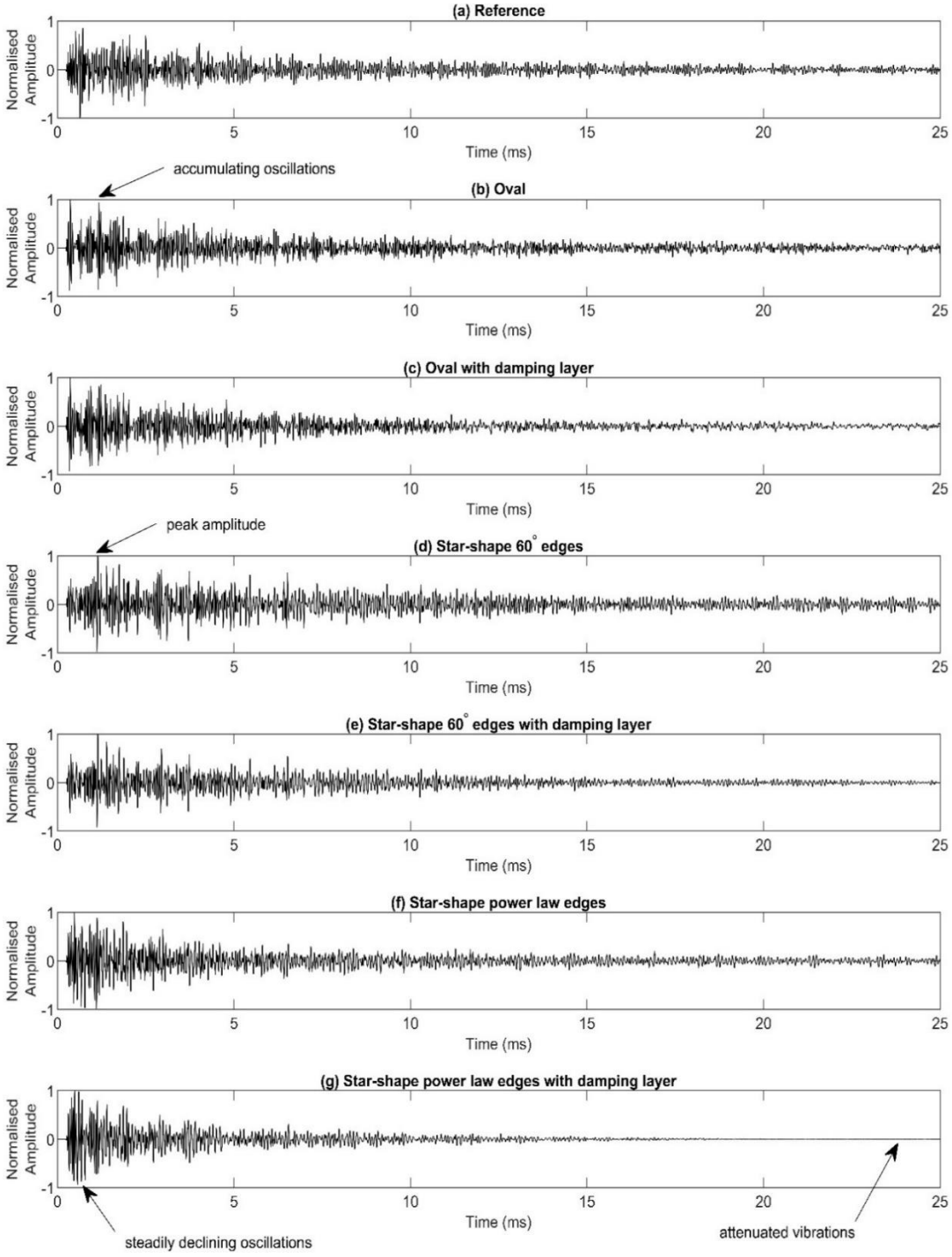

Figure 4-5: Typical vibration signals of the first test.

4.5.3 Second test scenario

Figure 4-6 presents the typical data of the vibrational signal for the plates tested in the second test scenario. The decay effect of damping is easily recognisable in the case of high-velocity impacts, as shown in Figure 4-6b (star-shaped plate with power-law edges with rubber damper). For the reference plate, the highest excitation level is delayed to 1 ms after the first oscillation is detected. The oscillations are still recognisable after 25 ms. Comparing the reference plate with the star-shaped plate with power-law edges and rubber damper, one can see a significant reverberation time reduction from over 200 ms to under 10 ms Figure 4-7.

However, the primary aim is to improve the information/loss ratio so that the signal contains a more substantial portion of impact information compared with the overall information. Since the signal is strongly reduced after the first few reflections, this aim is met by using the plate with a power-law shaped edge.

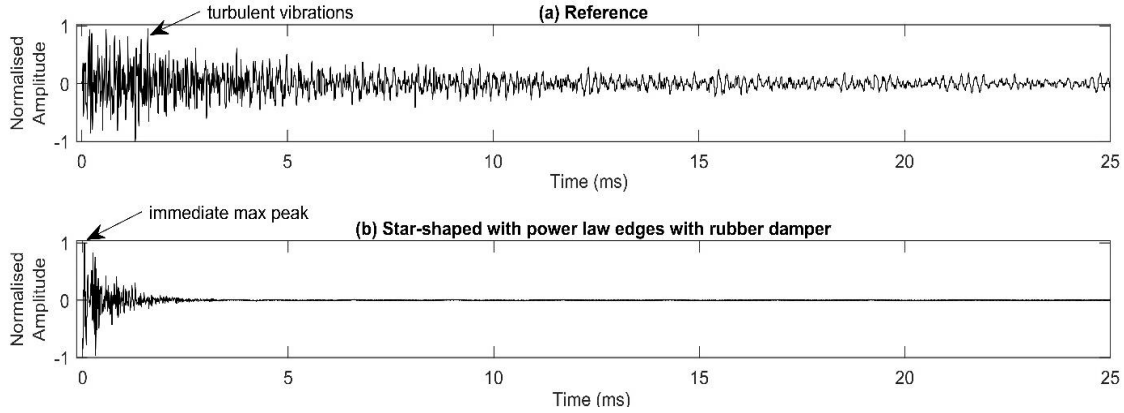

Figure 4-6: Typical vibration signals of the second test (impact of 9 mm projectile). (a) the reference (rectangular) plate which shows still some oscillations after 25 ms. (b) shows a significant signal decay after the initial excitation, after 4 ms one cannot see any remaining oscillations rising beyond the threshold.

Table 4-1: Averages and standard deviations of 9 measurements in the first test scenario.

Shape	average reverberation time (ms)	STD (ms)
Reference	135	7
Oval	158	1.2
Oval with a damping layer	134	2.4
Star shape	174	0.8
Star shape with a damping layer	63	0.6
star-shaped plate with power-law edges	147	1.1
star-shaped plate with power-law edges with a damping layer	37	0.1

Table 4-2: Averages and standard deviations of 9 measurements in the second test scenario.

Shape	average reverberation time (ms)	STD (ms)
Reference	214	2.9
star-shaped plate with power-law edges with a rubber damper	9	0.9

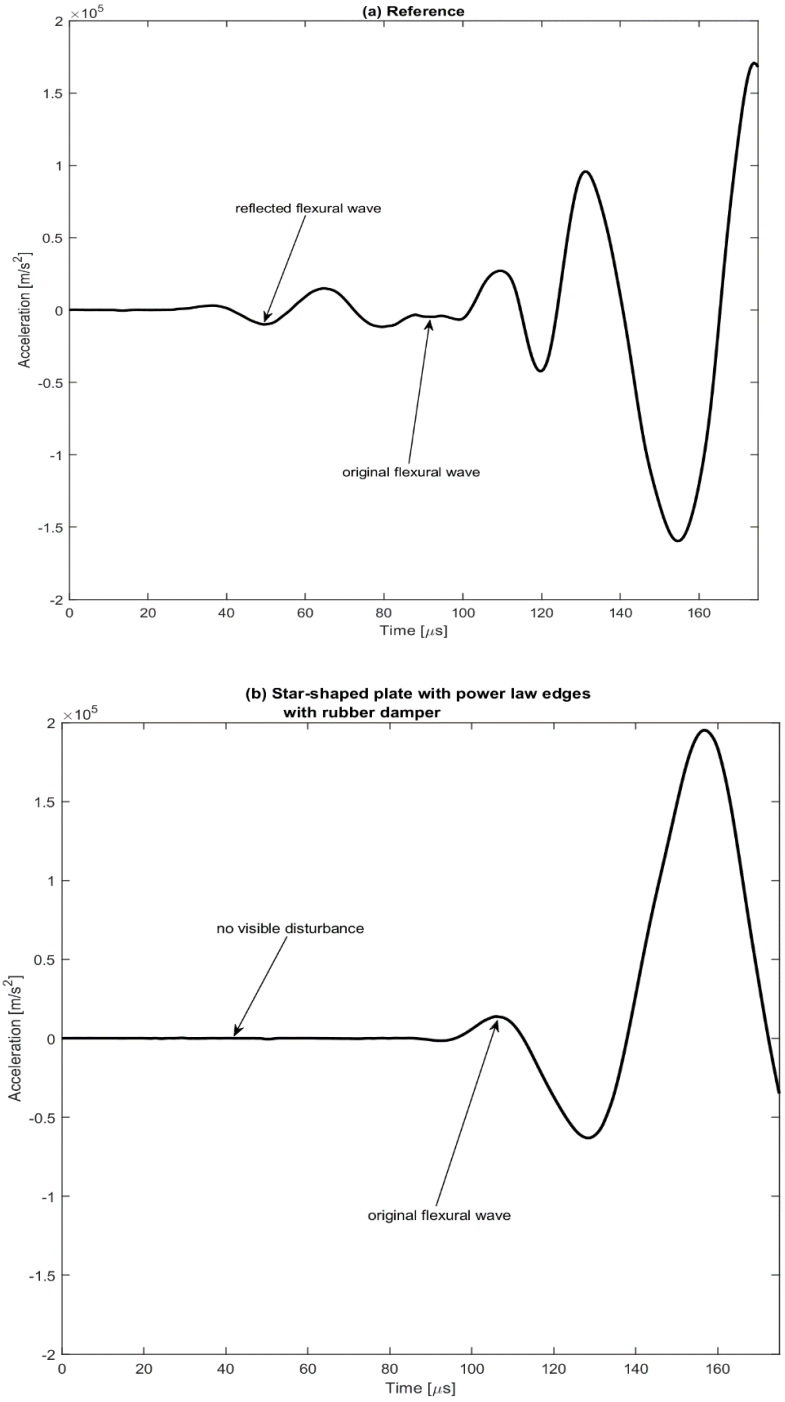

Figure 4-7: Acceleration signal acquired on (a) reference plate (b) star-shaped plate with power-law edges with rubber damper. This picture shows the benefit of the power-law edge design, the steady increase without disturbances of the wave amplitude after impact. Disturbances that can be recognised in the case of the reference plate lead to an inaccurate AT detection.

4.6 Conclusions

The results show that the plate shape has a significant influence on both vibration pattern and signal decay. The reverberation time is affected by vibration damping layers in combination with toothed edges. The effect of the damped 60° spike is less significant than the effect of the damped power-law shaped spike. Compared with the reference plates, it is possible to reduce the reverberation time by a factor of roughly 24, which is a huge advantage if one uses the witness plate as a measurement system.

Even though the kinetic energy from the impulse tests with a drop weight falling under gravity and a projectile flying at supersonic speed differ strongly, the oscillations resulting from vibration-time properties are comparable. The star-shaped plate, with power-law edges, can be used to design new devices which are suitable for ballistic impact investigations. For example, a ricochet measurement device could be built up. Furthermore, such measurement plates are also suitable for the location of multiple impacts in the same period.

It is known from the acoustic black-hole effect and from star-shaped flyer plates that they influence the wave propagation. This is particularly true with a combination of the two shapes and intense excitation bursts like ballistic impacts.

Another fact is that the sound appears to be less intensive since the acoustic reverberation time is shorter so that it is also possible to use this system for future sound and noise reduction applications. Directly applied examples are silent bed plates for punch presses, surface metal treatments in musical situations, quieter reciprocating engines and cyclical systems.

4.7 Publication references

[1] H. D. Espinosa and S. Nemat-Nasser, “Low-velocity impact testing,” *ASM Handb.*, vol. 8, pp. 539–559, 2000.

[2] H. D. Espinosa, G. Raiser, R. J. Clifton, and M. Ortiz, “Performance of the star-shaped flyer in the study of brittle materials: Three dimensional computer simulations and experimental observations,” *J. Appl. Phys.*, vol. 72, no. 8, pp. 3451–3457, 1992.

[3] R. Morsy, H. Marzouk, M. Haddara, and X. Gu, “Multi-channel random decrement smart sensing system for concrete bridge girders damage location identification,” *Eng. Struct.*, vol. 143, pp. 469–476, 2017.

[4] U. Dahlen, N. Ryden, and A. Jakobsson, “Damage identification in concrete using impact non-linear reverberation spectroscopy,” *NDT E Int.*, vol. 75, pp. 15–25, 2015.

[5] F. Allaeys, G. Luyckx, W. Van Paepegem, and J. Degrieck, “Characterization of real and substitute birds through experimental and numerical analysis of momentum, average impact force and residual energy in bird strike on three rigid targets: A flat plate, a wedge and a splitter,” *Int. J. Impact Eng.*, vol. 99, pp. 1–13, 2017.

[6] C. I. Hammetter, R. L. Jones, H. L. Stauffacher, and T. F. Schoenherr, “Measurement and modeling of supersonic hailstone impacts,” *Int. J. Impact Eng.*, vol. 99, pp. 48–57, 2017.

[7] A. Agnello, J. Dosch, R. Metz, R. Sill, and P. Walter, “Acceleration Sensing Technologies for Severe Mechanical Shock,” *Sound Vib.*, vol. 48, no. 2, pp. 8-19, 2014.

[8] T. H. and O. C. and G. D. and C. J. and S. R. and C. Touzé, “Wave turbulence in vibrating plates: The effect of damping,” *EPL (Europhysics Lett.*, vol. 102, no. 3, 2013.

[9] X. Xu, M. Zhao, J. Lin, and Y. Lei, “Envelope harmonic-to-noise ratio for

periodic impulses detection and its application to bearing diagnosis," *Meas. J. Int. Meas. Confed.*, vol. 91, pp. 385–397, 2016.

[10] A. Perelli, L. De Marchi, A. Marzani, and N. Speciale, "Frequency warped cross-wavelet multiresolution analysis of guided waves for impact localization," *Signal Processing*, vol. 96, pp. 51–62, 2014.

[11] D. Mušicki, R. Kaune, and W. Koch, "Mobile emitter geolocation and tracking using TDOA and FDOA measurements," *IEEE Trans. Signal Process.*, vol. 58, no. 3, pp. 1863–1874, 2010.

[12] F. Gustafsson and F. Gunnarsson, "Positioning using time-difference of arrival measurements," in *IEEE International Conference on Acoustics, Speech, and Signal Processing*, vol. 6, pp. VI–553, 2003.

[13] M. Liu, J. Yang, Y. Cao, W. Fu, and Y. Cao, "A new method for arrival time determination of impact signal based on HHT and AIC," *Mech. Syst. Signal Process.*, vol. 86, October, pp. 177–187, 2016.

[14] V. V. Krylov and F. J. B. S. Tilman, "Acoustic 'black holes' for flexural waves as effective vibration dampers," *J. Sound Vib.*, vol. 274, no. 3–5, pp. 605–619, 2004.

[15] V. V. Krylov and R. E. T. B. Winward, "Experimental investigation of the acoustic black hole effect for flexural waves in tapered plates," *J. Sound Vib.*, vol. 300, no. 2, pp. 43–49, 2007.

[16] E. Bowyer and V. Krylov, "Acoustic black hole manufacturing for practical applications and the effect of geometrical and material imperfections," no. 4, pp. 2411–2421, 2016.

[17] J. Y. Lee and W. Jeon, "Vibration damping using a spiral acoustic black hole," *J. Acoust. Soc. Am.*, vol. 141, no. 3, pp. 1437–1445, 2017.

[18] A. Howard, "Morphological control of tensile release in ceramic penetration," Cranfield University, 2014.

[19] Z.˘ Nakutis and P. Kaškonas, "Bridge vibration logarithmic decrement

estimation at the presence of amplitude beat," *Meas. J. Int. Meas. Confed.*, vol. 44, no. 2, pp. 487–492, 2011.

[20] M. Feldman and S. Braun, "Nonlinear vibrating system identification via Hilbert decomposition," *Mech. Syst. Signal Process.*, vol. 84, pp. 65–96, 2017.

[21] T. Humbert *et al.*, "Wave turbulence in vibrating plates : The effect of damping To cite this version : HAL Id : hal-01134801 Wave turbulence in vibrating plates : The effect of damping," 2016.

[22] Y. Liao and V. Wells, "Modal parameter identification using the log decrement method and band-pass filters," *J. Sound Vib.*, vol. 330, no. 21, pp. 5014–5023, 2011.

[23] J. Lardies and S. Gouttebroze, "Identification of modal parameters using the wavelet transform," *Int. J. Mech. Sci.*, vol. 44, no. 11, pp. 2263–2283, 2002.

[24] M. R. Schroeder, "New method of measuring reverberation time," *Journal of the Acoustical Society of America*, vol. 37. pp. 409–412, 1965.

[25] K. Arcas and A. Chaigne, "On the quality of plate reverberation," *Appl. Acoust.*, vol. 71, no. 2, pp. 147–156, 2010.

[26] V. Gomez Escobar and J. M. Barrigon Morillas, "Analysis of intelligibility and reverberation time recommendations in educational rooms," *Appl. Acoust.*, vol. 96, pp. 1–10, 2015.

[27] R. R. Boullosa, "Vibration measurements in the classical guitar," *Appl. Acoust.*, vol. 63, no. 3, pp. 311–322, 2002.

[28] W. Dudziński, Ł. Konat, and G. Pękalski, "Structural and strength characteristics of wear-resistant martensitic steels," *Arch. Foundry Eng.*, vol. 8, no. 2, pp. 21–26, 2008.

4.8 Connection to the next chapter

The fundamental research question of this thesis is, how do novel ballistic measurements affect recent safety considerations? This chapter is not a direct contribution to answering the question. To connect this chapter to the others, one has to put it into a broader context. The anticipated research is only possible with novel measurement devices.

This chapter describes a damping plate which will enhance the sensor signal for terminal ballistic investigations. However, the next chapter investigates the pushout force of the casing, which is an internal ballistic investigation.

The connection between this chapter and the next is devoted to the sensor layout and the measurement system. In this chapter is has been established that piezoelectric sensors are capable of sensing ballistic events in the range of microseconds. This time range of the physical event is investigated in this and also in the next chapter.

Furthermore, the knowledge of the best practice for signal processing of piezoelectric accelerometers has been established in this chapter and will be used and further refined in the next one.

One outcome of this chapter was that aluminium is not suitable for a measurement device in the field of ballistics due to the soft material. A best practice is to use hardened or tempered steel for ballistic investigations. This knowledge was essential for designing the breech described in the next chapter.

The chapter deals also with the vibration, acoustics and noise reduction methods. The publication covered in this chapter focuses on the proof of concept for one very crucial part of the research, namely the sensor plate. The sensor plate is subsequently differentiated into the ricochet and witness plate. These structures are described in detail later in chapter 6.

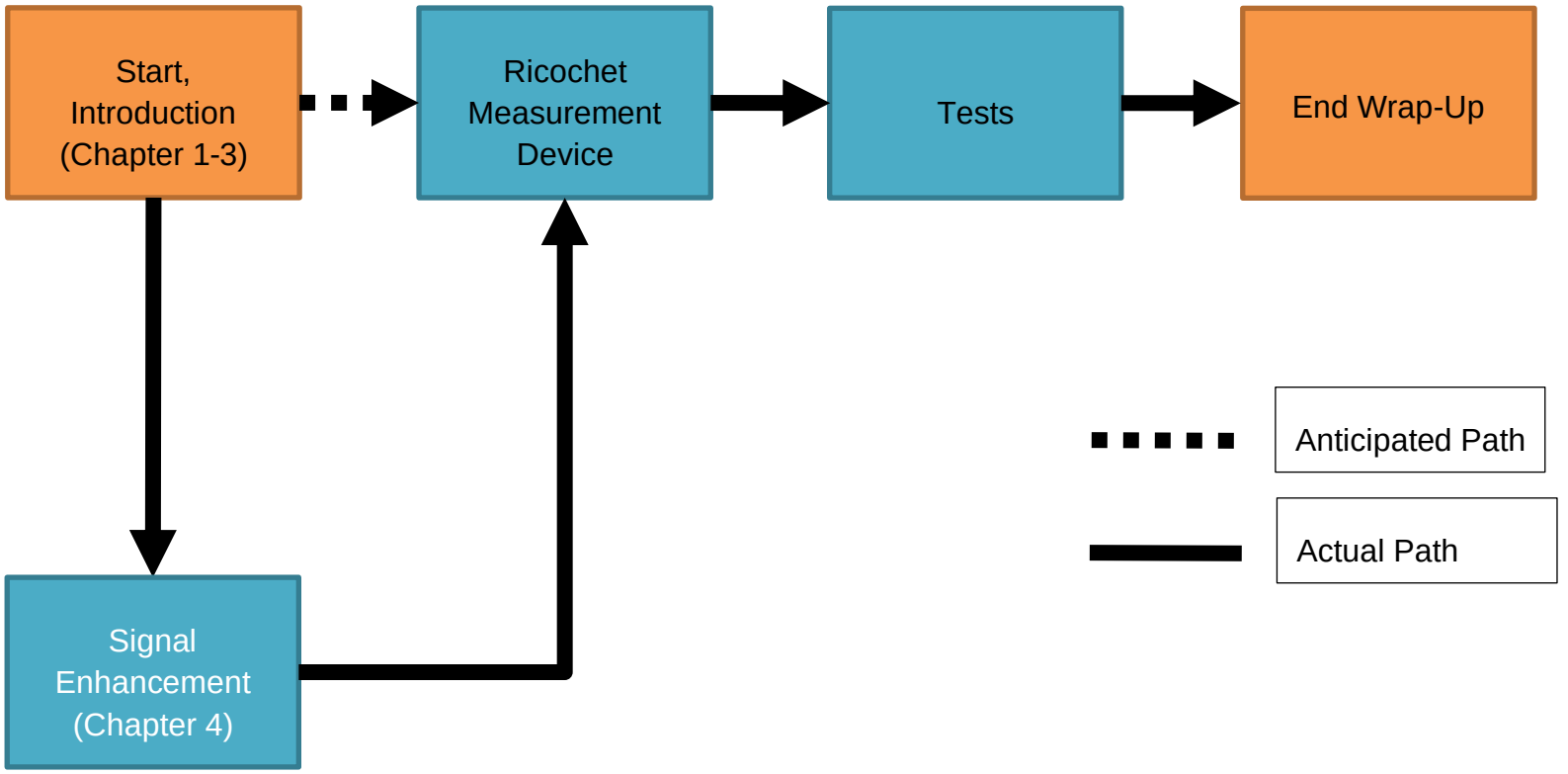

Figure 4-8: Comparison of the anticipated path and the actual path in relation to the chapters presented in the thesis. Chapter 2 was necessary to be capable of producing a ricochet measurement device.

4.9 Conclusion of chapter

This chapter was not directly connected to ballistics. However, this intermediate step was necessary to realise the ricochet measurement device. One key outcome of this chapter is that the ballistic impact is a prime example of a sound burst which produces all kinds of frequencies during impact. These broadband spectra can be controlled using power-law spiked plates

5 Pushout force measurement

5.1 Introduction to chapter

This chapter contains two publications which treat a similar topic. The first part is about the initial proof and verification of the concept. The second part assesses the usability for signal processing and the momentum measurement. Both parts together present a double cross-verification of the fact that surface-treated ammunition causes a significant rise in force. However, this chapter also shows the high reproducibility of internal ballistic processes. Section 5.2 describes the first accepted publication of the thesis.

5.2 Dynamic qualitative pushout force measurements for investigating influence factors on the pushout effect of small calibre ammunition

5.2.1 Author's contribution statement

Michael Muster developed this publication. Michael Muster contributed the main conceptual ideas concerning the sensor layout and its signal processing.

Michael Muster worked out almost all of the technical details and designed the measurement device with the help of Ralf Wahrenberg. Markus Grünig manufactured the novel breech.

Amer Hameed and Ralf Wahrenberg gave inputs for the test scenarios to prove the measurement concept.

Michael Muster wrote the paper with inputs from all authors.

Michael Muster, first author
Centre for Defence Engineering, Cranfield University, Defence Academy of the United Kingdom
Shrivenham, SN6 8LA, UK
michael.muster@cranfield.ac.uk

Amer Hameed, second author
Centre for Defence Engineering, Cranfield University, Defence Academy of the United Kingdom
Shrivenham, SN6 8LA, UK
a.hameed@cranfield.ac.uk

David Wood, third author
Centre for Defence Engineering, Cranfield University, Defence Academy of the United Kingdom
Shrivenham, SN6 8LA, UK
d.wood@cranfield.ac.uk

Keywords: lubrication, push-out force, small-calibre ammunition, internal ballistics

Abstract

A small calibre weapon system consists of the weapon and the ammunition. In the case of bolt action rifles during the process of firing, the breech is a rigid bearing which prevents the casing from being pushed out. However, not the whole pushout force is taken by the bolt. Because of friction forces at the casing boundary, the chamber of the weapon can absorb a significant part of the pushout force.

The duration of the pushout force is in the order of milliseconds. Piezoelectric strain gauges are capable of recording such short time events qualitatively. To increase the measurability of force obtained from the raw signal is filtered using a bandpass filter and applying a signal envelope. A piezoelectric force washer verifies the results from the strain gauges.

In this paper, two different lubrication states and two different casing materials are analysed to evaluate their influences on the force absorbed by the bolt.

The analysis indicated that lubricated casings lead to pushout forces which are more than three times higher when compared unlubricated casings. The unlubricated steel casing also showed a significant lower pushout force when compared with the regular brass casing. However, this effect is reversed if the casing is lubricated.

This work demonstrates how to measure dynamic events. The acquired results can be directly applied to 5.56x45 mm bolt action rifles. These measurements may also have a significant influence on self-loading rifles since the process of reloading is also dependent on the pushout force. The general application area is target competitive shooting and military purposes.

5.2.2 Introduction to publication

The process of firing a weapon system is a vivid example of the application of Newton's third law. The gas generated by the burning propellant accelerates the projectile in the weapon until it leaves the muzzle. This acceleration process leads to recoil. During the acceleration, the casing of the cartridge experiences high pressure. This leads to significant pushout forces, but for a minimal time. However, the chamber and the bolt of the weapon holds the cartridge in place during this time. See Figure 5-1.

The bolt of the weapon does not purely take the overall pushout force. The cartridge casing can be assumed as a pressure vessel which is plastically and elastically deformed during the time while the burns in the chamber. Through this behaviour, the casing is pushed against the walls of the chamber. The friction between the chamber walls and the casing provides some capabilities of taking some of the overall pushout force.

The pushout force depends mainly on four factors: The surface area of the case head, where the pressure applies; the pressure in the casing; the friction between the chamber wall and the case body; and the material properties of the chamber and the casing. The pressure curve in the chamber should be highly repeatable. Woodley et al. measured the projectile and the propellant mass, which resulted in comparable pressure maxima [1]. Since the cartridges are produced in tight tolerances, the area of the casing head can also be assumed as constant. In these experiments, the pushout force is mostly dependant on the material properties of the casing and the chamber and the friction coefficient between these materials.

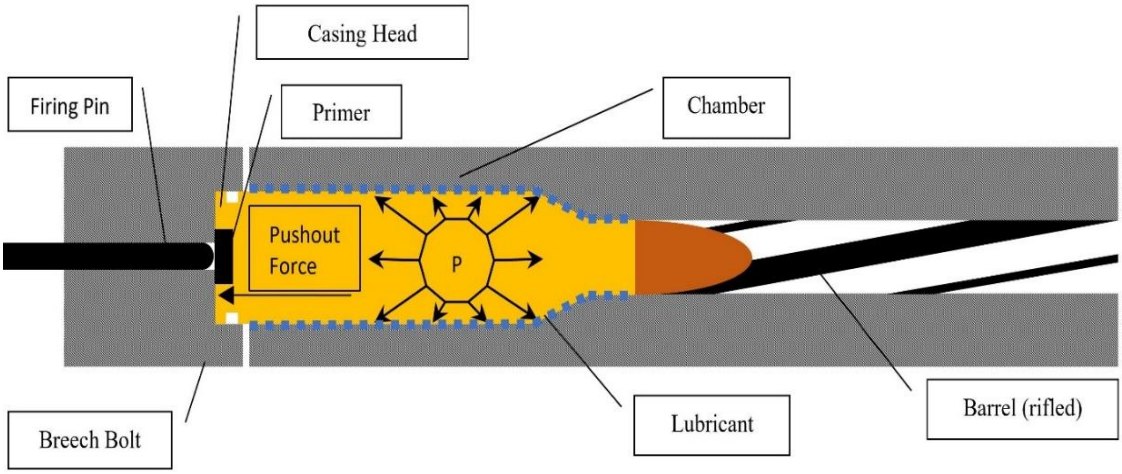

Figure 5-1: Schematic view of the cross-section of the barrel.

The behaviour of the dynamics of small arms weapons is often investigated using high-speed cameras. However, these cameras are suitable only for visible events, so are not appropriate for bolt action rifle measurements. A breech of a weapon holds the ammunition in place during firing. Often such short duration rigid or invisible processes have been modelled using finite element analysis [2], [3]. The advantage of finite element methods is that numerous parameters can be investigated within a single model by undertaking sensitivity studies. It is also possible to analyse geometric parameters with minor changes in the model. South et al. investigated an interior ballistic model which can be used to estimate the behaviour of a projectile while being pushed through the barrel. Some aspects of the model correlated almost exactly with the reality, but the wear mechanism of the groove formation during the firing was not represented realistically [4]. It is still challenging to simulate wear and tribological mechanisms such as friction and lubrication in thin-film environments [5].

It is also possible to measure these highly dynamic forces in a real environment. Ritter et al. presented a system to measure the in-chamber primer pushout force [6]. They used a force gauge to measure simultaneous the force on the breech and pressure inside the cartridge. However, with this system, it was only possible to measure the primer force, which is produced during a fire. It is not possible to measure the whole force at the bottom of the cartridge.

Another possibility to measure highly dynamic events, such as vibrations, are piezoelectric strain gauges. Michaelides et al. used such strain gauges to analyse the movements of a vibrating bridge [7]. In their investigations, they used the strain gauges for frequencies between 1 and 100 Hz. Such strain gauges are capable of quantifying much faster events. The raw signal quality is good with such encapsulated strain gauges so that it is possible to determine noisy but dynamical events with adequate signal processing [8].

Bin Tan et al. used standard flexible strain gauges to investigate the effect of steel balls, impacting at 200 m/s on military protection helmets. These strain gauges were used as a reference for validating the FE model [9].

One main problem of internal ballistics measurements systems is the noisy signals. The reason for this is that the acceleration process of a bullet is a short time event approximately 1 ms for the investigated calibre, which is comparable with a burst where a lot of mechanical oscillations are generated. In such a noisy environment, one has to determine the main physical event of interest. Phuong et al. suggested a de-noising approach with discrete wavelet decomposition in combination with a Hilbert Huang transformation for the detection of faults in roller bearings. They were more focused on reporting the time of occurrence of the error [10]. Wavelet decomposition is less suitable to measure the amplitude of an event. For internal ballistic pressure measurements, 20 kHz second-order Butterworth lowpass filters are generally used [11]. In the case of pressure measurements, it is simpler to determine the underlying physical event, such as oscillating pressure waves which may affect the whole measurement. However, in the case of the pushout measurement, more sophisticated filtering approaches are necessary.

Measuring force signals with piezoelectric force washers is widely used from the field of biomedical engineering [12] up to the rock drilling technology [13]. Groche et al. [14] used a force washer to indirectly measure the applied force on a punch in a high-speed press for a thick steel plate. The indirectly acquired signals were highly comparable to the signals of the measured directly. However, the system had to be calibrated for which they used a stroke rate of 300 strokes per minute. The duration of the event of interest was of the order of 100 ms.

More dynamical investigations were conducted by Jun et al. and Zhang et al. [15], [16]. Jun et al. investigated the behaviour of the spindle in a machining setup using an assembly of force washers. The rotation speed of the spindle and the cutting tool determines the cycle time, the cycle of the cutting process was between 50 and 5 ms, which is close with the internal ballistic process which is in the range of 50 µs to 1 ms. Jun et al. conducted an in-depth investigation of the force washer's properties under harsh circumstances. They obtained a very positive outcome for this dynamic application. Zhang et al. showed that ultrasonic forces could be measured with piezoelectric force washers.

5.2.3 Material and methods

Two different casing materials were chosen to investigate the influence of the lubrication on the pushout force. In both cases, the ammunition type M193 was used, it is a well-defined NATO standard ammunition stock number [17]. This ammunition type has a projectile diameter of 5.56 mm, and the length of the casing is 45 mm. The M193 has been extensively investigated by several researchers covering terminal ballistic studies [18] and [19]. Like some ammunition types, the M193 was produced with two types of casings, a regular brass casing and a steel casing.

A fluid called Klübersynt MZ 4-17 was used to lubricate the casings. This lubricant is recommended for small calibre weapons such as hunting and sporting rifles [20]. For the test, a thin layer of lubricant was applied onto the casing with a brush. The average weight of lubricant applied was 10 mg. The lubricant was equally distributed over the whole casing surface. The unlubricated ammunition was cleaned beforehand using acetone to remove any fat residuals, which might remain from the production process.

The ammunition was tested with a system similar to the Electronic Pressure Velocity and Action Time (EPVAT) measurement setup [21] which is known for NATO testings, see Figure 5-2. With this system; it was possible to measure the pushout force of the ammunition. Three piezoelectric strain gauges where pasted equidistant to the load cell with an adhesive, see Figure 5-3a and Figure 5-3b. The load cell consisted of stainless steel X5CrNi18-10, which is typically used in such experimental tests [22], [23]. This material is also resistant to residue from the burned propellant, which is of strong oxidising nature. Also, this load cell acted as a breech, providing a rigid bearing for the ammunition, see Figure 5-3c.

Multiple sensors were used to analyse the effect of inhomogeneous loading during the acceleration phase of the bullet firing. The measurement system housing was manufactured from the cast iron, to assist with vibration damping. The gun barrels were similar to those used in an EPVAT system and were interchangeable and could be used for multiple calibres. The Kistler 6215 pressure gauge with a Butterworth 20 kHz filter was used as a reference system.

The velocity was measured with a light gate. The pressure and velocity were measured in separate test setups.

The National Instruments USB-6366 data acquisition device was used for the tests. It can simultaneously acquire and record data every 0.5 µs.

The piezoelectric strain gauges were of type 740b02 (PCB, USA). They are capable of measuring frequencies up to 100 kHz. Also, a low pass filter to reduce the mechanical oscillations while measuring the pressure was used. The raw data

with a signal amplification rate of 1, was acquired without a filter using PCB-482C05 (PCB, USA) signal conditioner.

A precalibrated force washer was additionally used for strain gauge verification. This force washer gives a signal in volt, which can be directly converted into a force signal in Newtons. However, with this system, it is not possible to detect asymmetrical loads produced by the casing.

The used force washer was a Kistler 9041a (Kistler, Switzerland); this sensor type is capable of recording forces up to 90 kN. The signal conditioner was a Kistler 5073A (Kistler, Switzerland). Figure 5-4 shows the assembly of the force washer. In Figure 5-4a, one can see the sensor. However, this sensor needed to be protected by a steel protection plate (Figure 5-4b). The second reason for the steel plate was to provide a rigid bearing for the ammunition.

The data acquisition time was set to 20 ms. As the signal of interest was ca. 4 ms, this acquisition time was sufficient. The pre-trigger was set to 0.1 ms. The reason for this extended acquisition time was to ensure that the trigger started the data acquisition before releasing the spring-loaded igniter rather than later when the igniter hit the primer. In this experimental setup, it was possible to trigger the release time. Each test was repeated five times.

A servo press was used, to investigate the signal linearity of the load cell with the piezoelectric strain gauges and the force washer, which applied a defined load for a short time on the system. The servo press was controlled by a calibrated force detector and an additional sensor that controlled the servo press system. This double controlled system ensured the calibration accuracy.

After shooting, the empty cartridge casings where optically investigated for any scratches or shape deformations. In addition, a longitudinal sectional cut of the empty casings was performed to investigate the case head area and the maximum internal diameter, see Figure 5-5.

The tests were performed in a closed shooting range behind safety glass. The cartridge was ignited by a remote trigger.

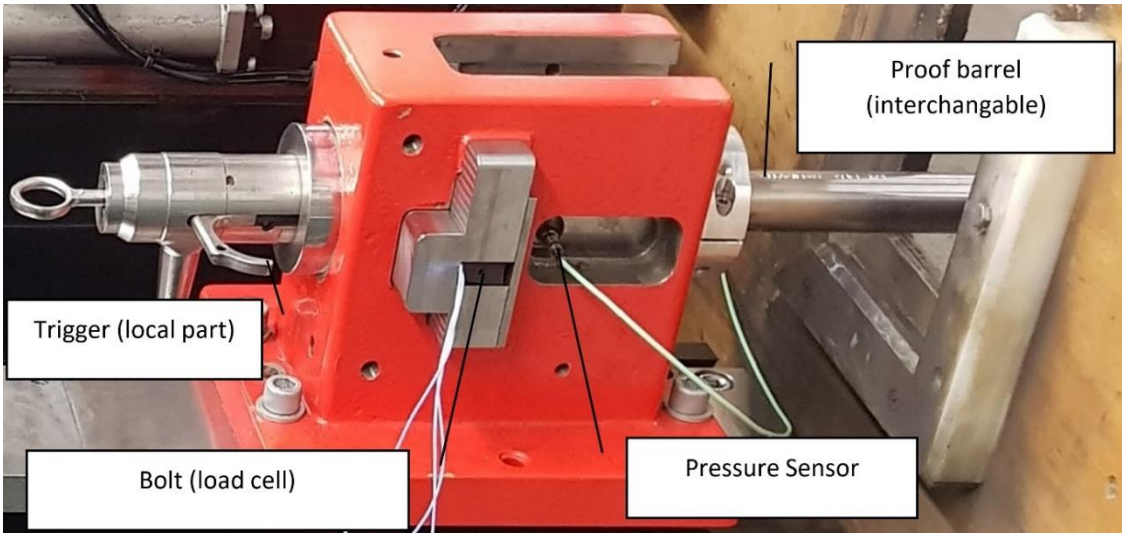

Figure 5-2: Measurement system.

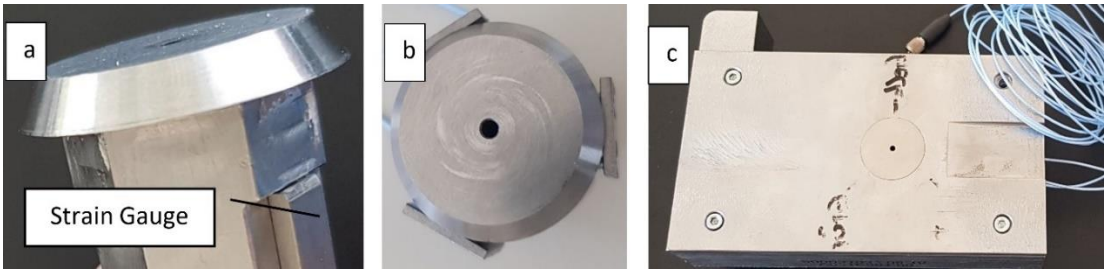

Figure 5-3: Qualitative measurement assembly of the load cell. (a) load cell with strain gauge, (b) assembled load cell, (c) fully assembled breech measurement plate.

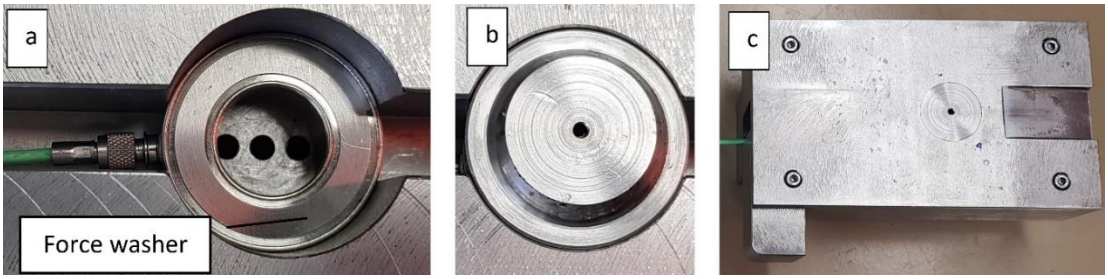

Figure 5-4: Quantitative measurement assembly. (a) force washer, (b) protection plate (c) fully assembled quantitative breech measurement plate.

5.2.4 Raw data processing of piezoelectric strain gauge signal

The Hilbert transformation which produces a signal envelope is a widely used function in signal processing, see [10], [24] and [25]. It is primarily used in the analysis of a signal that exhibits a rapid increase and decay similar to internal ballistics.

A general property of the signal envelope is that a signal wave which carries much high-frequency noise can be demodulated into a low-frequency signal which represents the main physical property if the signal is not cyclic. After transforming the signal into an envelope, as shown in Figure 5-6, it can be used as a stand-alone signal. The signal envelope approach is most suitable for our application because it filters out high-frequency peaks that are artefacts, deriving from reflections.

Tests showed that a reliable idea is to measure the force during firing with a combination of a bandpass filter and a signal envelope. Because of the signal characteristics, it is possible to work with the maximum value of the signal envelope to determine the maximum force.

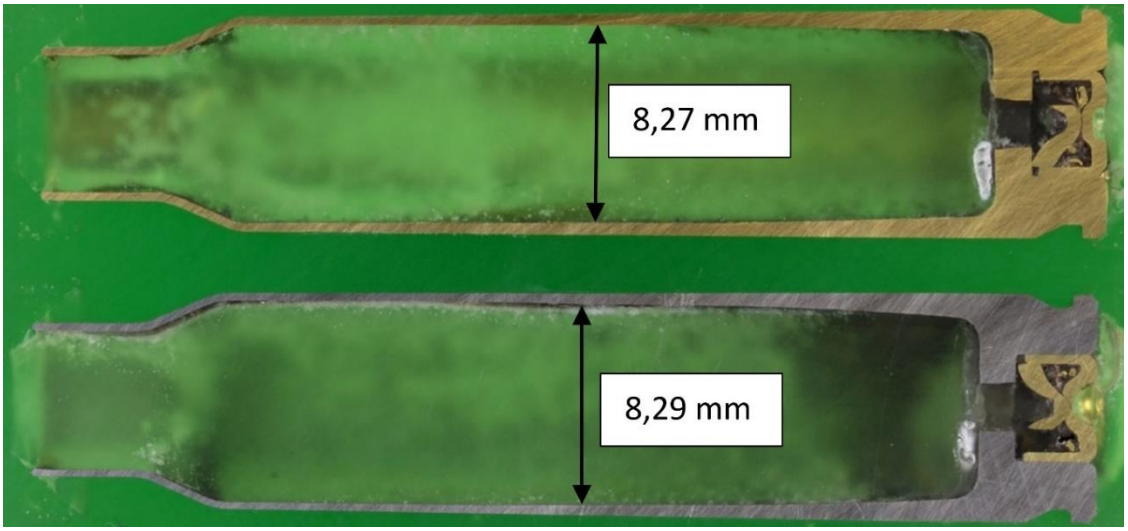

Figure 5-5: Analysed casing types and their maximal internal diameters. The upper is the brass casing, the lower the steel casing.

As already mentioned, a servo-press was used to investigate the linearity of the system. However, such a press only offers limited comparability with the real test situation. In the described system, the signal processing was undertaken exactly as in the real internal ballistic measurements. Therefore, the investigation was performed at its peak. This paper only investigates the linearity of the load cell; it is not aimed to calibrate the load cell to give fully quantitative results.

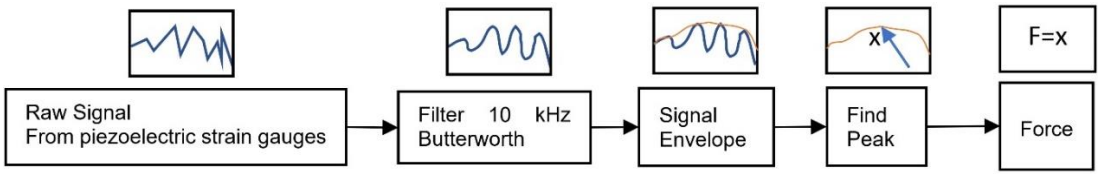

Figure 5-6: Signal processing of the raw data.

5.2.5 Results

Figure 5-7 presents the raw data (in blue) of a typical pushout force signal for all tested casing scenarios. The red dashed line represents the signal envelope: Only the signal envelope was used to compare the results. The duration of the signal is ca. 1 ms. One can note that the raw signal consisted of high-frequency components, especially during the ignition phase. These parts are sharply reduced by processing the signal through a 20 kHz filter and generating the signal envelope. The signal envelope exhibits a strong smoothening. However, the time of the first excitation of the envelope is strongly consistent with the thresholds excitation point of the raw signal. In the unlubricated brass case, testing's measured with strain gauges, the duration of the force is shorter compared to all other scenarios.

The force curves represented in Figure 5-8 show the post-processed raw signals of the lubricated and unlubricated brass casings measured with strain gauges. The amplitude is normalised relative to the regular case, which is considered to be the unlubricated brass casing. One can observe that the starting time of the force generation on the breech is at the same time for both the lubricated and unlubricated casing. However, the peak force of the unlubricated casing falls at 0.4 ms, which is earlier when compared to the lubricated casing falling at 0.55 ms. This observation is for both measurement scenarios valid, for the measuring system with strain gauges and the one with the force washer.

The unlubricated casing curves show a lower peak force and in case of the strain gauge measurement, a smaller deviation between the max and min peak force compared to the lubricated casings. The semi-quantitative difference is of the ratio of about 1:2 in both peak force and the deviation in the case of brass casings.

The difference between the lubrication scenarios can also be observed in Figure 5-9 and Figure 5-10. The variance in the case of steel casings is even stronger. The peak force both in the lubricated steel and the brass casing is exhibited at almost the same time.

However, the time when the force applies to the breech is marginally different for steel between the unlubricated and lubricated curves. These force measurements are contrary to both brass casing measurements, where the force from the cartridge applied on the breech for the unlubricated state acted for a markedly shorter time

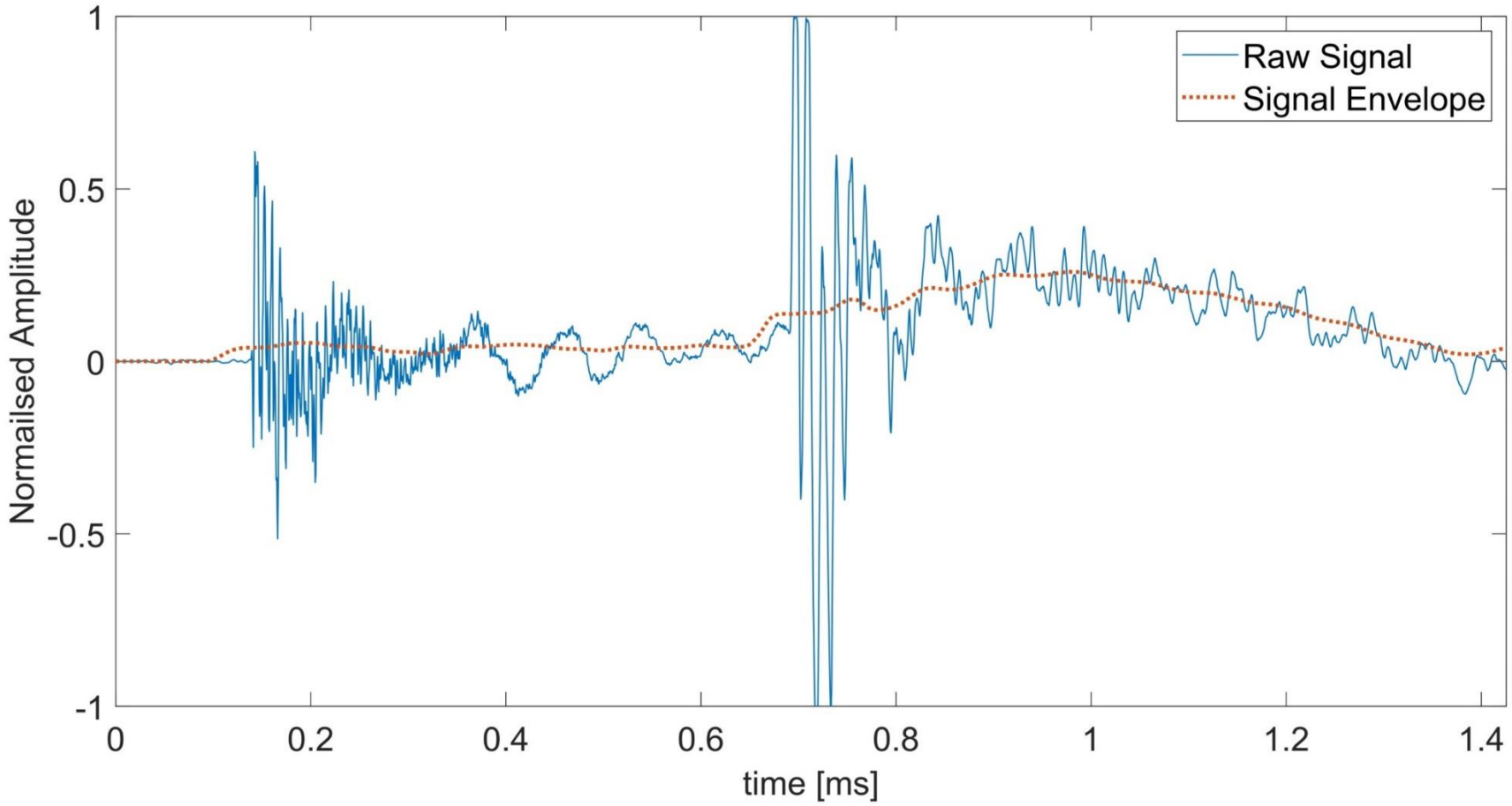

Figure 5-7: The raw signal of the strain gauges and its calculated envelope.

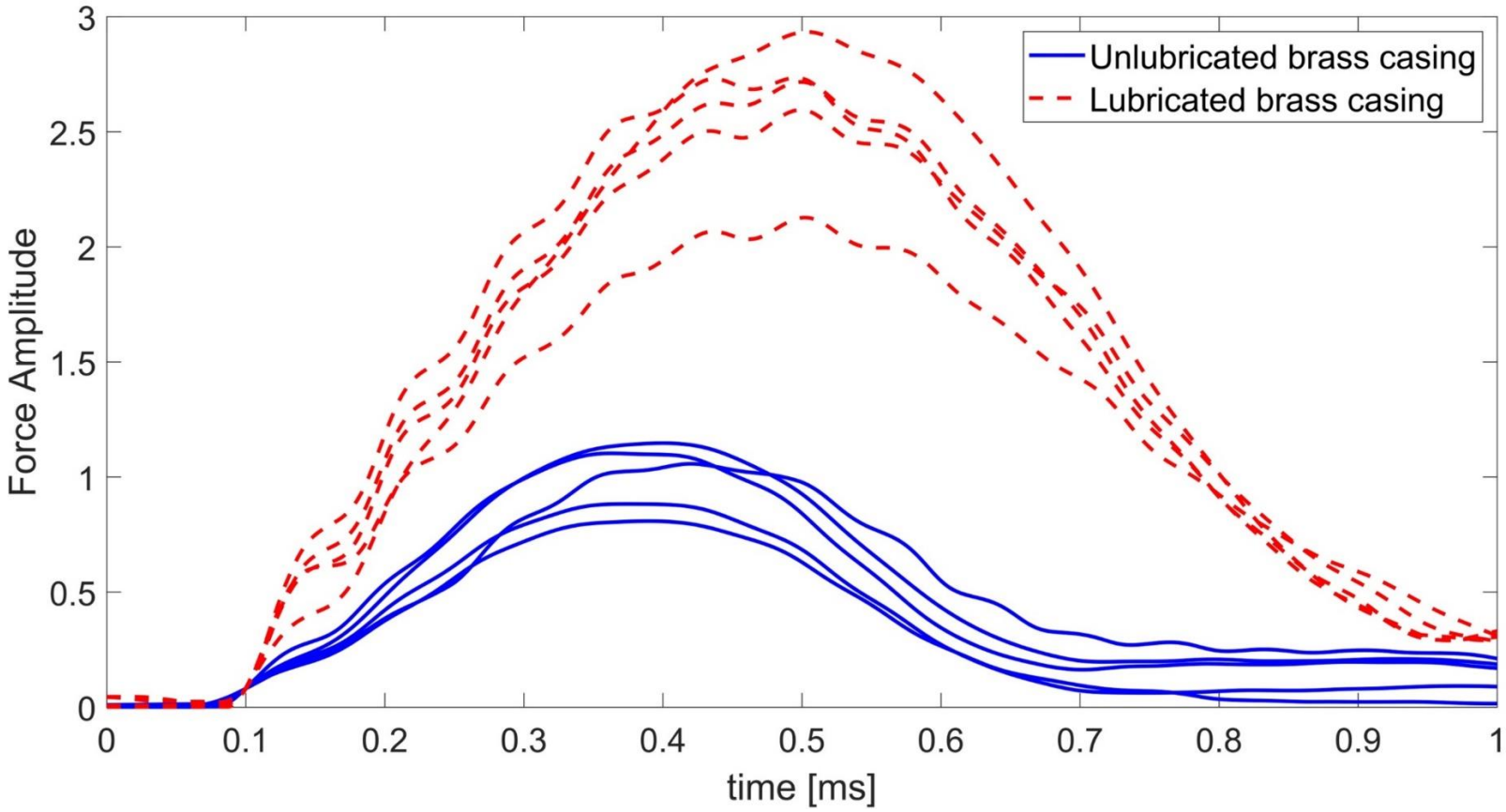

Figure 5-8: The peak pushout force measured with piezoelectric strain gauges showing lubricated and unlubricated brass casings.

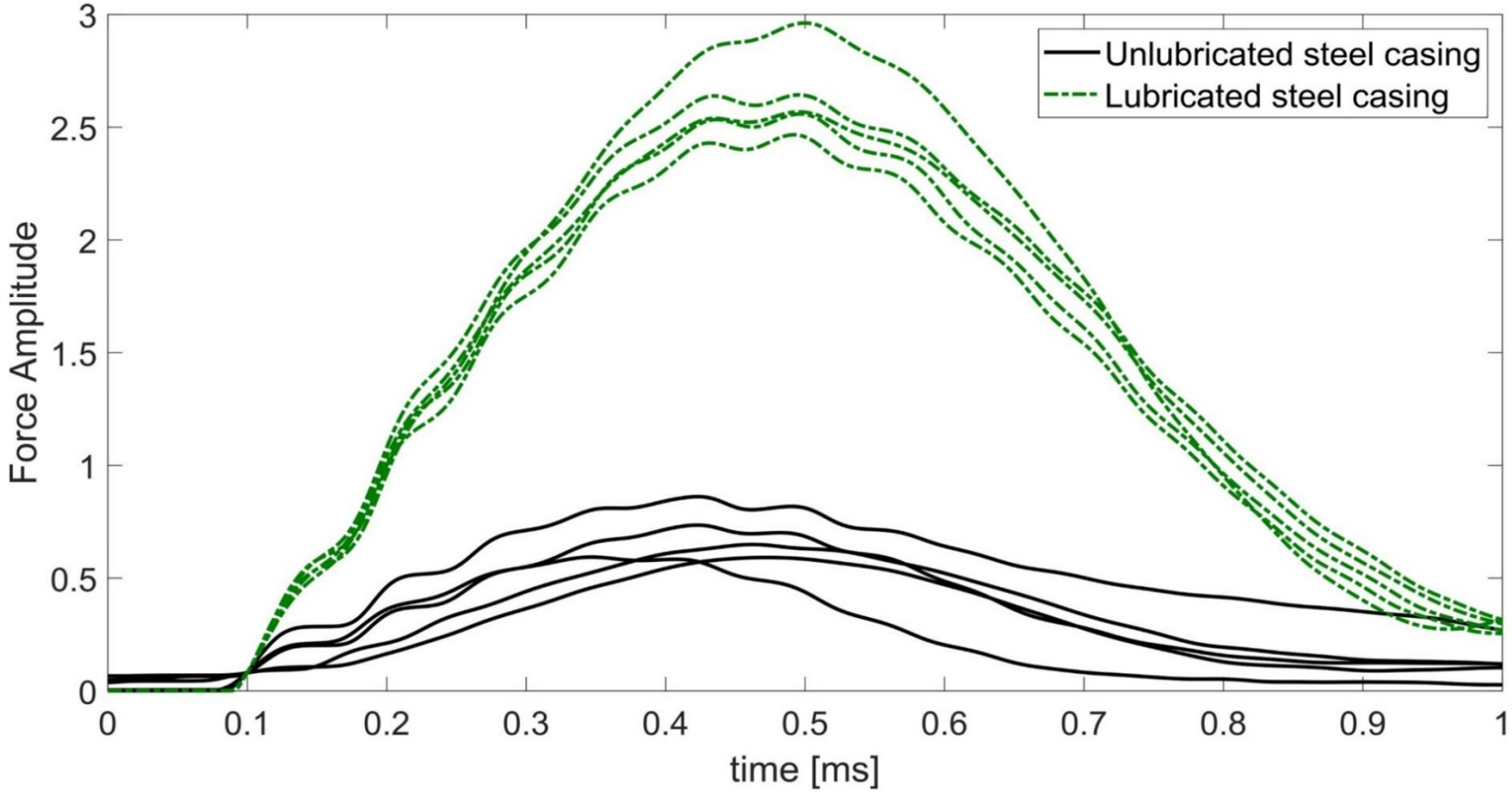

Figure 5-9: Comparison of the force signals of lubricated and unlubricated steel casings, referring to the unlubricated brass casing.

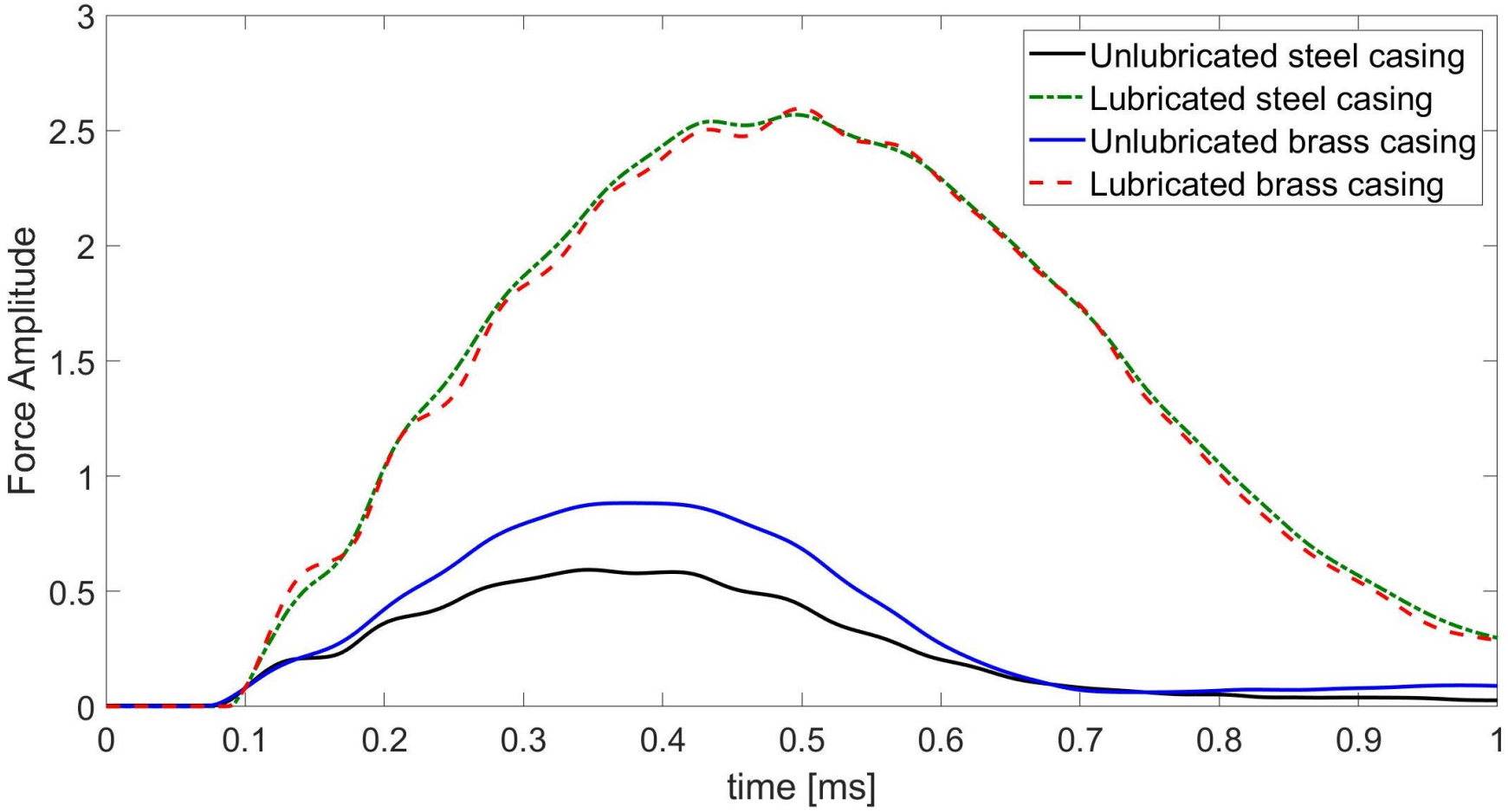

Figure 5-10: Graph of average signals of steel and brass casings.

The comparison of some neuralgic data is represented in Table 5-1. It shows a large difference in both the average and the maximum force between the baseline (unlubricated brass casing) and the lubricated casings, which is in both cases ca. factor 3. Even more dramatic is the difference between the minimal and the maximum force of the steel casing, which is approximately exhibiting a ratio of 1:5. In general, unlubricated steel casings produce less force on the breech compared to brass casings. The average reference pressure was acquired with a different measurement system. Each pressure test scenario was also repeated five times. The range of average pressures was comparable between the scenarios and overall, differences were negligible.

Table 5-1: Relative comparison of the peak values of strain gauge measurements.

Description	Average Force	Min Force	Max Force	Average Pressure [Bar]
Brass Unlubricated	100 %*	81 %	114 %	3510
Brass Lubricated	268 %	212 %	293 %	3560
Steel Unlubricated	68 %	59 %	86 %	3590
Steel Lubricated	264 %	247 %	296 %	3509

* Normalised to the average of the unlubricated brass casing

The results of the strain gauge equipped load cell were compared and verified by the force washer. The same apparatus such as the proof barrel, the housing of the load cell and the trigger mechanism was used for all the experiments, to ensure consistency. Figure 5-11shows the acquired data of the brass casings comparing the results from the force washer with the strain gauge measurements. The force washer signal was filtered with a 20 kHz filter. No signal envelope was applied during the experiments. In general, the results between the force washer measurements and the strain gauge based load cell are comparable. In the case of the force washer, a comparatively slightly faster decay to zero was observed in the lubricated brass casing. The comparative difference in the peak force decay is also noticeable in the lubricated casings.

The relative average force, tabulated in Table 5-2, indicates that the difference between the lubricated and unlubricated casing is around ca. 2.2 times. The strain gauges captured similar magnitudes of relative peak measurements.

Table 5-2: Peak force of the force washer measurements.

Description	Relative average Force	Average Force [kN]	Min Force[kN]	Max Force[kN]
Brass Unlubricated	100 %	9.77	9.23	10.42
Brass Lubricated	217 %	21.2	20.5	21.72

5.2.6 Discussion

The results are consistent with the published models that used finite element analysis [2]. The measurements are conducted with two different approaches and are comparable, which strengthens the outcome of key results. A change in lubrication leads to a significant difference in the pushout force. The signal processing approach described here is suitable for these force measurements. It was proven that the initial times of excitation remain the same while the primary signal is strongly smoothened using a signal envelope approach, which leads to good comparability.

The engineered piezoelectric load cell as well as the force washer are suitable means of data acquisition devices to proof and measure the pushout force during the firing process. The main advantage of the force washer is that it is easy to get absolute values. If one wants to investigate the load distribution, the measurement system with three strain gauges is more applicable.

The time during which the force is measured is comparable with the duration during which a projectile is pushed through the barrel, despite the fact that forces are still expected in the chamber well after the projectile exits the barrel. This expected force is because of residual gas pressure in the chamber.

One significant observation from the analysis of these tests is that the lubrication in the chamber or on the ammunition leads to higher pushout forces. For reference, we have taken the unlubricated brass case as a baseline.

The mechanical material properties of the two casing types differ strongly. However, the fact that the lubricated brass casing produces the same pushout force as the lubricated steel casing leads to the conclusion that the pushout force is mainly depending on the friction between the boundaries.

The comparison of the unlubricated steel and brass casing indicates that the steel casing produces a significantly lower force on the breech. However, the duration of the load cycle in the case of the steel casing is comparatively longer, and in some cases, is more than 1 ms. The pushout energy remained comparable between the unlubricated steel casing and the unlubricated brass casing. It is important to note that the steel surface is treated with a lacquer. Using a treated surface it is not possible to make statements about the steel casing-chamber interaction which has not been studied in this investigation, for a lacquered casing, the interaction is between the polymer and the steel chamber.

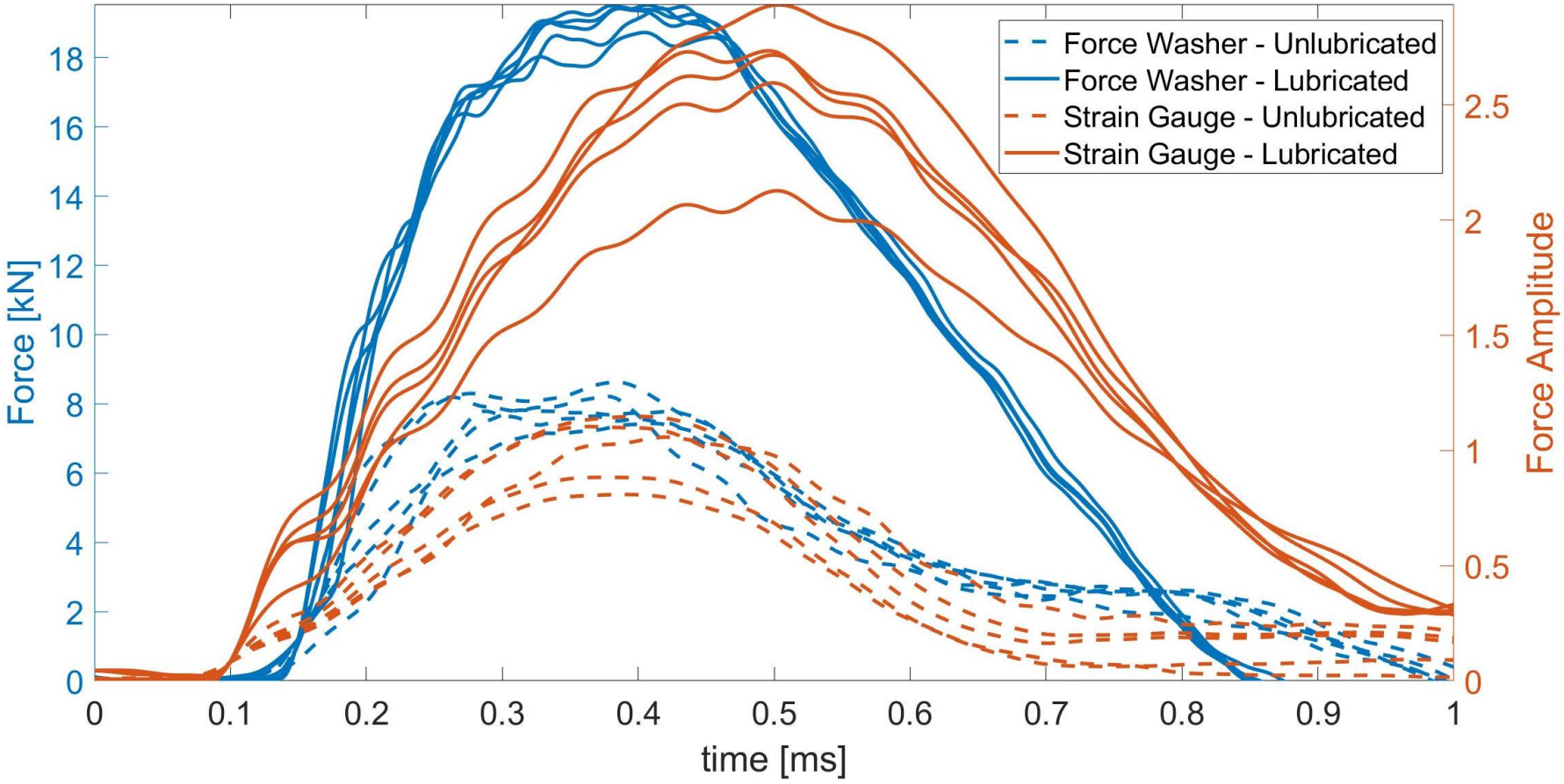

Figure 5-11: Force washer signals during the process of firing in comparison to the signal from the strain gauge.

5.2.7 Conclusion and future work

This paper demonstrates two approaches to measure the pushout force of the casing on the breech. The benefit of this system is that it can be used for calibres, such as 8.6x70 mm, which is frequently used by long-range shootings with breech rifles. An enhancement to this investigation is further tests with different small arms calibres, to investigate what parameter influences the pushout force significantly.

These results might also be applicable for repeating rifles since their mechanism is strongly dependant on the pushout energy, which strongly changes if the casing is lubricated. It is also worth investigating the effect of water or ice in the chamber, which may exhibit similar results. This technique would also be applicable for investigating the forces involved in breeches in larger gun systems such as autocannons and tank guns.

5.2.8 Acknowledgement

RUAG Ammotec AG, Thun Switzerland supported this research. I want to thank the R&D team and the ballistic testing team. Especially Dr Ralf Wahrenberg, who provided valuable expertise in the field of ballistic test settings.

5.3 Publication references

[1] C. Woodley, A. Carriere, P. Franco, J. Nussbaum, X. Chabaux, and B. Longuet, “Comparisons of Internal Ballistics Simulations of 40mm Gun Firings,” in *23rd Int. Symp. Ballist.*, 2007, pp. 359–367.

[2] D. Gubernat and C. Fischer, “Explicit finite element model for determing influence of cartridge case material properties on small caliber weapon function,” in *26th Int. Symp. Ballist.*, 2011, pp. 806–817.

[3] D. K. Kankane and S. N. Ranade, “Computation of In-bore Velocity-time and Travel-time profiles from Breech Pressure Measurements,” *Def. Sci. J.*, vol. 53, no. 4, p. 351, 2003.

[4] J. T. South, K. Dipak, and M. Minnicino, “Small Caliber Modeling From Design to Manufacture to Launch,” in *23rd Int. Symp. Ballist.*, 2007, pp. 557–564.

[5] H. Rahnejat, P. M. Johns-Rahnejat, M. Teodorescu, V. Votsios, and M. Kushwaha, “A review of some tribo-dynamics phenomena from micro- to nano-scale conjunctions,” *Tribol. Int.*, vol. 42, no. 11, pp. 1531–1541, 2009.

[6] J. J. Ritter, R. A. Beyer, and A. Canami, “In-Chamber Primer Force and Case Pressure Measurements of the 5 . 56-mm Cartridge,” *Army Res. Lab.*, 2012.

[7] P. Michaelides, P. Apostolellis, and S. Fassois, “Vibration-Based Damage Diagnosis in a Laboratory Cable–Stayed Bridge Model via an RCP–ARX Model Based Method,” *J. Phys. Conf. Ser.*, vol. 305, 2011.

[8] N. K. Kadim Abid AL-Sahib and Al-khawarizmi, “Monitoring Process in Turning Operations for Cracked Material Alloy Using Strain and Vibration Sensor with Neural Network,” *J. Eng.*, vol. 13, no. 3, 2006.

[9] L. Bin Tan, K. M. Tse, H. P. Lee, V. C. Tan, and S. P. Lim, “Performance of an advanced combat helmet with different interior cushioning systems in ballistic impact : Experiments and finite element simulations,” *Int. J. Impact Eng.*, vol. 50, pp. 99–112, 2012.

[10] P. Nguyen, M. Kang, J.-M. Kim, B.-H. Ahn, J.-M. Ha, and B.-K. Choi, “Robust condition monitoring of rolling element bearings using de-noising and envelope analysis with signal decomposition techniques,” *Expert Syst. Appl.*, vol. 42, no. 22, pp. 9024–9032, 2015.

[11] “American National Standard Voluntary Industry Performance Standards for Pressure and Velocity of Shotshell Ammunition for the Use of Commercial Manufacturers,” *American National Standards Institute*. 2015.

[12] J. Slavi, L. Knez, and M. Bolte, “International Journal of Mechanical Sciences The importance of harmonic versus random excitation for a human finger,” vol. 132, pp. 507–515, 2017.

[13] D. Che, W. Le Zhu, and K. F. Ehmann, “Chipping and crushing mechanisms in orthogonal rock cutting,” *Int. J. Mech. Sci.*, vol. 119, pp. 224–236, 2016.

[14] P. Groche, J. Hohmann, and D. Übelacker, “Overview and comparison of different sensor positions and measuring methods for the process force measurement in stamping operations,” *Measurement*, vol. 135, pp. 122–130, 2019.

[15] M. B. Jun, O. B. Ozdoganlar, R. E. DeVor, S. G. Kapoor, A. Kirchheim, and G. Schaffner, “Evaluation of a spindle-based force sensor for monitoring and fault diagnosis of machining operations,” *Int. J. Mach. Tools Manuf.*, vol. 42, no. 6, pp. 741–751, 2020.

[16] X. Zhang, H. Sui, D. Zhang, and X. Jiang, “Measurement of ultrasonic-frequency repetitive impulse cutting force signal,” *Measurement*, vol. 129, pp. 653–663, 2017.

[17] “Hand Receipt for Contents of Components of end Item (COEI), Basic issue item (BII), and Additional Autorization List (AAL) item for M85 Machine Gun.” Headquarters Department of the Army, Washington D.C., 1997.

[18] B. Sturtevant, “Shock wave effects in biomechanics,” *Sadhana*, vol. 23, no. 5, pp. 579–596, 1998.

[19] B. Ragsdale and S. Sohn, “Comparison of the Terminal Ballistics of Full Metal Jacket 7.62-mm M80 (NATO) and 5.56-mm M193 Military Bullets: A Study in Ornance Gelatin BT,” *J. Forensic Sci*., vol. 33, no. 3, pp. 676–696, 1988.

[20] “Klübersynth MZ 4-17,” pp. 3–4, 2014.

[21] “Defence Standard 05-101 Part 1 Proof of Ordnance, Munitions, Armour and Explosives,” MoD , 2005.

[22] H. Uzun, C. Dalle, A. Argagnotto, T. Ghidini, and C. Gambaro, “Materials & Design Friction stir welding of dissimilar Al 6013-T4 To X5CrNi18-10

stainless steel," vol. 26, pp. 41–46, 2005.

[23] H. Köhler, K. Partes, J. R. Kornmeier, and F. Vollertsen, "Residual Stresses in Steel Specimens Induced by Laser Cladding and their Effect on Fatigue Strength," *Phys. Procedia*, vol. 39, pp. 354–361, 2012.

[24] R. Rubini and U. Mengetti, "Application of the Envelope and Wavelet Transform Analyses for the Diagnosis of Incipient Faults in Ball Bearings," *Mech. Syst. Signal Process.*, vol. 15, no. 2, pp. 287–302, 2001.

[25] A. Egaña, F. Seco, and R. Ceres, "Processing of ultrasonic echo envelopes for object location with nearby receivers," *IEEE Trans. Instrum. Meas.*, vol. 57, no. 12, pp. 2751–2755, 2008.

5.3.1 Connection to the next section

This section, showed that the pushout force measurement device can be used for the investigation of different casing surfaces. Based on the results of this section it was decided that it is worth further investigating the topic of pushout force.

The aim of the next section was to investigate many different small arms ammunition types under different lubrication states because this influences the usage and danger potential of weapons.

From this section it is also known that the pushout force is a reproducible process if the casings are treated in the same manner. With this knowledge it was possible to further refine the filtering algorithm of the raw data.The refinement of this section was necessary because one of the main aims of the next section is the assessment of the momentum/impulse delivered on the breech.

The connections to the next section can be summarised as follows:

- The same measurement device is used
- The same lubrication for the casing is used
- The same force washer is used for the whole calibre range
- The same signal processing approach
- Published in the same journal

Differences to the next section are as follows

- Momentum/impulse measurement
- Assessment of ice layer treated ammunition
- Assessment of the whole calibre range

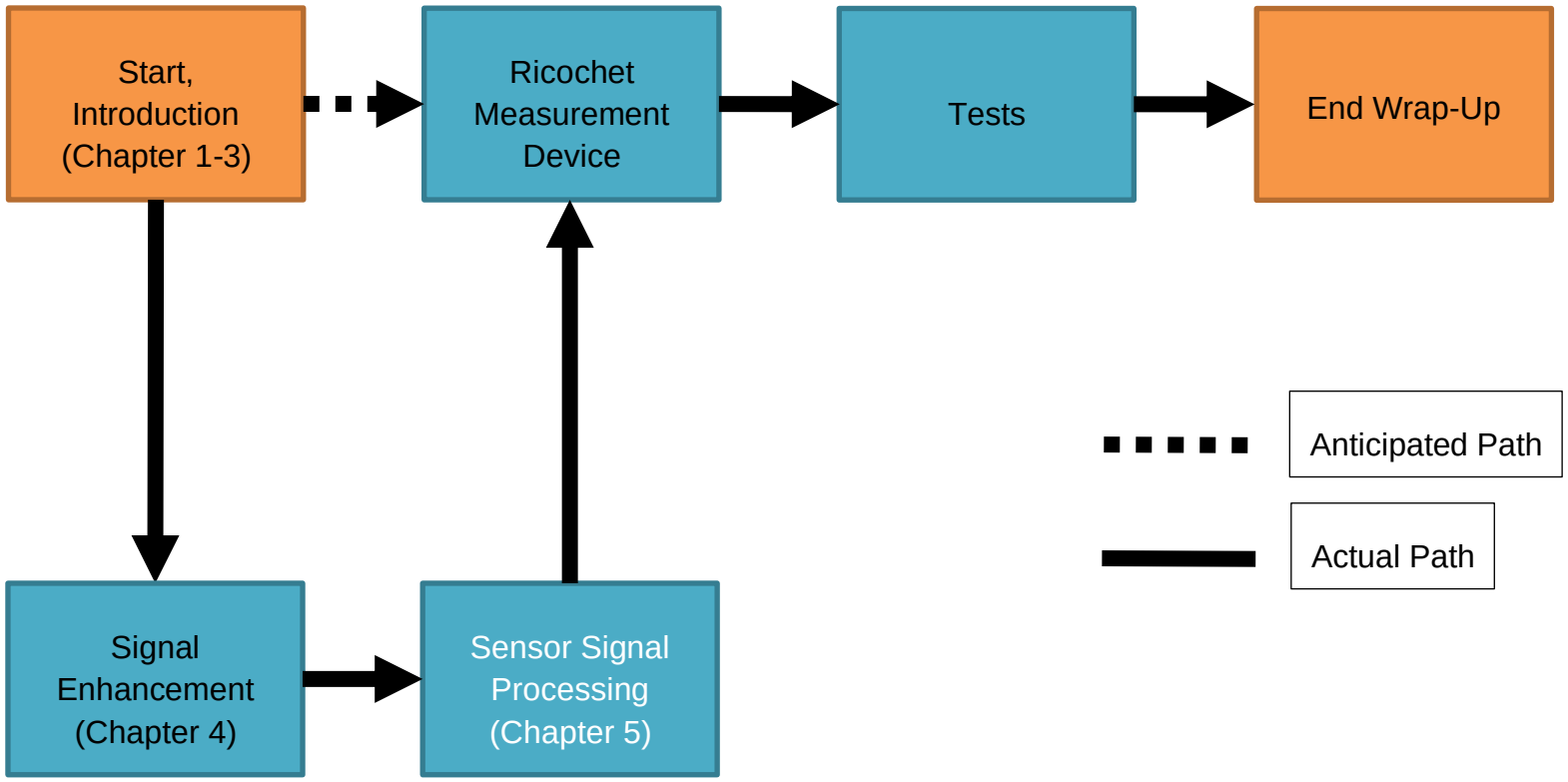

Figure 5-12: Comparison of the anticipated path and the actual path in relation to the chapters presented in the thesis. Section 5.2 was necessary for the proof of concept of a proper signal processing algorithm which is less dependent on the raw signal.

5.4 Pushout force and impulse measurement of seven types of small arms ammunition with three different surface states

5.4.1 Author's contribution statement

Michael Muster, Amer Hameed and Ralf Wahrenberg designed the study for this publication. Michael Muster performed the ballistic experiments. Peter Biedermann and Markus Hoffmann performed the FEA tests. Michael Muster analysed and discussed the data and wrote the paper with inputs from all authors

Michael Muster, first author
Centre for Defence Engineering, Cranfield University, Defence Academy of the United Kingdom
Shrivenham, SN6 8LA, UK
michael.muster@cranfield.ac.uk

Amer Hameed, second author
Centre for Defence Engineering, Cranfield University, Defence Academy of the United Kingdom
Shrivenham, SN6 8LA, UK
a.hameed@cranfield.ac.uk

David Wood, third author
Centre for Defence Engineering, Cranfield University, Defence Academy of the United Kingdom
Shrivenham, SN6 8LA, UK
d.wood@cranfield.ac.uk

Kilian Wasmer, forth author
Laboratory for Advanced Materials Processing, EMPA, Swiss Federal Laboratories for Materials Science and Technology
3602 Thun, Switzerland, CH
kilian.wasmer@empa.ch

Keywords: force, small caliber ammunition, momentum

Abstract

This study analyses the influence of lubrication treatments on the force absorbed by the breech. The results are of interest for weapon-safety and durability studies, especially when it comes to weapon maintenance.

A barrel-ammunition combination represents an expanding vessel under high pressure. The pressure rises from ambient up to 420 MPa in less than a millisecond. During such a highly dynamic process, purely static equations, describing the problem of the casing pushout force, may not be applied. Besides the dynamic behaviour, the surface properties and geometry also play a crucial role. To investigate the pushout force, a measurement system based on force washer was built. This system was validated using a crusher method and Finite Element Analysis. The impulse was calculated using the data of the measured force to obtain additional information about the force-time properties of the push-out behaviour.

Untreated ammunition and two lubrication systems: “ice layer” and “oil lubricated” as well as seven different ammunition sizes ranging from 5.56 and 12.7 mm were considered. The response was the force absorbed by the breech while the cartridge provides rear obturating to the combustion gases. It was found that both the casing geometry and its treatments have a significant influence on the pushout force.

5.4.2 Introduction to publication

This contribution aims to measure the influence of differently treated cartridge surfaces on the breech force in a range of small arms ammunition. Treatment types analysed were untreated, ice layer and oil lubricated. Ammunition types investigated were 50 Browning., 375 SWISS P, 338 Lapua Mag, 7,5 x 55 Suisse., 308 Win, 223 Rem and 9 mm Luger.

Because of safety and functionality reasons, the chamber of the weapon needs to be sealed by the casing during the process of firing. This sealing process also decreases the breech force. During the acceleration phase of the projectile, the casing experiences a dynamic environment. Under such circumstances, the cartridge casing can be considered as a pressure vessel, which undergoes a plastic deformation while the propellant burns in the chamber. The plastic deformation of the cartridge that prevents the rearward escape of firing gases between the weapon chamber and cartridge is called obturation and is closely related to the pushout force. For safety reasons, the obturation of the casing needs to produce a seal. Otherwise, unpredictable gap flows may occur, known as the dangerous burn-through or gas-wash phenomenon.

A thermodynamic gap flow investigation was made by Squire and Donnard [1]. They described the efflux of luminous gases at the weapon breech, which is abrasive and can lead to severe damage of the weapon. At worst, it can harm the rifle person. Squire and Donnard described the problem in detail, referring to classical melting theory. They investigated this experimentally by drilling a small hole in the head of the casing. They observed that even a minor scratch might result in a burn-through. This investigation was made with aluminium casings, which have a significantly lower melting point as compared to regular brass casings. However, the possible risks reveal the importance of a controlled obturation process guaranteeing the sealing of the pressure vessel system.

Hence, in recent years, several patent applications, describing possible technical approaches to solve the sealing problem of the ammunition barrel system for small-calibre ammunition [2], [3], but also large-calibre applications [4], [5], have been filed.

The obturation of the casing affects not only the sealing process but also has an influence on the force taken/supported by the breech. In the case when the pushout force exceeds a certain level, the breech can break, which leads to severe damage or even can harm the operator.

With a combination of internal pressure and the obturation, the casing is pushed against the wall of the chamber. In other words, it means that the overall pushout force is not entirely taken by the breech. The friction between the chamber wall and casing bears some of the overall pushout force. The friction between the interface boundaries is a crucial factor for breech force assessments, which is described in the literature, in particular for steel and brass systems. According to Aida [6], the static and dry Coefficient of Friction (COF) of brass and steel is in the order of 0.19 [6]. In the case of the oil lubricated and kinetic brass-steel combination, the COF is around 0.09, which is consistent with recent publications [7]. In terms of lubrication, it is found that thin water layers may also act as a performant lubricant [8]. However, lubrication is only one of the six main factors the breech force depends on; the other five factors are:

- The surface area of the case head where the pressure acts
- The pressure in the casing
- The friction between the chamber wall and the case body
- The material properties of the chamber and casing
- The chamber geometry, i.e. fluted or smooth

By controlling these five factors and measuring the pushout force, it is possible to get information about the effect of the lubricant on the obturation process during firing. Processes such as obturation are challenging to measure and are nowadays simulated using Finite Element Analysis (FEA) [9], [10]. The advantage of FEA is that numerous parameters can be investigated within one single model by sensitivity studies. With only minor changes in the model, one can analyse geometric parameters.

Besides numerical approaches, it is also possible to investigate the pushout force analytically at the breech, as suggested by Allsop et al. [11]. The extraction force equation can be used to estimate the pushout force. Such an approach is unsuitable for solving the dynamical problem of the obturation and cartridge sealing since only part of the analytical model can be applied. The main reason is that in the equation of Allsop et al., the friction is assumed to have a constant value. Specific properties of the propellant, such as pressure oscillations, described by Elkarous et al. [12], are neglected.

Several types of small-calibre ammunition are available for both military and law enforcement purposes. The most often-used cartridge type is the 9 mm Luger. This type of ammunition is standardised and utilised in pistols all over the world [13]. The most powerful calibre belonging to the family of small-calibre ammunition, exploited by many armies, is the 12.7x99 mm, also known as 50 Browning or 50 BMG. This calibre is mostly for the heavy machine gun Browning M2, which has its origins in 1918 [14]. The 50 BMG is especially worth for investigation since this ammunition type caused problems concerning the reloading cycle and breech/pushout force and was therefore profoundly investigated using FEA methods [15].

Besides FEA investigations, it is also possible to measure forces at the case head using force washers. Ritter et al. [16] measured the force on the igniter and pressure inside the cartridge with a piezoelectric force sensor. This provided confidence in predicting the behaviour occurring in the barrel chamber. They mentioned that the impulse has a significant influence on the system.

Sensors relying on the piezoelectric effect are often selected for standardised pressure measurements [17]–[19] and so are very suitable for ballistic investigations. However, ballistic pressure investigations rank among the most challenging types of measurement to be conducted.

These measurements were previously conducted using a simple copper crusher method. The copper crusher method consists of a copper cylinder which is deformed depending on the pressure produced in the chamber of the weapon during the firing process [20], [21]. Even today, the copper has its legitimation for cross- reference purposes. Elkarous et al. [22] investigated the sensing behaviour of two piezoelectric pressure sensors and compared the results with a copper crusher. They investigated the amount of deformation of the copper cylinders after the shooting tests, using FEA to obtain quantitative results about the pressure applied. An approach to apply the crusher method directly on the casing is to turn notches into the head of the casing. Similar to copper, the brass of the casing is also a highly defined material and can be investigated as the crusher method.

However, ballistic pressure measurements in the chamber of a weapon are regularly conducted for security assessments. In contrast, breech force measurements are rarely made, even though the breech is a main part of the weapon. The force on the breech has a significant influence on the firing process, weapon functionality, and safety. This paper confirms that the breech force depends significantly on the surface treatment, which is one of the relevant issues. Consequently, this study is a supplement to and enrichment of existing studies on diagnosis associated with the firing process for small arms ammunition.

5.4.3 Experimental procedures

Full Metal Jacket (FMJ) projectiles need a lower push-through force as compared to Monolithic (Solid) projectiles [23]. All types of ammunition were certified according to the most recent Commission Internationale Permanente (CIP) regulations [17]. The 9 mm Luger is the only casing without bottleneck design investigated. By comparing the bottleneck-type casings, the differences are in the angle and diameter-length ratio. For the ammunition, three surface states were selected; untreated, oil lubricated and ice layer and they can be seen in Figure 5-13b. The surface lubrications oil lubricated and ice layer are highly defined and may occur in real-world usage.

The oil lubricated case simulates the case where the ammunition might have some lubricant at the boundaries of the inner chamber of the weapon. This is the case when the weapon is cleaned and oiled before use. To oil lubricate the casings, a fluid referred to as Klübersynth MZ 4-17 was applied. This lubricant is recommended for the maintenance of small arms such as hunting and sporting rifles [24]. The casing surface was treated with 0.4 mg/cm^2 lubrication oil.

In contrast, the ice layer state reproduces the situation where the ammunition is significantly colder than the weapon so that it is possible that the ammunition condensates quickly. In this study, to investigate the ice layer treatments, the ammunition was cooled to -30 °C for 1 hour and then exposed two minutes to ambient temperature. This approach permitted to build a highly defined thin ice layer with a mass of 0.5 mg/cm^2, as shown in Figure 5-13b. The condensation process was controlled with an analytical balance (Mettler, Switzerland) and a stopwatch. The resulting water film is very thin and does not increase the gap between the chamber and the casing. Furthermore, it is melted immediately after putting it into the barrel.

The ammunition was first tested using an Electronic Pressure Velocity and Action Time (EPVAT) (HPI, Austria) measurement setup [25]; recognised by NATO and CIP testings. The amount of propellant is known from production certificates, and the casing surface can be calculated from the specific dimensions published in the CIP documents [17].

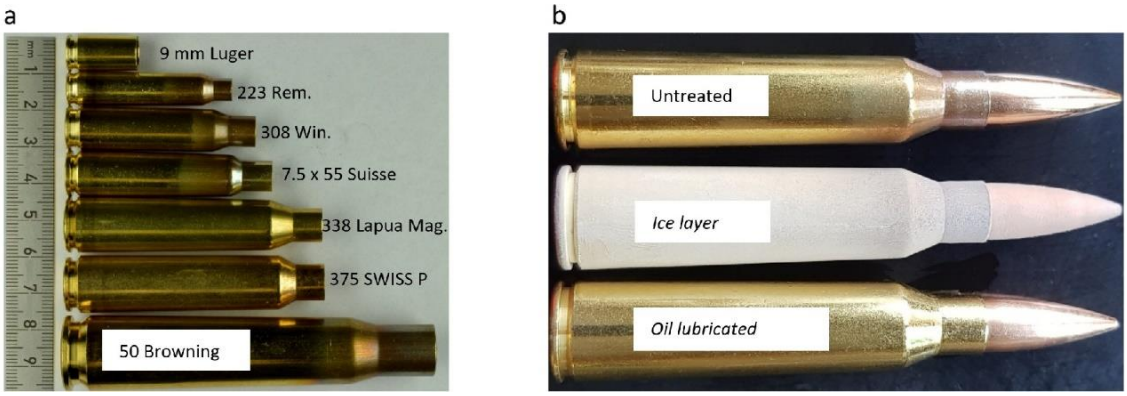

Figure 5-13: (a) picture of casings tested (b) picture of the different surface states.

Table 5-3: Specifications of the investigated ammunition types.

Name	Muzzle diameter [mm]	Bullet weight [g]	V_0 [m/s]	Muzzle energy [Joule]	Projectile type	Casing surface [mm^2]
50 Browning	12.70	48.5	825	16505	Solid	5219
375 SWISS P	9.50	22.7	850	8200	FMJ	3005
338 Lapua Mag.	8.60	16.3	860	6028	FMJ	2802
7,5 x 55 Suisse	7.50	11.3	780	3437	FMJ	1878
308 Win.	7.62	11.4	770	3380	FMJ	1654
223 Rem.	5.56	3.6	980	1729	FMJ	1152
9 mm Luger	9.00	8.0	365	533	FMJ	497

5.4.3.1 Piezoelectric measurements

The piezoelectric force measurement was conducted ten times for each ammunition type so that the reproducibility and associated errors are statistically relevant. The pushout force measurement device is similar to the EPVAT system, as shown in Figure 5-14. It includes an interchangeable proof barrel, rigid housing that is made of cast iron to reduce the effect of vibrations during shooting. In addition, it has a trigger device attached to the force measurement plate, which is shown in Figure 5-15, this acts at the same time as breech. The trigger device and the force measurement plate, which also serves as a breech, needs to be disassembled after every shot performed. The difference to a regular EPVAT system was that the breech was equipped with a force washer Kistler 9041a (Kistler, Switzerland), shown in Figure 5-15. This sensor has an Eigen frequency of 65 kHz and is capable of measuring short time events. A National Instruments USB-6366 (NI, USA) data acquisition device was used for all tests. A trustful time and amplitude raw signal were necessary for the impulse measurements. Hence, the data acquisition rate was 2 MHz (0.5 µs step size) with a 16-bit resolution. The impulse was calculated using the time integral of the force signal. The filtering of the acquired raw data was identical in all cases. The filtering was a combination of 20 kHz Butterworth low-pass filter is known from NATO standards concerning small-calibre ammunition [19] and an RMS signal envelope [26] with a step size of 170 samples. The filtering approach and the overall measurement system with a force washer are the same as the one described in Muster et al. [27]. The effect of this filtering as compared with the raw signal can be seen in Figure 5-16. The signal is not loaded with high-frequency parts over 20 kHz. However, the time property of the first rise remains persistent.

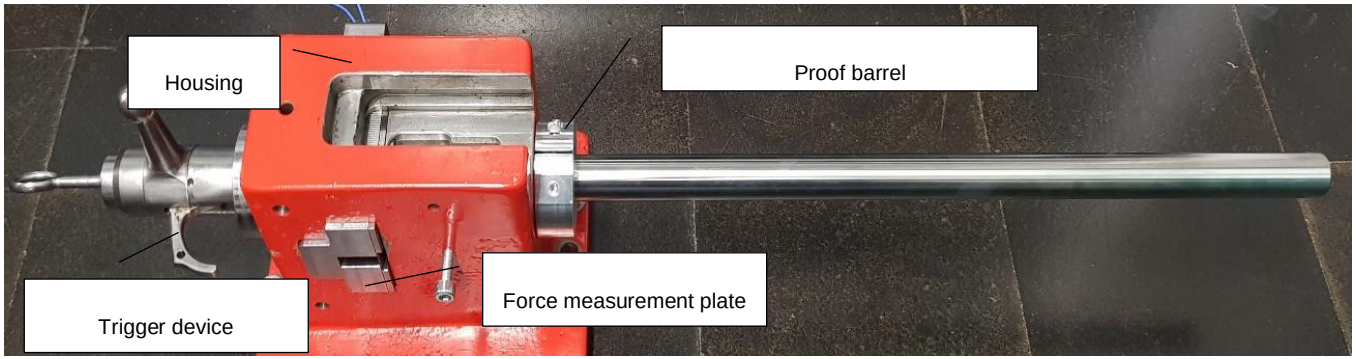

Figure 5-14: Measurement setup with a measurement plate.

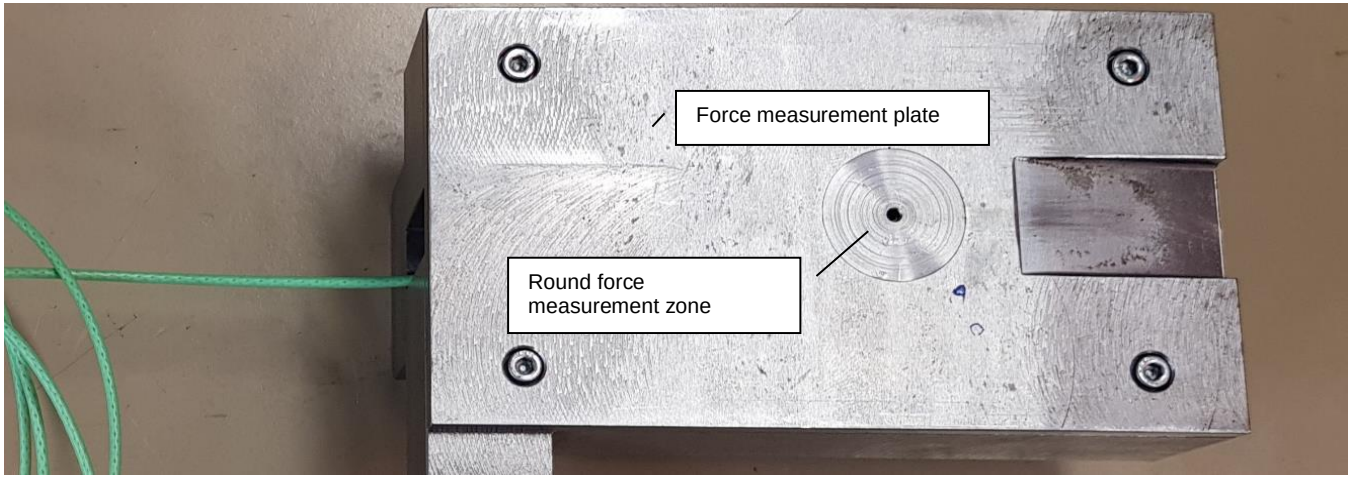

Figure 5-15: Force measurement plate which is at the same time a breech.

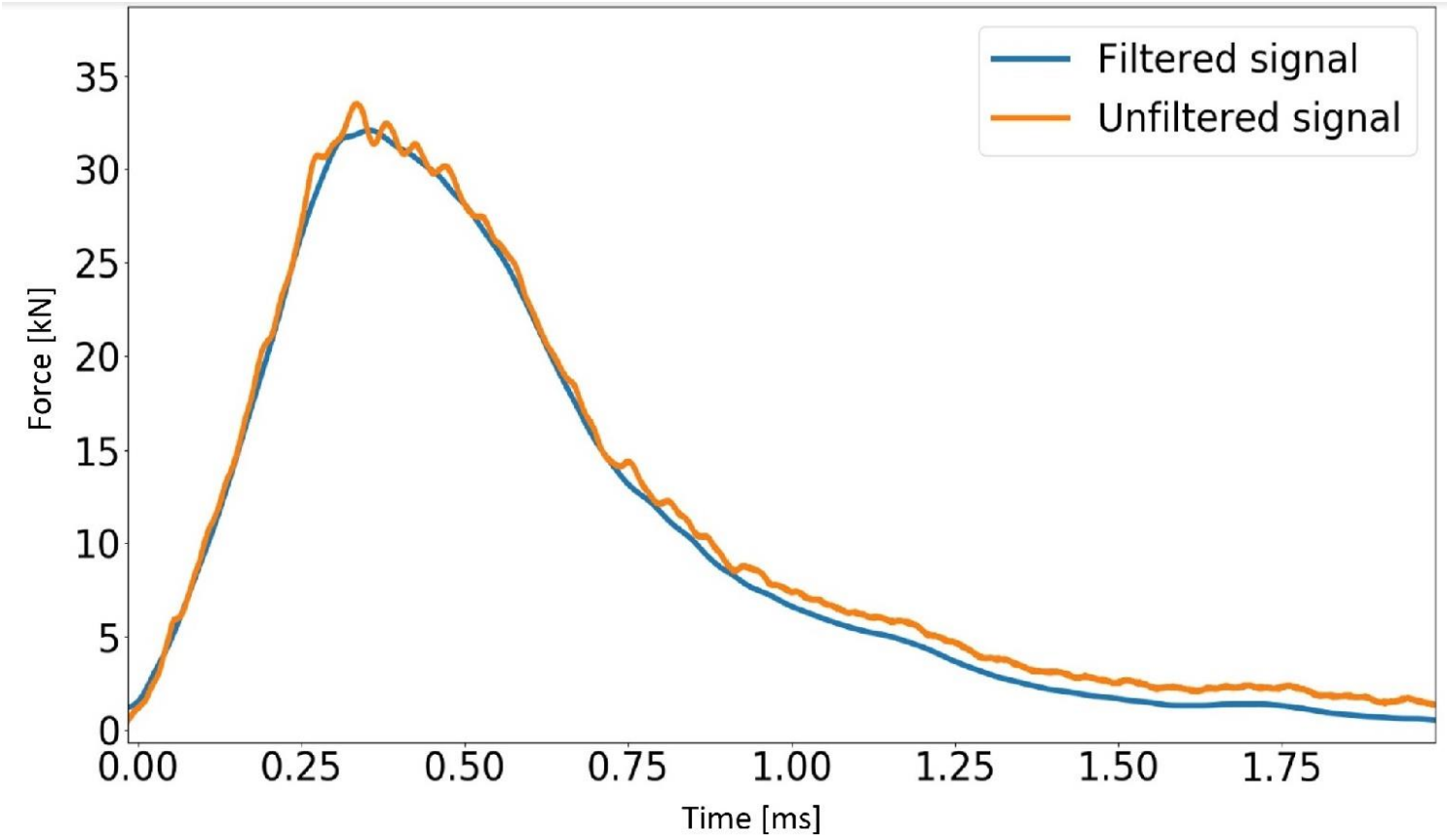

Figure 5-16: Typical force versus time curve of *oil lubricated* 308 Win ammunition. Filtered and not filtered. For the filtering process, a bandpass, RMS signal envelope approach was applied.

5.4.3.2 Case head crusher assessment

The 338 Lapua Mag. was chosen to conduct the cross-verification of the piezoelectric measurements for two reasons. First, it is a calibre mainly used in sniper rifles. Second, it has a rigid breech. Bolt-action rifles are with rigid bearings of main interest for pushout force and safety investigations. In addition, the 338 Lapua Mag. was assessed since it provides enough material at the casing head to drill notches, which is necessary for later crusher investigations. These notches have resulted in defined spikes, which deform under the high forces occurring during the firing process. This deformation was measured using an analogue microscope with a measurement X-Y table (Wild Heerbrugg, Germany).

The unloaded notch pattern of the case head, see Figure 5-17, was replicated using a CAD package of a FEA software. The FEA software applied for this investigation was FORGE® Version 4.6.2.1 (Transvalor, USA), optimised for metal forming processes [28]. The casing hardness was assumed to be homogenous with the constant hardness value of 180 Hardness Vickers (HV30). This drawn casing head was placed between two bearings, which were assumed to be fully rigid. A quarter symmetry model was constructed, to save computation time. The load was built up stepwise on a gradient, to obtain a force-step curve. No oscillations were assumed. The element and mesh size was set to "automatic”. The force was applied “static”, and the mesh for the analysis was generated automatically and dynamically. Each surface state type was assessed three times. With this approach, we were able to replicate the deformation under an applied force to obtain a semi-quantitative result. The reason for this verification system is the same as presented by Elkarous et al. [22], which is to obtain a result from a different measurement approach.

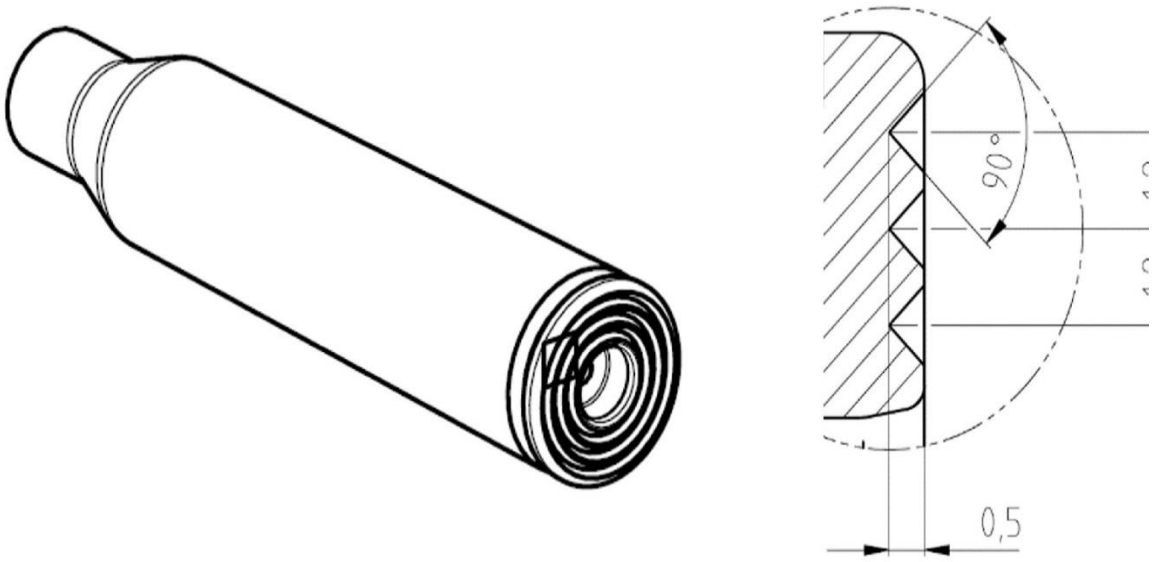

Figure 5-17: Modified "crusher" casing head using notches turned into the casing head.

5.4.3.3 Analytic calculations

Besides the crusher gauge and FEA, the calculated maximum force (F_{max}) is another straightforward method that can be used for an analytic calculation of the pushout forces of the ammunition types investigated. This method assumes that the maximum possible force is delivered on the breech. The calculation of the theoretical Fmax can be simplified since it depends only on two factors. The peak pressure (P_{peak}), a measured value, and the casing head diameter (DCH) see Figure 5-18, which is taken from the CIP regulations. Then, $F_{max} = P_{peak} * DHC$ and the results are given in Table 5-5. This maximal force scenario applies only if no obturation and no friction exists between the boundaries of the casing and the chamber. Under such circumstances, it is obvious that the theoretical F_{max} cannot be exceeded in real-world measurements and so must be taken as a maximum reference.

More complex equations for push-out measurements rely on several parameters such as the friction coefficient, materials, geometrical properties and the peak pressure [11]. These parameters are hard to measure during the experiment and so must be simplified. Another drawback of this approach is that the dynamic properties of the projectile acceleration process are neglected.

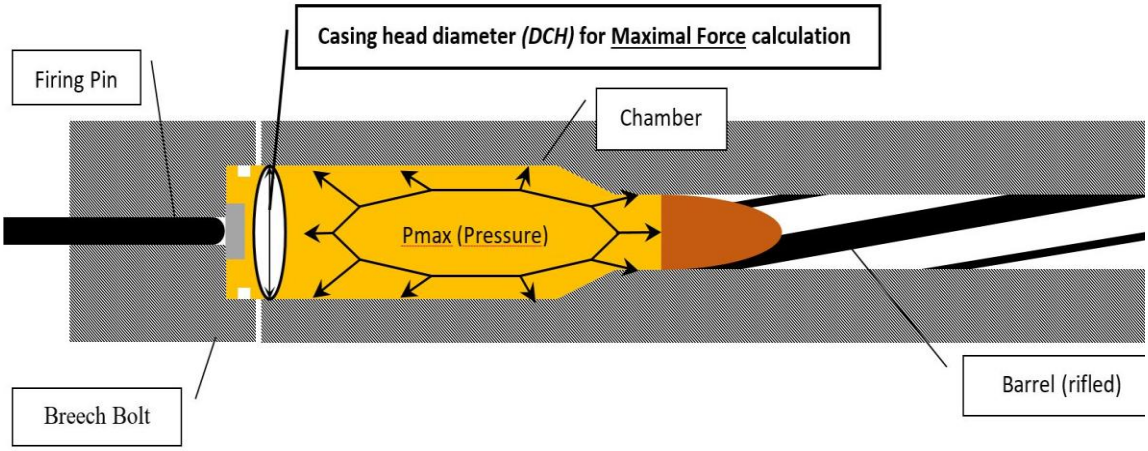

Figure 5-18: Schematic view of the barrel cross-section. The maximum possible is calculated according to $F_{max} = P_{peak}$ *·DCH.

5.4.4 Results and discussion

The results section are into two sections, the piezoelectric measurements and the case head crusher assessment. The piezoelectric measurements are divided into four parts. Single force curves according to the different ammunition types are presented. They give an impression about the force-time behaviour. Third, boxplots summarised the statistics of the acquired results. Finally, the measurements are then cross verified using a crusher method with FEA.

5.4.5 Piezoelectric measurements

Figure 5-19, Figure 5-20 and Figure 5-21 show typical pushout force vs time curves acquired with the force measurement instrument for the seven casing types. As expected, after firing, the forces increase drastically before decreasing gradually. Most of the sharp rise takes place within 1 ms, whereas the force decreases take places between 0.8 and 3 ms depending on the casing. The 9 mm Luger is the only casing without a bottleneck and has a unique push-out curve as compared to the other curves. After a short rising time, the maximum force (F_{peak}) measured is lower than the other casing type followed by a decrease to zero force within only one millisecond, and evidence of this is in Figure 5-19, Figure 5-20 and Figure 5-21. The reason is that 9 mm Luger proof barrel (100 mm) is much shorter as compared to the other barrels. In contrast, the .50 BMG has a much longer barrel (1200 mm), and this leads to longer acceleration time. The difference in acceleration time is independent on the surface state.

Figure 5-19, Figure 5-20 and Figure 5-21 are closely related to Table 5-4, which summarises the measured but also the calculated forces for the three surface states. The P_{peak} was acquired according to the CIP regulations. It represents the average value from the pressure maxima's of ten single shots. For each ammunition and surface state, F_{peak} was averaged over a set of ten shots and F_{max} was the maximum pushout force value in the system. This table also contains an important value which is defined as F_{peak}/F_{max}. This value shows the measured force in relation to the absolute maximal possible force (F_{max}). Also, one main relation between the figures and the table is the average force (F_{peak}), which is an average value of peak values of the force curve shown in Figure 5-19. This is a very artificial value, since there is always some obturation and friction in the system which lowers the push-out force.

In Table 5-4, no significant difference is observed in the average maximum pressure (P_{peak}) and F_{max} for the untreated and oil lubricated ammunition. In contrast, a slight difference (but significant) is visible in the Ppeak between the untreated and ice layer ammunition. This is because of the burning properties of the propellant and igniter that are affected during cold conditions.

The results of the untreated surface state are shown in Figure 5-19 and Table 5-4. In Figure 5-19, force oscillations, which are caused by the stick-slip effect, can be observed and was detected in all untreated surface states. Some oscillations are high in amplitude and reach up to 1/10 of the maximum pushout force; this affects the reproducibility of the measurements. For the untreated surface state, it is possible to identify three different casing groups. The first group is made by the 9 mm Luger only, which shows a sharp peak and reaches up to 72 % of Fmax, see Table 5-4. The second group is made of 375 SWISS P, 338 Lapua Mag., 308 Win and 7.5x55 Suisse. These casings showed a similar relation for F_{peak}/F_{max} values ranging from 42 and 61 %. The third group is worth mentioning as it comprises the largest and smallest projectile diameter investigated (223 Rem. and .50 BMG, see Table 5-4). These two ammunition types showed only 25- 26 % of the maximum possible pushout force, see in Table 5-4, which is a strong indication of a good obturation process. The reason for this behaviour might be the similar geometrical constraints of the casings; see the geometry of these two casing types (Figure 5-13a). For the untreated surface state, it is also to note that, although the 50 BMG has twice of the muzzle energy of the 375 SWISS P, see Table 5-3, the 50 BMG has lower pushout force as compared to the 375 SWISS P. Actually, the peak-force of the 50 BMG is reached more than 1.5 ms after the first signal rises. All other casing types reached the peak-force between 0.3 and 0.5 ms after. One reason is that the propellant used for this largest investigated caliber is less vigilant; this leads to delayed peak pressure. Another possible reason for the delayed peak-force is the stick-slip phenomenon of the ammunition; an effect that can be observed between 0.2 and 0.7 ms in the case of the 50 BMG.

In contrast, the 375 SWISS P produces the most significant force at the bottom of the casing (up to 49 kN), see Figure 5-19, a behaviour true for all force curves investigated in this work. This caliber reaches on average 53 % of the maximum pushout force, see Table 5-4.

The surface state ice layer influences not only the coefficient of friction of the casing but also the burning properties of the propellant. However, no significant difference concerning the pressure and velocity of the projectile was observed.

The ice layer surface state rises the pushout force significantly for every ammunition type and affects the obturation process. All ammunition types show between 73 and 97 % of the maximal force, which is remarkably high when considering the safety of the system. The ice layer state revealed significant influence on the force oscillations of all bottlenecked casings. All force signals are steadily rising and falling. Compared to the untreated surface state, fewer oscillations occur. The force signal from this surface state is comparable with the signal from the regular pressure measurements. The peak-force is correlated with the muzzle energy, which is an indication that the thin water layer affects the obturation process significantly. This is consistent with the statement of Paliy et al.[8], who reported that, under certain circumstances, water acts as a high-performance lubricant.

For the oil lubricated, a thin film Klübersynth MZ 4-17 was applied. The resulting push-out forces are comparable with those from the ice layer. However, for example, the 338 Lapua Mag. casings are subjected to fewer stick-slip effects; compare the green lines in Figure 5-20 and Figure 5-21.

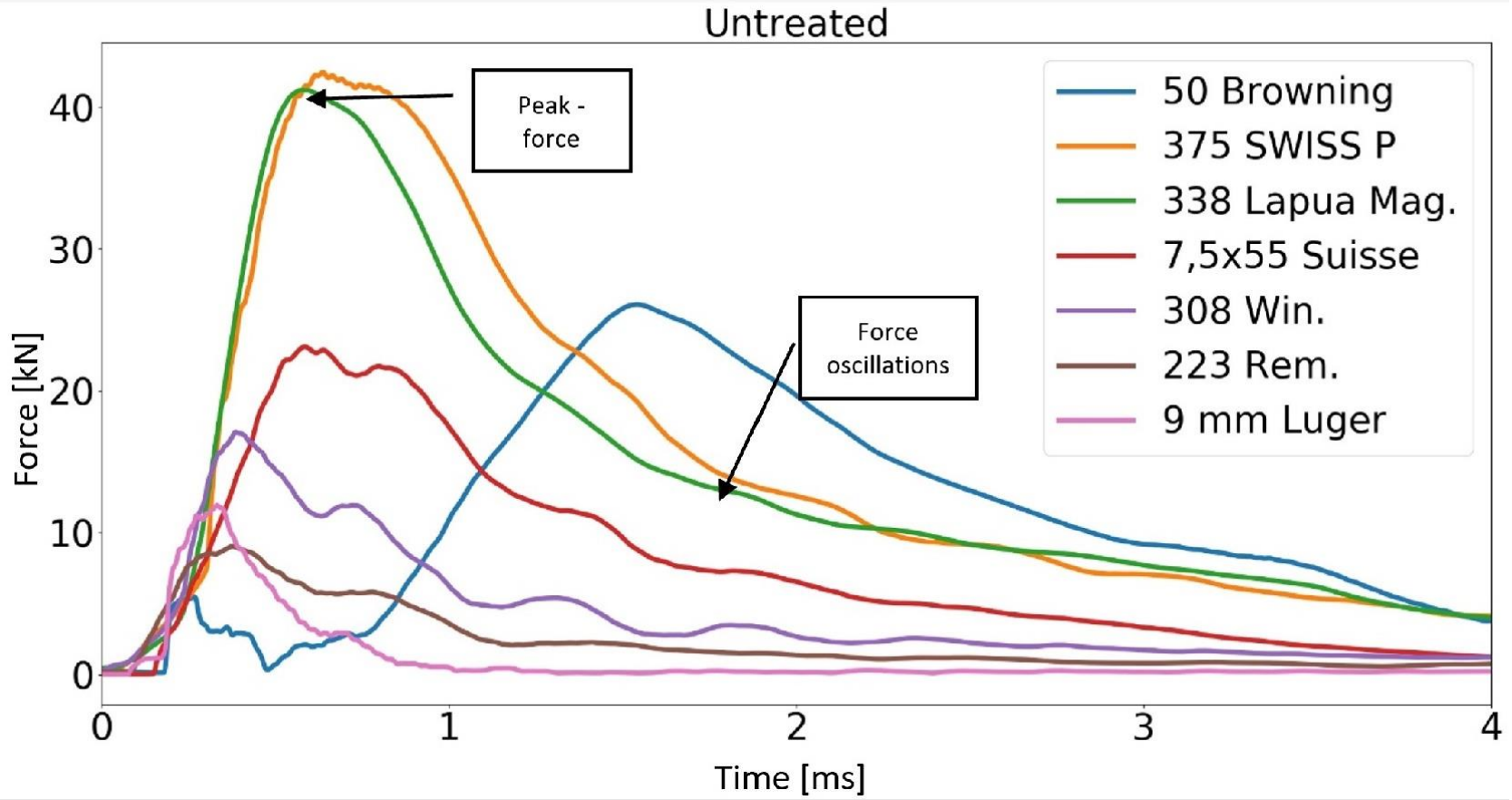

Figure 5-19: Typical force signals acquired from the untreated ammunition.

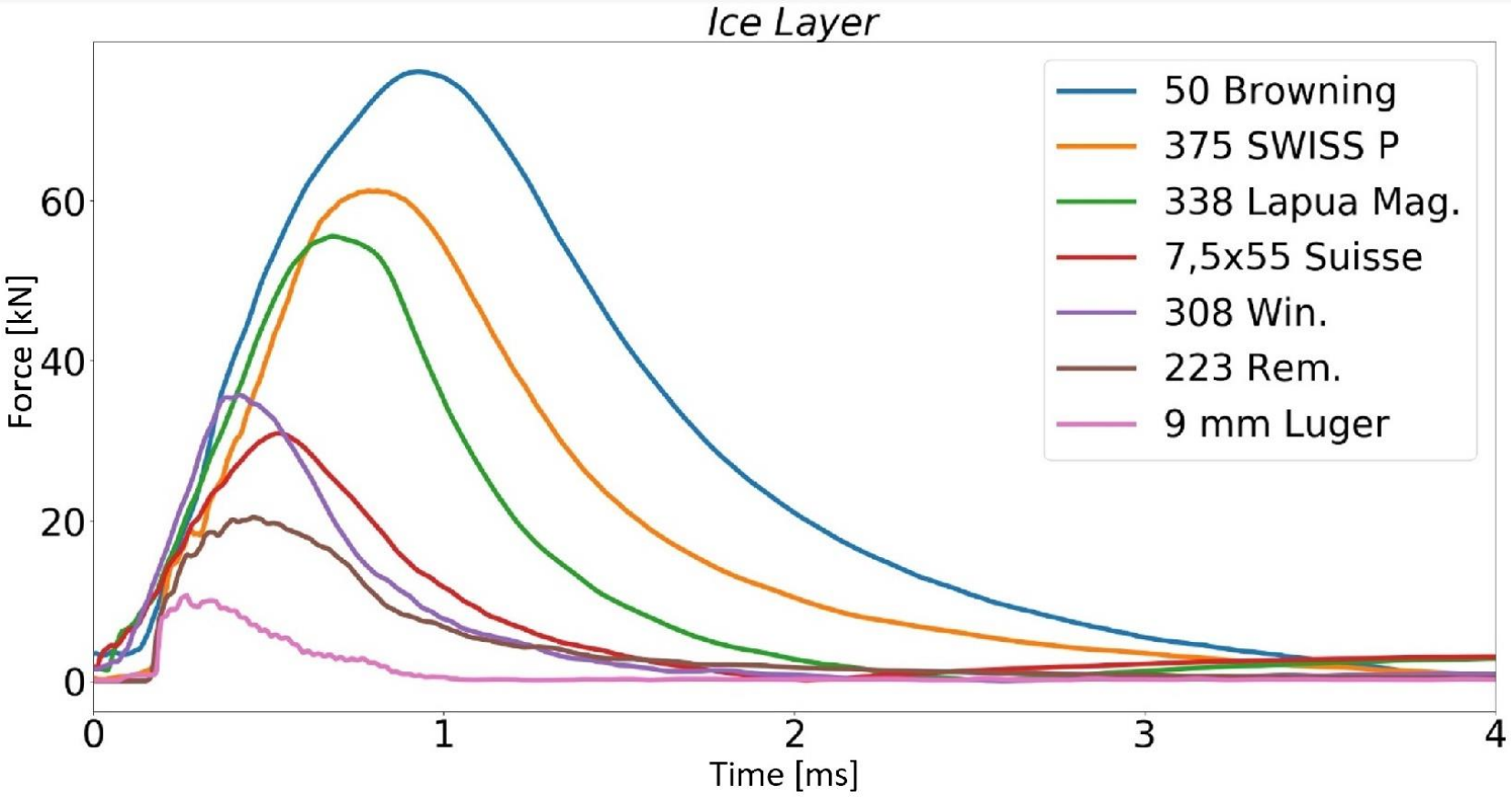

Figure 5-20: Typical force signals acquired from the ice-layer-treated ammunition.

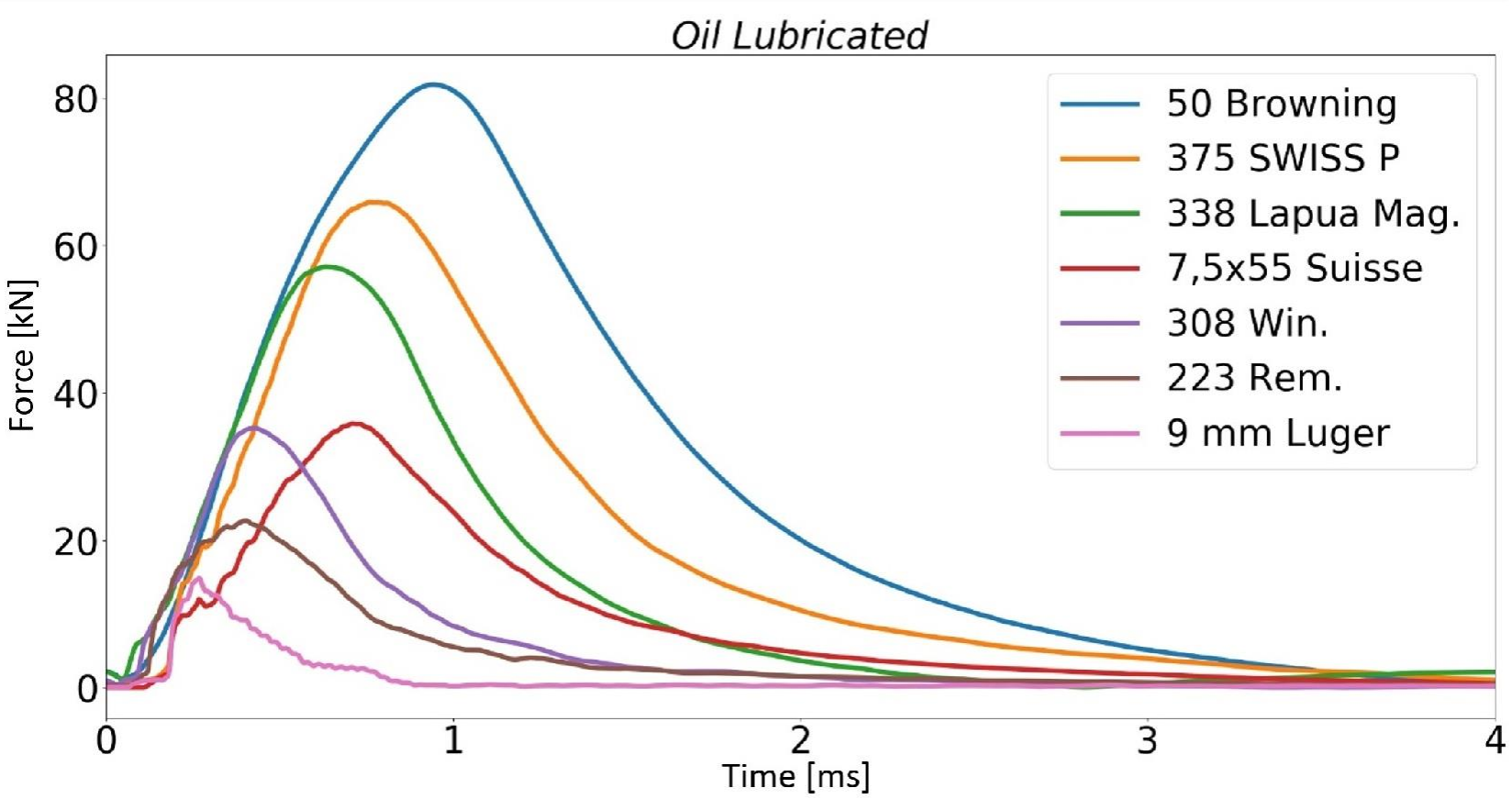

Figure 5-21: Typical force signals acquired from oil lubricated ammunition.

Table 5-4: Tabular representation of the measured properties. The "F_{peak}/F_{max} " represents a very meaningful value. A high value indicates that almost no obturation takes place and may affect weapon safety.

Cartridge	Surface state	F_{peak} [MPa]	F_{max} [kN]	F_{peak} [kN]	F_{peak}/F_{max} [%]
50 Browning	Untreated	310	102.0	25,00	25
	Ice Layer	305	100.0	85,38	85
	Oil Lubricated	310	102.0	85,38	84
375 SWISS P	Untreated	390	76.0	40,10	53
	Ice Layer	385	75.0	64,80	86
	Oil Lubricated	390	76.0	64,80	85
338 Lapua Mag.	Untreated	380	66.0	40,40	61
	Ice Layer	382	66.0	56,40	85
	Oil Lubricated	380	66.0	56,40	85
7,5 x 55 Suisse	Untreated	320	40.0	21,10	53
	Ice Layer	310	39.0	34,75	89
	Oil Lubricated	320	40.0	34,75	87
308 Win.	Untreated	330	37.0	15,70	42
	Ice Layer	315	36.0	35,00	97
	Oil Lubricated	330	37.0	35,70	96
223 Rem.	Untreated	400	29.0	7,50	26
	Ice Layer	390	28.0	21,60	77
	Oil Lubricated	400	29.0	21,60	74
9 mm Luger	Untreated	200	17.0	12,30	72
	Ice Layer	205	17,5	12,80	73
	Oil Lubricated	200	17.0	12,80	75

To compare the statistical results of the experiments, one decided to separate the ammunition into two groups: smaller and larger ammunition types based on their muzzle energy delivered. The smaller ammunition types were defined for ammunition delivering muzzle energy of less than 3500 Joule and the statistical results are given in Figure 5-22a and Figure 5-23a. The smaller ammunition types are normally used in self-loading firearms. In contrast, the larger ammunition types are delivering muzzle energy higher than 6000 Joule, and their statistical results are shown in Figure 5-22b and Figure 5-23b. These calibres are used by snipers and are often used in weapons with bolt-action. Bolt-action rifles with a rigid bearing are stronger affected by insufficient obturation processes and large pushout forces. A comparison of the different smaller and larger ammunition types are presented in the boxplots in Figure 5-22 containing the information about all force measurements performed in this study. They represent median, quartiles as well as extreme values.

We can see that the force delivered on the breech bolt increases in the treated surface states with increasing muzzle energy; compare Figure 5-22 with Table 5-4. For all bottleneck casings, it is seen that in the untreated surface state has a relatively low push-out force whereas the pushout forces for the treated surface states are significantly higher. The ice layer causes a less significant rise in the pushout force than the oil lubricated.

It is worth comparing the 7,5 x 55 Suisse with the 308 Win casings as both have almost the same muzzle energy values, and they are the only caliber investigated with interchangeable projectiles. However, the casing geometry differs slightly, which leads to different pushout force patterns. By comparing both casings, we can conclude that the overall geometry influences the pushout force. This observation of a geometrical dependency is supported by the different sized calibres 50 BMG and 223 Rem, see Figure 5-13a. They react with a similar force pattern on the surface state. The absolute force value and its spread are low in the case of the untreated surface, and both rise significantly after changing the surface state with lubricant. Some of the measured 9 mm Luger peak-forces are so high that they reach almost the calculated maximum possible force. In this case, the sealing of the casing in the chamber might break and thereby release some of the hot and highly compressed gas into the weapon. The scatter in the results of the non-bottlenecked 9 mm Luger is the largest as compared to all other types of ammunition investigated. For the bottleneck casings investigated, the 338 Lapua Mag. shows a large scatter.

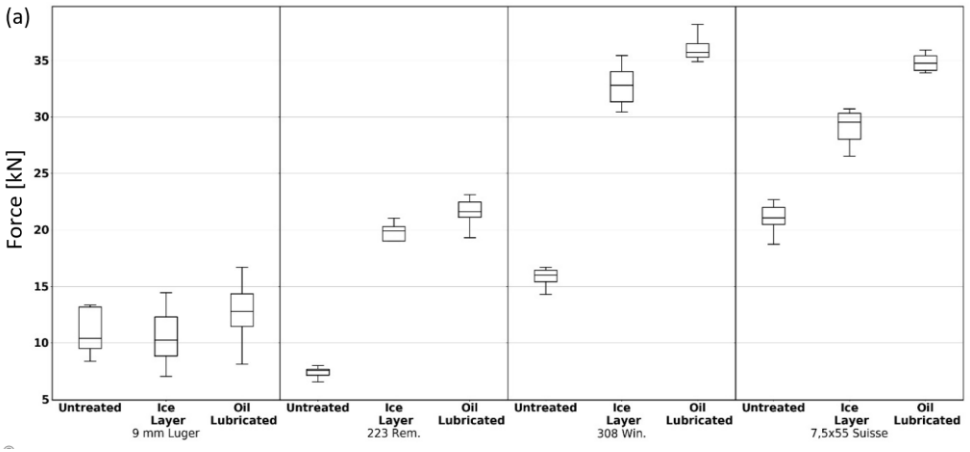

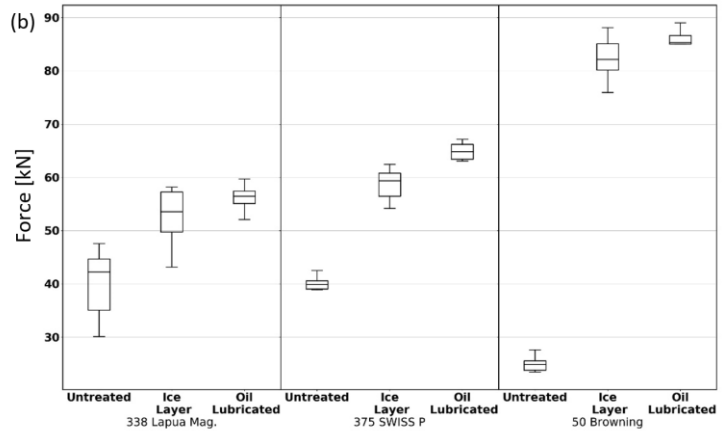

Figure 5-22: Force boxplots of the investigated caliber range, (a) represents the smaller cartridge types, (b) represents the larger cartridge types.

Figure 5-23 presents the results of the impulse transmitted to the breech. The impulse gives information about the duration of the force applied on the breech. This factor is meaningful because some breech systems like breech bolts are more sensitive when a load applies for a certain time. The impulse transmitted at the base is represented by the integral of the force-time curve, and it also depends on the length of the barrel. Based on Figure 5-23, no evident difference in the impulses was observed between the treated and untreated 9 mm Luger ammunition. The average impulses transmitted to the breech bolt varies between 7 and 59 Ns in the untreated surfaces states. This range is larger for the lubricated surfaces, which varies between 6 and 120 Ns. The lack of stick-slip effect in the treated surfaces prevent the chamber from taking big amounts of impulse leading to an enlargement of the range between min and max value. In contrast, all treated bottleneck casing types show a decrease in impulse variation. This decrease in impulse variation supports the theory that the barrel chamber cannot take significant amounts of impulse if the casings are treated.

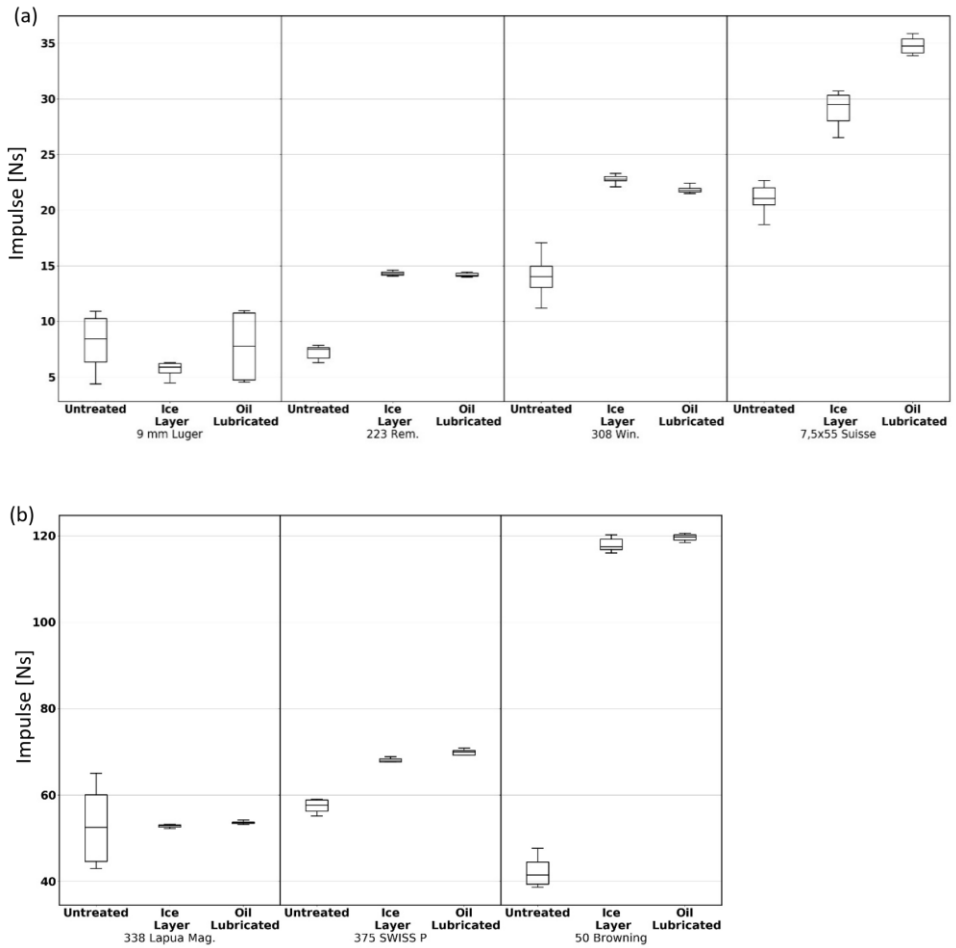

Figure 5-23: Impulse boxplots of the investigated caliber range, (a) represents the smaller cartridge types, (b) represents the larger cartridge types.

5.4.5.1 Case head crusher assessment

The case head crusher assessment for the .338 Lapua Mag. was used to cross-verify the electronic measurements. In such highly dynamic environments, there is a distinct possibility that parts or tolerances of the measurement system influence the quality of measurements themselves. The verification was conducted in a two-stage approach; via optical investigation and FEA. Figure 5-24 presents pictures of the case heads before firing (Figure 5-24a) and after for the three surface states. This optical investigation showed already noticeable differences concerning the casing-head deformation. For example, the less flattened ring contour in Figure 5-24d is due to the different hardness of the casing and is prominent in the outer ring.

Furthermore, the extraction groove supports the outer ring less effective. In a second step, the FEA was performed and their results compared with the force-washer measurements. The oil lubricated casing showed a less significant flattening of the casing head. However, this might be because of the intrinsic force spread of this calibre (338 Lapua Mag.). This is interesting since the flattening of the casing head might also lead to different internal ballistics or, in the worst-case scenario, affect the obturation process further. Such an effect was not observed in the presented study. Figure 5-25a shows the setup of the FEA, a rigid structure (black bearing) presses a simplified ductile case head against a rigid plate which is not represented. The results of the FEA are presented in Figure 5-25 for the three surface states, and the comparison is given in Table 5-5. The Crusher FEA average peak-force (F_{peak}) analysis is remarkably close to the measured F_{peak} by the force washer, and evidence of this is in Table 5-5.

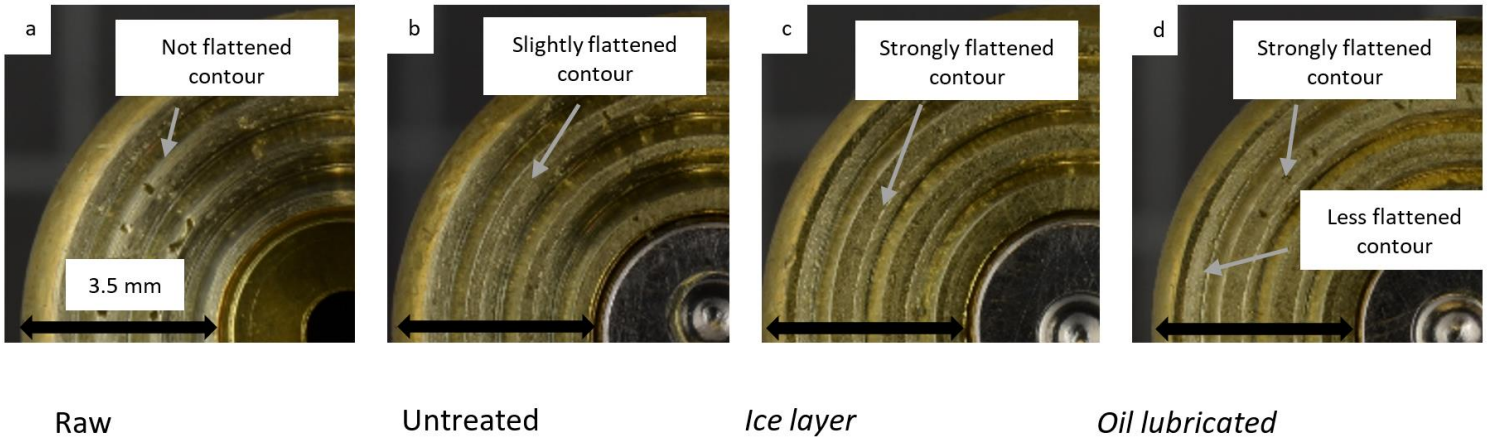

Figure 5-24: Pictures of flattened casing heads.

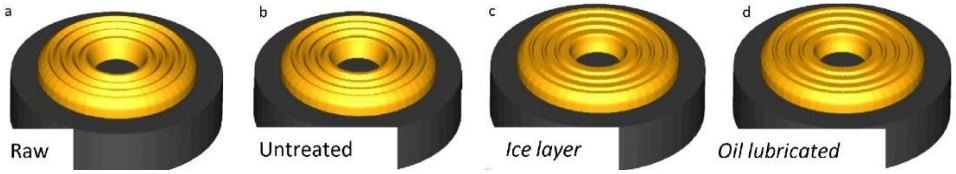

Figure 5-25: FEA recalculation of the flattened casing heads.

Table 5-5: Comparison of the semi-quantitative FEA measurements and the force washer experiments.

Surface state	Crusher FEA [kN]	from force washer [kN]
Untreated	35	40
Ice layer	58	56
Oil Lubricated	51	56

5.4.6 Conclusion

This contribution investigated the effect of casings and surface states on the push-out force and transmitted impulse. Seven casings (50 Browning., 375 SWISS P, 338 Lapua Mag, 7,5 x 55 Suisse., 308 Win, 223 Rem and 9 mm Luger) and three surface states (untreated, ice layer and oil lubricated) were selected. We established the pushout force, and transmitted impulse often depends on the surface state. Using lubricants such as water or oil increase the average peak-force (F_{peak}) up to a factor of 3.5 and affect the obturation process. These are safety-relevant features since a good obturation process is necessary to ensure the functionality of a weapon. However, large, oscillating and unpredictable loads on a breech, especially on the breech bolt may lead to its breakage and harm the operator severely.

We demonstrated that our proposed measurement system is suitable for analysing a wide range of forces and impulses in small arms weapon systems. It has been validated using a case-head crusher method, aided by FEA. The three different surface states; untreated, ice layer and oil lubricated showed that already small changes on the ammunition surface have a significant influence on the pushout force and so on the obturation process.

The geometry of the casing, also, influences the pushout force to a major extent, which is valid for all sizes of bottleneck casings. The investigated non-bottlenecked casing (9 mm Luger) behave differently concerning the overall spread of the momentum or push-out force. The acquired results can be used to estimate the maximum force at the breech, which is a very important and safety-critical factor in the design and operation of a weapon.

The dispersion of the impulse is reduced in all surface-treated bottleneck casings. This is a secure sign that for the lubricated surface state, no stick-slip phenomenon occurs and that the obturation process has a minor influence on the pushout force.

The recommendation to users is to apply lubricant during barrel maintenance but to remove the lubricant before firing. To weapon manufacturers, the relevant recommendation is that a weapon should be capable of withstanding at least the maximal possible force which depends on the maximal possible peak pressure and the diameter of the case head. A gap between the breech and casing head leads to strong collisions between the two during weapon firing.

5.4.7 Acknowledgement

I want to express my thanks to RUAG Ammotec AG, Switzerland, for making the test facilities available. The use of measurement devices would not have been possible without the great help of Markus Gruenig and Gregoire Pache. I am also grateful to Markus Hofmann and Peter Biedermann, who contributed their expertise in the “casing crusher method” and FEA simulation.

5.5 Publication references

[1] W. H. Squire and R. E. Donnard, “An Analysis of 5, 56mm Aluminum Cartridge Case Burn-Through Phenomenon,” Natl. Techical Infomation Sevice, Philadelphia, 1972.

[2] D. Carpenter, H. Engel, B. Recchia, and P. Shipley, “Ballistic sealing, component retention, and projectile launch control for an ammunition cartridge assembly,” 2012.

[3] B. Peterson, E. Carlson, A. Moser, and H. Lawrence, “Projectile Assembly with Stabilization Enhancement,” 2015.

[4] P. Morin *et al.*, “Case Base for Large-Caliber Ammunition,” 2002.

[5] U. Wagner, H. J. Limburgerhof, K. Henrici, H. ; Kuessner, K. Volkamer, and E. Fuerst, “Self-Obturating, Expellable Cartridge Case,” 1982.

[6] R. Aida, “Measurment of Coefficient of Static Friction of Metals,” *Sci. reports Res. Institutes, Tohoku Univ. Ser. A, Physics, Chem. Metall.*, vol. 2, pp. 380–395, 1950.

[7] M. A. Chowdhury, D. M. Nuruzzaman, A. H. Mia, and M. L. Rahaman, “Friction coefficient of different material pairs under different normal loads and sliding velocities,” *Tribol. Ind.*, vol. 34, no. 1, pp. 18–23, 2012.

[8] M. Paliy, O. M. Braun, and S. Consta, “The friction properties of an ultrathin confined water film,” *Tribol. Lett.*, vol. 23, no. 1, pp. 7–14, 2006.

[9] D. K. Kankane and S. N. Ranade, “Computation of In-bore Velocity-time and Travel-time profiles from Breech Pressure Measurements,” *Def. Sci. J.*, vol. 53, no. 4, p. 351, 2003.

[10] J. T. South, K. Dipak, and M. Minnicino, “Small Caliber Modeling From Design to Manufacture to Launch,” in *23rd Int. Symp. Ballist.*, 2007, April, pp. 557–564.

[11] D. F. Allsop, *Brassey’s Essential Guide to Military Small Arms: Design Principles and Operating Methods*. Brassey’s, 1997.

[12] L. Elkarous, M. Pirlot, J.-C. Golinval, and M. Maldague, “Investigation on gas pressure measurement inside small caliber weapons with piezoelectric transducers,” *Meas. Sci. Conf. 2012*, pp. 1–8, 2012.

[13] G. Langer, “Neue Polizeimunition,” *PVT*, pp. 1–3, 2004.

[14] M. Thommen, “Browning Machine Gun, Caliber .50 12,7 mm Mg 64,” in *Gesellschaft für Waffen und Militaria*, 2006.

[15] D. Gubernat and C. Fischer, “Explicit finite element model for determing influence of cartridge case material properties on small caliber weapon function,” *Proc. 26th Int. Symp. Ballist.*, pp. 806–817, 2011.

[16] J. J. Ritter, R. A. Beyer, and A. Canami, “In-Chamber Primer Force and Case Pressure Measurements of the 5 . 56-mm Cartridge,” *Army Res. Lab.*, vol. ARL-TR-586, no. 1, 2012.

[17] “CIP (Commission internationale permanente pour l’épreuve des armes à feu portatives).” Bruxelles, 2019.

[18] “American National Standard Voluntary Industry Performance Standards for Pressure and Velocity of Shotshell Ammunition for the Use of Commercial Manufacturers,” *American National Standards Institute*. 2015.

[19] AEP-97, *Multi calibre manual of proof and inspection (M-C MOPI) for 5.56 mm, 7.62 mm, 9 mm and 12.7 mm ammunition*, vol. 23, 2013.

[20] C. E. Waters, “Technologic Papers Bureau of Standards,” p. 26, 1921.

[21] F. I. Du Pont, “Ballistic gun.”, 1906.

[22] L. Elkarous, F. Coghe, M. Pirlot, and J.-C. Golinval, “Experimental techniques for ballistic pressure measurements and recent development in means of calibration,” *Journal of Physics: Conference Series*, vol. 459, no. 1, 2013.

[23] L. White and J. Siewert, “Final Report of the Rifling Profile Push Test,” 2007.

[24] “Klübersynth MZ 4-17,” pp. 3–4, 2014.

[25] “Defence Standard 05-101 Part 1 Proof of Ordnance, Munitions, Armour and Explosives,” no. 1. MoD, 2005.

[26] C. Jarne, “An heuristic approach to obtain signal envelope with a simple software implementation,” pp. 1–9, 2017.

[27] M. Muster, A. Hameed, and D. Wood, “Dynamic qualitative bolt force measurements for investigating influence factors on the pushout effect of small calibre ammunition,” *AIP Adv.*, vol. 9, no. 6, 2019.

[28] P. De Micheli *et al.*, “Towards the simulation of the whole manufacturing chain processes with FORGE,” *Proc. Int. Conf. ‘New Dev. Forg. Technol.*, pp. 1–25, 2015.

5.5.1 Connection to the next chapter

This chapter deals with the pushout effects of different ammunition types. It revealed essential findings for weapon design purposes and further considerations. It also showed the lubrication- dependent pushout force which can affect the breech bolt of a weapon. This is of interest for the weapon and eventually the operator's safety.

The ricochet measurement is of relevance to operational safety. Even if the fundamental research question remains the same, the next chapter elucidates the terminal ballistics.

Besides this change from internal to terminal ballistics, the next chapter is a consolidation of the knowledge developed in this thesis. The knowledge about a signal processing of short- time physical events from chapter 5 as well as the knowledge about ballistic momentum measurements are applied to the next chapter.

The measurements described in this chapter are highly reproducible. This is because internal ballistics needs to be as reproducible as possible for the sake of weapon functionality and precision. However, this is not the case in the next chapter devoted to the ricochet, which is, in general, not a well reproducible ballistic phenomenon, as it depends on many factors.

Although signal processing and the evaluation of the ballistic event are interlinked in this and the next chapter, one needs to connect to chapter 4 as well. It is only with the power-law profiled damping plate that, the ricochet measurement device can be built up. This is because of the filtering requirements of the terminal ballistic impact since the ricochet is less reproducible and experiences even higher decelerations.

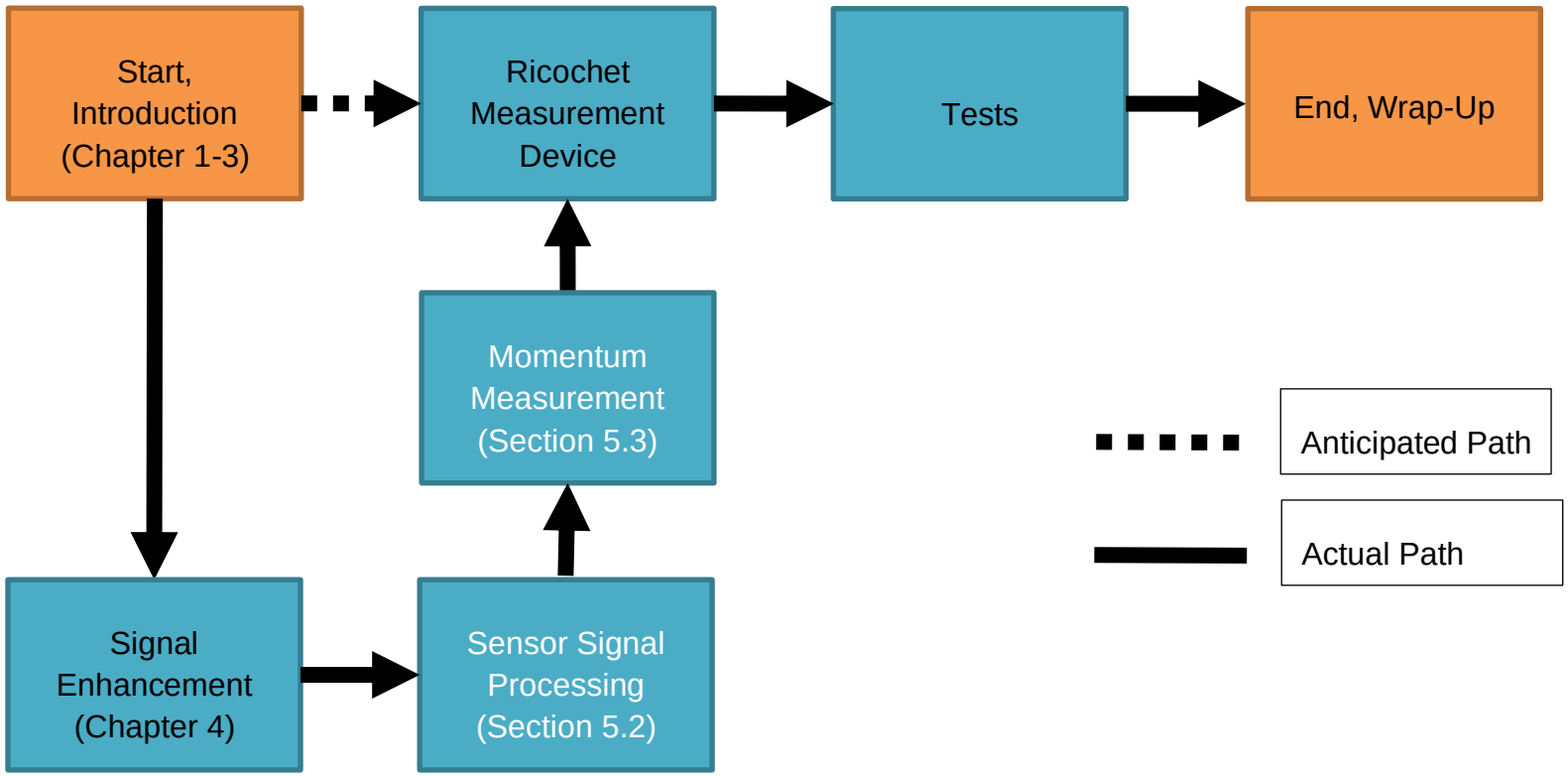

Figure 5-26: Comparison of the anticipated path and the actual path in relation to the chapters presented in the thesis.

5.6 Conclusion of chapter

The significant outcome of this chapter is the high-frequency measurement capabilities of piezoelectric sensors. Piezoelectric sensors are capable of measuring ballistic processes independent on the sensor purpose. Piezoelectric strain gauges deliver comparable signals to force washers and accelerometers. The measurement range of the sensor is very linear and thus applicable to a wide range of forces accelerations and momentums. Due to this fact, the investigated sensor concept is also suitable for ricochet measurements.

6 Ricochet quantification using a multiple sensor approach

6.1 Introduction to chapter

This chapter deals with the overall measurement system. It is a combination of all previously generated knowledge. The concept of the ricochet measurement device is proved using piezoelectric shock accelerometers and two damped sensor plates called ricochet plate and witness plate. Besides the measurement device, the ricochets of different projectile designs of 5.56 mm ammunition are investigated in this chapter.

6.2 Author's contribution statement

Michael Muster performed all measurements, Amer Hameed was involved in planning and supervised the work. Michael Muster processed the experimental data, performed the analysis, drafted the manuscript and designed the figures. Marlies Jenni manufactured the ammunition samples under the supervision of Michael Muster. Michael Muster wrote the manuscript. Amer Hameed aided in interpreting the results. All authors discussed the results and commented on the manuscript.

Michael Muster, first author
Centre for Defence Engineering, Cranfield University, Defence Academy of the United Kingdom
Shrivenham, SN6 8LA, UK
michael.muster@cranfield.ac.uk

Amer Hameed, second author
Centre for Defence Engineering, Cranfield University, Defence Academy of the United Kingdom
Shrivenham, SN6 8LA, UK
a.hameed@cranfield.ac.uk

David Wood, third author
Centre for Defence Engineering, Cranfield University, Defence Academy of the United Kingdom
Shrivenham, SN6 8LA, UK
d.wood@cranfield.ac.uk

Keywords: Ricochet analysis, small-calibre ammunition, velocity measurement, thermography

Abstract

This study investigates the ricochet behaviour of three different types of small arms projectiles using a novel ricochet measuring device. The results can be used to estimate the danger potential of ricochets on shooting ranges. A ricochet is a projectile or parts thereof changing direction and velocity after impacting an oblique surface. This impact produces strong vibrations in a rigid plate. During this impact, flexural waves travel radially outwards from the point of impact. These waves are used to determine the properties of the impactor with accelerometers situated on the target surface. With the use of two measurement plates, it is possible to produce a ricochet and detect its velocity at the same time. Accelerometers are suitable for accurate momentum measurements of single impacts. However, depending on the strike velocity and the impact angle, a ricochet can separate in multiple fragments after being deflected. From the operational safety perspective, these fragments must be detected, also. The concept of a coupled sensor was chosen to solve this problem. Thermographic sensors were additionally used to visualise the heat produced by the penetration of a rubber layer applied to the front surface of the steel target plate. With this approach, one was able to detect the position of the impact. The investigations showed that the measurement system's performance is better if a multiple sensor design is used, which includes accelerometers for the velocity, impact strength and partly the position measurement; In contrast, the thermographic sensor takes care of the position measurement and partly the momentum measurement. The investigated ammunition showed a plausible fragmentation behaviour, and the results can already be used to estimate the danger potential of different ammunition types.

Frangible projectiles fragment into small particles after deflection already under a small angle. Full Metal Jacket projectiles with or without a steel core, on the other hand, do not fragment under angles of less than 5°. The objective of the paper is to demonstrate the possibility of measuring the complex ricochet mechanics of small projectiles using standard accelerometers coupled with adequate signal processing techniques. The measuring system relies on an off-the-shelf thermographic camera.

6.3 Introduction to publication

This work aims to investigate the performance of a novel measurement device capable of measuring ricochets of small-calibre ammunition. Small arms are extensively used during manoeuvre-based operations.

Any high-speed fragment ricocheting from fragmenting projectiles is a safety hazard for personnel operating in the vicinity. It is essential, therefore, to evaluate the potential danger zone of ricocheting particles generated by projectiles.

Small-calibre projectiles are objects that weigh from 2 to 10 g, which travel at supersonic speed and produce strong acceleration signals on impacting an object such as witness plate which are used for ballistic investigations. Due to their high speed and rotation rates, projectiles are generally challenging to characterise during flight and impact, even with high-frequency sensors.

Sensors mounted on small arms projectiles, for ballistic tests, would be too bulky and affect the flight path. Ricochet characterisation is necessary for important applications like the estimation of range danger areas of shooting ranges. For the desired applications, one needs to know the position of impact and the momentum transmitted into the plate. To be known are also the time and distance between the first and second impact, where the ricochets are finally stopped. Using this information, one can measure the residual energy, fragment weight and deflection angle of the projectile after impact, as well as the velocity.

The velocity can be derived easily by using a Time of Flight (TOF) approach with two trigger devices. In the proposed system, the two sensor plates are considered as trigger devices. However, the procedure is similar to the well-known trigger-foil system, which is often used to trigger ballistic events such as, e.g. ballistic events in high-speed imaging [1] or general investigations like multiple impacts [2]. The idea behind foil triggers is that two electrically conductive foils (preferably of aluminium) are set up directly behind each other. During the penetration process, a short circuit is generated which can be used as a trigger.

Using two trigger devices, and with the known distance between them, one can calculate the velocity by applying the TOF. This approach is shown by Yan *et al*. [3].

The triggering system in the case proposed here relies on wave propagation in the plate material. The idea is similar to the acoustical approach described in the notes of Michael Courtney [4]. He investigated the time of flight with a high-resolution microphone and placed this microphone equidistant between the target and the barrel muzzle. With the known distance between target and barrel muzzle, plus the time difference of the two acoustic signals, one could recalculate the mean velocity of the projectile. The acoustic signals coming from the muzzle burst, and the impact sound burst when the projectile hits the target (in this case, a steel plate). The main challenge for in detail impact quantification on steel plates has to do with enormous decelerations and significant deformations in a short time. This is why sensors mounted on witness plates, in the proposed case of steel, are widely used for impact detection.

Impact detection units with plates rely on, e.g. Impact Soft-Recovery Experiments [5]. In this case, the target under investigation is a brittle plate, monitored by an interferometer. The projectile's impact generates strong vibrations, which can be used to characterise the nature of the impact. Espinosa *et al*. [6] revealed that it is possible to get a cleaner raw signal from the target plate by using a star-shaped geometry. Their tests showed that one could significantly minimise the effect of the outer layer of the plate on the impact zone itself. Like interferometers, accelerometers are frequently used to determine properties of the impact, such as the impact position or the momentum [7]–[9]. One of the major sources of measurement inaccuracies are random and reflected vibrations [10]. Hammetter *et al*. used an array of accelerometers fixed on the plate to determine the momentum transferred. He showed that geometrical properties of the detecting plate itself might lead to inaccurate measurements.

Another source of measurement inaccuracy is electronic filtering of the acceleration data. As a best practice for shock investigations, accelerometers are mechanically insulated [11]. Severe mechanical shocks such as bullet impact typically lead to six degrees of freedom accelerations represented in broadband frequencies. These frequencies make it difficult to determine the overall momentum [6] or the position. Mechanical insulators combined with electrical filters were found to be an appropriate way to overcome this problem.

The impacting body excites the witness plate within a very short time in a non-linear and random vibration regime, where scattering and reflections of vibrations at boundaries occur [12], [13]. Right after the impact is the moment where the point of interest occurs, this moment is called the Arrival Time (AT). The AT is defined as the time when the sensor detects the first set of waves, which originates from the impact position.

Consequently, knowing the accurate AT is necessary to recalculate the exact impact position with the Time Difference of Arrival (TDOA) algorithms [14]. TDOA algorithms are nowadays often used and optimised for passive tracking of wireless communication systems [15]. However, the underlying computations for wireless devices tracking and the impact location are the same. The main issue for an accurate triangulation of impact remains accurate AT detection. For flexural group waves travelling in steel at a speed of over 2500 m/s, even minor time errors lead to significant positioning errors. Knowing the speed of sound in the target material and the AT difference are necessary for positioning. Furthermore, by knowing the sensor positions, one can calculate the location of the impact/of the origin of the waves by numerical approaches [16].

Mingzhou *et al*. showed the possibility of precisely detecting the AT of flexural waves using accelerometers after the impact of a dropped test weight on a large steel plate. This investigation was done in noisy environments like power plants [17]. They used a sophisticated decomposition algorithm combined with the Hilbert Huang Transformation. They found that the proposed algorithm was capable of detecting the AT with a precision of several milliseconds.

The main reason for the inaccuracies was still the noise in the signal. In an idealised case, to lower the noise, flexural and compression waves emitted from the origin of impact would not be reflected.

Using a plate significantly larger compared with the investigated area (this approach is presented in [13]), or using a special damping plate with wave filters can be used.

An interesting approach is a plate of unique shape with decreasing thickness at the edge (called a wedge shape) in a power-law profile [18]. The different waveforms are eliminated due to internal refraction. However, the power-law shape is challenging to manufacture, which is why it is not used in practical vibration dampers [19].

Possible approaches to manufacture this wedge shape are 3D milling or casting [20], which are cost-intensive. Where hardened steel and supersonic impacts are concerned, such delicate and large structures are unsuitable for ballistic applications. For impact analysis, shapes for more robust structures are desirable.

For hardened steel wear plates suitable to resist supersonic impacts, 2D shapes should be used. Waterjet cutting or plasma cutting could produce such plate designs. Possible shapes that can be manufactured easily are any polygons or any round but two-dimensional shapes.

Star-shaped (polygonal) flyer plates are also able to trap compression waves, as used for standard impact soft-recovery experiments [6]. In the star-shaped plate, much lower-level reflection is observed during impact, which enhances the quality of the raw data in ballistic tests. The edge morphology is capable of serving as a trap for waves and was investigated computationally in [21].

A combination of star-shaped damping plate, enhanced by using an acoustic black-hole shape for ballistic investigations, is proposed by Muster *et al.* [22]. A witness and ricochet plate like this are capable of measuring the momentum of an impact accurately.

For more accurate projectile impact position investigations, especially for multiple impacts, it makes sense to search for a different solution. Manrad and Doty [23] describe in their patent an application which captures an impact on an elastic screen which heats up during the penetration process of the projectile. The idea of the patent is to calculate the exact impact coordinates of a single impact. Using this information, it is possible to get a real-time signal out of the computations, which the operator may apply during the most realistic possible training. The information about heating up is used to calculate the virtual trajectory of the projectile, not to make any statement about the impact. The process of heating up and the amount of energy transmitted into the screen are not of interest. However, it shows the basic idea and the performance of such thermographic systems.

Thermography in ballistics is also often used to investigate failure mechanisms in composite structures [24]–[26]. The reason for using high-speed thermography is that different materials of the composite structure are heated for a short time during the penetration process, and this can affect the matrix material, which is often thermoplastic or epoxy resin. These thermal differences are only of short duration and need to be investigated by high-speed thermography.

However, thermography has also its benefits for the investigation of materials like ballistic composite structures, without the need for frame rates over 30 per second. Gopalakrishnan *et al*. [27] showed that it is possible to investigate the damage point of impact on a ballistic sheet impacted by a medium-velocity body using a 50 Hz camera. The studied material with fibres acts more like a monolithic material, as can be seen in the picture taken after several milliseconds.

Another interesting approach to investigate materials using low frame-rate thermography is shown by Duan *et al*. [28]. They described a system, which assesses the material after damage. They took a general heat source and heated the specimen. This heating-up process was filmed with a low-framerate thermal camera.

The outcome was that, with this low-cost approach, it was possible to investigate the failure in the specimen itself accurately. The accuracy was better compared to the state-of-the-art ultrasonic transmission assessment. Soonkyu *et al*. [29] described a way to inspect wind turbine blades with the use of a laser and thermography. Fractures on large blades are assessed by laser preheating. In case, the damage is allocated to the surface, the specific heat capacity changes. The blade with the damaged zone heats up faster. With such a system, the defect can be precisely detected and investigated.

The sought sensor system is a combination of Gopalakrishnan with the low-framerate thermography of impacts, combined with a similar approach of Soonkyu *et al*.. During the penetration of a rubber layer, an impacting projectile dissipates its kinetic energy in lower form by producing heat. This heat is stored so that it can be seen for several seconds after impact.

To increase the positioning accuracy of multiple impacts, a thermographic sensor is used additionally. With this combination, a measurement device can be realised, which is capable of working with all kinds of projectiles and quantifying their ricochets. To get a broader picture of the accelerometer measurements, a second sensor type is used as a so-called piezoelectric strain gauge. Thanks to their broadband signal acquisition capabilities, these sensor types can identify the condition of large structures [30].

This paper describes a sensor method for ballistic analysis using two plates equipped with four acceleration sensors and a thermographic sensor in combination with a witness rubber layer. The momentum measurement of the projectile or its ricochets is made with specially shaped plates equipped with accelerometers capable of measuring uniaxial accelerations. They are placed in a normal position relative to the plate, which means that only flexural waves will be measured.

6.4 Material and methods

The ricochet measurement device consists of two main parts. The schematic idea of the system is described in Figure 6-1.

A heavy ricochet table which is attached to a pushcart with reliable brakes to ensure that it does not move due to the impact see Figure 6-2a and b. The table can be adjusted in height and angle. The ricochet plate is equipped with accelerometers to localise the point where the projectile touches the plate for the first time and deflects the projectile depending on the angle of the plate.

Second, a heavy metal frame, see Figure 6-2c and d, equipped with a second sensor plate at the back, called witness plate. The witness plate is significantly larger than the ricochet plate because the spread of the second impact (from the deflected projectile or its fragments) is significantly larger compared with the first impact. The weight of the metal frame is 950 kg. This is necessary due to the strong impulse transmitted into the system during impact.

Each of the two plate types (ricochet and witness plate) is equipped with four accelerometers. The acceleration sensors are designed for severe-shock investigations up to 100,000 G 350B01 (PCB, USA) [31]. These sensors are mechanically filtered to prevent overshooting oscillations [11] and augment the capabilities to detect the incident first flexural wave. A piezoelectric strain gauge type 740B02 (PCB, USA) is also mounted on the witness plate to crosscheck the sensor signal of the accelerometer, see Figure 6-3. The sensor plates are equipped with damping structures, which can be seen in Figure 6-2a and c.

The ricochet plate has three major tasks, namely the deflection of the projectile, the position measurement, and the exact time measurement when the projectile impacts the first time. The momentum transmitted into the ricochet plate is also measured during impact, but this is not this plate's primary task. The momentum measurement in the witness plate is more in focus.

The witness plate's tasks are to measure the momentum and the exact point-in-time. The measurement capabilities of the witness plate need to be augmented by a thermography camera. This, because it is complex to locate different impact positions at the same time using just four accelerometers. This capability is needed because a ricochet can consist of several simultaneously impacting fragments. The thermography camera shows on the rubber screen the heat produced when a piece penetrated the thin rubber layer. The material used for the layer was a special silicone of Shore hardness 60. The layer was 0.6 mm thick. A typical picture of several impacts, which penetrated the thin rubber layer, can be seen in Figure 6-4. These impacts were by subsonic projectiles weighing less than 3 g each. This penetration process showed already significant heating of the layer.

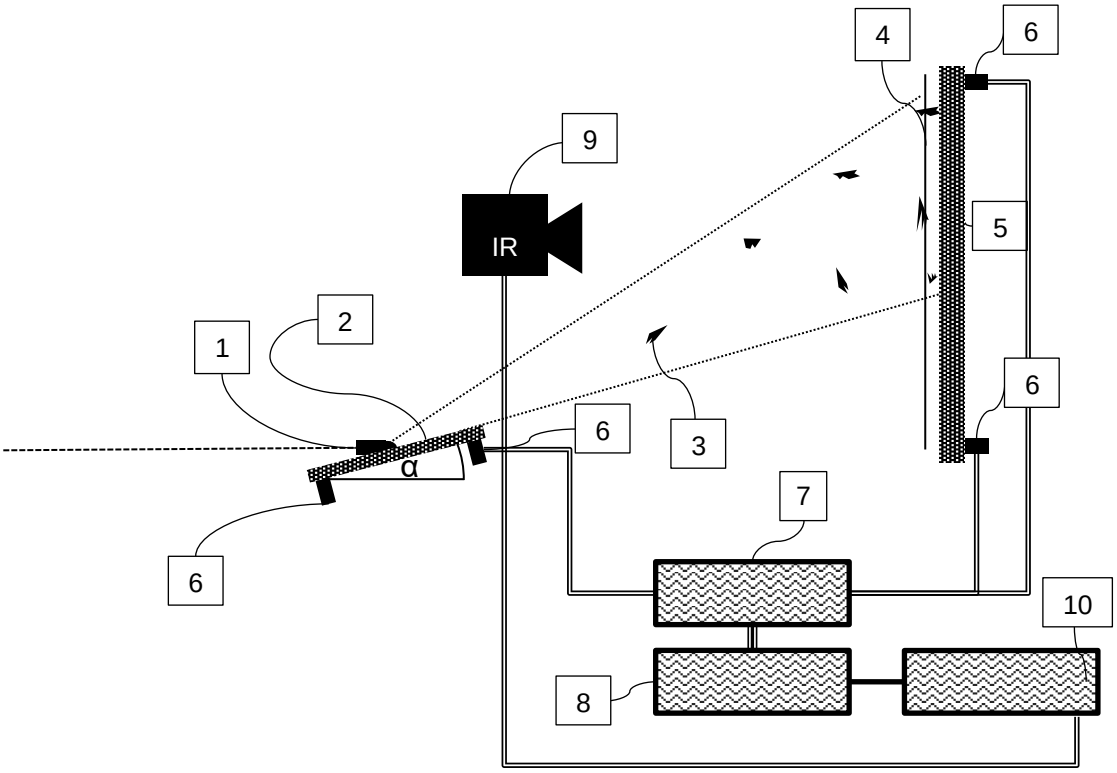

1. Projectile 2. Ricochet Plate 3. Ricochets 4. Rubber layer 5. Witness Plate
6.Accelerometers 7.Conditioner 8. Data Acquisition 9. Thermographic 10.Processing

Figure 6-1: System layout: Under an incident trajectory, the projectile (1) impacts on the ricochet plate under the angle α . 0° means a fully flat plate 90° means a direct impact (2). The deflected fragments (3) fly in the direction of the rubber layer (4) and penetrate it. After penetration, the fragments get stopped on the witness plate (5) which is, like the ricochet plate, equipped with four accelerometers (6). The raw signal of the accelerometers is first conditioned (7) so that it can be digitalised by the Data Acquisition Device (8). The rubber layer, heated up during the penetration process, is observed under thermographic (9) to determine the point of impact with the help of the raw signal of the accelerometers. All signals are processed in the processing unit (10).

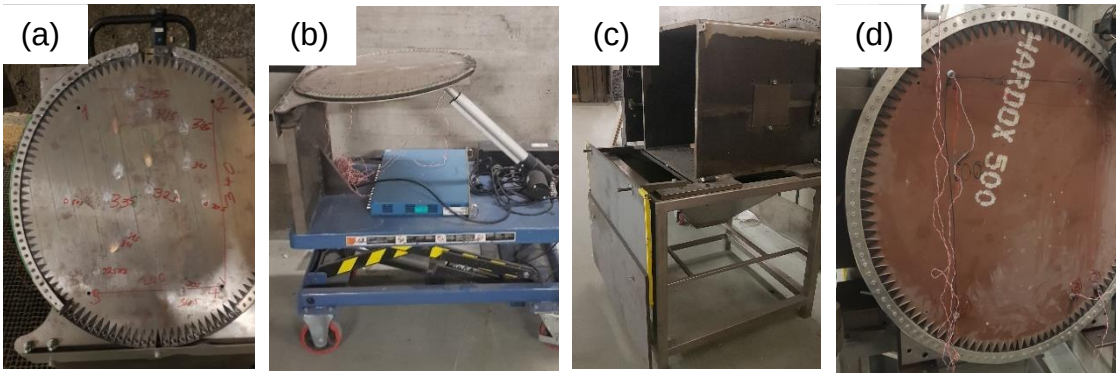

Figure 6-2 a-d: Picture (a) shows the ricochet plate. The spikes of the plate are damping structures which allow a better AT detection, which is important for the precise triangulation. The measurement area is 340x200 mm, (b) is the ricochet plate assembled on the pushcart. In this picture, the impact angle is just 2°. The structure of (c) represents the heavy metal frame to which the large witness plate is screwed (d). The witness plate has the same type of spikes at the boundaries for damping purposes. The size of the measurement area is 600x345 mm.

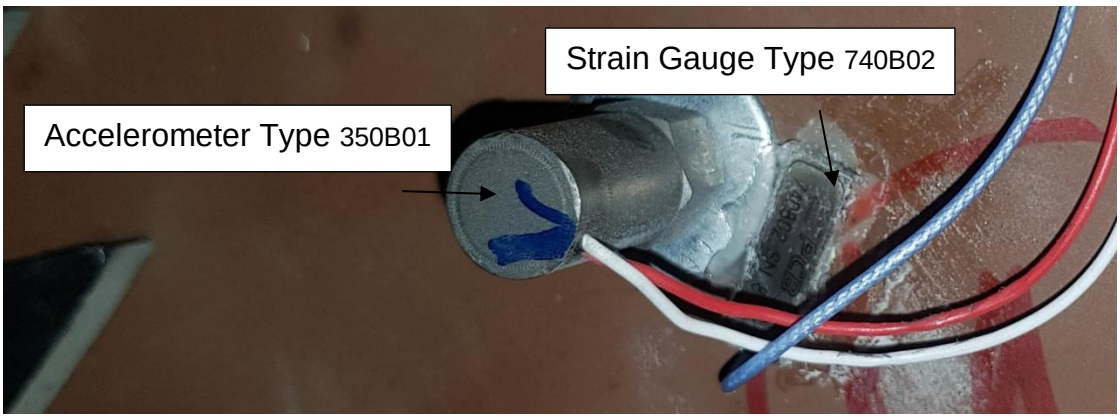

Figure 6-3: Accelerometer strain gauge assembly on the witness plate.

Three different ammunition types of the same calibre are investigated, as shown in Figure 6-5. They have a projectile diameter of 5.56 mm, and the length of the casing is 45 mm. This calibre type was chosen to investigate the influence of the tilt angle of the ricochet plate and the different ricochet behaviour of the particular designs.

The first projectile tested is different projectile in that; it is a 5.56 mm training ammunition weighing 2.9 g. This projectile is optimised for fragmentation, see Figure 6-5a. It consists of copper particles and a polymer matrix, called a frangible compound. These projectile types are described less often in the scientific field. The brittle material can cause severe wounds if a person is hit by this projectile type [32], [33]. For the ricochet investigation, it is an unorthodox and interesting projectile.

The second projectile type tested is the SS109, which is common and investigated extensively by tests [34] or simulation [35]. The primary reason for the development of the SS109 was to enhance the penetration capabilities of the 5.56 mm projectiles [36]. It also has a Full Metal Jacket (FMJ), but additionally features small steel core in the front of the projectile, shown in Figure 6-5b. Such double-core projectiles can act differently compared to a purely lead-filled FMJ when it comes to ricochet behaviour. The steel core can fly longer distances compared with the other projectiles. The weight of the SS109 of 4 g is the heaviest investigated.

The third ammunition type (M193) is used is a well-defined NATO standard ammunition stock number [37]. The M193 has been extensively investigated by several researchers studying terminal ballistics[38] and [39]. The M193 is a standard FMJ, see Figure 6-5c, which makes it also a reference for ricochet measurements. The weight of the projectile is 3.6 g.

Figure 6-4: Thermal picture of 4 impacts with .22LR, the rise in temperature is approx. 10 °C which can easily be detected.

According to the presentation of Rottenberger [40], typical deflection angles for ricochets are 5°, 10°, 15° and 25°. Chosen for this investigation were the angles 5°, 10°, 15°, 20° and 25°. The test scope was the same as presented by the ricochet analysis of Rottenberger [40] and according to the ricochet investigations of Mattijssen and Kerkhoff [41]. Each ammunition and tilt-angle test scenario was performed five times, which means that 45 tests had to be made. The distance between the ricochet plate and the witness plate was on average 180 cm. The length was measured after every shot and noted.

The ammunition was tested with a system similar to the Electronic Pressure Velocity and Action Time (EPVAT) measurement setup [42] known for NATO tests. The National Instruments (NI, USA) USB-6366 data acquisition device was used for the tests. It can simultaneously acquire and record one set of data points every 0.5 µs. The piezoelectric accelerometers are capable of measuring frequencies up to 35 kHz. The raw data with a signal amplification rate of 1 was acquired without filter, using the PCB-482C05 (PCB, USA) signal conditioner. The data acquisition time was set to 20 ms. As the signal of interest was approx. 4 ms, this acquisition time was sufficient. The pre-trigger was set to 0.1 ms. to increase the accuracy and redundancy of the measurement. The velocity was first measured ten times using a projectile light gate B471 (HPI, Austria). During the ricochet measurements, the velocity was also measured before the projectile impacts, this using a small LS260 Light Gate (Kurzzeit, Germany).

The ricochet and witness plates were calibrated with 9 mm Luger calibration shots. A standard 9 mm projectile was accelerated to different velocities, from 290-350 m/s. The upper limit of the transmitted momentum was investigated using an SS109 projectile for both plate types. Both plate types were made of Hardox 500 tempered steel plate exhibiting a yield strength of 1300 MPa as a target [43]. They are regularly used for devices which are resistant to impacting supersonic projectiles [44].

This measurement was also verified by a fast-flying frangible projectile which transmitted the same momentum as the M193. All projectile types impacted orthogonal on the plates to ensure that the impact is fully inelastic. The systems can only be calibrated accurately on the assumption that the impact is inelastic. The thermal image was taken by a SeeK Compact PRO (SeeK, USA) camera. The focus of this investigation was more on the fragmentation behaviour than on the accurate triangulation. However, it was also an objective to prove that such a system can be used to enhance the positioning of impacts. The signal processing approach of this ballistic impact was the same as presented by Muster et al. [45]. An RMS envelope with low-pass filtering was applied for both detection systems, the positioning and the momentum transmitted, see Figure 6-6.

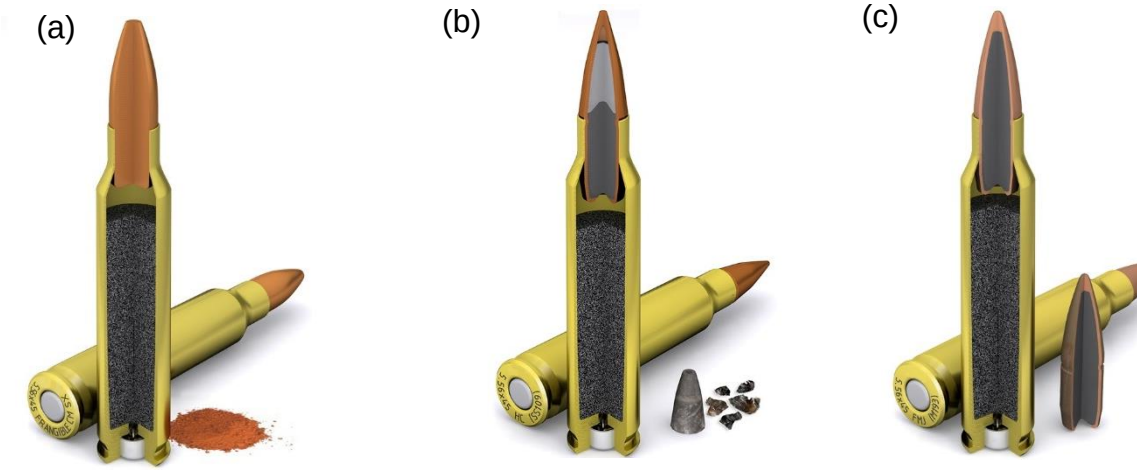

Figure 6-5: Picture of the three ammunition types investigated. Figure 4c represents the regular FMJ projectile (M193), (b) represents the SS109 projectile with a hardened steel core. However, the basic design is still a lead core and a metal jacket. A different approach is described in (a). Frangible projectiles are just copper particles with a matrix, which should be transferred again to copper particles after hitting a hard target.

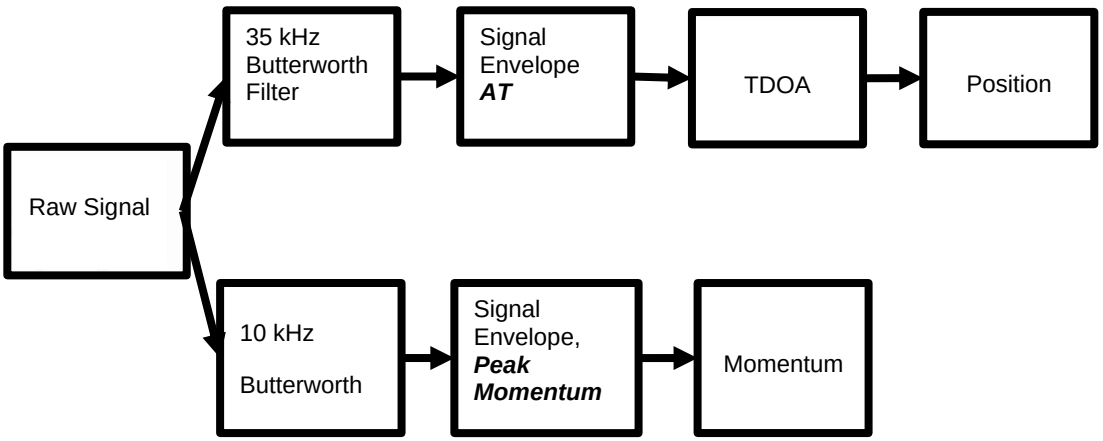

Figure 6-6: Signal processing of the raw accelerometer data.

6.5 Results

The raw data acquired from a typical accelerometer and strain gauge signal is presented in Figure 6-7. The strain gauge signal rises to approximately ten µs before the accelerometer signal. This earlier rise is due to the strain gauge being slightly more sensitive than the accelerometer. However, the strain gauge shows a negative offset after being excited for one millisecond. This behaviour is even more present in the filtered case, as Figure 6-8 shows. The time of the rise of the strain gauge signal is still similar to the accelerometer signal, which is important for cross-proofing purposes.

However, the strain gauge has a significantly longer recovery time compared to the accelerometers. This dynamic offset makes the sensor unusable for momentum detection. However, the first excitation, which is vital for the AT detection, is prominent. The AT of all four accelerometers on one plate is represented in Figure 6-9. The signal rises with some small sinusoidal variations. These variations are not present in the case of the strain gauge. However, the accelerometer shows a better overall performance for the performed ballistic test scenarios.

Figure 6-10 shows a typical accelerometer signal pattern of the tests. An M193 projectile generated this pattern under an impact angle of 15°. The first four accelerometer signals are from the ricochet plate, and they rise significantly higher compared with the second set of peaks, which come from the witness plate. This difference in maximum acceleration comes not only from the different impact strength but also from the different stiffness's of the plates. The ricochet plate is 12 mm thick, the witness plate 30 mm. The distance between the two impacts divided by the time difference between the two sets of waves determines the ricochet velocity.

This triangulation process of the ricochet plate is more straightforward compared to the witness plate because the pre-processed acceleration signal rises strongly. The arrival time is detected by a simple threshold trigger. The acceleration pattern of the witness plate is loaded with different peaks and, just on proper AT, not visible, see Figure 6-10. This pattern gives already an indication that a separation of the projectile took place, or that the projectile flies under a stronger precession and impacts diagonally. Positioning on the witness plate can be measured more accurately using a thermographic camera.

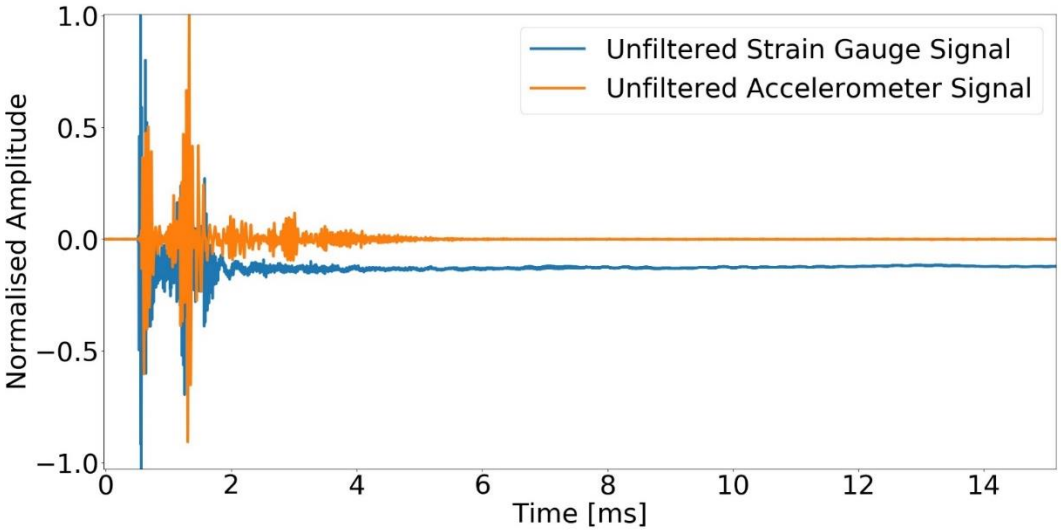

Figure 6-7: Unfiltered accelerometer /strain gauge signal.

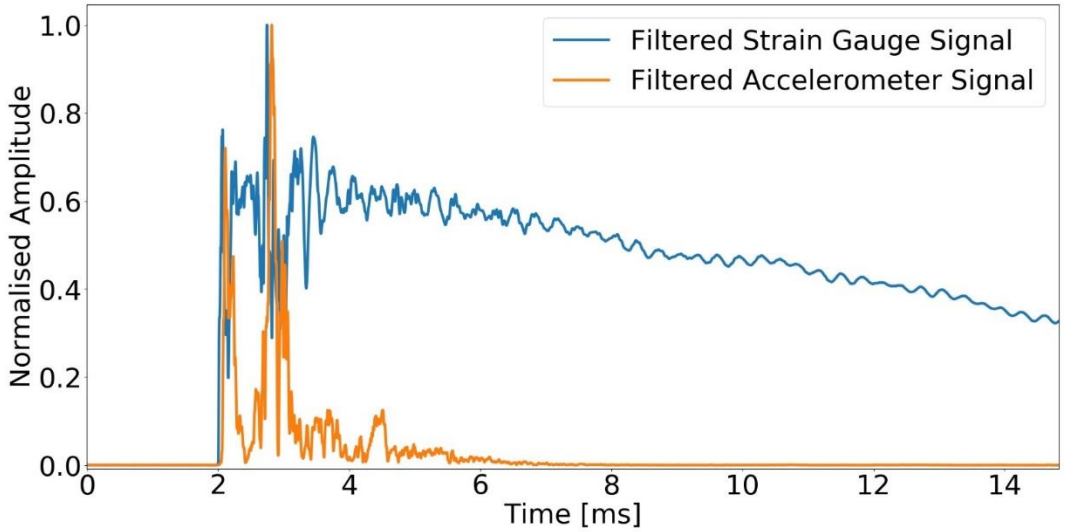

Figure 6-8: Filtered accelerometer / strain gauge signal.

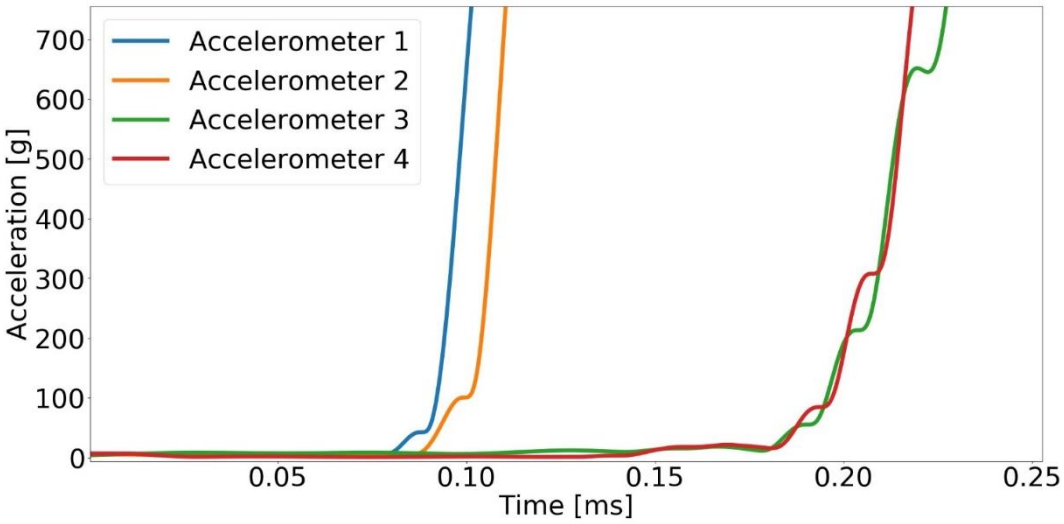

Figure 6-9: Different AT of the accelerometers. This picture shows that the position of the impact was equidistant from accelerometers 1 + 2 and 3 + 4. It indicates that the impact is closer to accelerometers 1 and 2.

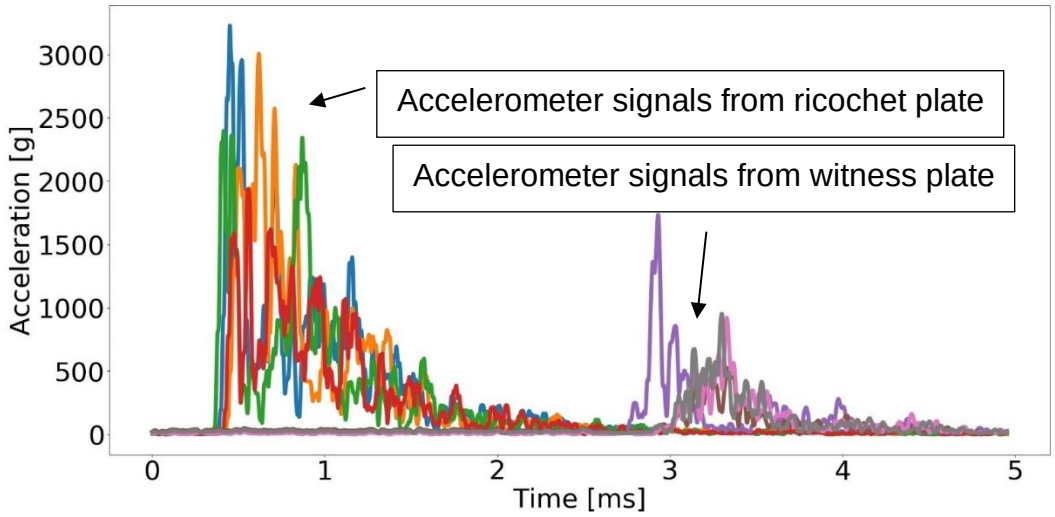

Figure 6-10: Typical raw signal. The first peaks represent the acceleration signal produced on the ricochet plate. The second set of signals represents the signals of the witness plate where the ricochet impacts finally.

Figure 6-11 shows the velocity of the impact on the witness plate. The direct impact was a scenario where the projectile was shot directly at the witness plate, undeflected. It represents the normal velocity occurring 25 m after leaving the muzzle. The error bars show the standard deviation of the measured velocity. With an increasing impact angle, the velocity decreases. The velocity drop has two reasons:

Firstly, the impact wear on the steel ricochet plate. This first hit slows the projectile down, the amount of impact wear depends on the projectile material.

Secondly, the change of projectile shape. The projectile is less aerodynamic and tumbles after hitting the oblique ricochet plate.

Looking at the heavier projectiles (M193 and SS109), one can recognise a steady velocity drop. However, the slightly heavier SS109 shows a less steep linear decay than the M193. In the case of the M193, the spread of the velocity increases with an increasing ricochet plate angle. The increasing spread might be because the M193 starts to fragment and the lead fragments are of different sizes, which results in a different drag coefficient and thereby different velocities.

However, the most significant change in velocity is experienced by the frangible projectile fragments after hitting the ricochet plate. The velocity of the frangible fragments seems to plateau between 20 and 25°. This plateau effect might be because the copper powder behaves similar to a fluid after total fragmentation.

Figure 6-12 shows the results of the same test scenario as in Figure 6-11. This time, however, the momentum is analysed. The momentum also decreases in this case with increasing impact angle. However, with all ammunition types tested, the transmitted momentum is very low after impact on a 25° plate. Figure 6-12 shows, like a fingerprint of a specific projectile design, a distinct specific momentum distribution. In the case of frangible projectiles, the momentum decays before 10° to a certain threshold below 0.1 Ns. In the case of the SS109, the signal also decays to a threshold. However, this threshold is reached at 20° impact. The M193 is in between in both scenarios.

The M193 shows an S-curve decay, which has its main momentum decay between 5° and 10° impact angle. Both the velocity and especially the projectile weight of the SS109 are high compared with the other ammunition types investigated, see Table 6-1. The momentum of the SS109 is more persistent and decays not as fast as the other projectiles. This might be due to the steel core, which behaves rigid and bounces away from the ricochet plate without substantial momentum loss.

The logarithmic decay pattern of the frangible projectile is even more present in the case of the momentum than in case of the velocity. Interestingly, the dispersion and the velocity of the 15° and 25° impacts are almost in the same range and decreased significantly compared with the initial momentum. Under these angles, the frangible projectile already fragmented into fine copper particles. These excellent disintegration properties are also the general purpose of frangible ammunition [46], namely the diminution of the range danger area after hitting any surface. This diminution can be quantified using the ricochet measurement device.

In Figure 6-13 till Figure 6-17, one can see the fragmentation process on a thermal picture of the investigated projectiles. The thermal image is plausible after reading the momentum graph in Figure 6-12. Many impacts and a wide spread of the residuals lead to a lower overall momentum. A low total momentum is crucial for a shorter-range danger area.

Interestingly, Figure 6-13 (M193) shows just one single impact, which can occur if the ricochet plate deflects the projectile more smoothly. However, this is not the case all the time; the thermal pictures represent just a possible pattern. A problem was the temperature shift and the blurring out of the camera one can recognize this shift in the background of the Figure 6-13a. Due to this fact, only the maximum temperature was indicated in the thermal images.

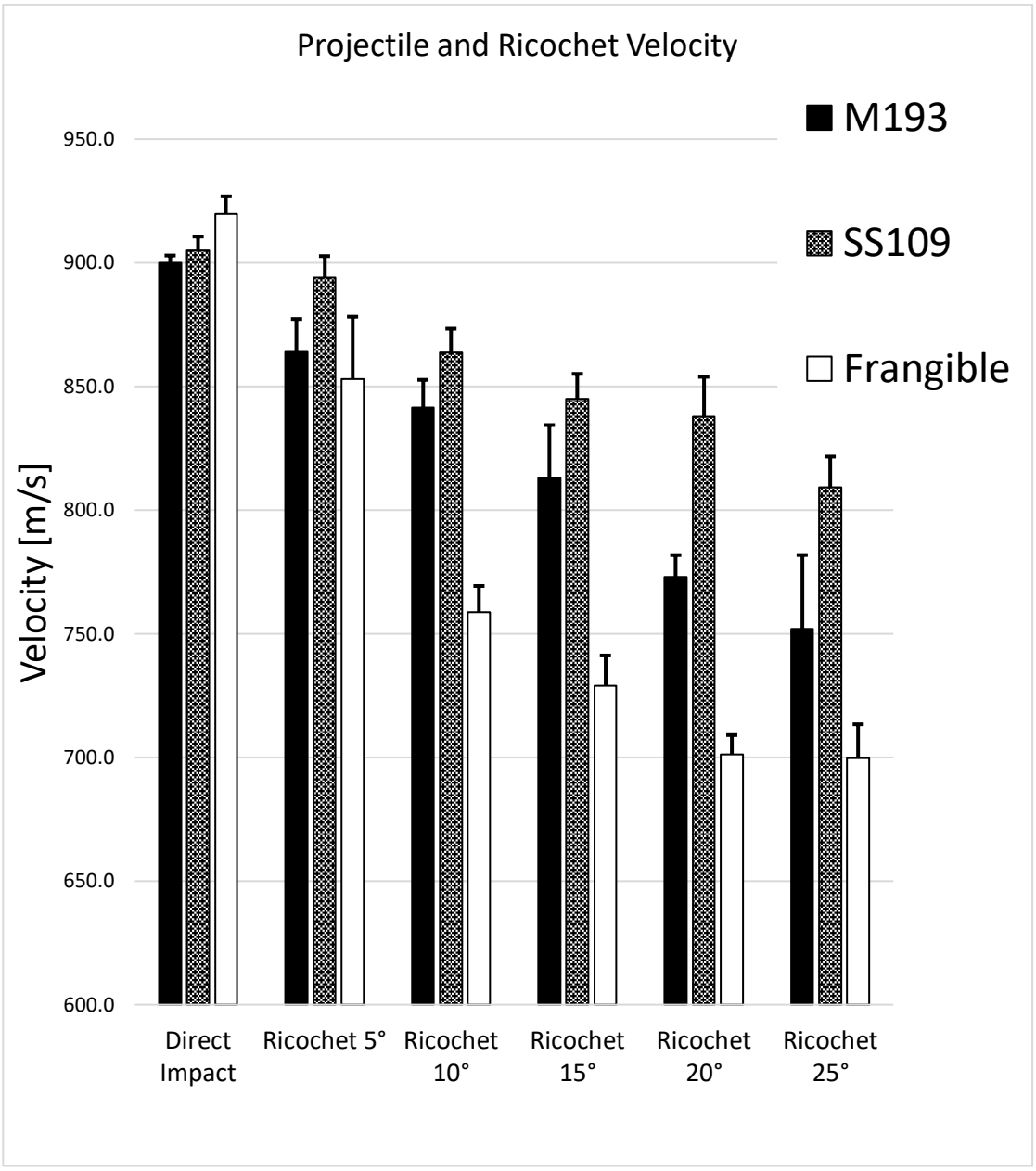

Figure 6-11: Velocity graph. The direct impact shows the scenario when the projectile hits the witness plate without prior deflection. All ricochet scenarios describe the velocity after being deflected on the ricochet plate. 5° is the smallest angle investigated. Due to the small impact angle, the projectile is also just marginally deflected and loses less velocity compared to the other angles.

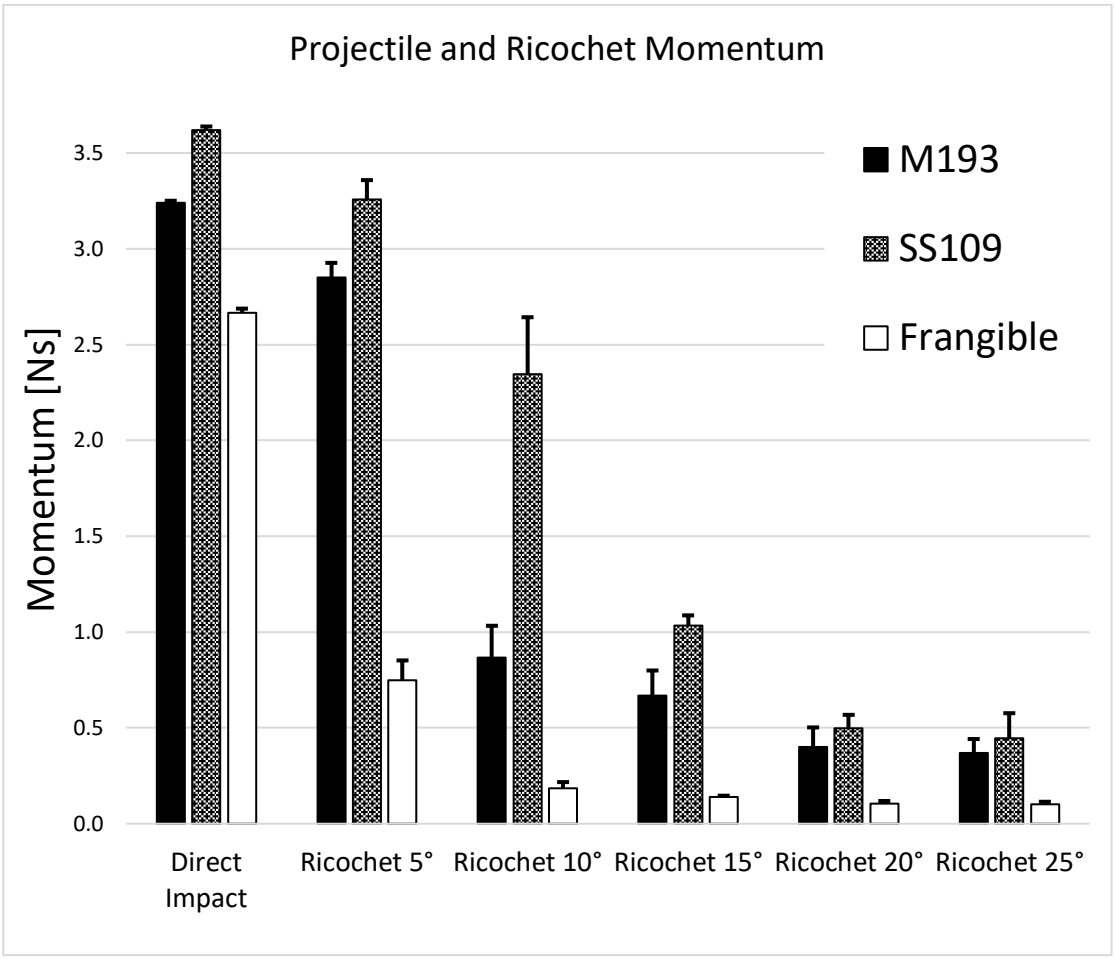

Figure 6-12: Momentum graph. The direct impact shows the scenario when the projectile hits the witness plate without prior deflection. In the orthogonal direct impact scenario, the projectile transfers the largest amount of momentum into the witness plate. All ricochet scenarios describe the momentum transmitted into the witness plate after being deflected on the ricochet plate. 5° is the scenario after a deflection on an almost flat plate. Due to the small impact angle, the projectile is also just marginally deflected and transfers more momentum into the witness plate compared to the other angles which deflect the projectile stronger.

Table 6-1: Comparison of projectile designs.

Projectile Type	Projectile Weight [g]	Impact Angle [°]	Impact Velocity [m/s]	Ricochet Velocity [m/s]	Velocity Drop [m/s]	Momentum before Impact [Ns]	Mom. Witness Plate [Ns]	Mom. Loss before vs. after Deflection [%]
Frangible	2,9	5	920	853	67	2,67	0,75	72
Frangible	2,9	10	923	759	164	2,67	0,19	93
Frangible	2,9	15	916	729	187	2,66	0,14	95
Frangible	2,9	20	921	701	220	2,67	0,13	95
Frangible	2,9	25	917	700	217	2,66	0,10	96
M193	3,6	5	900	864	36	3,24	2,85	12
M193	3,6	10	901	841	60	3,24	0,87	73
M193	3,6	15	900	813	87	3,24	0,67	79
M193	3,6	20	900	773	127	3,24	0,41	87
M193	3,6	25	899	752	147	3,23	0,37	89
SS109	4	5	908	894	14	3,63	3,26	10
SS109	4	10	905	864	41	3,63	2,35	35
SS109	4	15	900	845	55	3,60	1,03	71
SS109	4	20	904	838	66	3,62	0,50	86
SS109	4	25	901	809	92	3,60	0,45	88

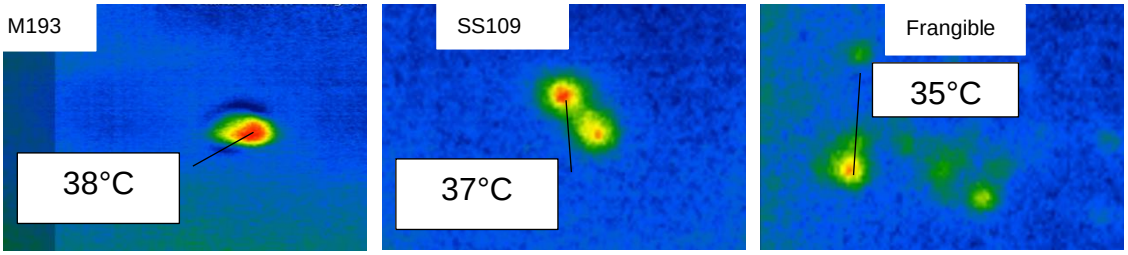

Figure 6-13: Thermal impact pattern of projectiles investigated under the impact angle of 5°. The M193 does not fragmentise; the SS109 is separated into two pieces, which is a general behaviour of two cored projectiles.

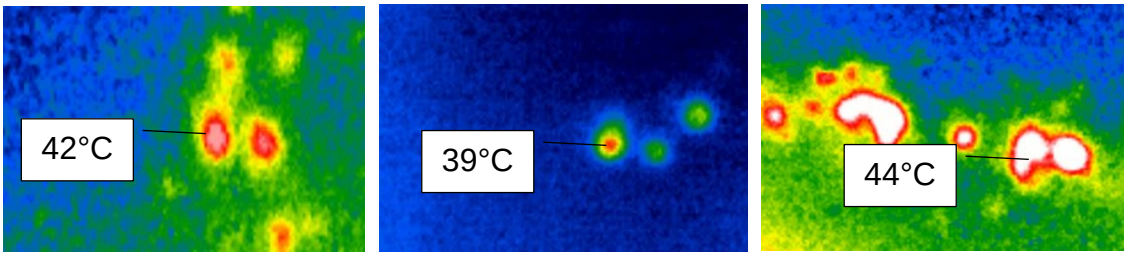

Figure 6-14: Thermal impact pattern of projectiles investigated under the impact angle of 10°. The M193 fragmentise under this angle. The blurred picture of the M193 and the frangible projectile is due to temperature drifts of the thermal camera. The increase in fragmentation is recognisable primarily in the case of the frangible.

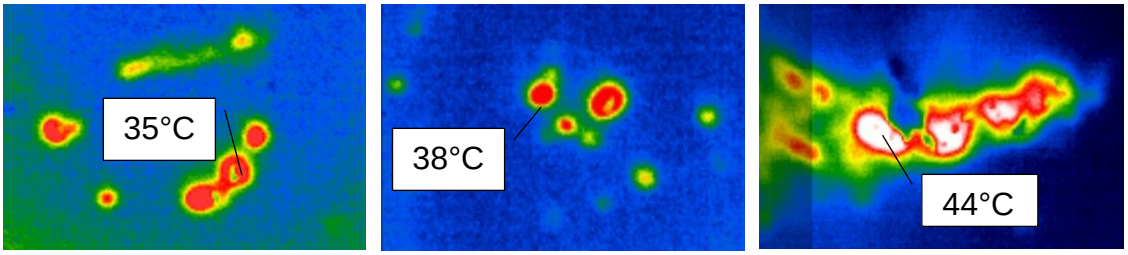

Figure 6-15: Under the impact angle of 15°, all projectiles start to fragmentise. In the case of the frangible projectile, a continuous thermal pattern can be recognised. This is the impact angle, where all projectile types show a significant momentum drop.

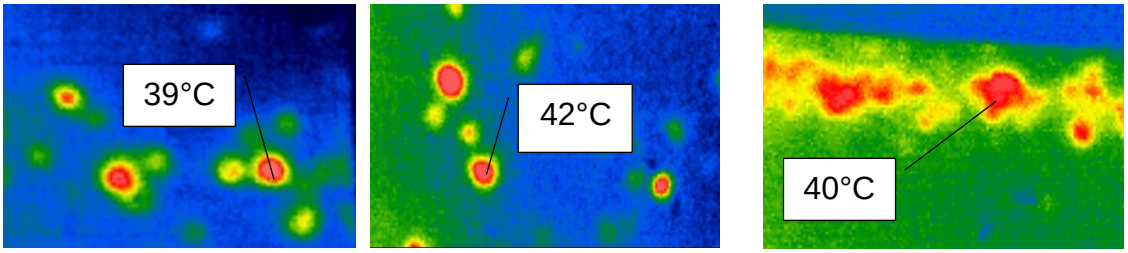

Figure 6-16: Under the angle of 20°, the fragmentation spread increases for all projectiles investigated. Under this angle, the franglible projectile is entirely disintegrated.

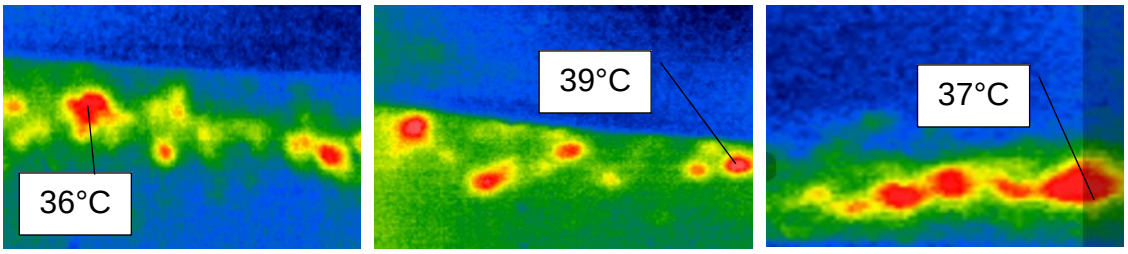

Figure 6-17: Under the angle of 25°, all projectiles are entirely disintegrated and show a horizontal line pattern. This is because the projectiles are reflected under a similar angle, independent of the material and design of the projectile.

6.6 Discussion

In this ballistic experiment, positioning was performed manually by visual investigation. The results of the frangible projectile ricochets, small particles, showed that the rubber layer does not influence the test results. Even these small particles penetrate the layer easily, and the velocity is not affected by the rubber layer. In future, exact positioning with thermal imaging should be done using an algorithm-based approach.

It was not possible to conclude from the thermal signature direct to the impact strength or the shape of the ricochet. However, with a more in-depth investigation and using a camera capable of several hundred frames per second, which is more suitable for general ballistic analysis, this would be possible as part of the future work plans. Concerning the camera, there is an additional drawback that involves the temperature shift over time and the blurring of the temperature pattern, especially the background. This was the reason why only the maximal temperature was indicated. This drawback can be resolved by using a camera featuring an accurate temperature shift filter.

The momentum measurement was performed with accelerometers and a calibration step using different ammunition types. It is possible to augment the precision of the momentum measurement with precisely defined metal balls shot on the measurement plates using accurately defined acceleration machines like gas guns.

The ricochet measurement device was in this publication used to investigate 5.56 mm projectiles and 9 mm projectiles. It is also possible to use this device to investigate all small-calibre types and all different projectile types like armour-piercing projectiles with a tungsten core or solid projectiles made of brass or copper.

6.7 Conclusion

The goal of this work was to assess the performance and trustworthiness of a novel ricochet measurement device with ammunition types of interest. The ballistic study showed that it is possible to quantify complicated and fast-flying structures like projectiles or its ricochets with regular signal processing approaches.

A Measurement system is proposed for ballistic impact investigations, which is suitable to measure ricochet velocities and impact momentums in the typical small-calibre range.

For ballistic momentum measurements, strain gauges are less suitable than accelerometers because the signal drifts strongly in the investigated time domain. However, AT detection is possible using both strain gauges and accelerometers. For multiple impact positioning of projectile fragments, the used thermovision device is appropriate to investigate the impact pattern. However, a more precise camera with an image-processing unit would enhance the performance of this sensor approach. The momentum measured using accelerometers is a valuable property for ballistic investigations like the estimation of danger potentials of specific projectile types and their fragments.

The transmitted momentum is further connected to the range safety. A large momentum loss after a deflection on an oblique plate indicates a projectile, which has good properties for a reduced ricochet danger.

Three different ammunition types showed that the basic design of the projectiles has a significant influence on the deflection process and with this on the range danger area. The results presented here are plausible. The acquired results can be used to estimate the danger potential of the different investigated ammunition types. The investigations also confirmed that a slight deflection of regular projectile types could lead to ricochets, which are still dangerous.

The main message is that quantifying of ricochets is possible using cost-effective and straightforward devices. The concept itself can also be applied to larger or smaller calibres to support the projectile design and development process.

6.8 Acknowledgement

Special thanks go to Donald Meyer and Dr Peter Spatz who made these measurements possible. The authors would like to thank RUAG Ammotec AG Switzerland for the provision of the test facilities and equipment. The use of measurement devices would not have been possible without the great help of Markus Gruenig and Roland Niederhaeuser.

6.9 Publication references

[1] H. Kusano, Y. Aoki, Y. Hirano, Y. Kondo, and Y. Nagao, “High-speed imaging on static tensile test for unidirectional CFRP,” in *Proc.SPIE*, 2009.

[2] P. C. Chou and R. H. Toland, “Experimental study of multiple interior impacts,” *Exp. Mech.*, vol. 17, no. 6, pp. 201–206, 1977.

[3] X. L. Yan et al., “Characterization of a double Time-Of-Flight detector system for accurate velocity measurement in a storage ring using laser beams,” *Nucl. Inst. Andm. Phys. Res. A*, vol. 931, no. March, pp. 52–59, 2019.

[4] M. Courtney, “Acoustic methods for measuring bullet velocity,” *Appl. Acoust.*, vol. 69, pp. 925–928, 2008.

[5] H. D. Espinosa and S. Nemat-Nasser, “Low-velocity impact testing,” *ASM Handb.*, vol. 8, pp. 539–559, 2000.

[6] H. D. Espinosa, G. Raiser, R. J. Clifton, and M. Ortiz, “Performance of the star-shaped flyer in the study of brittle materials: Three dimensional computer simulations and experimental observations,” *J. Appl. Phys.*, vol. 72, no. 8, pp. 3451–3457, 1992.

[7] R. Morsy, H. Marzouk, M. Haddara, and X. Gu, “Multi-channel random decrement smart sensing system for concrete bridge girders damage location identification,” *Eng. Struct.*, vol. 143, pp. 469–476, 2017.

[8] U. Dahlen, N. Ryden, and A. Jakobsson, “Damage identification in concrete using impact non-linear reverberation spectroscopy,” *NDT E Int.*, vol. 75, pp. 15–25, 2015.

[9] F. Allaeys, G. Luyckx, W. Van Paepegem, and J. Degrieck, “Development and validation of a set-up to measure the transferred multi-axial impact momentum of a bird strike on a booster vane,” *Int. J. Impact Eng.*, vol. 99, pp. 102–110, 2017.

[10] C. I. Hammetter, R. L. Jones, H. L. Stauffacher, and T. F. Schoenherr, “Measurement and modeling of supersonic hailstone impacts,” *Int. J. Impact Eng.*, vol. 99, pp. 48–57, 2017.

[11] A. Agnello, J. Dosch, R. Metz, R. Sill, and P. Walter, “Acceleration Sensing Technologies for Severe Mechanical Shock,” *Sound Vib.*, vol. 48, no. 2, pp. 8-19, 2014.

[12] T. H. and O. C. and G. D. and C. J. and S. R. and C. Touzé, “Wave turbulence in vibrating plates: The effect of damping,” *EPL (Europhysics Lett.*, vol. 102, no. 3, 2013.

[13] G. Zhao, H. Hu, S. Li, L. Liu, and K. Li, “Localization of impact on composite plates based on integrated wavelet transform and hybrid minimization algorithm,” *Compos. Struct.*, 2017.

[14] A. Perelli, L. De Marchi, A. Marzani, and N. Speciale, “Frequency warped cross-wavelet multiresolution analysis of guided waves for impact localization,” *Signal Processing*, vol. 96, pp. 51–62, 2014.

[15] D. Mušicki, R. Kaune, and W. Koch, “Mobile emitter geolocation and tracking using TDOA and FDOA measurements,” *IEEE Trans. Signal Process.*, vol. 58, no. 3, pp. 1863–1874, 2010.

[16] F. Gustafsson and F. Gunnarsson, “Positioning using time-difference of arrival measurements,” in *IEEE International Conference on Acoustics, Speech, and Signal Processing*, vol. 6, pp. VI–553, 2003.

[17] M. Liu, J. Yang, Y. Cao, W. Fu, and Y. Cao, “A new method for arrival time determination of impact signal based on HHT and AIC,” *Mech. Syst. Signal Process.*, vol. 86, pp. 177–187, 2017.

[18] V. V. Krylov and F. J. B. S. Tilman, “Acoustic ‘black holes’ for flexural waves as effective vibration dampers,” *J. Sound Vib.*, vol. 274, no. 5, pp. 605–619, 2004.

[19] V. V. Krylov and R. E. T. B. Winward, “Experimental investigation of the acoustic black hole effect for flexural waves in tapered plates,” *J. Sound Vib.*, vol. 300, no. 2, pp. 43–49, 2007.

[20] E. Bowyer and V. Krylov, “Acoustic black hole manufacturing for practical applications and the effect of geometrical and material imperfections,” no. 4, pp. 2411–2421, 2016.

[21] A. Howard, “Morphological control of tensile release in ceramic penetration,” Cranfield University, 2014.

[22] M. Muster, A. Hameed, D. Wood, G. Appleby-Thomas, and K. Wasmer, “Damping of post-impact vibrations,” *Appl. Acoust.*, vol. 156, pp. 427–433, 2019.

[23] P. Manrad, “System And Method for Calculating Projectile Impact Coordinates,” 2008.

[24] J. P. Johnston, J. M. Pereira, C. R. Ruggeri, and G. D. Roberts, “High-speed infrared thermal imaging during ballistic impact of triaxially braided composites,” *J. Compos. Mater.*, vol. 52, no. 25, pp. 3549–3562, 2018.

[25] N. Domun *et al.*, “Ballistic impact behaviour of glass fibre reinforced polymer composite with 1D/2D nanomodified epoxy matrices,” *Compos. Part B Eng.*, vol. 167, no. December 2018, pp. 497–506, 2019.

[26] W. Swiderski and P. Hlosta, “Non-Destructive Evaluation of Impacted CFRP by IR Thermography,” *Materials*, vol. 956, no. 12, 2019.

[27] S. Gopalakrishnan and V. Senthil, “Failure Analysis of Ballistic Material,” *Int. Conf. Adv. Mater. Eng.*, vol. 15, pp. 95–100, 2011.

[28] Y. Duan *et al.*, “Reliability assessment of pulsed thermography and ultrasonic testing for impact damage of CFRP panels,” *NDT E Int.*, vol. 102, pp. 77–83, 2018.

[29] S. Hwang, Y. K. An, and H. Sohn, “Continuous Line Laser Thermography for Damage Imaging of Rotating Wind Turbine Blades,” *Procedia Eng.*, vol. 188, pp. 225–232, 2017.

[30] M. D. Spiridonakos and S. D. Fassois, “Vibration based fault detection in a time-varying link structure via non-stationary FS-VTAR models,” *Int. Oper. Modal Anal. Conf.*, 2009.

[31] PCB, “High Shock ICP ® Accelerometer.”

[32] J. Komenda *et al.*, “Forensic and clinical issues in the use of frangible projectile,” *J. Forensic Leg. Med.*, vol. 20, no. 6, pp. 697–702, 2013.

[33] L. Martrille, A. Artuso, C. Cattaneo, and E. Baccino, “A deceptive case of gunshot entry wounds - Beware of frangible bullets,” *J. Forensic Leg. Med.*, vol. 14, no. 3, pp. 161–164, 2007.

[34] I. Horsfall and I. R. Crewther, “Proc 19th International Symposium on ballistics,” in *Glass ceramic armour systems for light armour applications*, 2001.

[35] T. Vanichayangkuranont, K. Maneeratana, and N. Chollacoop, “Numerical Simulations of Level 3A Ballistic Impact on Ceramic / Steel Armor,” pp. 2–7, 2006.

[36] P. G. Arvidsson, “Is there a problem with the lethality of the 5.56 NATO caliber,” 2009.

[37] U. States and R. Arms, “5.56×45mm NATO,” 1963.

[38] B. Ragsdale and S. Sohn, “Comparison of the Terminal Ballistics of Full Metal Jacket 7.62-mm M80 (NATO) and 5.56-mm M193 Military Bullets: A Study in Ornance Gelatin BT,” *J. Forensic Sci*., vol. 33, no. 3, pp. 676–696, 1988.

[39] B. Sturtevant, “Shock wave effects in biomechanics,” *Sadhana*, vol. 23, no. 5, pp. 579–596, 1998.

[40] I. Rottenberger, “Abprallverhalten von Jagdmunition,” *DEVA*, Altenbeken, Germany, 2011.

[41] E. J. A. T. Mattijssen and W. Kerkhoff, “Bullet trajectory reconstruction - Methods, accuracy and precision,” *Forensic Sci. Int.*, vol. 262, pp. 204–211, 2016.

[42] AEP-97, *Multi calibre manual of proof and inspection (M-C MOPI) for 5.56 mm, 7.62 mm, 9 mm and 12.7 mm ammunition*, vol. 23, 2013.

[43] W. Dudziński, Ł. Konat, and G. Pękalski, “Structural and strength characteristics of wear-resistant martensitic steels,” *Arch. Foundry Eng.*, vol. 8, no. 2, pp. 21–26, 2008.

[44] J. Hub and J. Komenda, “Ballistic resistance of steel plate hardox upon impact of non-penetrating projectiles,” *Adv. Mil. Technol.*, vol. 4, no. 2, pp. 79–91, 2009.

[45] M. Muster, A. Hameed, and D. Wood, “Dynamic qualitative bolt force measurements for investigating influence factors on the pushout effect of small calibre ammunition,” *AIP Adv.*, vol. 9, no. 6, p. 065020, 2019.

[46] S. P. Mates, R. Rhorer, S. Banovic, E. Whitenton, and R. Fields, “Tensile strength measurements of frangible bullets using the diametral compression test,” *Int. J. Impact Eng.*, vol. 35, no. 6, pp. 511–520, 2008.

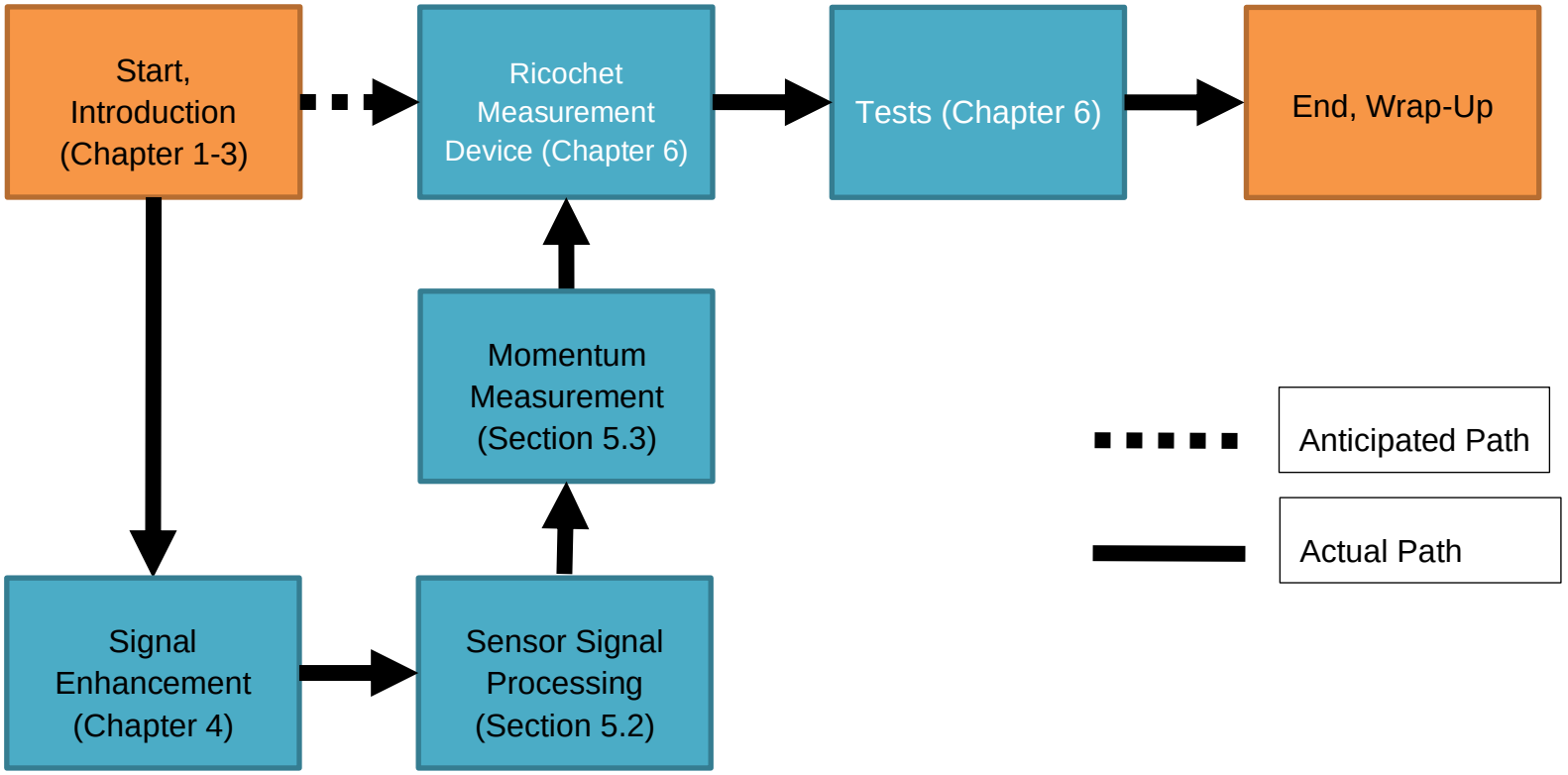

Figure 6-18: Comparison be the anticipated path and the actual path in relation to the chapters presented in the thesis.

6.10 Conclusion of chapter

The momentum loss of a projectile after deflection is in close relation to the loss of danger potential. This key fact shows that it is not sufficient to investigate just the velocity drop of the projectile after a deflection. The measurement device validated in this chapter showed the capability to measure in-situ multiple physical properties, relevant to ricochet investigation. The knowledge published in this chapter will be a significant contribution to future ricochet measurements.

7 Discussions, conclusions and future work

7.1 Introduction

This final chapter includes the three final points, the discussions and conclusions of all results concerning the fundamental research question.

7.2 Author’s contribution statement

Michael Muster wrote this chapter. However, Amer Hameed helped to describe and formulate the potential novel parts of the thesis. Michael Muster designed all CAD drawings of the novel damping structures. Meyer Donald was involved in the future work section; he rated the potential of the new findings.

7.3 Discussion

7.3.1 Introduction

The knowledge about the safety of shooters in the near and far fields has been extended during this thesis. This is in line with the fundamental research question. It has been further proved that modern measurement devices can investigate different ballistic phenomena using the same sensor principle.

The purpose of this study was to show the influence of novel ballistic measurement devices on recent safety considerations. Experiments showed that interesting and new aspects are found using the developed measurement device.

One important measurement system was the pushout force device which can be used for very accurate short-time measurements. The pushout force rises by factors using a lubricated casing compared to the unlubricated casing.

The ricochet can be quantified using the proposed two-plate measurement approach. The relevant implication from the ricochet research is that the projectile design can be assessed using the momentum change after deflection. This specific momentum change influences the danger potential of the projectile. A projectile with low danger potential after ricocheting is beneficial, because a smaller SDZ can be used.

The proposed ricochet measurement device is capable of comparing different projectile designs amongst each other. With the assessment of projectile designs, especially the measurement of their danger potential, one is able to establish design guidelines. Proof that frangible ammunition has a significantly lower risk of dangerous particles compared to other designs could be worked out with the novel measurement device.

Besides the developed measurement system, the thesis also describes a novel way for damping flexural waves in plates. This knowledge can be applied to many other applications, not only ricochet measurements — for example, the reduction of noise in piston engines.

7.3.2 Measurement Instruments

Two different measurement devices are developed. One for the pushout force investigation and the other for the ricochet measurement. Both measurement devices are operated by piezoelectric sensors and enable an accurate assessment of the short time physical events during the process of firing and projectile impact.

The force measurement was conducted using piezoelectric strain gauges and piezoelectric force washers. The ricochet measurement device was equipped with piezoelectric accelerometers. These sensor types showed a very good overall performance and are suitable for the devices. It has been identified that the signal processing of accelerometers and the strain gauge are more demanding compared with signal processing of the force washer sensor. A reason for this is that force washers are better pre filtered than strain gauges or accelerometers.

Both developed devices are of a modular design and capable of measuring in the whole range of small caliber ammunition. Another main aspect was that they needed to be bulky and rugged to withstand the extreme pulsed load. Furthermore, the environment is rather harsh and no fragile measurement systems could be used. This statement is valid for both measurement devices. In general, the developed devices were rugged enough for the intended purpose and, no device failed. The only damage observed during all experiments were a few cables cut due to the debris. And one accelerometer was destroyed. However, this accelerometer failed due to wrong handling and got hit directly by a projectile.

The ricochet measurement system and the pushout force measurement were conducted with the same filtering approach. It was evident that a bandpass filter enhanced with an RMS envelope is best practice to measure short time physical events. All events measured were in the time range between 10 µs and 1000 µs. Modern, sophisticated deep learning or machine learning signal processing approaches would be appropriate for longer duration signals or other sensor principles.

It is possible that the used software would not be suitable for sophisticated deep learning signal processing. However, for the measurements conducted, the open source spyder software tool was absolutely appropriate. The programming language is in python, which enabled a short working- in time. This language serves a huge amount of online tutorials and thr help community is large.

The two proposed measurement devices including the open source software enabled the research for novel safety considerations which are part of the main scope of this thesis.

7.3.3 Safety considerations

The pushout force investigations have a direct impact on the knowledge of weapon safety. This directly affects the operator in the form of near-field safety considerations, connected to the near field ballistics. The ricochet measurement, on the other hand, concerns the safety of civilians living near the shooting range or the safety of colleagues working nearby. In short, this work leads to the identification of the hazard zone to prevent collateral damage. The ricochet measurement is under the scope of far-field safety and connected to terminal ballistics.

Knowledge is acquired that a lubrication film influences the stick-slip effect between the boundaries of the casing and the chamber of the weapon. It also affects the overall obturation process of small-calibre rifles. Previously, this knowledge was not accessible to the wide public. The newly acquired knowledge should give the ammunition manufacturers reason to investigate the possibilities of treating the surface of brass casings differently.

The weapon manufacturers should search for possibilities of dampening these high forces or, even better, the weapon itself should be capable of withstanding forces produced at the breech during weapon firing. This is especially true for breech-bolt weapons. User- the relevant recommendation is to lubricate the weapon according to the cleaning protocol. However, the chamber and the ammunition should be unlubricated and free from any residuals.

The results of the pushout force measurements were proven by applying a method which relies on a strain gauge and a load cell to measure the deformation, and FEA analysis.

The most relevant parameter for the ricochet quantification is the momentum loss between the projectile before and after impact. This parameter holds the most SDZ-relevant information as it is the product of the velocity and the fragment weight. Experiments conducted in this research have demonstrated that the velocity drop is not as significant as the momentum drop, which means that the fragmentation is the driving factor which reduces the danger of the ricochet.

The main sources of error while estimating the SDZ remain the drag coefficient of the largest fragment (spin-stabilised or not) and the type of soil with which the projectile is confronted during impact. Both parameters have a strong influence, meaning that best practice would be to assume a worst-case scenario. With this knowledge, the recommendation for best practice of SDZ calculation is to take the momentum-loss values from steel plate ricochets and combine these with the already existing statistical models. With this approach, it should be possible to make SDZ more reliable and safer.

7.4 Conclusion

A novel way of quantifying impacts of small-calibre ammunition has been found. Short- time physical processes can be investigated using piezoelectric sensors and spiked plate designs. To use the described system for a real ricochet quantification and investigation, one needs to apply statistics, depending on the underlying safety requirements. Conclusions on the parts of the overall system are as follows:

- Nowadays, ballistic measurements are possible with COTS sensors and data acquisition systems. Especially piezoelectric sensors are broadly suitable for most ballistic investigations. However, the filtering process is crucial for successful measurementa.
- Most dangerous physical events which can destroy a device, take place in periods from several microseconds up to a hundred microseconds. Investigations of high-velocity impacts on the measurement device confirmed this as well as the powerful oscillating forces acting on the casing bottom of 9 mm ammunition.
- Open-source signal processing tools like Spyder are entirely suitable for filtering processes. Since they are written in Python language, it is equally possible to create user interfaces, which are easier to handle than scripts. A massive advantage of open-source software is that it is suitable for cluster computing. This might well be required because a large amount of data is collected within one second, which calls for a significant computational effort.
- Short-time events require mechanical filtering. The shock accelerometers need to be insulated mechanically. It was possible to significantly reduce the noise in the signal with the help of a particular shape. As mentioned, it is necessary to filter out events, which occur within microseconds.
- Different projectile designs display very different ricocheting behaviours if they are in the same range as regards their energy. It is, in fact, the bullet design which determines the danger potential, not the diameter or energy of the ricochet.

7.5 Future work

This chapter is split into two sections to enhance the readability. The first section treats the future work of the main topic, which is ballistic measurements and quantification. The focus is on projectile/ricochet quantification. The second section mainly addresses possible applications of some of the research findings, for example, other uses of invented power-law damping structure.

This PhD thesis defined four main objectives; *signal processing, momentum measurement, triangulation and ammunition influence*. Each can be developed further.

7.5.1 Future work related to ricochet/ammunition quantification

7.5.1.1 Process data to suit into mathematical prediction models

The data acquired with the ricochet measurement device should be used to develop a probabilistic ricochet analysis model, which gives information about the fragmentation behaviour and the range danger area. The ricochet measurement device provides values like incident velocity, deflected velocity, fragment weight, impact pattern and momentum transmitted to the witness plate. All these values can be used to feed the mathematical model of the ricochet analysis software of an army or a law enforcement institution. However, one major drawback is that the ricochet measurement device quantifies the impact on a steel plate and depends on the impact angle.

A straight forward method would be to define, for example, tree impact angles. And consider the momentum drop between the incident projectile and the deflected ricochet. The momentum is already a compilation of all physical properties measured. This approach can be used to minimise the amount of data which is needed to be processed to develop a mathematical prediction model.

The ultimate target would be the momentum loss used as a factor which rounds out a regular datasheet of an ammunition manufacturer. Figure 7-1 shows the already existing datasheet of a conventional 5.56 mm M193 ammunition enhanced with the *Momentum loss* (red).

The *momentum loss* would be a part of the performance data sheet and a solid decision bases to consider to procure a specific ammunition type. Such a standardised model might be beneficial to estimate range danger areas more reliable in future.

Cartridge	**5.56x45 / .223 Rem.**	
projectile	FMJ, 3.6 g / 55 gr	
projectile material	tombac jacket, lead core	
ballistic coefficient C1	0.280 (ICAO)	
primer / propellant	SINOXID / double base powder	
case material	CuZn - alloy	
cartridge weight	11.6 g	
Performance		
term of reference	MCMOPI	
temperature range	-54°C to +52°C	
mean case mouth pressure + 3s	max. 4 450 bar	(21°C)
muzzle velocity	990 m/s (3 248 fps)	510 mm barrel
muzzle energy	1 764 J	
accuracy at 300 m	s_H ; $s_V \leq 85$ mm	
penetration at 300 m	5 mm steel plate, St 37, 60°	
Momentum loss (5°, 10°, 20°)	**3 %, 20 %, 50 %** ◀	
Packaging	10 rds/clip, 50 rds/cardboard box, 1 000 rds/M2A1	

Technical specification and numerical data are given as an indication only and are of no contractual nature.
10.2013

Figure 7-1: A standardised extract from the fact sheet of the M193 ammunition type. A possible quantification value stands in the performance section.

Objectives, which will be required: *momentum measurement, triangulation and ammunition influence*

7.5.1.2 Tests with different ammunition types

During the ricochet assessment, only a set of military 5.56 ammunition was tested. However, ricochets are also worth being investigated for other calibres.

Only a selected set of ammunition types have been tested up until now. However, the measuring device can measure all kinds of ammunition up to 12.7x99 mm. Differences for further tests might be typical hunting projectiles compared with military projectiles. It is assumed that the regular double-core projectiles with two different lead harnesses in the core break up during the deflection in two or three fragments. It is possible that, at a certain point of wall thickness, the projectile reacts more similar to solid projectiles compared with regular-jacketed shells.

Objectives, which will be required: *ammunition influence*

7.5.1.3 Safety system for vehicles; real-time projectile assessment

With the development of the ricochet measurement plate, the idea emerged that such plates might also enhance the performance of armour plates. A part of the penetration process is always because of the high-frequency vibrations, which propagate through the plate during the penetration. These vibrations propagate radially outwards from the point of impact. These vibrations are strongly reduced with the use of acoustic black holes.

Furthermore, as described in the paper of chapter 4, the signal is purified and contains much information, which can be analysed and used to make a statement about the projectile itself. In the ideal, case it also possible to make a statement about the damage caused by the projectile. Figure 7-2 shows rugged vehicles with regular plates. Spline edged plates may enhance the protection against projectiles.

Figure 7-2: Armoured vehicle which could be equipped with plates with spline edges.

Objectives which will be required: *signal processing, momentum measurement and triangulation*

7.5.1.4 Force investigations for different chamber types

Barrel chamber flutes are longitudinal grooves cut in the chamber of a firearm that allows propellant gases to surround the fired casing. The flutes were thereby equalising internal and external gas pressures, which facilitate extraction or bolt operation for delayed blow-back firearm design [1], [2]. However, for high- performance sniper rifles, this augmented force might be a problem, especially if the casing is lubricated. The proposed measurement device may also quantify the effect of the flutes in the barrel chamber. Using new processing technologies in combination with the measurement device will enable novel designs for barrel fluting. Figure 7-3 shows a possible approach to modify chambers under consideration of the know-how that lubrication has a significant influence on the overall pushout force, which is taken by the breech bolt. The proposed design in Figure 7-3b is an approach to reduce the influence of lubricant. Since the high pressure presses the ductile casing against small spots of the chamber, the lubricant will be pushed away and reduce its influence on the pushout force. A chamber design independent on the surface treatment behaves more reliable. This enhances the system accuracy, which is crucial for a sniper. Furthermore, it improves also the weapon safety, which is of interest for the operator.

a

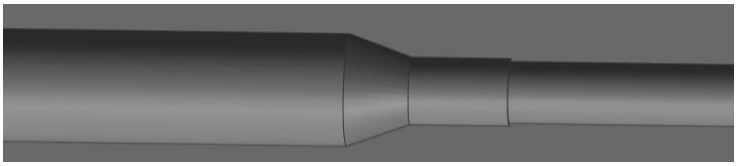

b

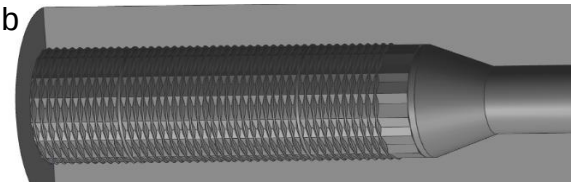

Figure 7-3: Different types of chambers can be assessed easily with the developed push out measurement device. (a) shows a regular smooth chamber of a rifle, whereas (b) shows a fluted chamber which is optimised for wet or oiled ammunition.

Objectives which will be required: *Signal processing, momentum measurement*

7.5.2 Applications for the novel vibration-damping structures

The Proposed applications are straight forward. The vibration damping approach gives a large amount of possibilities.

7.5.2.1 Gun barrel with power-law profile

Fluted gun barrels have advantages for heat flow and weight. There are many different approaches and designs for fluting the barrel around for the best overall benefit. However, for sniper rifles, the benefit of these flutings at the outer shell of the gun barrel has attracted some controversy. According to Chaturvedi [3] and Twafik [4], vibrations have a significant influence on the accuracy of the barrel.

Small manufacturing tolerances for the flutes are therefore necessary. The process of firing gives a tremendous impulse on the gun barrel, which ends in all kinds of vibrations and frequencies. The barrel needs to oscillate “symmetrically”, otherwise, the projectile is affected during an acceleration process in such a way that it does not leave the muzzle of the gun barrel in a reproducible manner. However, a reproducible muzzle is a crucial aspect of accuracy and first- round hit probability.

Because of this sensitivity to intolerances, some sniper rifle barrels are still unfluted, as presented in Figure 7-4a. Unfluted barrels have the big advantage that the vibrations are more predictable.

Power law structured gun barrels, shown in Figure 7-4b, are a possible approach to lower the influence of vibrations. The impulse emitted from the firing process can be immediately damped out. Positive facts are; the advantage concerning weight and heat flow remains the same; manufacturing tolerances of the flutings can be reduced. In an ideal world, it will result in a better accuracy weapon.

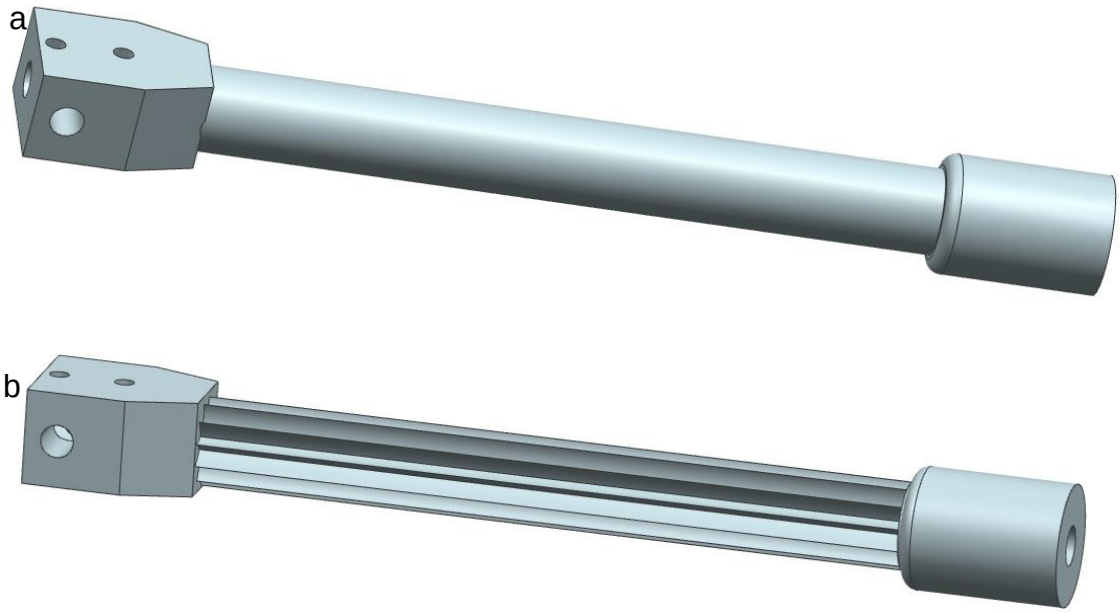

Figure 7-4: (a) represents an unfluted gun barrel, (b) shows a power-law fluted gun barrel. Sniper rifle barrels and medium calibre gun barrels are often fluted in the middle part to achieve weight savings and better heat flow. Power law fluted gun barrels might reduce the effect of vibrations and thus increase the accuracy and overall reliability.

7.5.2.2 Silencer of a weapon

A silencer for a weapon is generally considered, state of the art system within the small arms by the army and law enforcement community. Nowadays, Hunters have also started using silencers because it augments the safety of the hunter that the sound burst does not damage the ear [5].

Figure 7-5 shows a drawing of a power-law profiled silencer. The structures are challenging to manufacture. However, modern manufacturing processes, like additive manufacturing, may solve this issue.

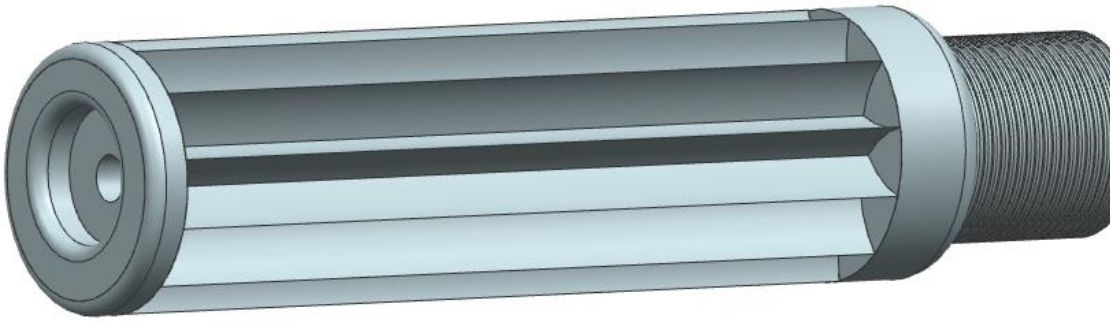

Figure 7-5: (a) shows a regular silencer for weapons, whereas (b) shows a novel approach. The sound is damped because of the use of acoustic black holes. The gas flow still needs to be broken down in the silencer. However, using additive manufacturing, such structures could also be realised.

7.5.2.3 Damped exhaust system

Noise is considered according to the World Health Organisation (WHO) as a significant environmental hazard of the 21st century [6]. Environmental noise from the road gives a substantial burden to people who live near such places: according to recent studies, one-third population living in the vicinity of highway can be affected by noise [6]. Because of this trend, it does make sense to investigate applications where the power-law noise-damping approach is applicable on a larger scale. One possible application is the noise reduction using more silent exhausting systems of any combustion engines.

Similar to the silencer of a weapon, it could use the advantage of power-law spikes to catch the vibrations directly in the catalytic converter or the exhaust system. Figure 7-6 shows a rough drawing of such a device. This device, applied to different kinds of vehicles, could lower the burden of environmental noise around crowded places in big cities.

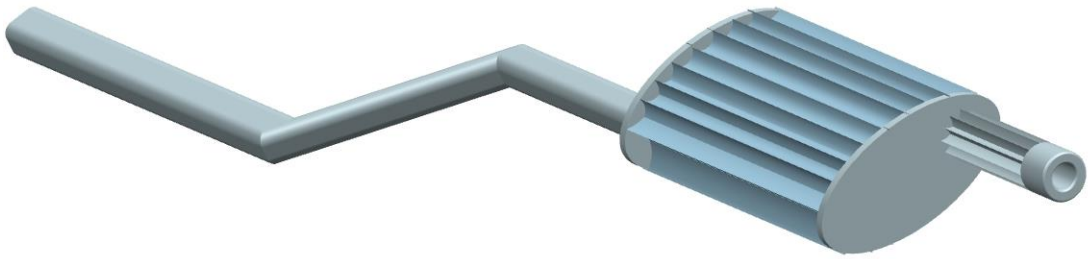

Figure 7-6: One of the major sources of noise from combustion engines are the exhaust systems. With a simple power-law profile in the outer shell, it will be possible to realise less noisy exhaust systems.

7.5.2.4 Damped steel plates as an example of truck beds

An approach similar to the exhaust system can be applied for damping of all kinds of steel plates. During the assessment of the witness plate of the ricochet measurement device, one recognised as a side effect that the impact of the projectile on the steel plate appears significantly less loud. Because of this finding, possible other direct applications could be identified. One immediate application of the damped steel plate represents Figure 7-7, the loading area of a pick-up truck is equipped with a power-law steel plate. With this solution, significantly less noise is emitted to the environment if the truck is loaded or unloaded.

Another possible application is the application on punch presses. A factory, which uses punch presses is always very loud; employees have to wear ear protection. Punch presses could be modified with power-law plates to reduce the overall noise of the factory. In an ideal case, it would be possible to get rid of ear protection. However, there are a lot more applications where damped steel plates, directly connected to the ricochet measurement plate, can be used.

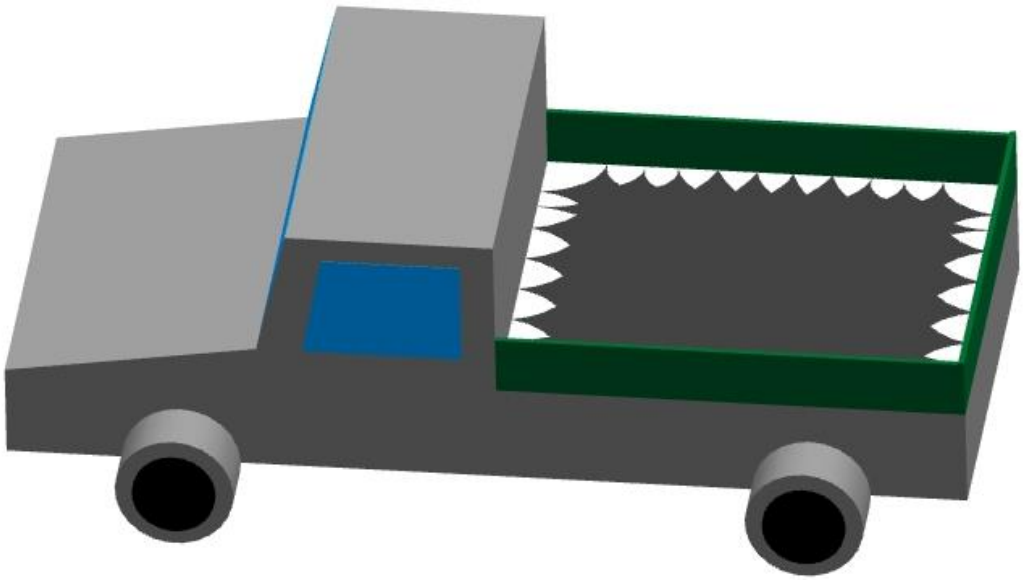

Figure 7-7: Represents a possible application of power-law shaped plates. If plane steel plates are loaded with an impulse force, they emit loud noise. With the use of power-law shaped plates, this noise can be significantly reduced.

7.6 Final conclusion

The aim of the thesis is the measurement of ricochet mechanics with a novel and fast measurement approach. The ricochet measurement is important for the accurate estimation of danger areas.

The aim of the thesis has been met using a separately developed device which is capable of measuring ricochets which are made from different materials. This aim has been met with the use of additional developments.

The enhanced measurement plate with acoustic black holes which was used for the ricochet plate and the measurement system for the breech force was one of the main developments. This two additional development where necessary to fulfil the final aim of the thesis.

The necessary developments for the final aim are in close relation to significant findings of the thesis. The significant findings are as follows:

- Power-law edged impact plates are capable of measuring projectile impacts and their ricochets accurately. The power-law edge of the plate can be considered as an acoustic black hole which prevents the reflection of flexural waves in the steel plate.
- From a time and force range perspective, pushout force measurements are comparable to the ricochet measurements. However, pushout force measurements are much more reproducible. It is also found that lubrication has a significant influence on the pushout force.
- Using the ricochet measurement device, which is developed during this thesis showed that the design and the material of the projectile has a significant influence on the danger potential of the projectile. This fact is up to now not taken into account for most SDZ considerations.

The publication in Applied Acoustics is one key publication. It covers the investigation of a novel measurement plate which is necessary for the overall ricochet measurement system. A second publication treats the investigation of the momentum and the force transmitted on the breech. These findings are published in AIP Advances. The fourth essential publication is about the overall ricochet measurement device to proof the concept are also different projectile types investigated.

In the future work section are a number of ideas proposed which can be taken forward. Some of the ideas have significant benefit both the commercial and defence sector while others will deliver improved performance.

7.7 References

[1] V. Krcma, “Fluted and Annular Grooved Barrel Chambers in Firearms,” *J. Forensic Sci.*, vol. 41, no. 3, p. 407-417, 1996.

[2] V. J. M. DiMaio, *Gunshot wounds: practical aspects of firearms, ballistics, and forensic techniques*. CRC press, 2015.

[3] E. Chaturvedi, “Numerical investigation of dynamic interaction with projectile and harmonic behaviour for T-finned machine gun barrels,” *Def. Technol*., vol. 16, no. 2, pp. 460–469, 2020.

[4] M. Tawfik, “Dynamics and Stability of Stepped Gun-Barrels with Moving Bullets,” *Adv. Acoust. Vib.*, pp. 1–6, 2008.

[5] Bundesministerium des Innern, *Zulassung von Schalldämpfern zur Jagd*. Germany: Bundeskriminalamt Wiesbaden, 2013.

[6] WHO, *Burden of disease from environmental noise*. Copenhagen, 2011.

Appendix

Appendix I– Published Papers

Applied Acoustics 156 (2019) 427–433

Contents lists available at ScienceDirect

Applied Acoustics

journal homepage: www.elsevier.com/locate/apacoust

Technical note

Damping of post-impact vibrations

Michael Muster [a,*], Amer Hameed [a], David Wood [a], Gareth Appleby-Thomas [a], Kilian Wasmer [b]

[a] Centre for Defence Engineering, Cranfield University, Defence Academy of the United Kingdom, Shrivenham SN6 8LA, UK
[b] Laboratory for Advanced Materials Processing, EMPA, Swiss Federal Laboratories for Materials Science And Technology, 3602 Thun, Switzerland

ARTICLE INFO

Article history:
Received 1 October 2018
Received in revised form 28 July 2019
Accepted 30 July 2019

Keywords:
Flexural vibrations
Damping
Metallic plate
Boundary reflection

ABSTRACT

Impacts of solid bodies on rigid plates produce loud noise and strong vibrations. During this impact, flexural waves travel circularly outwards from the point of impact. These waves are used to determine the properties of the impacting body. For accurate location and momentum measurements, it is necessary that the set of flexural waves pass acceleration sensors just once without being disturbed by reflections.

Different plate designs are tested with the aim of evaluating the shape, which offers the best damping properties against strong single impacts.

The investigations showed that the damping properties are significantly better if the plates are of a star-shaped design and feature a damping layer.

The work offers a solution to achieve significantly better damping properties and a better signal for the investigation of impacts. The results demonstrate that it is a promising approach for an impact detection system, which could be equally applicable to acoustic damping applications.

1. Introduction

This study investigates the effect of different plate shapes on their damping behaviour after a single excitation burst. The focus is on a short-time scale from microseconds up to milliseconds. Small-arms projectiles are structures that weigh from 2 to 10 grams, which travel at supersonic speed and produce strong acceleration and acoustic signals when they impact. Due to their high speed and rotation rates, they are generally difficult to characterise during flight and impact. The impact characterisation is used for applications like the estimation of range-danger areas after deflection of the projectile on oblique plates. For such purposes one needs to know the position of impact and the momentum transmitted into the plate. With this information, one can estimate the residual energy and deflection angle of the projectile after impact. The main challenge of the impact detection is connected to huge decelerations and large deformations in a short time regime. Such projectiles are often too small to be equipped with sensors. Therefore, sensors mounted on witness plates are widely used for impact detection devices. So-called Impact Soft-Recovery Experiments [1] are made, for example, with impact detection devices. In this case, the target under investigation is a brittle plate, monitored by an interferometer. The projectile impact generates strong vibrations, the characterisation of which helps to calculate the location and nature of the impact. Espinosa et al. [2] showed that it is possible to get a cleaner raw signal from the target plate by using a star-shaped flyer geometry. Their tests revealed that the effect of the outer layer of the plate on the impact zone itself could be minimised significantly. Besides interferometers, accelerometers are frequently used to determine properties of the impact like the impact position or the transferred momentum [3]–[5]. One of the major sources for measurement inaccuracies are random and reflected vibrations [6]. Hammetter et al. used an array of accelerometers fixed on the plate to determine the momentum transferred. They showed that geometrical properties of the detecting plate itself might lead to inaccurate measurements. Another source of measurement inaccuracy is electronic filtering of the acceleration data. Best practice for severe-shock investigations is to use mechanically insulated accelerometers [7]. Severe mechanical shocks such as caused by bullet impact, typically lead to six degrees of freedom accelerations represented in broadband frequencies. This makes it difficult to determine the overall momentum [6], or the position. Mechanical insulators combined with electrical filters were found to be an appropriate way to overcome this problem. The impacting body excites the witness plate within a very short time in a non-linear and random vibration regime, where scattering and reflections of vibrations at boundaries will occur [8], [9]. Right after the impact is the moment when the point of interest occurs. This moment is called the Arrival Time

* Corresponding author.
E-mail addresses: michael.muster@cranfield.ac.uk (M. Muster), a.hameed@cranfield.ac.uk (A. Hameed), d.wood@cranfield.ac.uk (D. Wood), g.thomas@cranfield.ac.uk (G. Appleby-Thomas), kilian.wasmer@empa.ch (K. Wasmer).

https://doi.org/10.1016/j.apacoust.2019.07.040
0003-682X/

(AT). The AT is defined as the time when the sensor detects the first set of waves, which originate from the impact position. Consequently, knowing the exact AT is necessary to recalculate the exact impact position [10] with the Time Difference of Arrival (TDOA) algorithms. TDOA algorithms are often used nowadays, and optimised for passive tracking of wireless communication systems [11]. The underlying computations for wireless-devices tracking and impact location, however, are the same. The main issue for an accurate triangulation of impact remains the accurate AT detection. For flexural group waves travelling in steel at a speed of more than 2500 m/s, even minor errors lead to large positioning errors. The speed of sound in the target material and the AT difference must be known for positioning. Furthermore, by knowing the sensors' positions, one can easily calculate the position of the impact/of the origin of the waves by numerical methods [12]. Mingzhou et al. showed the possibility of precisely detecting the AT of flexural waves using accelerometers after the impact of a test weight dropped on a large steel plate, even in noisy environments like power plants [13]. They used a sophisticated decomposition algorithm combined with the Hilbert Huang Transformation. They found that the proposed algorithm was capable of detecting the AT with a precision of several milliseconds. The main reason for the inaccuracies was still the noise in the signal. During a ballistic impact on a plate, stochastic waves appear inevitably, which affects the precision of the AT calculation. In an idealised case, flexural and compression waves emitted from the origin of impact would not be reflected. This can be realised by two approaches: Using a plate significantly larger in comparison with the investigated area (this approach is presented in [9]), or using a special damping plate. A very interesting approach is a plate of special shape which decreases in thickness at the edge (called a wedge shape) in a power-law profile [14]. The different waveforms are eliminated due to internal refraction. However, the power-law shape is difficult to manufacture, which is why it is not used in practical vibration dampers [15]. Possible ways of manufacturing this wedge shape are 3D milling or casting [16], both of which are expensive. For hardened-steel and supersonic impacts, such delicate and large structures are normally unsuitable to be made by industrial methods. There are some highly effective damping alternatives which are easier to manufacture, i.e. the application of a thin absorbing layer to the plate surface [14]. Another possibility is an acoustic black hole, reduced in its space requirements as proposed by [17]. This showed that a damping layer covering and wrapping the acoustic black hole results in a reduced vibration. However, for impact analysis purposes, other shapes are more desirable. From a manufacturing point of view, if one wants to process a hardened wear plate, just 2D shapes should be used. Such plate designs can be produced by water-jet or plasma cutting. Possible shapes that can be produced easily are polygons or any kind of round, but two-dimensional. Star-shaped (polygonal) flyer plates are also able to trap compression waves, as used for normal impact soft-recovery experiments [2]. With the star-shaped plate, much lower level reflection is observed during impact. This enhances the quality of the raw data in ballistic experiments. The edge morphology can serve as a trap for waves and was investigated computationally in [18]. Apart from the computational investigations, the real noise-damping properties of the plates need to be quantified. The plate experiences random vibrations after significant impulse is applied. The plate's response cannot be assessed using purely analytical models [8]. The random-decrement method is a possible way to quantify the damping factor of a system. This approach is suitable for systems which are randomly excited, for example fluid flow against rigid structures like ships or bridges [19]. Using the logarithmic decrement to determine the damping ratio is widely used for such damped systems [20]. However, this system is unsuitable for the present application because the plate is just excited once with a strong burst, then recovers fully as the vibration decays down to non-excited state. The random decrement method would be more applicable if the system was excited by many fragments impacting simultaneously. In the case of a strong excitation burst, the plate vibrates stochastically. According to the experimental results of Humbert et al. [8], all frequencies are abundant during the first 70 ms after excitation with one strong mechanical burst. All frequency bands of the broadband spectra of the free vibrational decay have different decay rates. Itis not possible to calculate just one valid damping ratio [21], especially if one wants to calculate the AT, which is the case in this investigation. In this case, one can use band-pass filters to determine each specific damping ratio. The drawback of this system is that the results are strongly dependent on the chosen bandwidth of the band-pass filter [22]. The information about the properties of the impacting mass and the AT is retained in flexural waves only for the first few post-impact milliseconds. To get a meaningful result, it is desirable that the first 100 μs are not disturbed by reflections. It is possible to sort out specific reflections using wave separation [23]. This approach, however, works for ultrasonic signals because small changes in frequency may be detected with such systems. Severe shock signals need to be detected with mechanically prefiltered accelerometers. The recorded acceleration broadband signal decays exponentially after a single excitation event. This is comparable to the decay of sound in room acoustics. In room acoustics, the "reverberation time" is a common way of describing a signal decay pattern. The reverberation time is defined as an exponential decay fit, which has the advantage that there is just one main decay rate, which includes all frequencies. This reverberation time was introduced by Schroeder [24] in 1965. He used filtered pistol shots to produce a single excitation event comparable to the application described in this paper. Since the damping is directly related to the reverberation time [25], this is a meaningful quantity for the system performance in the present case. The reverberation time is mostly measured to determine room acoustics [26], but can also be measured for any solid plates, for instance in musical equipment [27]. This paper describes different plate shapes and their capabilities to attenuate the noise, relative to a reference plate. The increased damping properties enhance the detection of the AT. The vibrations are detected with accelerometers capable of measuring uniaxial accelerations. They are normally positioned on the plate. This means that only flexural waves will be measured. Because of the similarities to the acoustical reverberation of a sound burst (or filtered pistol shot), the reverberation time is chosen as quantification method. In an initial study, a drop test is performed in a small-scale experiment to determine the most efficient plate shape. This shape is produced in a larger scale model and used for ballistic impact tests.

1.1. Experimental procedures and materials tested

1.1.1. Test procedures

Two different test scenarios were chosen to estimate the scalability of the system. The goal of the two scenarios is to evaluate and assess the damping properties of plate shapes after impact. The most promising design after the first test scenario is verified on a larger scale. All shapes were produced using the water-jet cutting technique which results in a surface roughness of Ra 25 μm. This is comparable to standard sandblasting. The overall tolerances is 0.1 mm, independent of the plate thickness. Concave edges are produced with radii of 0.75 mm, convex edges with minimum radii of 0.08 mm. In the case of the shapes subject to the power law, the exponent was approx. 2.8 for both test scenarios. The surface of the plate has a Ra of 8 μm, which is relatively smooth. The surface of the plate has no disturbances except for the screwed-in accelerom-

eters. The data acquisition system for the accelerometers was the NI USB-6366 (National Instruments, USA) in both scenarios, with simultaneous sampling, acquiring and recording data every 0.5 μs. Simultaneous sampling is very important for such tests, so that the exact time shift between the excitation events is measured. The acceleration sensors used for both scenarios are shock sensors 350B01 (PCB, USA), mechanically isolated and electrically filtered. The signal conditioner was the 483C40 (PCB, USA).

The data acquisition time was set to 150 ms, i.e. long enough to investigate the signal decay. Each test was repeated three times. The maximum signal amplitude acquired was normalised to ± 1. With this approach, one can compare low-momentum impacts with high-momentum impacts. The time from primary wave detection until 1% of the max amplitude is reached, was used to calculate the reverberation time of the different plates. This was necessary to quantify and compare the results.

1.1.2. First test scenario

The first test scenario was a small-scale setup; plates of four different shapes were used to acquire information about their damping behaviour. All plates for the first set of experiments consisted of 5 mm thick S275J2 steel. As a reference, a simple rectangular plate was analysed. This had four additional small rectangles attached for fixation purposes as shown in Fig. 1a–d. Most ballistic standard tests rely on square or rectangular plate shapes. Square plates are used in the interest of simplicity and cost savings. A second reference plate of oval shape was used to examine whether this would enhance the damping properties. The third plate was made with projections featuring a 60° angle in accordance to the findings of [2] and [18], called the "star-shaped with 60° edge" plate. The height of the triangle is 35 mm. It is assumed that, with this shape, the damping rate increases significantly. The fourth shape is the combination of the power-law profile and the star-shape called "star-shape with power-law edge", the edges are shown in Fig. 2c. The number of spikes of the fourth shape is the same as in the case of the star-shaped plate. The width between the corners remained the same. However, the length of the edge increased to 98 mm. As suggested in [14], the surface was treated with an absorbing surface, a magnetic polymer compound. This layer can be removed if required. The star-shaped with 60° edge plate and the star-shaped plate with power-law edges were equipped with three thread bores each to accommodate three sensors. One of these bores is closer to the centre, while the second is near the concave edge of the spike and the third in the centre of the convex edge as shown in Fig. 2b. In this way, reflections and backscatter can be detected by monitoring and comparing the sensor data. However, sensor position and the speed of sound in a given material are parameters which can be controlled very accurately.

The plates were impacted by a falling steel roller bearing ball, its layout shown in Fig. 2a. The ball's mass was 16.84 g, representing a widely used 16 mm ball bearing. The reason for using such an object was that it consists of 100cr6 hardened steel. These drop weights can sustain several drops without any deformation. The release height was 3.8 m, the release mechanism an electromagnet

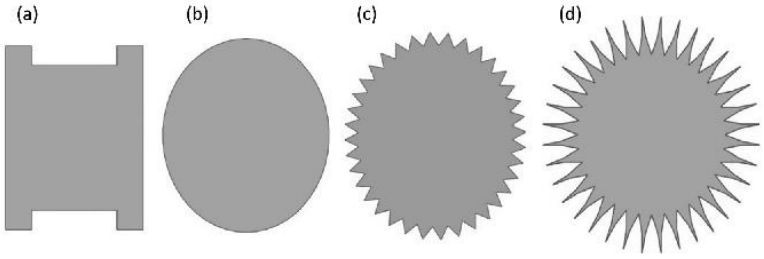

Fig. 1. Different plate shapes: (a) reference, (b) oval (c) star Shape with 60° edge (d) star shape with power-law edge. The reference consists of five rectangles, with the large one representing the main impact zone. The four small rectangles are fixation points. The oval plate is a second reference which has, like (c) and (d), an oval main impact zone, but no spikes.

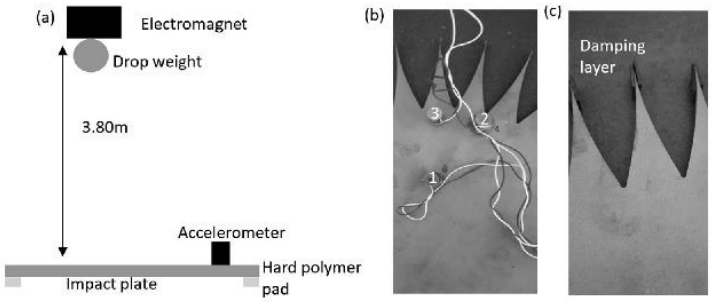

Fig. 2. First test scenario: (a) schematic test layout, (b) accelerometer with the sensor numbers, sensor 1 is most proximal to the centre, the other two are at the same distance from the centre. Sensor 2 is exactly in front of the concave edge to see if this edge influences the signal. Sensor 3 is in line to the spike of the plate. (c) damping layer which is basically a magnetic polymer compound which "sticks" perfectly to the contour of the plate.

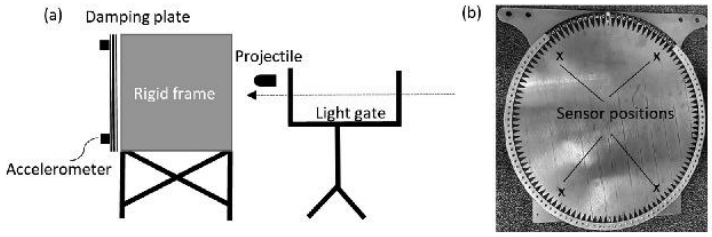

Fig. 3. Second test scenario: (a) schematic test layout with the heavy (800 kg) metal frame and the plate attached to the back of the frame. (b) star-shaped plate with power-law edges with rubber damper. The plate is placed in an assembly of rubber pieces and a fixation plate suitable for mounting in the heavy metal frame.

switched by a transistor. The standard deviation of the overall drop accuracy was 0.1 mm. This drop height delivered a kinetic energy of 0.62 Joule.

The damping layer was applied only to the last section of the power-law spikes. The size of the damping layer material (10 mm × 20 mm × 1 mm) was the same in all analysed cases as shown in Fig. 2c. The damping layer was placed on the oval plate, the star-shaped 60° edge plate and the star-shaped plate with power-law edges.

For the plates with geometries such as the ones in Fig. 1b, c and d, it was possible to add an equally distributed magnetic damping layer on the spikes or attach an equally distributed magnetic damping layer to the oval plate. This is not possible in the case of the rectangular plate. The reason is that the rectangular geometry has less edges and they are not equidistant.

1.1.3. Second test scenario

The second experiment was made using a 12 mm thick Hardox 500 tempered steel plate exhibiting a yield strength of 1300 MPa [28] as target, against a supersonic impacting projectile.

Two different plates were tested in this scenario: A rectangular reference plate (Fig. 1a) and a star-shaped plate with power-law edge (Fig. 1d). Both plates had a thickness of 12 mm, the reference plate was 700 mm wide and 800 mm long, while the star-shaped plate with power-law edge (Fig. 1d) had a diameter of approx.800 mm. The reference plate was fixed in a rigid frame at the four corners as shown in the Fig. 3a. The power-law edged plate was mounted between a frame consisting of two steel rings and then fixed into the rigid frame shown in Fig. 3a. A rubber inlay (called rubber damper) was mounted between the spikes and served for both damping and fixation purposes.

The plates were tested with a 9 mm 7.5 g Full Metal Jacket (FMJ) projectile with a velocity of 380 m/s. These projectiles were chosen because of the low occurrence of backscattering. Another reason is that they are NATO-compliant and widely available for such tests.

The velocity was measured 15 m before impact, using a BMC 31 (Kurzzeit, Germany) ballistic data processing system and an LS 260 (Kurzzeit, Germany) light gate for velocity measuring. The velocity drop within the light gate is considered, using the known drag coefficient of the specific FMJ projectile type. Knowing the velocity drop between measurement system and impact is very important to determine the reference impact velocity. In this case all four sensors are equidistant from the centre as shown in Fig. 3.b. This is easier for triangulation, which will be applied in future.

2. Results and discussion

2.1. General observations

In the case of the plate with power-law edge and rubber damper, the highest excitation level occurs 10–20 μs after impact. A similar decay pattern was observed in both experimental scenarios. This in spite of the fact that the impact energy in the second experiment was approx. 900 times higher and the plate was 30 times heavier than in the first test scenario. The results of the experiments conducted for the first and second test scenarios differ greatly in their repeatability of the impact position. In the case of the first test scenario, the radial standard deviation was less than 1 mm. The second test scenario, performed with 9 mm projectiles, showed a radial standard deviation of impacts of 40 mm. The reason for this impact distribution is the performance of the projectile acceleration system.

Interestingly, the distribution of impact positions does not affect the standard deviation between the measurements of the reverberation time shown in Tables 1 and 2. The reason for this stable reverberation time might be that, in all cases, there are some flexural waves reflected by the boundaries which keep the plate in oscillation during a few milliseconds.

One of the most important tasks of the damped plate is to reduce the vibrations occurring after an impact event. By damping the plate, one ensures that the detected vibrations originate directly from the impact itself and not from the boundary reflections.

Fig. 6 shows the acceleration signal acquired for the reference plate (shape like Fig. 1a) and the star-shaped plate with power-law edges (shape like Fig. 1f). In this figure, the reference plate shows a package of small flexural waves which are detected by the accelerometer 30 μs before the main wave packages arrive. These packages disturb the positioning and the momentum measurement process, since it is not possible to distinguish between

Table 1
Averages and standard deviations of 9 measurements in the first test scenario.

Shape	Average reverberation time (ms)	STD (ms)
Reference	135	7
Oval	158	1.2
Oval with damping layer	134	2.4
Star shape	174	0.8
Star shape with damping layer	63	0.6
Star-shaped plate with power-law edges	147	1.1
Star-shaped plate with power-law edges with damping layer	37	0.1

Table 2
Averages and standard deviations of 9 measurements in the second test scenario.

Shape	Average reverberation time (ms)	STD (ms)
Reference	214	2.9
Star-shaped plate with power-law edges with rubber damper	9	0.9

the small reflected flexural waves and the wave package which is emitted directly from the impact. This is especially true if the two wave packages are overlapping more than the ones represented in Fig. 6a. With the proposed design, a very pure impact signal can be produced, as seen in Fig. 6b. In this signal, no disturbances are visible before the main wave package arrives. This enhances the accuracy of the impact measurement significantly.

The magnitude of the peaks is rising steadily and no significant disturbance in the signal can be detected before the first small excitation occurs. In the case of the star-shaped plate with power-law edges with rubber damper, the acquired signal is significantly different. The package of small waves does not occur. In both cases the magnitude of the acceleration peak is about 20,000 m/s^2.

The best plate shape for damping single impacts is the star-shaped plate with the power-law edges with the damping layer. This shape is a combination of the shape of acoustic black holes and the star-shaped flyer plate. The damping effect of general acoustic black holes, as in the case of the power-law shapes, is strongly reduced, since acoustic black holes react sensitively to

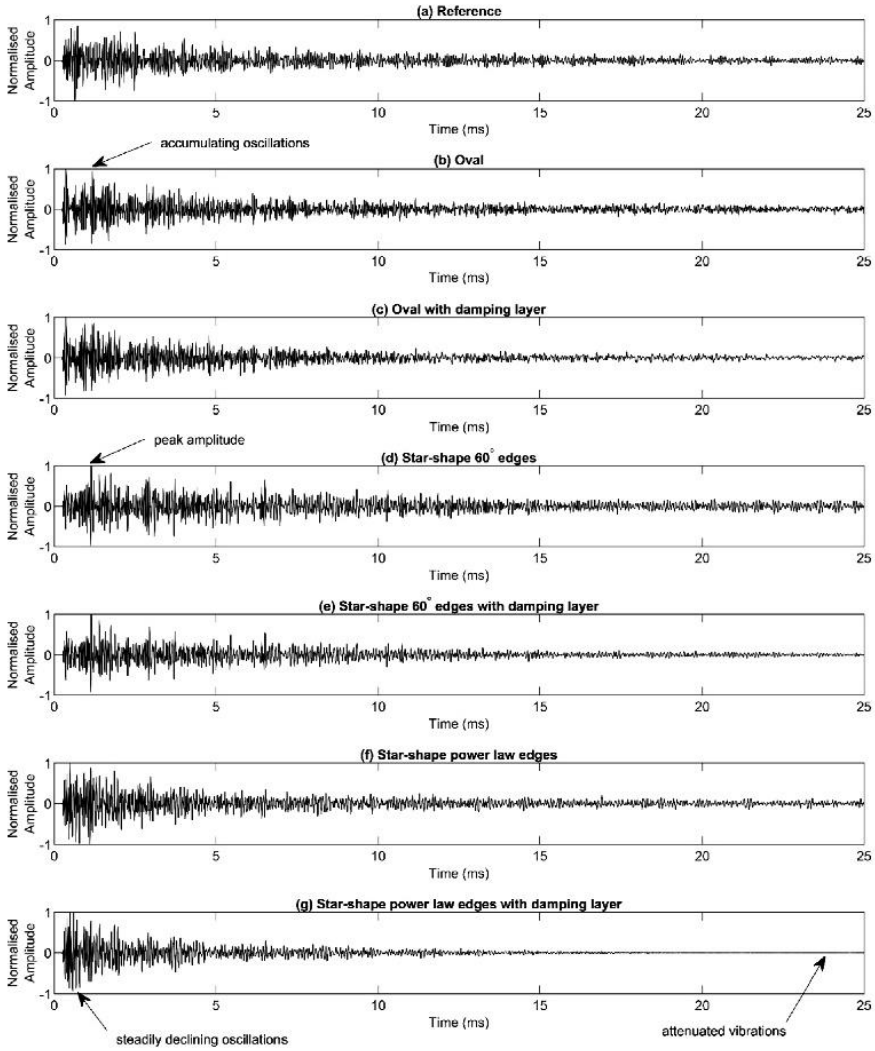

Fig. 4a–g. Typical vibration signals of the first test.

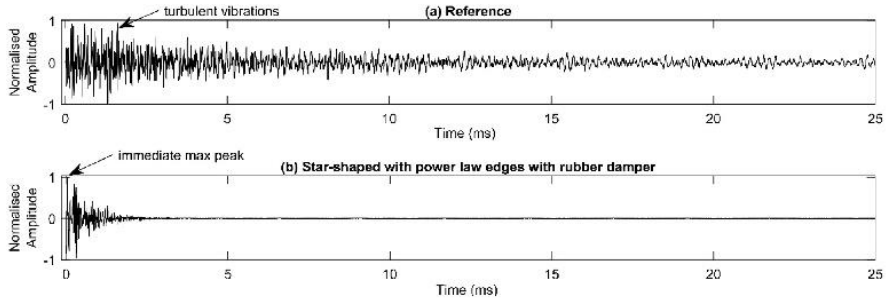

Fig. 5. Typical vibration signals of the second test (impact of 9 mm projectile). (a) The reference (rectangular) plate which shows still some oscillations after 25 ms. (b) Shows a significant signal decay after the initial excitation, after 4 ms one cannot see any remaining oscillations rising beyond the threshold.

truncation imperfections, material failures, surface roughness and reduced length of the last part of the spike [16]. However, with the use of rubber dampers, the damping effect is still significantly better than compared with the star-shape 60° edge with the damping layer. This can only be explained by the fact that the acoustic black hole is an additional help for the star-shape geometry.

In all measurements, there is a fast-oscillating signal body followed by sharp peaks. These peaks are occurring stochastically because the plate is excited in a turbulent regime. This makes the quantification of the damping system challenging, since the peaks of the signal decay faster than the noise.

The reverberation time was chosen as the most stable value to quantify the system. It does not depend on a specific frequency, which is very important for such turbulent systems. The results reported here are promising and a method can be developed to analyse more sophisticated impact detection systems.

2.1.1. First test scenario

The data presented in Fig. 4 are the raw data representing typical plate vibrational signals for all plates tested in the first test scenario. One can see that the plate shape influences the signal decay pattern.

The damped and undamped power-law edged plate exhibits a steady signal decay, whereas the oval plate shows a more oscillating behaviour after the initial excitation. It is also recognisable that the peak amplitude occurs shortly after impact in the case of the power-law shaped structures. In the case of other structural shapes, especially the star-shaped plate with 60° edge, however, slow rising amplitudes of the acceleration signal may occur due to internal compressive waves reflecting at the boundaries.

Compression waves travel through the plate at almost twice the velocity of flexural waves. The accelerometers detect in one direction only, and therefore do not detect these initial in-plane com-

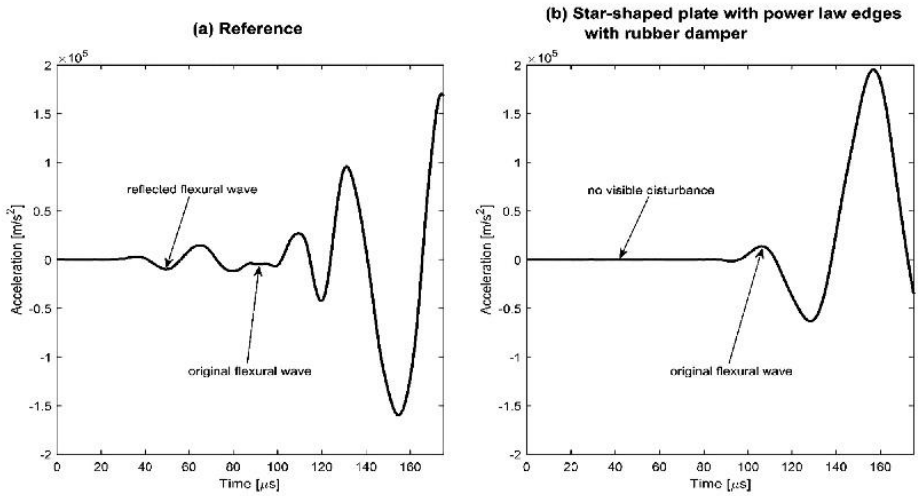

Fig. 6. Acceleration signal acquired on (a) reference plate (b) star-shaped plate with power-law edges with rubber damper. This picture shows the benefit of the power-law edge design, the steady increase without disturbances of the wave amplitude after impact. Disturbances that can be recognised in the case of the reference plate lead to an inaccurate AT detection.

pressive waves. At the boundary, the compressive waves are reflected and partly converted to flexural waves. These reflected flexural waves are unwanted for the triangulation process, since they conflict with the arrival time of the unreflected flexural wave caused directly by the impact. Such a behaviour can be seen in Fig. 6a.

The damping layer has a significant influence, reducing or eliminating the low magnitude vibrations after 20 ms, evidence of which is observed in Fig. 4g. This is in keeping with the experimental investigations of Kyrlov and Winward [15]. The small damping layer can absorb the energy of small magnitude vibrations. However, this effect is not recognisable in the oval damped case.

2.1.2. Second test scenario

Fig. 5 presents the typical data of the vibrational signal for the plates tested in the second test scenario. The decay effect of damping is easily recognisable in the case of high-velocity impacts as shown in Fig. 5b (star-shaped plate with power-law edges with rubber damper). For the reference plate, the highest excitation level is delayed to 1 ms after the first oscillation is detected. The oscillations are still recognisable after 25 ms. Comparing the reference plate with the star-shaped plate with power-law edges and rubber damper, one can see a significant reverberation time reduction from over 200 to under 10. Fig. 6

However, the primary aim is to improve the information/loss ratio so that the signal contains a larger portion of impact information compared with the overall information. Since the signal is strongly reduced after the first few reflections, this aim is met by using the plate with power-law shaped edge.

3. Conclusions

Single-impact tests on differently shaped steel plates have been shown. The major test criteria were the reverberation time between the first excitation and the point of time when the plate does not vibrate any more. This property is of interest because it enhances the measurement of impact properties. Filtered shock accelerometers were used to acquire the signals. The tests were performed in two scenarios. First, on a small scale with four different plate shapes and a low-energy impact. The second test scenario was performed with 30 times heavier plates with a high-energy supersonic bullet impact.

The results show that the plate shape has a significant influence on both vibration pattern and signal decay. The reverberation time is affected by vibration damping layers in combination with toothed edges. The effect of the damped 60° spike is less significant than the effect of the damped power-law shaped spike. Compared with the reference plates, it is possible to reduce the reverberation time by a factor of roughly 24, which is a huge advantage if one uses the witness plate as measurement system.

Despite the fact that the kinetic energy from the impulse tests with a drop weight falling under gravity and a projectile flying at supersonic speed differs strongly, the oscillations resulting from vibration-time properties are comparable. The star-shaped plate with power-law edges which performed best with respect to the reverberation time, can be used to design new devices which are suitable for ballistic impact investigations. For example, a ricochet measurement device capable of measuring the point of deflection on a first plate and the point of impact on a second. Furthermore, such measurement plates are also suitable for the location of multiple impacts in the same period.

It is known from the acoustic black-hole effect and from star-shaped flyer plates that they influence the wave propagation. This is particularly true with a combination of the two shapes and strong excitation bursts like ballistic impacts.

Another interesting fact is that the sound appears to be less intensive, since the acoustic reverberation time is shorter, so that it is also possible to use this system for future sound and noise reduction applications. Directly applied examples are silent bed plates for punch presses, surface metal treatments in musical situations, quieter reciprocating engines and cyclical systems.

References

[1] H.D. Espinosa, Low-Velocity Impact Testing, vol. 8; 2000. p. 539–59.
[2] Espinosa HD, Raiser G, Clifton RJ, Ortiz M. Performance of the star-shaped flyer in the study of brittle materials: three-dimensional computer simulations and experimental observations. J Appl Phys 1992;72(8):3451–7.
[3] Morsy R, Marzouk H, Haddara M, Gu X. Multi-channel random decrement smart sensing system for concrete bridge girders damage location identification. Eng Struct 2017;143:469–76.
[4] Dahlen U, Ryden N, Jakobsson A. Damage identification in concrete using impact non-linear reverberation spectroscopy. NDT E Int. 2015;75:15–25.
[5] Allaeys F, Luyckx G, Van Paepegem W, Degrieck J. Characterization of real and substitute birds through experimental and numerical analysis of momentum, average impact force and residual energy in bird strike on three rigid targets: a flat plate, a wedge and a splitter. Int J Impact Eng 2016.
[6] Hammetter CI, Jones RL, Stauffacher HL, Schoenherr TF. Measurement and modeling of supersonic hailstone impacts. Int J Impact Eng 2017;99:48–57.
[7] Agnello A, Dosch J, Metz R, Sill R, Walter P. Acceleration sensing technologies for severe mechanical shock. Sound Vib. 2014;48(2):8–U20.
[8] Humbert T, Cadot O, Düring G, Josserand C, Rica S, Touzé C. Wave turbulence in vibrating plates: the effect of damping. EPL (Europhysics Lett. 2013;102(3):30002.
[9] Zhao G, Hu H, Li S, Liu L, Li K. Localization of impact on composite plates based on integrated wavelet transform and hybrid minimization algorithm. Compos Struct 2017.
[10] Perelli A, De Marchi L, Marzani A, Speciale N. Frequency warped cross-wavelet multiresolution analysis of guided waves for impact localization. Signal Process 2014;96(PART A):51–62.
[11] Mušicki D, Kaune R, Koch W. Mobile emitter geolocation and tracking using TDOA and FDOA measurements. IEEE Trans Signal Process 2010;58(3 PART 2):1863–74.
[12] Gustafsson F, Gunnarsson F. Positioning using time-difference of arrival measurements. IEEE Int Conf Acoust Speech Signal Process 2003;6. VI-553-6.
[13] Liu M, Yang J, Cao Y, Fu W, Cao Y. A new method for arrival time determination of impact signal based on HHT and AIC. Mech Syst Signal Process 2017;,86:177–87.
[14] Krylov VV, Tilman FJBS. Acoustic 'black holes' for flexural waves as effective vibration dampers. J Sound Vib 2004;274(3–5):605–19.
[15] Krylov VV, Winward RETB. Experimental investigation of the acoustic black hole effect for flexural waves in tapered plates. J Sound Vib 2007;300(1–2):43–9.
[16] E. Bowyer, V. Krylov, Acoustic black hole manufacturing for practical applications and the effect of geometrical and material imperfections, no. 4; 2016. p. 2411–21.
[17] Lee JY, Jeon W. Vibration damping using a spiral acoustic black hole. J Acoust Soc Am 2017;141(3):1437–45.
[18] Howard A. Morphological control of censile release in ceramic penetration. Cranfield University; 2014.
[19] Nakutis Z, Kaškonas P. Bridge vibration logarithmic decrement estimation at the presence of amplitude beat. Meas J Int Meas Confed 2011;44(2):487–92.
[20] Feldman M, Braun S. Nonlinear vibrating system identification via Hilbert decomposition. Mech Syst Signal Process 2017;84:65–96.
[21] Liao Y, Wells V. Modal parameter identification using the log decrement method and band-pass filters. J Sound Vib 2011;330(21):5014–23.
[22] Lardies J, Gouttebroze S. Identification of modal parameters using the wavelet transform. Int J Mech Sci 2002;44(11):2263–83.
[23] Avanesians P, Momayez M. Wave separation: application for arrival time detection in ultrasonic signals. Ultrasonics 2015;55(1):15–25.
[24] Schroeder MR. New method of measuring reverberation time. J Acoust Soc Am 1965;37:409–12.
[25] Arcas K, Chaigne A. On the quality of plate reverberation. Appl Acoust 2010;71(2):147–56.
[26] Gomez V, Escobar JM, Morillas Barrigon. Analysis of intelligibility and reverberation time recommendations in educational rooms. Appl Acoust 2015;96:1–10.
[27] Boullosa RR. Vibration measurements in the classical guitar. Appl Acoust 2002;63(3):311–22.
[28] Dudziński W, Konat Ł, Pękalski G. Structural and strength characteristics of wear-resistant martensitic steels. Arch Foundry Eng 2008;8(2):21–6.

AIP Advances

Dynamic qualitative bolt force measurements for investigating influence factors on the pushout effect of small calibre ammunition

Cite as: AIP Advances 9, 065020 (2019); https://doi.org/10.1063/1.5092167
Submitted: 08 February 2019 . Accepted: 14 June 2019 . Published Online: 25 June 2019

Michael Muster, Amer Hameed, and David Wood




AIP Advances ARTICLE scitation.org/journal/adv

Dynamic qualitative bolt force measurements for investigating influence factors on the pushout effect of small calibre ammunition

Cite as: AIP Advances 9, 065020 (2019); doi: 10.1063/1.5092167
Submitted: 8 February 2019 • Accepted: 14 June 2019 •
Published Online: 25 June 2019

Michael Muster,[a] Amer Hameed, and David Wood

AFFILIATIONS

Centre for Defence Engineering, Cranfield University, Defence Academy of the United Kingdom, Shrivenham SN6 8LA, UK

[a]Corresponding author. E-mail address: michael.muster@cranfield.ac.uk (M. Muster).

ABSTRACT

A small calibre weapon system consists of the weapon and the ammunition. In the case of bolt action rifles during the process of firing, the breech is a rigid bearing which prevents the casing from being pushed out. However, not the whole pushout force is taken by the bolt. Due to friction forces at the casing boundary, the chamber of the weapon can absorb a significant part of the pushout force. The duration of the pushout force is in the order of milliseconds. Piezoelectric strain gauges are capable of recording such short time events qualitatively. To increase the measurability of force obtained from raw signal, is filtered using a bandpass filter and applying a signal envelope. The results from the strain gauges are verified by a piezoelectric force washer. In this paper, two different lubrication states and two different casing materials are analysed to evaluate their influences on the force absorbed by the bolt. The analysis indicated that lubricated casings lead to bolt forces which are more than three times higher when compared unlubricated casings. The unlubricated steel casing also showed a significant lower bolt force when compared with the regular brass casing. However, this effect is reversed, if the casing is lubricated. This work demonstrates how to measure highly dynamic events. The acquired results can be directly applied to 5.56x45 bolt action rifles. These measurements may also have a significant influence on self-loading rifles, since the process of reloading is also dependent on the pushout force. The general application area is target competitive shooting and military purposes.

INTRODUCTION

The process of firing a weapon system is a vivid example of the application of the Newton's third law. The gas generated by the burning propellant accelerates the projectile in the weapon until it leaves the muzzle. This acceleration process leads to recoil. During the acceleration, the casing of the cartridge experiences high pressure. This leads to high pushout forces, but for an extremely limited time. However, the chamber and the bolt of the weapon holds the cartridge in place during this time. See Figure 1.

The overall pushout force is not purely taken by the bolt of the weapon. The cartridge casing can be assumed as a pressure vessel which is plastically and elastically deformed during the time while the propellant burns in the chamber. Through this behaviour the casing is pushed against the walls of the chamber. Due to the friction between the chamber walls and the casing, the chamber of the barrel itself is capable of taking some of the overall pushout force.

The bolt force depends mainly on four factors: The surface area of the case head, where the pressure applies; the pressure in the casing; the friction between the chamber wall and the casebody; and the material properties of the chamber and the casing. The pressure curve in the chamber should be highly repeatable. Woodley et al. measured the projectile and the propellant mass which resulted in comparable pressure maximas.[1] Since the cartridges are produced in tight tolerances, the area of the casing head can also be assumed as constant. In these experiments, the pushout force is mostly dependant on the material properties of the casing and the chamber and the friction coefficient between these materials.

The behaviour of the dynamics of small arm weapons are often investigated using high speed cameras. However, these cameras are

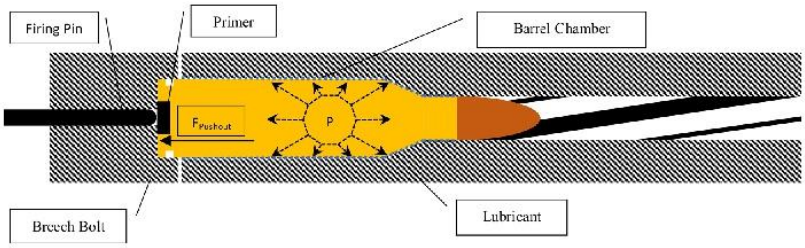

FIG. 1. Schematic view of the cross section of the barrel.

suitable only for visible events, so are not appropriate for bolt action rifle measurements. A breech bolt of a weapon holds the ammunition in place during firing. Often such short duration rigid or invisible processes have been modelled using finite element analysis.[2,3] The advantage of finite element methods is that numerous parameters can be investigated within in a single model by undertaking sensitivity studies. It is also possible to analyse geometric parameters with minor changes in the model. South et al. investigated an interesting interior ballistic model which can be used to estimate the behaviour of a projectile while being pushed through the barrel. Some aspects of the model correlated almost exactly with the reality, but the wear mechanism of the groove formation during the firing was not represented realistically.[4] It is still very difficult to simulate wear and tribological mechanisms such as friction and lubrication in thin film environments.[5]

It is also possible to measure these highly dynamic forces in a real environment. Ritter et al. presented a system to measure the in-chamber primer pushout force.[6] They used a force gauge to measure simultaneous the force on the breech and pressure inside the cartridge. This gave the confidence to predict what occurs in the chamber of the barrel. However, with this system it was only possible to measure the primer force which is produced during a fire. It is not possible to measure the whole force at the bottom of the cartridge.

Another possibility to measure highly dynamic events, such as vibrations, are piezoelectric strain gauges. Michaelides et al. used such strain gauges to analyse the movements of a vibrating bridge.[7] In their investigations they used the strain gauges for frequencies between 1 and 100 Hz. Such strain gauges are capable to quantify much faster events. The raw signal quality is good with such encapsulated strain gauges, so that it is possible to determine noisy but dynamical events with an adequate signal processing.[8]

Bin Tan et al. used standard flexible strain gauges to investigate the effect of steel balls, impacting at 200 m/s on military protection helmets. These strain gauges where used as a reference for validating the FE model.[9] Nevertheless, due to the rigid shape of the military helmets, piezoelectric strain gauges are not suitable for such an application.

One main problem of internal ballistics measurements systems is the noisy signals. The reason for this is that the acceleration process of a bullet is a short time event approximately 1 ms for the investigated calibre, which is comparable with a burst where a lot of mechanical oscillations are generated. In such a noisy environment one has to determine the main physical event of interest. A de-noising approach with discrete wavelet decomposition in combination with a Hilbert Huang transformation for the detection of faults in roller bearings was suggested by Phuong et al. They were more focused on reporting the time of occurrence of the fault.[10] To measure the amplitude of an event, wavelet decomposition is less suitable. For internal ballistic pressure measurements 20 kHz second order Butterworth lowpass filters are generally used.[11] In the case of pressure measurements it is simpler to determine the underlying physical event, such as oscillating pressure waves which may affect the whole measurement. However, in the case of the pushout measurement, more sophisticated filtering approaches are necessary.

Measuring force signals with piezoelectric force washers is widely used from the field of biomedical engineering[12] and the rock drilling technology.[13] Groche et al.[14] used a force washer to indirectly measure the applied force on a punch in a high speed press for a thick steel plate. The indirectly acquired signals where highly comparable to the signals of the measured directly. However, the system had to be calibrated for which they used a stroke rate of 300 strokes per minute. This meant that the duration of the event of interest was of the order of 100 ms.

More dynamical investigations conducted by Jun et al. and Zhang et al.[15,16] Jun et al. investigated the behaviour of spindle in a machining setup using an assembly of force washers. Due to the rotation speed of the spindle and the cutting tool, the cycle of the cutting process was between 50 and 5 ms, which is more comparable with the internal ballistic process which is in the range of 1µs to 1ms. Jun et al. conducted the in-depth investigation of the force washers properties under harsh circumstances. They obtained a very positive outcome for this dynamic application. Zhang et al. showed that even ultrasonic forces can be measured with piezoelectric force washers. Repetitive loads which are applied only for 40 µs applied can be accurately detected. Such timescales are comparable with ballistic tests.

MATERIAL AND METHODS

Two different casing materials were chosen to investigate the influence of the lubrication on the pushout force. In both cases the ammunition type M193 was used, it is a well-defined NATO

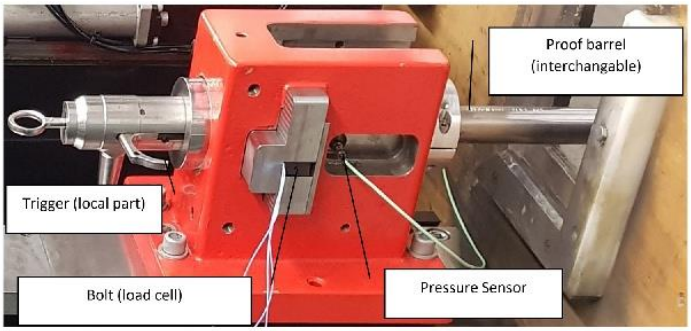

FIG. 2. Measurement System.

standard ammunition stock number.[17] This ammunition type has a projectile diameter of 5.56 mm and the length of the casing is 45 mm. The M193 has been extensively investigated by a number of researchers covering terminal ballistic studies.[18,19] Like some ammunition types, the M193 was produced with two types of casings, a regular brass casing and a steel casing.

To lubricate the casings a fluid called Klübersynt MZ 4-17 was used. This lubricant is recommended for small calibre weapons such as hunting and sporting rifles.[20] For the test, a thin layer of lubricant was applied onto the casing with a brush. The average weight of lubricant applied was 10 mg. The lubricant was equally distributed over the whole casing surface. The unlubricated ammunition was cleaned beforehand using acetone to remove any fat residuals, which might remain from the production process.

The ammunition was tested with a system similar to the Electronic Pressure Velocity and Action Time (EPVAT) measurement setup[21] which is known for NATO testings, see Figure 2. With this system, it was possible to measure the pushout force of the ammunition. Three piezoelectric strain gauges where pasted equidistance to around the load cell with an adhesive, see Figure 3a and 3b. The load cell consisted of stainless steel X5CrNi18-10, which is typically used in such experimental tests.[22,23] This material is also resistant to residue from the burned propellant which is highly oxidising in nature. In addition this load cell also acted as breech bolt, providing a rigid bearing for the ammunition, see Figure 3c.

Multiple sensors were used to analyse the effect of inhomogeneous loading during the acceleration phase of the bullet firing. To assist with vibration damping, the measurement system housing was manufactured from the cast iron. The gun barrels were similar to those used in an EPVAT system and were interchangeable and could be used for multiple calibres. The Kistler 6215 pressure gauge with a Butterworth 20 kHz filter was used as a reference system. The velocity was measured with a light gate. The pressure and velocity were measured in separate test setups.

The National Instruments USB-6366 data acquisition device was used for the tests. It has the ability to simultaneously acquire and record data every 0.5 µs. The piezoelectric strain gauges were of type 740b02 (PCB, USA). They are capable of measuring frequencies up to 100 kHz. In addition, a low pass filter to reduce the mechanical oscillations while measuring the pressure was used. The raw data with a signal amplification rate of 1, was acquired without filter using PCB-482C05 (PCB, USA) signal conditioner.

To verify the results of the piezoelectric strain gauges a precalibrated force washer was additionally used. This force washer gives a signal in volt, which can be directly converted into a force

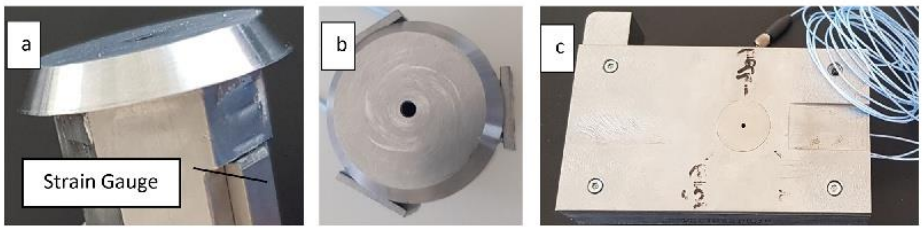

FIG. 3. Qualitative measurement assembly of the load cell (a) Load cell with strain gauge (b) Assembled load cell (c) Fully assembled breech measurement plate.

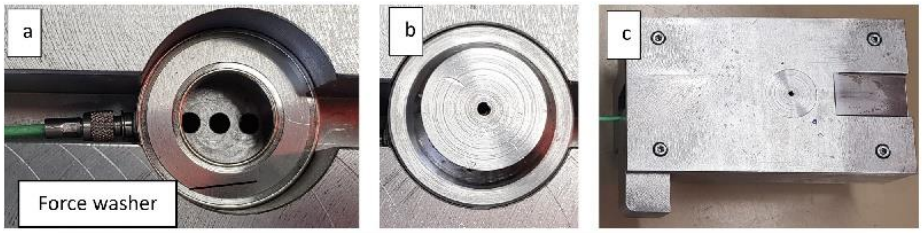

FIG. 4. Quantitative measurement assembly (a) Force washer (b) Protection Plate (c) Fully assembled quantitative breech measurement plate.

signal in Newtons. However, with this system it is not possible to detect asymmetrical loads produced by the casing.

The used force washer was a Kistler 9041a (Kistler, Switzerland), this sensor type is capable of recording forces up to 90 kN. The signal conditioner was a Kistler 5073A (Kistler, Switzerland). Figure 4 shows the assembly of the force washer. In Figure 4a one can see the sensor. However this sensor needed to be protected by a steel protection plate (Figure 4b). The second reason for the steel plate was to provide a rigid bearing for the ammunition. A large difference to the load cell which is equipped with piezoelectric strain gauges is that the measurement device and the rigid bearing is split into two parts.

The data acquisition time was set to 20 ms. As the signal of interest was ca. 4 ms, this acquisition time was sufficient. The pretrigger was set to 0.1 ms. The reason for this extended acquisition time was to ensure that the trigger started the data acquisition before releasing the spring loaded igniter rather than later when the igniter hit the primer. In this experimental set up, it was just possible to trigger the release time. Each test was repeated five times.

To investigate the signal linearity of the load cell with the piezoelectric strain gauges and the force washer, a servo press was used, which applied a defined load for a short time on the system. The servo press was controlled by a calibrated force detector and an additional sensor that controlled the servo press system. This double controlled system ensured the calibration accuracy.

After the shooting, the empty cartridge casings where optically investigated for any scratches or shape deformations. In addition, a longitudinal sectional cut of the empty casings was performed to investigate the case head area and the maximum internal diameter, see Figure 5.

The tests were performed in a closed shooting range behind safety glass. The cartridge was ignited by a remote trigger.

RAW DATA PROCESSING OF PIEZOELECTRIC STRAIN GAUGE SIGNAL

The Hilbert transformation which produces a signal envelope is a widely used function in signal processing, see Refs. 10, 24, and 25. It is especially used in the analysis of a signal that exhibits rapid increase and decay similar to internal ballistics.

A general property of the signal envelope is that a signal wave which carries a lot of high frequency noise can be demodulated into a low frequency signal which represents the main physical property, even if the signal is not cyclic. After transforming the signal into an envelope as shown in Figure 6, it can be used as a stand-alone signal. The signal envelop approach is most suitable for our application because it filters out high frequency peaks that are artefacts, deriving from reflections.

Tests showed that a reliable approach is to measure the force during firing with a combination of a bandpass filter and a signal

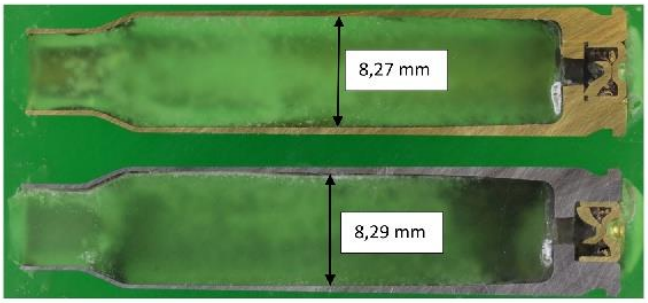

FIG. 5. Analysed casing types and their maximal internal diameter, the upper is the brass casing and the lower is the steel casing.

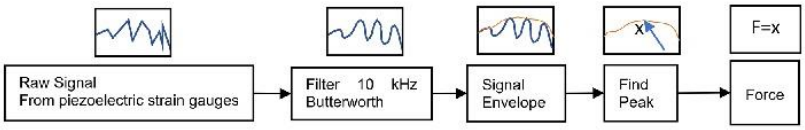

FIG. 6. Signal processing of the raw data.

envelope. Because of the signal characteristics, it is possible to work with the maximum value of the signal envelope to determine the maximum force.

As already mentioned, a servo-press was used to investigate the linearity of the system. However, such a press, only offers limited comparability with the real test situation. In the described system, the signal processing was undertaken exactly as in the real internal ballistic measurements. Therefore, the investigation was performed at its peak. This paper only investigates the linearity of the load cell, it is not aimed to calibrate the load cell to give fully quantitative results.

RESULTS

Figure 7 presents the raw data (in blue) of a typical force signal for all tested casing scenarios. The red dashed line represents the signal envelope: To compare the results, only the signal envelope was used. The duration of the signal is ca. 1 ms. One can note that the raw signal consisted of high frequency components, especially during the ignition phase. These parts are strongly reduced by processing the signal through a 20 kHz filter and generating the signal envelope. The signal envelope exhibits a strong smoothening. However, the time of the first excitation of the envelope is strongly consistent with the impact point of the raw signal. In the unlubricated brass case scenario, measured with strain gauges, the duration of the force is shorter compared to all other scenarios.

The force curves represented in Figure 8 show the post-processed raw signals of the lubricated and unlubricated brass casings measured with strain gauges. The amplitude is normalised relative to the regular case which is considered to be the unlubricated brass casing. One can observe that the starting time of the force generation on the breech is at the same time for both the lubricated and unlubricated casing. However, the peak force of the unlubricated casing falls at 0.4 ms, which is earlier when compared to the lubricated casing falling at 0.55 ms. This observation is for both measurement scenarios valid, for the measuring system with strain gauges and for the one with the force washer.

The unlubricated casing curves shows a lower peak force and in case of the strain gauge measurement a smaller deviation between the max and min peak force compared to the lubricated casings. The semi-quantitative difference is of the ratio of about 1:2 in both peak force and the deviation in the case of brass casings.

The difference between the lubrication scenarios can also be observed in Figure 9 and Figure 10. The variance in the case of steel casings is even stronger. The peak force both in the lubricated steel and the brass casing is exhibited at almost the same time.

However, the time when the force applies to the breech bolt is just marginally different for steel between the unlubricated and lubricated curves. This is contrary to both brass casing measurements, where the force from the cartridge applied on the breech for the unlubricated state acted for a markedly shorter time.

The comparison of some neuralgic data is represented in Table I. It shows a large difference in both the average and the maximum force between the baseline (unlubricated brass casing) and the lubricated casings, which is in both cases ca. factor 3. Even more

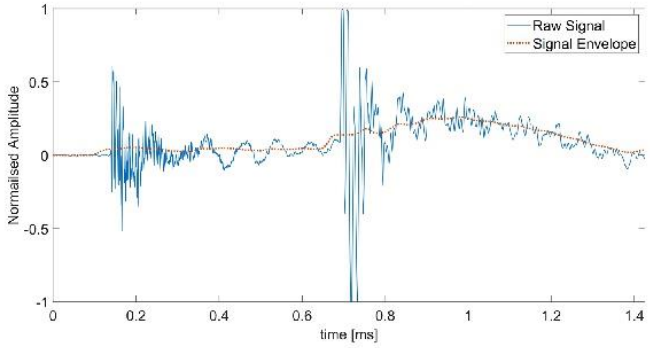

FIG. 7. The raw signal of the strain gauges and its calculated envelope.

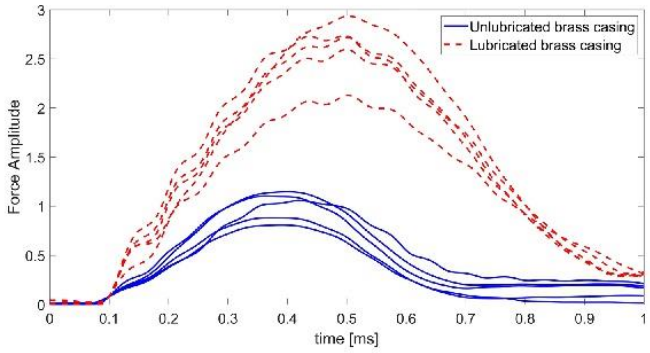

FIG. 8. The peak pushout force measured with piezoelectric strain gauges showing lubricated and unlubricated brass casings.

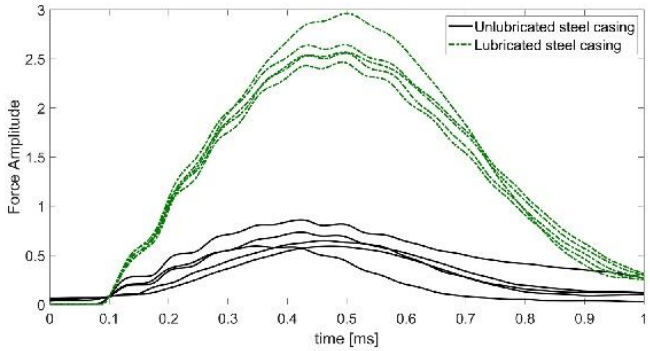

FIG. 9. Comparison of the force signals of lubricated and unlubricated steel casings, referring to the unlubricated brass casing.

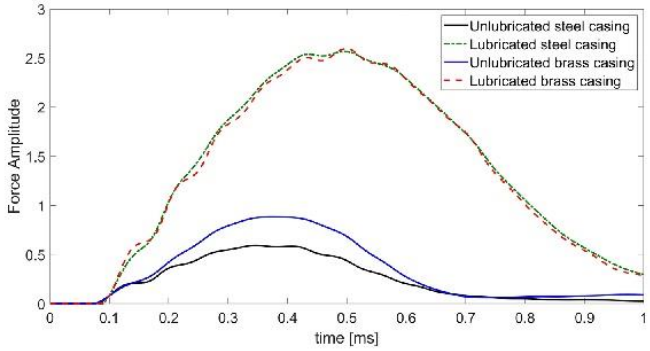

FIG. 10. Graph of average signals of steel and brass casings.

TABLE I. Relative comparison of the peek values of strain gauge measurements.

Description	Average Force	Min Force	Max Force	Average Pressure [Bar]
Brass Unlubricated	100%[a]	81%	114%	3510
Brass Lubricated	268%	212%	293%	3560
Steel Unlubricated	68%	59%	86%	3590
Steel Lubricated	264%	247%	296%	3509

[a]Normalised to the average of the unlubricated brass casing.

dramatic is the difference between the minimal and the maximum force of the steel casing which is approximately exhibiting a ratio of 1:5. In general, unlubricated steel casings produce less force on the breech compared to brass casings. The average reference pressure was acquired with a different measurement system. Each pressure test scenario was also repeated 5 times. The range of average pressures were highly comparable between the scenarios and overall, differences were negligible.

The results of the strain gauge equipped load cell were compared and verified by the force washer. To ensure consistency, the same apparatus such as the proof barrel, housing of the load cell and the trigger mechanism were used for all the experiments. Figure 11 shows the acquired data of the brass casings comparing the results from the force washer with the strain gauge measurements. The force washer signal was filtered with a 20 kHz filter. No signal envelope was applied during the experiments. In general, the results between the force washer measurements and the strain gauge based load cell are highly comparable. In the case of the force washer, a comparatively slightly faster decay to zero was observed in the lubricated brass casing. The comparative difference in the peak force decay is also noticeable in the lubricated casings. The relative average force, tabulated in Table II, indicates that the difference between the lubricated and unlubricated casing is around ca. 2.2 times. Similar magnitudes of relative peak measurements were captured by the strain gauges.

DISCUSSION

The results are consistent with the published models that used finite element analysis.[2] The measurements are conducted with two different approaches and are highly comparable which strengthens the outcome of key results. A change in lubrication leads to a significant difference in the pushout force. The signal processing approach described here is suitable for these force measurements. It was proven that the initial times of excitation remain the same while the main signal is strongly smoothened using signal envelop approach. This leads to a good comparability and comparison.

The engineered piezoelectric load cell as well as the force washer are suitable means of data acquisition devices to proof and measure the pushout force during the firing process. The main advantage of the force washer is that it is easy to get absolute values. If one wants to investigate the load distribution the measurement system with 3 strain gauges is more applicable.

The time during which the force is measured is comparable with the duration during which a projectile is pushed through the barrel. Despite the fact that forces are still expected in the chamber well after the projectile exits the barrel due to residual gas pressure in the chamber.

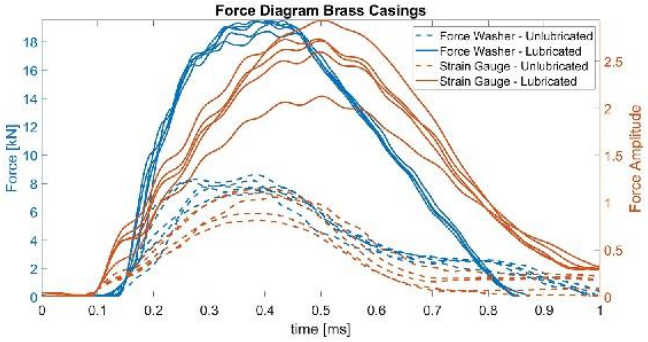

FIG. 11. Force washer signals during the process of firing in comparison to the signal from the strain gauge.

TABLE II. Peek force of the force washer measurements.

Description	Relative average Force	Average Force [kN]	Min Force [kN]	Max Force [kN]
Brass Unlubricated	100%	9.77	9.23	10.42
Brass Lubricated	217%	21.2	20.5	21.72

One significant observation from the analysis of these tests is that the lubrication in the chamber or on the ammunition leads to higher pushout forces. For reference, we have taken the unlubricated brass case as a baseline.

The mechanical material properties of the two casing types differ strongly. However, the fact that the lubricated brass casing produces the same pushout force as the lubricated steel casing leads to the conclusion that the pushout force is mainly depending on the friction between the boundary.

The comparison between the unlubricated steel and brass casing indicates that the steel casing produces significantly lower force on the breech. However, the duration of the load cycle in the case of the steel casing is comparatively longer, and in some cases, is more than 1 ms. The pushout energy remained comparable between the unlubricated steel casing and the unlubricated brass casing. It is important to note that the steel surface is treated with a lacquer. Due to this it is not possible to make statements about the steel casing-chamber interaction which has not been studied in this investigation, For a lacquered casing, the interaction is between the polymer and the steel chamber.

CONCLUSION AND FUTURE WORK

This paper demonstrates two approaches to measure the pushout force of the casing on the breech. The benefit of this system is that it can be used for calibres, such as 8.6x70 mm, which is frequently used by long range shootings with breech bolt rifles. An enhancement to this investigation are further tests with different small arm calibres, to investigate if casing geometries affect the push out force significantly.

These results might be also applicable for repeating rifles, since their mechanism is strongly dependant on the pushout energy, which strongly changes if casing is lubricated. It is also worth investigating the effect of water or ice in the chamber which may exhibit similar results. This technique would also be applicable for investigating the forces involved in breeches in larger gun systems such as autocannons and tank guns.

ACKNOWLEDGMENTS

This research was supported by RUAG Ammotec AG, Thun Switzerland. I would like to thank the R&D team and the ballistic testing team. Especially Dr. Ralf Wahrenberg who provided valuable expertise in the field of ballistic test settings.

REFERENCES

[1] C. Woodley, A. Carriere, P. Franco, J. Nussbaum, X. Chabaux, and B. Longuet, "Comparisons of Internal Ballistics Simulations of 40mm Gun Firings," *23rd Int. Symp. Ballist.*, no. April, pp. 359–367, 2007.

[2] D. Gubernat and C. Fischer, "Explicit finite element model for determining influence of cartridge case material properties on small caliber weapon function," *Proc. 26th Int. Symp. Ballist.*, pp. 806–817, 2011.

[3] D. K. Kankane and S. N. Ranade, "Computation of in-bore velocity-time and travel-time profiles from breech pressure measurements," pp. 1–6.

[4] J. T. South, K. Dipak, and M. Minnicino, "Small caliber modeling from design to manufacture to launch," in *23rd Int. Symp. Ballist.*, 2007, no. April, pp. 557–564.

[5] H. Rahnejat, P. M. Johns-Rahnejat, M. Teodorescu, V. Votsios, and M. Kushwaha, "A review of some tribo-dynamics phenomena from micro- to nano-scale conjunctions," Tribol. Int. **42**(11), 1531–1541 (2009).

[6] J. J. Ritter, R. A. Beyer, and A. Canami, "In-Chamber Primer force and case pressure measurements of the 5.56-mm cartridge," no. January, 2012.

[7] P. G. Michaelides, P. G. Apostolellis, and S. D. Fassois, "Vibration – Based Damage Diagnosis in a Laboratory Cable – Stayed Bridge Model via an RCP ARX Model Based Method," *DAMAS*, vol. 9, no. July, 2011.

[8] N. K. Kadim Abid AL-Sahib and Al-khawarizmi, "Monitoring process in turning operations for cracked material alloy using strain and vibration sensor with neural network," J. Eng. **13**(3) (2006).

[9] L. Bin Tan, K. M. Tse, H. P. Lee, V. C. Tan, and S. P. Lim, "Performance of an advanced combat helmet with different interior cushioning systems in ballistic impact: Experiments and finite element simulations," Int. J. Impact Eng. **50**, 99–112 (2012).

[10] P. Nguyen, M. Kang, J.-M. Kim, B.-H. Ahn, J.-M. Ha, and B.-K. Choi, "Robust condition monitoring of rolling element bearings using de-noising and envelope analysis with signal decomposition techniques," Expert Syst. Appl. **42**(22), 9024–9032 (2015).

[11] American National Standard Voluntary Industry Performance Standards for Pressure and Velocity of Shotshell Ammunition for the Use of Commercial Manufacturers, American National Standards Institute, 2015.

[12] J. Slavi, L. Knez, and M. Bolte, "The importance of harmonic versus random excitation for a human finger," International Journal of Mechanical Sciences **132**, 507–515 (2017).

[13] D. Che, W. Le Zhu, and K. F. Ehmann, "Chipping and crushing mechanisms in orthogonal rock cutting," Int. J. Mech. Sci. **119**(October), 224–236 (2016).

[14] P. Groche, J. Hohmann, and D. Übelacker, "Overview and comparison of different sensor positions and measuring methods for the process force measurement in stamping operations," Measurement **135**, 122–130 (2019).

[15] M. B. Jun, O. B. Ozdoganlar, R. E. Devor, S. G. Kapoor, A. Kirchheim, and G. Schaffner, "Evaluation of a spindle-based force sensor for monitoring and fault diagnosis of machining operations," International Journal of Machine Tools and Manufacture **42**, 741–751 (2002).

[16] X. Zhang, H. Sui, D. Zhang, and X. Jiang, "Measurement of ultrasonic-frequency repetitive impulse cutting force signal," Measurement **129**, 653–663 (2018).

[17] *Components of end Item Basic Issue Items and Additional Authorization List* (Headquarters Department of the Army, Washington D.C., 1997).

[18] B. Sturtevant, "Shock wave effects in biomechanics," Sadhana **23**(5), 579–596 (1998).

[19] B. Ragsdale and S. Sohn, Comparison of the Terminal Ballistics of Full Metal Jacket 7.62-mm M80 (NATO) and 5.56-mm M193 Military Bullets: A Study in Ornance Gelatin BT (1988).

[20] "Klübersynth MZ 4-17," pp. 3–4, 2014.

[21] Defence Standard 05-101 Part 1 Proof of Ordnance, Munitions, Armour and Explosives, no. 1, Ministry of Defence, 2005.

[22] H. Uzun, C. Dalle, A. Argagnotto, T. Ghidini, and C. Gambaro, "Friction stir welding of dissimilar Al 6013-T4 To X5CrNi18-10 stainless steel," Materials & Design **26**, 41–46 (2005).

[23] H. Köhler, K. Partes, J. R. Kornmeier, and F. Vollertsen, "Residual stresses in steel specimens induced by laser cladding and their effect on fatigue strength," Phys. Procedia **39**, 354–361 (2012).

[24] R. Rubini and U. Mengetti, "Application of the envelope and wavelet transform analyses for the diagnosis of incipient faults in ball bearings," Mech. Syst. Signal Process. **15**(2), 287–302 (2001).

[25] A. Egaña, F. Seco, and R. Ceres, "Processing of ultrasonic echo envelopes for object location with nearby receivers," IEEE Trans. Instrum. Meas. **57**(12), 2751–2755 (2008).

AIP Advances

Push-out force and impulse measurement of seven types of small arms ammunition with three different surface states

Cite as: AIP Advances 9, 115016 (2019); https://doi.org/10.1063/1.5128440
Submitted: 19 September 2019 . Accepted: 30 October 2019 . Published Online: 18 November 2019

Michael Muster, Amer Hameed, David Wood, and Kilian Wasmer

AIP Advances ARTICLE scitation.org/journal/adv

Push-out force and impulse measurement of seven types of small arms ammunition with three different surface states

Cite as: AIP Advances 9, 115016 (2019); doi: 10.1063/1.5128440
Submitted: 19 September 2019 • Accepted: 30 October 2019 •
Published Online: 18 November 2019

Michael Muster,[1,a)] Amer Hameed,[1,b)] David Wood,[1,c)] and Kilian Wasmer[2,d)]

AFFILIATIONS

[1]Centre for Defence Engineering, Cranfield University, Defence Academy of the United Kingdom, Shrivenham SN6 8LA, United Kingdom
[2]Laboratory for Advanced Materials Processing – Empa - Swiss Federal Laboratory for Materials Science and Technology, Feuerwerkerstrasse 39, CH 3602 Thun, Switzerland

[a)]Author to whom correspondence should be addressed: michael.muster@cranfield.ac.uk
[b)]a.hameed@cranfield.ac.uk
[c)]d.wood@cranfield.ac.uk
[d)]kilian.wasmer@empa.ch

ABSTRACT

This study analyzes the influence of lubrication treatments on the force absorbed by the breech bolt called push-out force. The results are of high interest for weapon-safety and durability studies, especially when it comes to weapon maintenance. A barrel-ammunition combination represents an expanding vessel under high pressure. The pressure rises from ambient up to 420 MPa in less than a millisecond. During such a highly dynamic process, purely static equations, describing the problem of the casing push-out force, may not be applied. Besides the dynamic behavior, the surface properties and geometry also play an important role. To investigate the push-out force, a measurement system based on a force washer was built. This system was validated using a crusher method and finite element analysis. The impulse was calculated using the data of the measured force to obtain additional information about the force-time properties of the push-out behavior. Untreated ammunition and two lubrication systems: "ice layer" and "oil lubricated," as well as seven different ammunition sizes ranging from 5.56 to 12.7 mm were considered. The response was the force absorbed by the bolt while the cartridge provides rear obturation to the combustion gases. It was found that both the casing geometry and its treatments have a significant influence on the push-out force.

INTRODUCTION

The aim of this contribution is to measure the influence of differently treated cartridge surfaces on the breech-bolt force in a range of small-arms ammunition. Treatment types analyzed were untreated, *ice layer*, and *oil lubricated*. Ammunition types investigated were 50 Browning, 375 SWISS P, 338 Lapua Mag., 7.5 × 55 Suisse, 308 Win., 223 Rem., and 9 mm Luger.

Due to safety and functionality reasons, the chamber of the weapon needs to be sealed by the casing during the process of firing. This sealing process also decreases the breech-bolt force. During the acceleration phase of the projectile, the casing experiences a highly dynamic environment. Under such circumstances, the cartridge casing can be considered as a pressure vessel, which undergoes a plastic deformation while the propellant burns in the chamber. The plastic deformation of the cartridge, which prevents the rearward escape of firing gases between the weapon chamber and cartridge, is called obturation and is closely related to the push-out force. For safety reasons, the obturation of the casing needs to produce a seal. Otherwise, unpredictable gap flows may occur, known as the dangerous burn-through or gas-wash phenomenon.

A thermodynamic gap flow investigation was made by Squire and Donnard.[1] They described the efflux of luminous gases at the weapon breech, which is highly abrasive and can lead to serious

damage of the weapon. At worst, it can harm the rifle person. Squire and Donnard described the problem in detail, referring to classical melting theory. They investigated this experimentally by drilling a small hole in the head of the casing. They observed that even a minor scratch might result in a burn-through. This investigation was made with aluminum casings, which have a significantly lower melting point as compared to regular brass casings. However, the possible risks reveal the importance of a controlled obturation process guaranteeing the sealing of the pressure vessel system. Hence, in recent years, several patent applications, describing possible technical approaches to solve the sealing problem of the ammunition barrel system for small-caliber ammunition[2,3] but also large-caliber applications,[4,5] have been filed. The obturation of the casing not only affects the sealing process but also has an influence on the force taken/supported by the breech bolt. In the case when the push-out force exceeds a certain level, the breech bolt can break, which leads to severe damage or even can harm the operator.

Due to the internal pressure and the obturation process, the casing is pushed against the wall of the chamber. In other words, it means that the overall push-out force is not entirely taken by the breech bolt. The friction between the chamber wall and casing bears some of the overall push-out force. The friction between the interface boundaries is an important factor for bolt force assessments, which is described in the literature, in particular for steel and brass systems. According to Aida,[6] the static and dry Coefficient of Friction (COF) of brass and steel is in the order of 0.19.[6] In the case of the *oil lubricated* and kinetic brass-steel combination, the COF is around 0.09, which is consistent with recent publications.[7] In terms of lubrication, it is found that thin water layers may also act as a performant lubricant.[8] However, lubrication is only one of the six main factors the bolt force depends on; the other five factors are as follows:

(1) The surface area of the case head where the pressure acts,
(2) The pressure in the casing,
(3) The friction between the chamber wall and the case body,
(4) The material properties of the chamber and casing,
(5) The chamber geometry, i.e., fluted or smooth.

By controlling these five factors and measuring the push-out force, it is possible to get information about the effect of the lubricant on the obturation process during firing. Processes such as obturation are difficult to measure and are nowadays simulated using Finite Element Analysis (FEA).[9,10] The advantage of FEA is that numerous parameters can be investigated within one single model by sensitivity studies. With only minor changes in the model, one can analyze geometric parameters.

Besides numerical approaches, it is also possible to investigate the push-out force analytically at the breech, as suggested by Allsop *et al.*[11] The extraction-force equation can be used to estimate the push-out force. Such an approach is unsuitable for solving the dynamical problem of the obturation and cartridge sealing since only part of the analytical model can be applied. The main reason is that in the equation of Allsop *et al.*, the friction is assumed to have a constant value. Specific properties of the propellant, such as pressure oscillations, described by Elkarous *et al.*,[12] are neglected.

Several types of small-caliber ammunition are available for both military and law enforcement purposes. The most often-used cartridge type is the 9 mm Luger. This type of ammunition is highly standardized and utilized in pistols all over the world.[13] The most powerful caliber belonging to the family of small-caliber ammunition, exploited by many armies, is the 12.7 × 99 mm, also known as 50 Browning or 50 BMG. This caliber is mostly for the heavy machine gun Browning M2, which has its origins in 1918.[14] The 50 BMG is especially interesting in this investigation since this ammunition type caused problems concerning the reloading cycle and bolt/push-out force and was therefore deeply investigated using FEA methods.[15] Besides FEA investigations, it is also possible to measure forces at the case head using force washers. Ritter *et al.*[16] measured the force on the igniter and pressure inside the cartridge with a piezoelectric force sensor. This provided confidence in predicting the behavior occurring in the barrel chamber. They mentioned that the impulse has a significant influence on the system.

Sensors relying on the piezoelectric effect are often selected for standardized pressure measurements[17–19] and so are very suitable for ballistic investigations. However, ballistic pressure investigations rank among the most challenging types of measurement to be conducted.

Decades ago, due to the lack of suitable electronic measuring equipment, these measurements were conducted using a simple copper crusher method. The copper crusher method consists of a copper cylinder which is deformed depending on the pressure produced in the chamber of the weapon during the firing process.[20,21] Even today, the copper has its legitimation for cross-reference purposes. Elkarous *et al.*[22] investigated the sensing behavior of two piezoelectric pressure sensors and compared the results with a copper crusher. They investigated the amount of deformation of the copper cylinders after the shooting tests, using FEA to obtain quantitative results about the pressure applied. An approach to apply the crusher method directly on the casing is to turn notches into the head of the casing. Similar to copper, the brass of the casing is also a highly defined material and can be investigated as the crusher method.

However, ballistic pressure measurements in the chamber of a weapon are regularly conducted and important for security assessments. In contrast, breech-bolt force measurements are rarely made even though the breech bolt is a very important part of the weapon. The force on the breech bolt has a significant influence on the firing process, weapon functionality, and safety. This paper confirms that the breech-bolt force depends significantly on the surface treatment, which is one of the relevant issues. Consequently, this study is a supplement to and enrichment of existing studies on diagnosis associated with the firing process for small-arms ammunition.

EXPERIMENTAL PROCEDURES

To investigate the influence of the ammunition on the push-out force, seven types of casings and three surface states were selected. The types of casings are 50 Browning, 375 SWISS P, 338 Lapua Mag., 7.5 × 55 Suisse, 308 Win., 223 Rem., and 9 mm Luger which are presented in Fig. 1(a). The push-out force relevant properties of the ammunition type are given in Table I. This table contains properties having a direct influence on the push-out force such as the muzzle energy, casing surface, and the diameter of the mouth of the casing. The bullet weight and the projectile type influence the

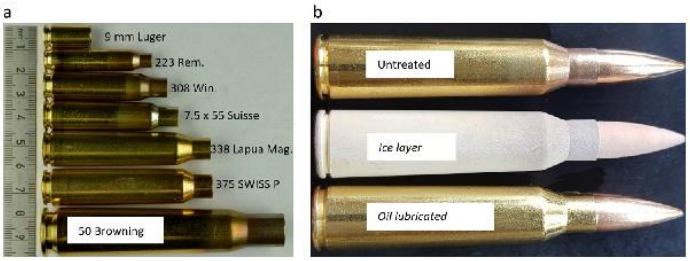

FIG. 1. (a) Picture of casings tested and (b) picture of the different surface states.

TABLE I. Specifications of the investigated ammunition types.

Name	Muzzle diameter (mm)	Bullet weight (g)	V_0 (m/s)	Muzzle energy (joule)	Projectile type	Casing surface (mm^2)
50 Browning	12.70	48.5	825	16 505	Solid	5219
375 SWISS P	9.50	22.7	850	8200	FMJ	3005
338 Lapua Mag.	8.60	16.3	860	6028	FMJ	2802
7.5 × 55 Suisse	7.50	11.3	780	3437	FMJ	1878
308 Win.	7.62	11.4	770	3380	FMJ	1654
223 Rem.	5.56	3.6	980	1729	FMJ	1152
9 mm Luger	9.00	8.0	365	533	FMJ	497

push-through force of the projectile in the barrel during acceleration, which also affects the push-out force. In general, Full Metal Jacket (FMJ) projectiles need a lower push-through force as compared to monolithic (solid) projectiles.[23] All types of ammunition were certified according to the most recent Commission Internationale Permanente (CIP) regulations.[17] The 9 mm Luger is the only casing without bottleneck design investigated. By comparing the bottleneck-type casings, the differences are in the angle and diameter-length ratio. For the ammunition, three surface states were selected: untreated, *oil lubricated*, and *ice layer*, which are seen in Fig. 1(b). The surface lubrications *oil lubricated* and *ice layer* are highly defined and may occur in real-world usage. The *oil lubricated* case simulates the case where the ammunition might have some lubricant at the boundaries of the inner chamber of the weapon. This is the case when the weapon is cleaned and oiled before use. To oil lubricate the casings, a fluid referred to as Klübersynth MZ 4-17 was applied. This lubricant is recommended for the maintenance of small arms such as hunting and sporting rifles.[24] The casing surface was treated with 0.4 mg/cm^2 lubrication oil.

In contrast, the *ice layer* state reproduces the situation where the ammunition is significantly colder than the weapon so that it is possible that the ammunition condensates quickly. In this study, to investigate the *ice layer* treatments, the ammunition was cooled to −30 °C for 1 h and then exposed 2 min to ambient temperature. This approach permitted to build a highly defined thin *ice layer* with a mass of 0.5 mg/cm^2, as shown in Fig. 1(b). The condensation process was controlled with an analytical balance (Mettler, Switzerland) and a stopwatch. The resulting water film is very thin and does not increase the gap between the chamber and the casing. Furthermore, it is melted immediately after putting it into the barrel.

The ammunition was first tested using an Electronic Pressure Velocity and Action Time (EPVAT) (HPI, Austria) measurement setup,[25] recognized by NATO and CIP testings. The amount of propellant is known from production certificates, and the casing surface can be calculated from the specific dimensions published in the CIP documents.[17]

Piezoelectric measurements

The piezoelectric force measurement was conducted ten times for each ammunition type so that the reproducibility and associated errors are statistically relevant. The push-out force measurement device is similar to the EPVAT system, as shown in Fig. 2. It includes an interchangeable proof barrel, rigid housing that is made of cast iron to reduce the effect of vibrations during shooting. In addition, it has a trigger device attached to the force measurement plate, which is shown in Fig. 3. The trigger device and the force measurement plate, which also serve as a breech bolt, need to be disassembled after every shot is performed. The key difference to a regular EPVAT system was that the breech bolt was equipped with a force washer Kistler 9041a (Kistler, Switzerland), shown in Fig. 3. This sensor has an eigen frequency of 65 kHz and is capable of measuring short time events. A National Instruments USB-6366 (NI, USA) data acquisition device was used for all tests. Accurate time and the amplitude raw signal were necessary for the impulse measurements. Hence, the data acquisition rate was 2 MHz (0.5 μs step size) with a 16-bit

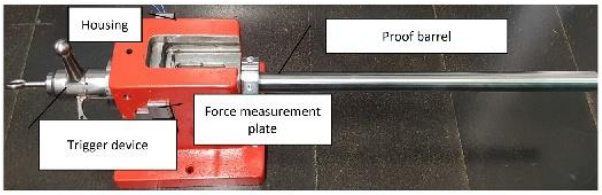

FIG. 2. Measurement setup with a measurement plate.

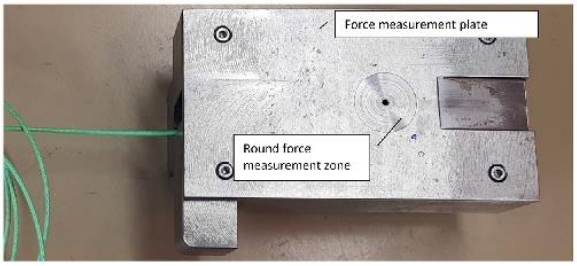

FIG. 3. Force measurement plate.

resolution. The impulse was calculated using the time integral of the force signal. The filtering of the acquired raw data was identical in all cases. The filtering was a combination of 20 kHz Butterworth low-pass filter which is known from NATO standards concerning small-caliber ammunition[19] and an RMS signal envelope[26] with a step size of 170 samples. The filtering approach and the overall measurement system with a force washer are the same as the one described in the work of Muster *et al.*[27] The effect of this filtering as compared to the raw signal can be seen in Fig. 4. The signal is not loaded with high-frequency parts over 20 kHz. However, the time property of the first rise remains persistent.

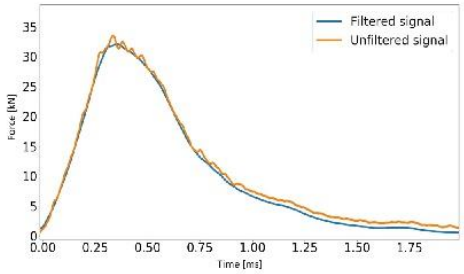

FIG. 4. Typical force vs time curve of *oil lubricated* 308 Win. ammunition. Filtered and not filtered. For the filtering process, a bandpass, RMS signal envelope approach was applied.

Case head crusher assessment

The 338 Lapua Mag. was chosen to conduct the cross-verification of the piezoelectric measurements for two reasons. First, it is a caliber mainly used in sniper rifles. Second, it has a rigid breech bolt. Bolt-action rifles are with rigid bearings of main interest for push-out force and safety investigations. In addition, the 338 Lapua Mag. was assessed since it provides enough material at the casing head to contain notches, which is necessary for later crusher investigations. These notches have resulted in defined spikes, which deform under the high forces occurring during the firing process. This deformation was measured using an analog microscope with a measurement *X-Y* table (Wild Heerbrugg, Germany).

The unloaded notch pattern of the case head (see Fig. 5) was replicated using a CAD package of a FEA software. The FEA software applied for this investigation was FORGE® Version 4.6.2.1 (Transvalor, USA), optimized for metal forming processes.[28] The casing hardness was assumed to be homogeneous with the constant hardness value of 180 Hardness Vickers (HV_{30}). This drawn casing head was placed between two bearings, which were assumed to be fully rigid. A quarter symmetry model was constructed, to save computation time. The load was built up stepwise on a gradient, to obtain a force-step curve. No oscillations were assumed. The element and mesh size were set to "*automatic.*" The force was applied "static," and the mesh for the analysis was generated automatically and dynamically. Each surface state type was assessed three times. With this approach, we were able to replicate the deformation under an applied force to obtain a semiquantitative result. The reason for this verification system is the same as presented by Elkarous *et al.*,[22] which is to obtain a result from a different measurement approach.

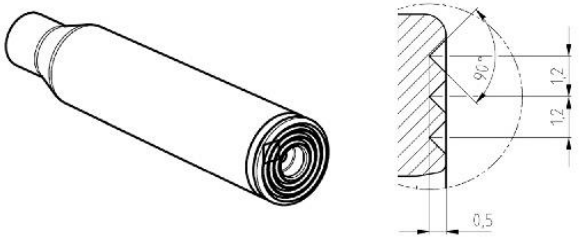

FIG. 5. Modified "crusher" casing head using notches which are turned in the casing head.

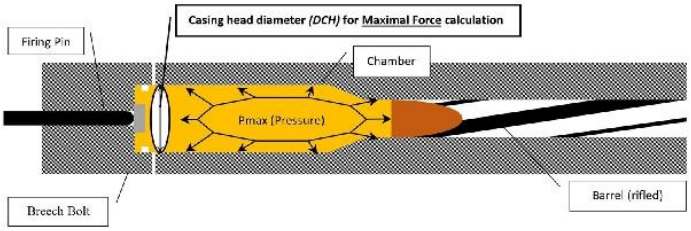

FIG. 6. Schematic view of the barrel cross section. The maximum possible is calculated according to $F_{max} = P_{peak} * DCH$.

Analytic calculations

Besides the crusher gauge and FEA, the calculated maximum force (F_{max}) is another straightforward method that can be used for an analytic calculation of the push-out forces of the ammunition types investigated. This method assumes that the maximum possible force is delivered on the breech bolt. The calculation of the theoretical F_{max} can be simplified since it depends only on two factors: the peak pressure (P_{peak}), a measured value, and the casing head diameter (DCH) (see Fig. 6) which is taken from the CIP regulations. Then, $F_{max} = P_{peak} * DHC$ and the results are given in Table III. This maximal force scenario applies only if no obturation and no friction exist between the boundaries of the casing and the chamber. Under such circumstances, it is obvious that the theoretical F_{max} cannot be exceeded in real-world measurements and so must be taken as a maximum reference.

More complex equations for push-out measurements rely on several parameters such as the friction coefficient, materials, geometrical properties, and the peak pressure.[11] These parameters are hard to measure during the experiment and so must be simplified. Another drawback of this approach is that the dynamic properties of the projectile acceleration process are neglected.

RESULTS AND DISCUSSION

This section is divided into two sections: the piezoelectric measurements and the case head crusher assessment. The piezoelectric measurements are divided into four parts. Single force curves according to the different ammunition types are presented. They give an impression about the force-time behavior. Then, a table summarizes the results, in particular an important factor between the measurement and the worst-case scenario. Third, boxplots summarized the statistics of the acquired results. Finally, the measurements are then cross verified using a crusher method with FEA.

Piezoelectric measurements

Figures 7–9 show typical push-out force vs time curves acquired with the force measurement instrument for the seven casing types. As expected, just after firing, the forces increase drastically before decreasing gradually. Most of the sharp rise takes place within 1 ms, whereas the force decreases take place between 0.8 and 3 ms

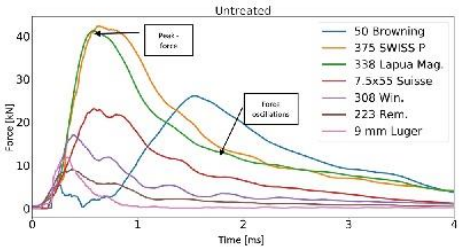

FIG. 7. Typical force signals acquired from the untreated ammunition.

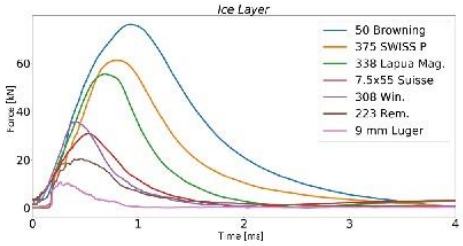

FIG. 8. Typical force signals acquired from the ice-layer-treated ammunition.

depending on the casing. The 9 mm Luger is the only casing without a bottleneck and has a unique push-out curve as compared to the other curves. After a short rising time, the maximum force (F_{peak}) measured is lower than the other casing type followed by a decrease to zero force within only 1 ms, and evidence of this is given in Figs. 7–9. The reason is that the 9 mm Luger proof barrel (100 mm) is much shorter as compared to the other barrels. In contrast, the 50 Browning has a much longer barrel (1200 mm), and this leads to longer acceleration time. The difference in acceleration time is independent of the surface state.

Figures 7–9 are closely related to Table II, which summarizes the measured but also the calculated forces for the three surface states. $\overline{P_{peak}}$ was acquired according to the CIP regulations. It represents the average value from the pressure maxima of ten single shots. For each ammunition and surface state, $\overline{F_{peak}}$ was averaged over a set of ten shots and F_{max} was the maximum push-out force value in the system. This table also contains an important value which is defined as $\overline{F_{peak}}/F_{max}$. This value shows the measured force in relation to the absolute maximal possible force (F_{max}). Also, one main relation between the figures and the table is the average force ($\overline{F_{peak}}$), which is an average value of peak values of the force curve shown in Fig. 7. This is a very artificial value since there is always some obturation and friction in the system which lower the push-out force.

In Table II, no significant difference is observed in the average maximum pressure ($\overline{P_{peak}}$) and F_{max} for the untreated and *oil lubricated* ammunition. In contrast, a slight difference (but significant) is visible in $\overline{P_{peak}}$ between the untreated and *ice layer* ammunition. This is due to the burning properties of the propellant and igniter that are affected during cold conditions.

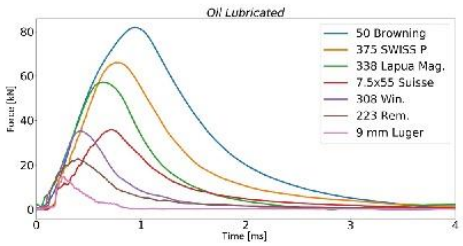

FIG. 9. Typical force signals acquired from *oil lubricated* ammunition.

The results of the untreated surface state are shown in Fig. 7 and Table II. In Fig. 7, force oscillations, which are caused by the stick-slip effect, can be observed and were detected in all untreated surface states. Some oscillations are high in amplitude and reach up to 1/10 of the maximum push-out force; this affects the reproducibility of the measurements. For the untreated surface state, it is possible to identify three different casing groups. The first group is made by the 9 mm Luger only, which shows a sharp peak and reaches up to 72% of F_{max}; see Table II. The second group is made of 375 SWISS P, 338 Lapua Mag., 308 Win., and 7.5 × 55 Suisse. These casings showed a similar relation for $\overline{F_{peak}}/F_{max}$ values ranging from 42% to 61%. The third group is very interesting as it comprises the largest and smallest projectile diameter investigated (223 Rem. and 50 Browning, see Table I). These two ammunition types showed only 25%–26% of the maximum possible push-out force (see Table II), which is a strong indication of a good obturation process. The reason for this behavior might be the similar geometrical constraints of the casings; see the geometry of these two casing types [Fig. 1(a)]. For the untreated surface state, it is also interesting to note that although the 50 Browning has twice of the muzzle energy of the 375 SWISS P (see Table I), the 50 Browning has lower push-out force as compared to the 375 SWISS P. Actually, the peak-force of the 50 Browning is reached more than 1.5 ms after the first signal rises. All other casing types reached the peak-force between 0.3 and 0.5 ms after. One reason is that the propellant used for this largest investigated caliber is less vigilant; this leads to delayed peak pressure. Another possible reason for the delayed peak-force is the stick-slip phenomenon of the ammunition, an effect that can be observed between 0.2 and 0.7 ms in the case of the 50 Browning. In contrast, the 375 SWISS P produces the most significant force at the bottom of the casing (up to 49 kN) (see Fig. 7), a behavior true for all force curves investigated in this work. This caliber reaches on average 53% of the maximum push-out force (see Table II).

The surface state *ice layer* influences not only the coefficient of friction of the casing but also the burning properties of the propellant. However, no significant difference concerning the pressure and velocity of the projectile was observed.

The *ice layer* surface state rises the push-out force significantly for every ammunition type and affects the obturation process. All ammunition types show between 73% and 97% of the maximal force, which is remarkably high when considering the safety of the system. The *ice layer* state revealed a significant influence on the force oscillations of all bottlenecked casings. All force signals are steadily rising and falling. Compared to the untreated surface state, fewer oscillations occur. The force signal from this surface state is comparable with the signal from the regular pressure measurements. The peak-force is correlated with the muzzle energy, which is an indication that the thin water layer affects the obturation process significantly. This is consistent with the statement of Paliy *et al.*,[8] who reported that, under certain circumstances, water acts as a high-performance lubricant.

For the *oil lubricated case*, a thin film of Klübersynth MZ 4-17 was applied. The resulting push-out forces are comparable with those from the *ice layer*. However, for example, the 338 Lapua Mag.

TABLE II. Tabular representation of the measured properties. The "$\overline{F_{peak}}/F_{max}$" represents a very important value. A high value indicates that almost no obturation takes place and may affect weapon safety.

Cartridge	Surface state	$\overline{P_{peak}}$ (MPa)	F_{max} (kN)	$\overline{F_{peak}}$ (kN)	$\overline{F_{peak}}/F_{max}$ (%)
50 Browning	Untreated	310	102.0	2500	25
	Ice layer	305	100.0	8538	85
	Oil lubricated	310	102.0	8538	84
375 SWISS P	Untreated	390	76.0	4010	53
	Ice layer	385	75.0	6480	86
	Oil lubricated	390	76.0	6480	85
338 Lapua Mag.	Untreated	380	66.0	4040	61
	Ice layer	382	66.0	5640	85
	Oil lubricated	380	66.0	5640	85
7.5 × 55 Suisse	Untreated	320	40.0	2110	53
	Ice layer	310	39.0	3475	89
	Oil lubricated	320	40.0	3475	87
308 Win.	Untreated	330	37.0	1570	42
	Ice layer	315	36.0	3500	97
	Oil lubricated	330	37.0	3570	96
223 Rem.	Untreated	400	29.0	750	26
	Ice layer	390	28.0	2160	77
	Oil lubricated	400	29.0	2160	74
9 mm Luger	Untreated	200	17.0	1230	72
	Ice layer	205	17.5	1280	73
	Oil lubricated	200	17.0	1280	75

casings are subjected to fewer stick-slip effects (compare the green lines in Figs. 8 and 9).

To compare the statistical results of the experiments, one decided to separate the ammunition into two groups: smaller and larger ammunition types based on their muzzle energy delivered. The smaller ammunition types were defined for ammunition delivering muzzle energy of less than 3500 J, and the statistical results are given in Figs. 10(a) and 11(a). The smaller ammunition types are normally used in self-loading firearms. In contrast, the larger ammunition types are delivering muzzle energy higher than 6000 J, and their statistical results are shown in Figs. 10(b) and 11(b). These calibers are used by snipers and are often used in weapons with bolt-action. Bolt-action rifles with a rigid bearing are strongly affected by insufficient obturation processes and large push-out forces. A comparison of the different smaller and larger ammunition types is presented in the boxplots in Fig. 10 containing the information about all force measurements performed in this study. They represent median, quartiles, as well as extreme values.

We can see that the force delivered on the breech bolt increases in the treated surface states with increasing muzzle energy (compare Fig. 10 with Table I). For all bottleneck casings, it is seen that the untreated surface state has a relatively low push-out force, whereas the push-out forces for the treated surface states are significantly higher. The *ice layer* causes a less significant rise in the push-out force than the *oil lubricated*.

It is worth comparing the 7.5 × 55 Suisse with the 308 Win. casings as both have almost the same muzzle energy values, and they are the only caliber investigated with interchangeable projectiles. However, the casing geometry differs slightly, which leads to different push-out force patterns. By comparing both casings, we can conclude that the overall geometry influences the push-out force. This observation of a geometrical dependency is supported by the different sized calibers 50 Browning and 223 Rem.; see Fig. 1(a). They react with a similar force pattern on the surface state. The absolute force value and its spread are low in the case of the untreated surface, and both rise significantly after changing the surface state with lubricant. Some of the measured 9 mm Luger peak-forces are so high that they reach almost the calculated maximum possible force. In this case, the sealing of the casing in the chamber might break and thereby release some of the hot and highly compressed gas into the weapon. The scatter in the results of the nonbottlenecked 9 mm Luger is the largest as compared to all other types of ammunition investigated. For the bottleneck casings investigated, the 338 Lapua Mag. shows a large scatter.

Figure 11 presents the results of the impulse transmitted to the breech bolt. The impulse gives information about the duration of the force applied on the breech bolt. This factor is important because

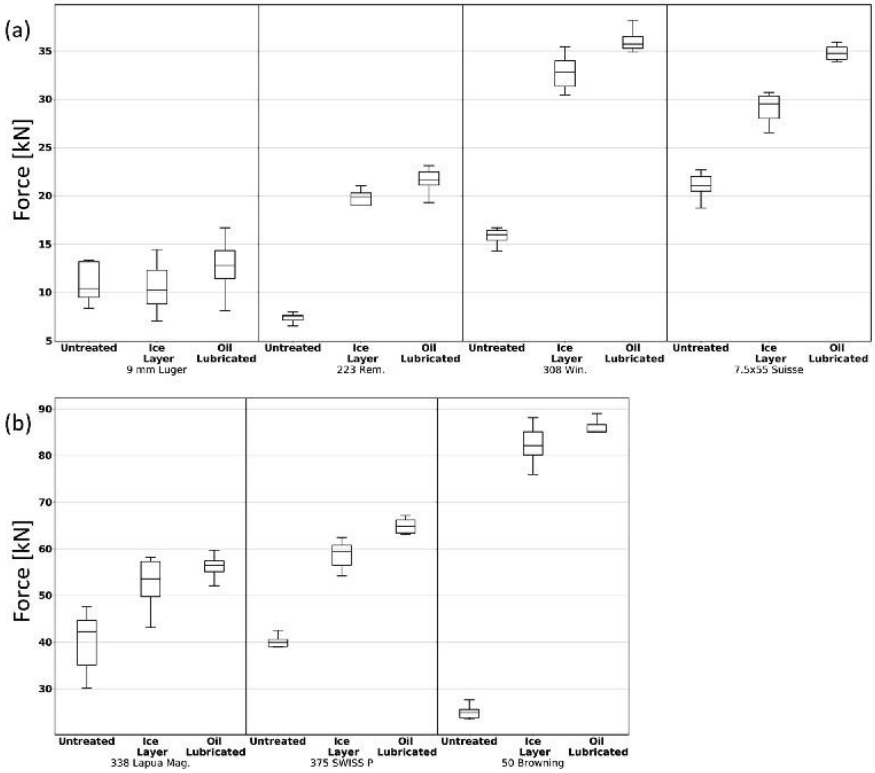

FIG. 10. Force boxplots of the investigated caliber range: (a) represents the smaller cartridge types and (b) represents the larger cartridge types.

some breech bolt systems are more sensitive when a load is applied for a certain time. The impulse transmitted at the base is represented by the integral of the force-time curve, and it also depends on the length of the barrel. Based on Fig. 11, no evident difference in the impulses was observed between the treated and untreated 9 mm Luger ammunition. The average impulses transmitted to the breech bolt vary between 7 and 59 N s in the untreated surface states. This range is larger for the lubricated surfaces, which varies between 6 and 120 N s. The lack of stick-slip effect in the treated surfaces prevents the chamber from taking big amounts of impulse leading to an enlargement of the range between the min and max value. In contrast, all treated bottleneck casing types show a decrease in impulse variation. The theory that the barrel chamber cannot take significant amounts of impulse if the casings are treated is supported by this decrease in impulse variation.

Case head crusher assessment

The case head crusher assessment for the 338 Lapua Mag. was used to cross verify the electronic measurements. In such highly dynamic environments, there is a distinct possibility that parts or tolerances of the measurement system influence the quality of measurements themselves. The verification was conducted in a two-stage approach, via optical investigation and FEA. Figure 12 presents pictures of the case heads before firing [Fig. 12(a)] and after for the three surface states. This optical investigation showed already obvious differences concerning the casing-head deformation. For example, the less flattened ring contour in Fig. 12(d) is due to the different hardness of the casing and is prominent in the outer ring.

Furthermore, the outer ring is less supported due to the extraction groove. In a second step, the FEA was performed and its results

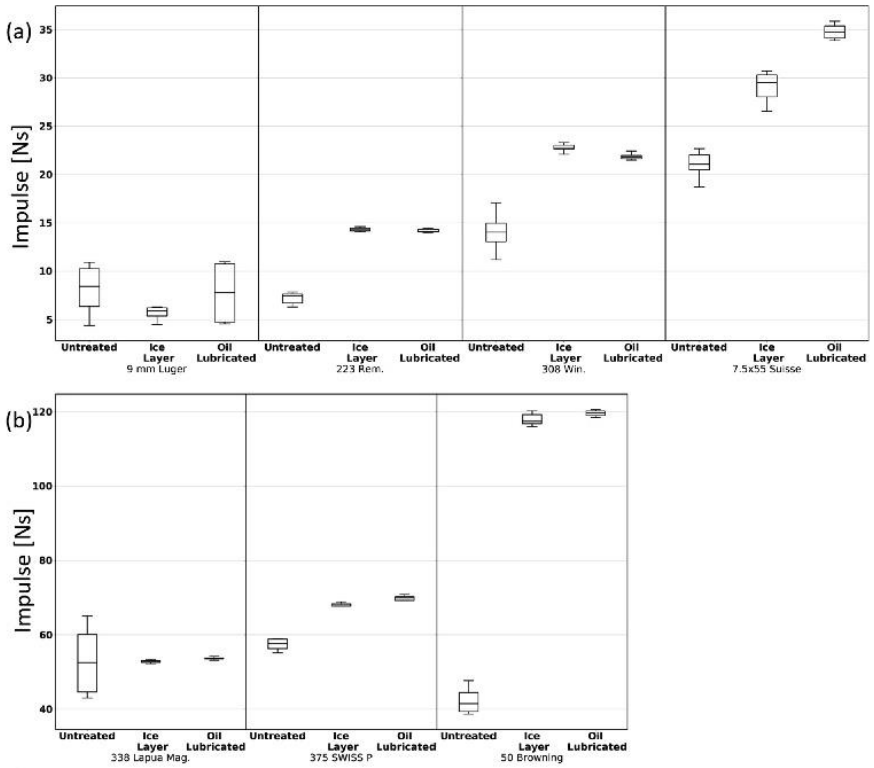

FIG. 11. Impulse boxplots of the investigated caliber range: (a) represents the smaller cartridge types and (b) represents the larger cartridge types.

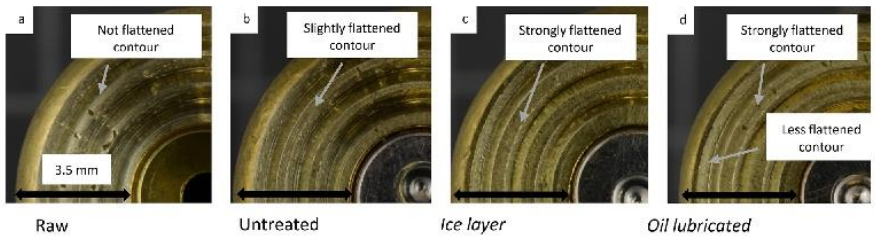

FIG. 12. Pictures of flattened casing heads.

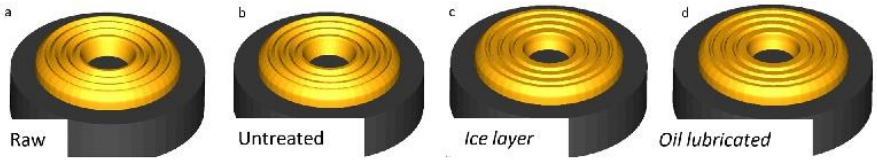

FIG. 13. FEA recalculation of the flattened casing heads.

TABLE III. Comparison between the semiquantitative FEA measurements and the force washer experiments.

Surface state	Crusher FEA $\overline{F_{peak}}$ (kN)	$\overline{F_{peak}}$ from force washer (kN)
Untreated	35	40
Ice layer	58	56
Oil lubricated	51	56

were compared with the force-washer measurements. The *oil lubricated* casing showed a less significant flattening of the casing head. However, this might be due to the intrinsic force spread of this caliber (338 Lapua Mag.). This is interesting since the flattening of the casing head might also lead to different internal ballistics or, in the worst-case scenario, affect the obturation process even further. Such an effect was not observed in the present study. Figure 13(a) shows the setup of the FEA, a rigid structure (black bearing) presses a simplified ductile case head against a rigid plate which is not represented. The results of the FEA are presented in Fig. 13 for the three surface states, and the comparison is given in Table III. The crusher FEA average peak-force ($\overline{F_{peak}}$) analysis is remarkably close to the measured $\overline{F_{peak}}$ by the force washer, and evidence of this is given in Table III.

CONCLUSION

This contribution investigated the effect of casings and surface states on the push-out force and transmitted impulse. Seven casings (50 Browning, 375 SWISS P, 338 Lapua Mag., 7.5 × 55 Suisse, 308 Win., 223 Rem., and 9 mm Luger) and three surface states (untreated, *ice layer*, and *oil lubricated*) were selected. We established the push-out force, and transmitted impulse often depends on the surface state. Using lubricants such as water or oil increases the average peak-force ($\overline{F_{peak}}$) up to a factor of 3.5 and affects the obturation process. These are safety-relevant features since a good obturation process is necessary to ensure the functionality of a weapon. However, large, oscillating, and unpredictable loads on a breech bolt may lead to its breakage and harm the operator severely.

We demonstrated that our proposed measurement system is suitable for analyzing a wide range of forces and impulses in small-arms weapon systems. It has been validated using a case-head crusher method, aided by FEA. The three different surface states: untreated, *ice layer*, and *oil lubricated*, showed that already small changes in the ammunition surface have a significant influence on the push-out force and so on the obturation process. The geometry of the casing, also, influences the push-out force to a major extent, which is true for all sizes of bottleneck casings. The investigated non-bottlenecked casing (9 mm Luger) behaves differently concerning the overall spread of the momentum or push-out force. The acquired results can be used to estimate the maximum force at the breech bolt, which is a very important and safety-critical factor in the design and operation of a weapon.

The dispersion of the impulse is reduced in all surface-treated bottleneck casings. This is a strong sign that for the lubricated surface state, no stick-slip phenomenon occurs and that the obturation process has a minor influence on the push-out force.

The recommendation to users is to apply lubricant during barrel maintenance but to remove the lubricant before firing. To weapon manufacturers, the relevant recommendation is that a weapon should be capable of withstanding at least the maximal possible force which depends on the maximal possible peak pressure and the diameter of the case head. A gap between the breech bolt and casing head leads to strong collisions between the two during weapon firing.

ACKNOWLEDGMENTS

I want to express my thanks to RUAG Ammotec AG, Switzerland, for making the test facilities available. The use of measurement devices would not have been possible without the great help of Markus Gruenig and Gregoire Pache. I am also grateful to Markus Hofmann and Peter Biedermann, who contributed their expertise in the "casing crusher method" and FEA simulation.

REFERENCES

[1] W. H. Squire and R. E. Donnard, "An analysis of 5.56 mm aluminium cartridge case burn-through phenomenon," National Techical Infomation Sevice, No. AD-750, pp. 385–399, 1972.
[2] D. Carpenter, H. Engel, B. Recchia, and P. Shipley, "Ballistic sealing, component retention, and projectile launch control for an ammunition cartridge assembly," U.S. patent US20140000471 (2 January 2014).
[3] B. Peterson, E. Carlson, A. Moser, and H. Lawrence, "Projectile assembly with stabilization enhancement," U.S. patent US9046332B2 (10 July 2014).
[4] T. Heitmann and T. Niemeyer, "Case base for large-caliber ammunition," U.S. patent US6408764 (25 June 2002).
[5] U. Wagner, H. J. Limburgerhof, K. Henrici, H. Kuessner, K. Volkamer, and E. Fuerst, "Self-obturating, expellable cartridge case," U.S. patent US3759184A (18 September 1973).

[6]R. Aida, "Measurment of coefficient of static friction of metals," Sci. Rep. Res. Inst., Tohoku Univ., Ser. A **2**, 380–395 (1950).
[7]M. A. Chowdhury, D. M. Nuruzzaman, A. H. Mia, and M. L. Rahaman, "Friction coefficient of different material pairs under different normal loads and sliding velocities," Tribol. Ind. **34**(1), 18–23 (2012).
[8]M. Paliy, O. M. Braun, and S. Consta, "The friction properties of an ultrathin confined water film," Tribol. Lett. **23**(1), 7–14 (2006).
[9]D. K. Kankane and S. N. Ranade, "Computation of in-bore velocity-time and travel-time profiles from breech pressure measurements," Def. Sci. J. **53**(4), 351–356 (2003).
[10]J. T. South, K. Dipak, and M. Minnicino, "Small caliber modeling from design to manufacture to launch," in *23rd International Symposium on Ballistics* (International Ballistic Society, 2007), No. April, pp. 557–564.
[11]D. F. Allsop, *Brassey's Essential Guide to Military Small Arms: Design Principles and Operating Methods* (Brassey's, 1997).
[12]L. Elkarous, M. Pirlot, J.-C. Golinval, and M. Maldague, "Investigation on gas pressure measurement inside small Caliber weapons with piezoelectric transducers," Meas. Sci. Conf. **2012**, 1–8 (2012).
[13]G. Langer, "Neue polizeimunition," PVT, No. 1166, pp. 1–3, 2004.
[14]M. Thommen, *Browning Machine Gun, Caliber .50 12, 7 mm Mg 64* (Gesellschaft für Waffen und Militaria, 2006).
[15]D. Gubernat and C. Fischer, "Explicit finite element model for determining influence of cartridge case material properties on small caliber weapon function," in *Proceedings of the 26th International Symposium on Ballistics* (International Ballistic Society, 2011), pp. 806–817.
[16]J. J. Ritter, R. A. Beyer, and A. Canami, *In-Chamber Primer Force and Case Pressure Measurements of the 5.56-mm Cartridge* (U.S. Army Research Laboratory, 2012), Vol. ARL-TR-586, No. January.
[17]"CIP (Commission Internationale Permanente pour l'épreuve des Armes à Feu Portatives)," Bruxelles, p. Ann., 2019.
[18]"American National standard voluntary industry performance standards for pressure and velocity of shotshell ammunition for the use of commercial manufacturers," American National Standards Institute, 2015.
[19]AEP-97, Multi calibre manual of proof and inspection (M-C MOPI) for 5.56 mm, 7.62 mm, 9 mm and 12.7 mm ammunition, Vol. 0023, No. December 2013, 2014.
[20]C. E. Waters, "Technologic Papers Bureau of Standards," p. 26, 1921.
[21]F. I. Du Pont, "Ballistic gun," U.S. patent US815468 (4 November 1905).
[22]L. Elkarous, F. Coghe, M. Pirlot, and J.-C. Golinval, "Experimental techniques for ballistic pressure measurements and recent development in means of calibration," J. Phys.: Conf. Ser. **459**(1), 012048 (2013).
[23]L. White and J. Siewert, "Final report of the rifling profile push test," No. June, 2007.
[24]"Klübersynth MZ 4-17," pp. 3–4, 2014.
[25]"Defence Standard 05-101 Part 1 Proof of Ordnance, Munitions, Armour and Explosives," No. 1, Ministry of Defence, 2005.
[26]C. Jarne, "An heuristic approach to obtain signal envelope with a simple software implementation," An. AFA **29**, 51–57 (2017).
[27]M. Muster, A. Hameed, and D. Wood, "Dynamic qualitative bolt force measurements for investigating influence factors on the pushout effect of small calibre ammunition," AIP Adv. **9**(6), 065020 (2019).
[28]P. De Micheli, A. Settefrati, S. Marie, J. Barlier, P. Lasne *et al.*, "Towards the simulation of the whole manufacturing chain processes with FORGE®," NEMU 2015–New Developments in Forging Technology, May 2015, Fellbach, Germany, hal–01247710.

Defence Technology xxx (xxxx) xxx

Contents lists available at ScienceDirect

Defence Technology

journal homepage: www.keaipublishing.com/en/journals/defence-technology

Ricochet quantification using a multiple sensor approach☆

Michael Muster*, Amer Hameed, David Wood

Centre for Defence Engineering, Cranfield University, Defence Academy of the United Kingdom, Shrivenham, SN6 8LA, UK

ARTICLE INFO

Article history:
Received 9 December 2019
Received in revised form
22 January 2020
Accepted 17 February 2020
Available online xxx

Keywords:
Ricochet analysis
Small-calibre ammunition
Velocity measurement
Thermography

ABSTRACT

This study investigates the ricochet behaviour of three different small-arms projectile types using a novel ricochet measuring device. The results can be used to estimate the danger potential of ricochets on shooting ranges.A ricochet is the change of direction and velocity of a projectile after impacting an oblique surface. This impact produces strong vibrations on a rigid plate.

During this impact, flexural waves travel radially outwards from the point of impact. These waves are used to determine the properties of the impactor with accelerometers situated on the target surface. With the use of two measurement plates, one can produce a ricochet and detect the velocity at the same time.

Accelerometers are suitable for accurate momentum measurements of single impacts. However, depending upon strike velocity and the impact angle, a ricochet can separate in multiple fragments after being deflected. From the operational safety perspective, these fragments need to be detected, as well. The approach of a coupled sensor concept was chosen to solve this problem.

Thermographic sensors were additionally used to visualise the heat which is produced after penetrating a rubber layer pasted in front of the steel target plate. With this approach one was able to detect the position of impact. The investigations showed that the measurement system performance is better with a multiple sensor design, which includes accelerometers for the velocity, impact strength and partly the position measurement, while the thermographic sensor was used for the position measurement and partly the momentum measurement.

The investigated ammunition showed plausible fragmentation behaviour, and the results can already be used to estimate the danger potential of different ammunition types. Frangible projectiles fragment to small particles already after being deflected under a small angle. However, Full Metal Jacket projectiles with or without a steel core do not fragment under angles which are less than 5°.

The objective of the paper is to demonstrate the possibility of measuring the complex ricochet mechanics of small projectiles using standard accelerometers with the adequate signal processing approach. This measuring system is supported by an off the shelf thermographic camera.

1. Introduction

The aim of this work is to investigate the performance of a novel measurement device capable of measuring ricochets of small-calibre ammunition. Small arms are extensively used during manoeuvre-based operations.

Any high-speed fragment ricocheting from fragmenting projectiles is a safety hazard for personnel operating in the vicinity. It is essential, therefore, to evaluate the potential danger zone of ricocheting particles generated by projectiles.

Small-calibre projectiles are objects that weigh from 2 to 10 g, which travel at supersonic speed and produce strong acceleration signals on impacting an object such as witness plate which are used for ballistic investigations. Due to their high speed and rotation rates, projectiles are generally challenging to characterise during flight and impact, even with high-frequency sensors.

Sensors mounted on small arms projectiles, for ballistic tests, would be too bulky and affect the flight path. Ricochet characterisation is necessary for important applications like the estimation of

* Cranfield Defence and Security, Cranfield University, Shrivenham, Swindon SN6 8LA, United Kingdom.
* Corresponding author.
E-mail addresses: michael.muster@cranfield.ac.uk (M. Muster), a.hameed@cranfield.ac.uk (A. Hameed), d.wood@cranfield.ac.uk (D. Wood).
Peer review under responsibility of China Ordnance Society

https://doi.org/10.1016/j.dt.2020.02.017

Please cite this article as: Muster M et al., Ricochet quantification using a multiple sensor approach, Defence Technology, https://doi.org/10.1016/j.dt.2020.02.017

range danger areas of shooting ranges. For the desired applications, one needs to know the position of impact and the momentum transmitted into the plate. To be known are also the time and distance between the first and second impact, where the ricochets are finally stopped. Using this information, one can measure the residual energy, fragment weight and deflection angle of the projectile after impact, as well as the velocity.

The velocity can be derived easily by using a Time of Flight (TOF) approach with two trigger devices. In the proposed system, the two sensor plates are considered as trigger devices. However, the procedure is similar to the well-known trigger-foil system, which is often used to trigger ballistic events such as e.g. ballistic events in high-speed imaging [1] or general investigations like multiple impacts [2]. The idea behind foil triggers is that two electrically conductive foils (preferably of aluminium) are set up directly behind each other. During the penetration process, a short circuit is generated which can be used as a trigger. Using two of these trigger devices and with the known distance between them, one can calculate the velocity by applying the TOF. This approach is shown by Yan et al. [3].

The triggering system in the case proposed here relies on wave propagation in the plate material. The idea is similar to the acoustical approach described in the notes of Michael Courtney [4]. He investigated the time of flight with a high-resolution microphone and placed this microphone equidistant between the target and the barrel muzzle. With the known distance between target and barrel muzzle, plus the time difference of the two acoustic signals, one could recalculate the mean velocity of the projectile. The acoustic signals come from the muzzle burst and the impact sound burst when the projectile hits the target (in this case a steel plate). The main challenge for in detail impact quantification on steel plates has to do with enormous decelerations and big deformations in a short time. This is why sensors mounted on witness plates, in the proposed case of steel, are widely used for impact detection.

Impact detection units with plates rely on e.g. Impact Soft-Recovery Experiments [5]. In this case, the target under investigation is a brittle plate, monitored by an interferometer. The projectile's impact generates strong vibrations, which can be used to characterise the nature of the impact. Espinosa et al. [6] revealed that it is possible to get a cleaner raw signal from the target plate by using a star-shaped geometry. Their tests showed that one can significantly minimise the effect of the outer layer of the plate on the impact zone itself. Like interferometers, accelerometers are frequently used to determine properties of the impact such as the impact position or the momentum [7–9]. One of the major sources of measurement inaccuracies are random and reflected vibrations [10]. Hammetter et al. used an array of accelerometers fixed on the plate to determine the momentum transferred. He showed that geometrical properties of the detecting plate itself might lead to inaccurate measurements.

Another source of measurement inaccuracy is electronic filtering of the acceleration data. As a best practice for shock investigations, accelerometers are mechanically insulated [11]. Severe mechanical shocks such as bullet impact typically lead to six degrees of freedom accelerations represented in broadband frequencies. These frequencies make it difficult to determine the overall momentum [6] or the position. Mechanical insulators combined with electrical filters were found to be an appropriate way to overcome this problem.

The impacting body excites the witness plate within a very short time in a non-linear and random vibration regime, where scattering and reflections of vibrations at boundaries will occur [12,13]. Right after the impact is the moment where the point of interest occurs, this moment is called the Arrival Time (AT). The AT is defined as the time when the sensor detects the first set of waves, which originates from the impact position.

Consequently, knowing the accurate AT is necessary to recalculate the exact impact position with the Time Difference of Arrival (TDOA) algorithms [14]. TDOA algorithms are nowadays often used and optimised for passive tracking of wireless communication systems [15]. However, the underlying computations for wireless devices tracking and the impact location are the same. The main issue for an accurate triangulation of impact remains accurate AT detection. For flexural group waves travelling in steel at a speed of over 2500 m/s, even minor time errors lead to significant positioning errors. Knowing the speed of sound in the target material and the AT difference are necessary for positioning. Furthermore, by knowing the sensor positions, one can calculate the location of the impact/of the origin of the waves by numerical approaches [16].

Mingzhou et al. showed the possibility of precisely detecting the AT of flexural waves using accelerometers after the impact of a dropped test weight on a large steel plate. This investigation was done in noisy environments like power plants [17]. They used a sophisticated decomposition algorithm combined with the Hilbert Huang Transformation. They found that the proposed algorithm was capable of detecting the AT with a precision of several milliseconds. The main reason for the inaccuracies was still the noise in the signal. In an idealised case, to lower the noise, flexural and compression waves emitted from the origin of impact would not be reflected.

The minimization of the reflections can be realised by two approaches: using a plate significantly larger compared with the investigated area (this approach is presented in Ref. [13]), or using a special damping plate. Unique damping plates are needed for both measurement types, momentum measurement and positioning.

An interesting approach is a plate of unique shape with decreasing thickness at the edge (called a wedge shape) in a power-law profile [18]. The different waveforms are eliminated due to internal refraction. However, the power-law shape is challenging to manufacture, which is why it is not used in practical vibration dampers [19].

Possible approaches to manufacture this wedge shape are 3D milling or casting [20], which are cost-intensive. Where hardened steel and supersonic impacts are concerned, such delicate and large structures are unsuitable for ballistic applications. For impact analysis, shapes for more robust structures are desirable.

For hardened steel wear plates suitable to resist supersonic impacts, 2D shapes should be used. Waterjet cutting or plasma cutting could produce such plate designs. Possible shapes that can be manufactured easily are any polygons or any round but two-dimensional shapes.

Star-shaped (polygonal) flyer plates are also able to trap compression waves, as used for standard impact soft-recovery experiments [6]. In the star-shaped plate, much lower-level reflection is observed during impact, which enhances the quality of the raw data in ballistic tests. The edge morphology is capable of serving as a trap for waves and was investigated computationally in Ref. [21].

A combination of star-shaped damping plate, enhanced by using an acoustic black-hole shape for ballistic investigations, is proposed by Muster et al. [22]. A witness and ricochet plate like this are capable of measuring the momentum of an impact accurately.

For more accurate projectile impact position investigations, especially for multiple impacts, it makes sense to search for a different solution. Manrad and Doty [23] describe in their patent an application which captures an impact on an elastic screen which heats up during the penetration process of the projectile. The idea of the patent is to calculate the exact impact coordinates of a single impact. Using this information, it is possible to get a real-time signal out of the computations, which the operator may apply

Please cite this article as: Muster M et al., Ricochet quantification using a multiple sensor approach, Defence Technology, https://doi.org/10.1016/j.dt.2020.02.017

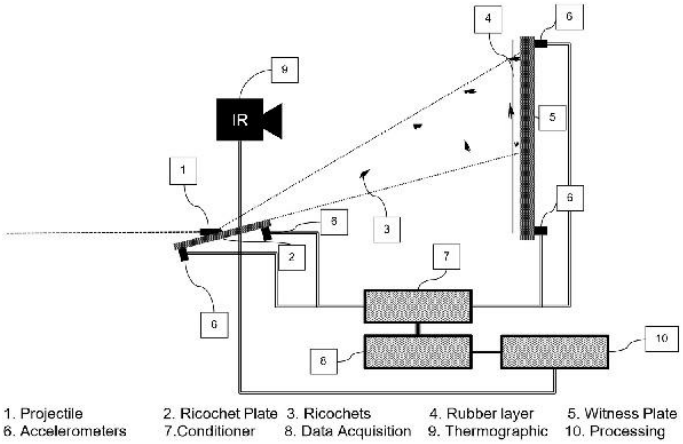

Fig. 1. System layout: under an incident trajectory, the projectile (1) impacts the ricochet plate (2) and gets fragmented and deflected under a certain angle. The deflected fragments (3) fly in the direction of the rubber layer (4) and penetrate it. After penetration, the fragments get stopped on the witness plate (5) which is, like the ricochet plate, equipped with four accelerometers (6). The raw signal of the accelerometers is first conditioned (7) so that it can be digitalised by the Data Acquisition Device (8). The rubber layer, heated up during the penetration process, is observed under thermographic (9) to determine the point of impact with the help of the raw signal of the accelerometers. All signals are processed in the processing unit (10).

during the most realistic possible training. The information about heating up is used to calculate the virtual trajectory of the projectile, not to make any statement about the impact. The process of heating up and the amount of energy transmitted into the screen are not of interest. However, it shows the basic idea and the performance of such thermographic systems.

Thermography in ballistics is also often used to investigate failure mechanisms in composite structures [24–26]. The reason for using high-speed thermography is that different materials of the composite structure are heated for a short time during the penetration process, and this can affect the matrix material, which is often thermoplastic or epoxy resin. These thermal differences are only of short duration and need to be investigated by high-speed thermography.

However, thermography has also its benefits for the investigation of materials like ballistic composite structures, without need for frame rates over 30 per second. Gopalakrishnan et al. [27] showed that it is possible to investigate the damage point of impact on a ballistic sheet impacted by a medium-velocity body using a 50 Hz camera. The studied material with fibres acts more like a monolithic material, as can be seen in the picture taken after several milliseconds.

Another interesting approach to investigate materials using low frame-rate thermography is shown by Duan et al. [28]. They described a system, which assesses the material after damage. They took a general heat source and heated the specimen. This heating-up process was filmed with a low-framerate thermal camera. The outcome was that, with this low-cost approach, it was possible to investigate the failure in the specimen itself accurately. The accuracy was better compared to the state-of-the-art ultrasonic transmission assessment. Soonkyu et al. [29] described a way to inspect wind turbine blades with the use of a laser and thermography. Fractures on large blades are assessed by laser preheating. In case, the damage is allocated to the surface, the specific heat capacity changes. The blade with the damaged zone heats up faster. With such a system, the defect can be precisely detected and investigated.

The sought sensor system is a combination of Gopalakrishnan with the low-framerate thermography of impacts, and the reversed approach of Soonkyu et al. During the penetration of a rubber layer, an impacting projectile dissipates its kinetic energy in lower form by producing heat. This heat is stored so that it can be seen for several seconds after impact.

To increase the positioning accuracy of multiple impacts, a thermographic sensor is used additionally. With this combination, a measurement device can be realised which is capable of working with all kinds of projectiles and quantifying their ricochets. To get a broader picture of the accelerometer measurements, a second sensor type is used a so-called piezoelectric strain gauge. Thanks to their broadband signal acquisition capabilities, these sensor types can identify the condition of large structures [30].

This paper describes a sensor method for ballistic analysis using two plates equipped with four acceleration sensors and a thermographic sensor in combination with a witness rubber layer. The momentum measurement of the projectile or its ricochets is made with specially shaped plates equipped with accelerometers capable of measuring uniaxial accelerations. They are placed in the normal position relative to the plate, which means that only flexural waves will be measured.

2. Material and methods

The ricochet measurement device consists of two main parts. The schematic idea of the system is described in Fig. 1.

First, a heavy ricochet table, see Fig. 2a and b, attached to a pushcart with reliable brakes to ensure that it does not move during impact. The table can be adjusted in height and angle. The ricochet plate is equipped with accelerometers to localise the point where the projectile touches the plate for the first time, and deflects the projectile depending on the angle of the plate.

Second, a heavy metal frame, see Fig. 2c and d, equipped with a second sensor plate at the back, called witness plate. The witness

Please cite this article as: Muster M et al., Ricochet quantification using a multiple sensor approach, Defence Technology, https://doi.org/10.1016/j.dt.2020.02.017

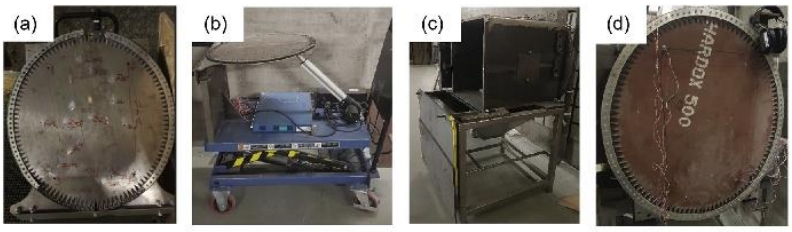

Fig. 2. a–d: Picture (a) shows the ricochet plate, the spikes of the plate are damping structures which allow a better AT detection, which is important for the precise triangulation. The measurement area is 340 mm × 200 mm. Fig. 1b is the ricochet plate assembled on the pushcart. The structure of (c) represents the heavy metal frame to which the large witness plate is screwed (d). The witness plate has the same type of spikes at the boundaries for damping purposes. The size of the measurement area is 600 mm × 345 mm.

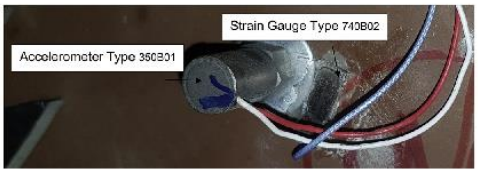

Fig. 3. Accelerometer strain gauge assembly on the witness plate.

plate is significantly larger than the ricochet plate because the spread of the second impact (from the deflected projectile or its fragments) is significantly larger compared with the first impact. The weight of the metal frame is 950 kg. This is necessary due to the strong impulse transmitted into the system during impact.

Each of the two plate types (ricochet and witness plate) is equipped with four accelerometers. The acceleration sensors are designed for severe-shock investigations up to 100,000 g 350B01 (PCB, USA) [31]. These sensors are mechanically filtered to prevent overshooting oscillations [11] and augment the capabilities to detect the incident first flexural wave. A piezoelectric strain gauge type 740B02 (PCB, USA) is also mounted on the witness plate to crosscheck the sensor signal of the accelerometer, see Fig. 3. Furthermore, the sensor plates are equipped with damping structures, which can be seen in Fig. 2a and c.

The ricochet plate has three major tasks, namely the deflection of the projectile, the position measurement, and the exact time measurement when the projectile impacts the first time. The momentum transmitted into the ricochet plate is also measured during impact, but this is not this plate's main task. The momentum measurement in the witness plate is more in focus.

Fig. 4. Thermal picture of 4 impacts with .22LR, the rise in temperature is ca. 10 °C which can easily be detected.

The witness plate's tasks are to measure the momentum and the exact point-in-time. The measurement capabilities of the witness plate need to be augmented by a thermography camera. This, because it is complex to locate different impact positions at the same time using just four accelerometers. This capability is needed because a ricochet can consist of several simultaneously impacting fragments. The thermography camera shows on the rubber screen the heat produced when a piece penetrated the thin rubber layer. The material used for the layer was a special silicone of Shore hardness 60. The layer was 0.6 mm thick. A typical picture of several impacts, which penetrated the thin rubber layer, can be seen in Fig. 4. These impacts were by subsonic projectiles weighing less than 3 g each. This penetration process showed already significant heating of the layer.

Three different ammunition types of the same calibre are investigated, as shown in Fig. 5. They have a projectile diameter of 5.56 mm, and the length of the casing is 45 mm. This calibre type was chosen to investigate the influence of the tilt angle of the ricochet plate and the different ricochet behaviour of the particular designs.

The first projectile tested is different projectile in that; it is a 5.56 mm training ammunition weighing 2.9 g. This projectile is optimised for fragmentation, see Fig. 5a. It consists of copper particles and a polymer matrix, called frangible compound. These projectile types are described less often in the scientific field. The brittle material can cause severe wounds if a person is hit by this projectile type [32,33]. For the ricochet investigation, it is an unorthodox and interesting projectile.

The second projectile type tested is the SS109, which is common and investigated extensively by tests [34] or simulation [35]. The primary reason for the development of the SS109 was to enhance the penetration capabilities of the 5.56 mm projectiles [36]. It also has a Full Metal Jacket (FMJ), but additionally features small steel core in the front of the projectile, shown in Fig. 5b. Such double-core projectiles can act differently when it comes to ricochet behaviour. The steel core can fly longer distances compared with the other projectiles. The weight of the SS109 of 4 g is the heaviest investigated.

The third ammunition type (M193) is used is a well-defined NATO standard ammunition stock number [37]. The M193 has been extensively investigated by several researchers studying terminal ballistics[38,39]. The M193 is a standard FMJ, see Fig. 5c, which makes it also a reference for ricochet measurements. The weight of the projectile is 3.6 g.

Please cite this article as: Muster M et al., Ricochet quantification using a multiple sensor approach, Defence Technology, https://doi.org/10.1016/j.dt.2020.02.017

Fig. 5. Picture of the tree ammunition types investigated. Fig. 4c represents the regular FMJ projectile (M193), (b) represents the SS109 projectile with a hardened steel core. However, the basic design is still a lead core and a Metal Jacket. A different approach is described in (a). Frangible projectiles are just copper particles with a matrix, which should be transferred again to copper particles after hitting a hard target.

According to the presentation of Rottenberger [40], typical deflection angles for ricochets are 5°, 10°, 15° and 25°. Chosen for this investigation were the angles 5°, 10°, 15°, 20° and 25°. The test scope was the same as presented by the ricochet analysis of Rottenberger [40] and according to the ricochet investigations of Mattijssen and Kerkhoff [41]. Each ammunition and tilt-angle test scenario was performed five times, which means that 45 tests had to be made. The distance between the ricochet plate and the witness plate was on average 180 cm. The length was measured after every shot and noted.

The ammunition was tested with a system similar to the Electronic Pressure Velocity and Action Time (EPVAT) measurement setup [42] known for NATO tests. The National Instruments (NI, USA) USB-6366 data acquisition device was used for the tests. It can simultaneously acquire and record one set of data points every 0.5 μs The piezoelectric accelerometers are capable of measuring frequencies up to 35 kHz. The raw data with a signal amplification rate of 1 was acquired without filter, using the PCB-482C05 (PCB, USA) signal conditioner. The data acquisition time was set to 20 ms. As the signal of interest was approx. 4 ms, this acquisition time was sufficient. The pre-trigger was set to 0.1 ms. To increase the accuracy and redundancy of the measurement. The velocity was first measured ten times using a projectile light gate B471 (HPI, Austria). During the ricochet measurements, the velocity was also measured before the projectile impacts, this using a small LS260 Light Gate (Kurzzeit, Germany).

The ricochet and witness plates were calibrated with 9 mm calibration shots. A standard 9 mm projectile was accelerated to different velocities, from 290 to 350 m/s. The upper limit of the transmitted momentum was investigated using an SS109 projectile

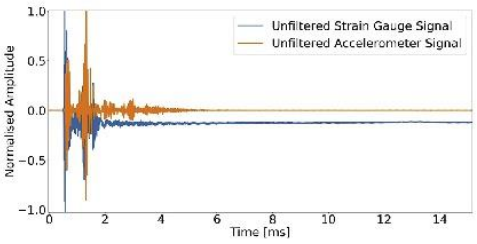

Fig. 7. Unfiltered accelerometer/strain gauge signal.

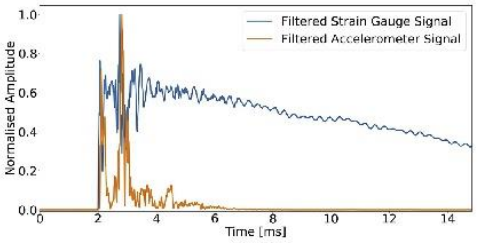

Fig. 8. Filtered accelerometer/strain gauge signal.

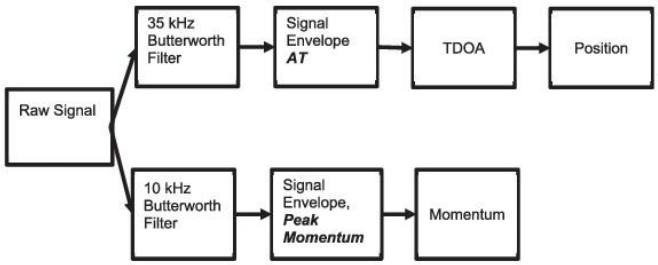

Fig. 6. Signal processing of the raw accelerometer data.

Please cite this article as: Muster M et al., Ricochet quantification using a multiple sensor approach, Defence Technology, https://doi.org/10.1016/j.dt.2020.02.017

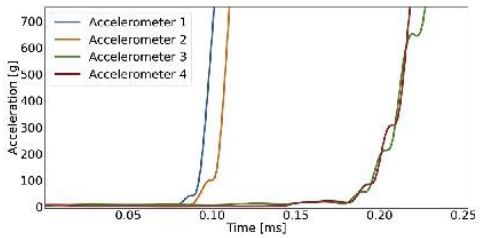

Fig. 9. Different Arrival Times of the accelerometers. This picture shows that the position of the impact was equidistant from Accelerometers 1 + 2 and 3 + 4. It also indicates that the impact is closer to accelerometers 1 and 2.

for both plate types. Both plate types were made of Hardox 500 tempered steel plate exhibiting a yield strength of 1300 MPa as a target [43]. They are regularly used for devices which are resistant to impacting supersonic projectiles [44].

This measurement was also verified by a fast-flying frangible projectile which transmitted the same momentum as the M193. All projectile types impacted orthogonal on the plates to ensure that the impact is fully inelastic. The systems can only be calibrated accurately on the assumption that the impact is inelastic. The thermal image was taken by a SeeK Compact PRO (SeeK, USA) camera. The focus of this investigation was more on the fragmentation behaviour than on the accurate triangulation. However, it was also an objective to prove that such a system can be used to enhance the positioning of impacts. The signal processing approach of this ballistic impact was the same as presented by Muster et al. [45]. An RMS envelope with low-pass filtering was applied for both detection systems, the positioning and the momentum transmitted, see Fig. 6.

3. Results

The raw data acquired from a typical accelerometer and strain gauge signal is presented in Fig. 7. The strain gauge signal rises to approximately ten µs before the accelerometer signal. This earlier rise is due to the strain gauge being slightly more sensitive than the accelerometer. However, the strain gauge shows a negative offset after being excited for 1 ms. This behaviour is even more present in the filtered case, as Fig. 8 shows. The time of the rise of the strain gauge signal is still similar to the accelerometer signal, which is important for cross-proofing purposes.

However, the strain gauge has a significantly longer recovery

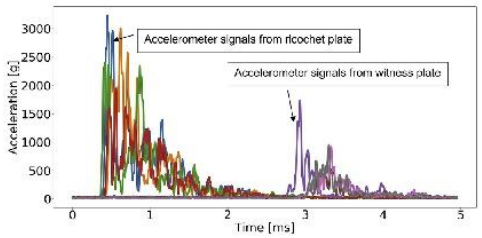

Fig. 10. Typical raw signal. The first peaks represent the acceleration signal produced on the ricochet plate. The second set of signals represents the signals of the witness plate where the ricochet impacts finally.

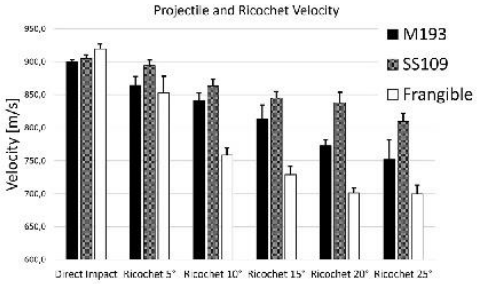

Fig. 11. Graph of the velocity the direct Impact velocity is measured using a light gate, whereas the ricochet velocities are measured using the time difference and the distance between the impact on the ricochet plate and the witness plate.

time compared to the accelerometers. This dynamic offset makes the sensor unusable for momentum detection. However, the first excitation, which is vital for the AT detection, is prominent. The AT of all four accelerometers on one plate is represented in Fig. 9. The signal rises with some small sinusoidal variations. These variations are not present in the case of the strain gauge. However, the accelerometer shows a better overall performance for the performed ballistic test scenarios.

Fig. 10 shows a typical accelerometer signal pattern of the tests. This pattern was generated by an M193 projectile under an impact angle of 15°. The first four accelerometer signals are from the ricochet plate, and they rise significantly higher compared with the second set of peaks, which come from the witness plate. This difference in maximum acceleration comes not only from the different impact strength, but also from the different stiffness's of the plates. The ricochet plate is 12 mm thick, the witness plate 30 mm. The distance between the two impacts divided by the time difference between the two sets of waves determines the ricochet velocity.

This triangulation process of the ricochet plate is more straightforward because the pre-processed acceleration signal rises strongly. The arrival time is detected by a simple threshold trigger. The acceleration pattern of the witness plate is loaded with different peaks and, just on proper AT, not visible, see Fig. 10. This pattern gives already an indication that a separation of the projectile took place, or that the projectile flies under a stronger precession and impacts diagonally. Positioning on the witness plate can be measured more accurately using a thermographic camera.

Fig. 11 shows the velocity of the impact on the witness plate. The

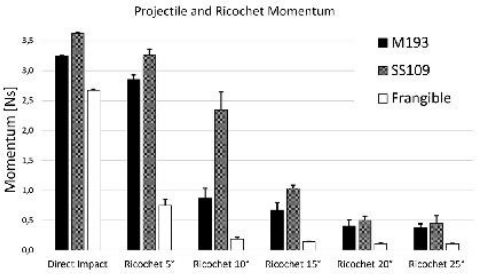

Fig. 12. Graph of the different impact momentums on the witness plate, the direct impact represents the momentum of the impact of a directly impacting projectile.

Please cite this article as: Muster M et al., Ricochet quantification using a multiple sensor approach, Defence Technology, https://doi.org/10.1016/j.dt.2020.02.017

Table 1
Comparison of projectile designs.

Projectile Type	Projectile Weight [g]	Impact Angle [°]	Impact Velocity [m/s]	Ricochet Velocity [m/s]	Velocity Drop [m/s]	Momentum before Impact [Ns]	Momentum Witness Plate [Ns]	Momentum Loss before vs. after Deflection [%]
Frangible	2,9	5	920	853	67	2,67	0,75	72
Frangible	2,9	10	923	759	164	2,67	0,19	93
Frangible	2,9	15	916	729	187	2,66	0,14	95
Frangible	2,9	20	921	701	220	2,67	0,13	95
Frangible	2,9	25	917	700	217	2,66	0,10	96
M193	3,6	5	900	864	36	3,24	2,85	12
M193	3,6	10	901	841	60	3,24	0,87	73
M193	3,6	15	900	813	87	3,24	0,67	79
M193	3,6	20	900	773	127	3,24	0,41	87
M193	3,6	25	899	752	147	3,23	0,37	89
SS109	4	5	908	894	14	3,63	3,26	10
SS109	4	10	905	864	41	3,63	2,35	35
SS109	4	15	900	845	55	3,60	1,03	71
SS109	4	20	904	838	66	3,62	0,50	86
SS109	4	25	901	809	92	3,60	0,45	88

direct impact was a scenario where the projectile was shot directly at the witness plate, undeflected. It represents the normal velocity occurring 25 m after leaving the muzzle. The error bars show the standard deviation of the measured velocity. With an increasing impact angle, the velocity decreases. The velocity drop has two reasons:

Firstly, the impact wear on the steel ricochet plate. This first hit slows the projectile down, the amount of impact wear depends on the projectile material.

Secondly, the change of projectile shape. The projectile is less aerodynamic and tumbles after hitting the oblique ricochet plate.

Looking at the heavier projectiles (M193 and SS109), one can recognise a steady velocity drop. However, the slightly heavier SS109 shows a less steep linear decay than the M193. In the case of the M193, the spread of the velocity increases with an increasing ricochet plate angle. The increasing spread might be because the M193 starts to fragment and the lead fragments are of different sizes, which results in a different drag coefficient and thereby different velocities.

However, the most significant change in velocity is experienced by the frangible projectile fragments after hitting the ricochet plate. The velocity of the frangible fragments seems to plateau between 20 and 25°. This plateau effect might be because the copper powder behaves similar to a fluid after total fragmentation.

Fig. 12 shows the results of the same test scenario as in Fig. 11. This time, however, the momentum is analysed. The momentum decreases also in this case with increasing impact angle. However, with all ammunition types tested, the transmitted momentum is very low after impact on a 25° plate. Fig. 12 shows, like a fingerprint of a specific projectile design, a distinct specific momentum distribution. In the case of frangible projectiles, the momentum decays before 10° to a certain threshold below 0.1 N. In the case of the SS109, the signal decays also to a threshold. However, this threshold is reached at 20° impact. The M193 is in between in both scenarios.

The M193 shows an S-curve decay, which has its main momentum decay between 5° and 10° impact angle. Both the velocity and especially the projectile weight of the SS109 are high compared with the other ammunition types investigated, see Table 1. The momentum of the SS109 is more persistent and decays not as fast as the other projectiles. This might be due to the steel core, which behaves rigid and bounces away from the ricochet plate without substantial momentum loss.

The logarithmic decay pattern of the frangible projectile is even more present in the case of the momentum than in case of the velocity. Interestingly, the dispersion and the velocity of the 15° and 25° impacts are almost in the same range and decreased significantly compared with the initial momentum. Under these angles, the frangible projectile already fragmented into fine copper particles. These good disintegration properties are also the general purpose of frangible ammunition [46], namely the diminution of the range danger area after hitting any surface. This diminution can be quantified using the ricochet measurement device.

In Fig. 13–17, one can see the fragmentation process on a thermal picture of the investigated projectiles. The thermal image is plausible after reading the momentum graph in Fig. 12. Many impacts and a wide spread of the residuals lead to a lower overall momentum. A low total momentum is crucial for a shorter-range danger area.

Interestingly, Fig. 13 (M193) shows just one single impact, which can occur if the ricochet plate deflects the projectile more smoothly. However, this is not the case all the time; the thermal pictures

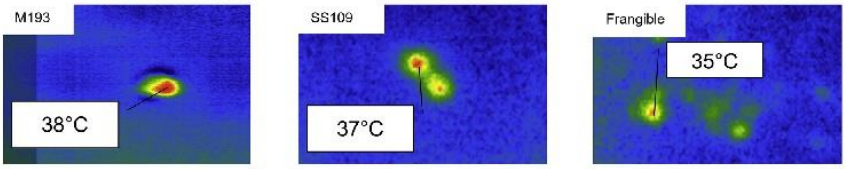

Fig. 13. Thermal impact pattern of projectiles investigated under the impact angle of 5°. The M193 does not fragmentise; the SS109 is separated into two pieces, which is a general behaviour of two cored projectiles. In the case of the frangible ammunition, one can detect already many small fragments.

Please cite this article as: Muster M et al., Ricochet quantification using a multiple sensor approach, Defence Technology, https://doi.org/10.1016/j.dt.2020.02.017

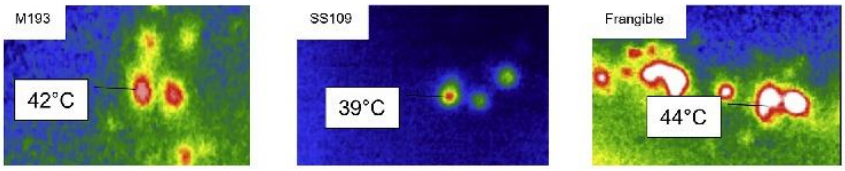

Fig. 14. Thermal impact pattern of projectiles investigated under the impact angle of 10°. The M193 fragmentise under this angle. The blurred picture of the M193 and the frangible projectile is due to temperature drifts of the thermal camera. The increase in fragmentation is recognisable primarily in the case of the frangible.

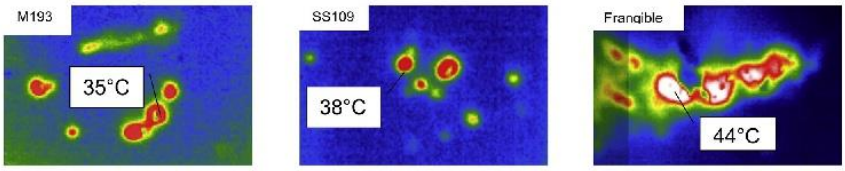

Fig. 15. Under the impact angle of 15°, all projectiles start to fragmentise. In the case of the frangible projectile, a continuous thermal pattern can be recognised. This is the impact angle, where all projectile types show a significant momentum drop.

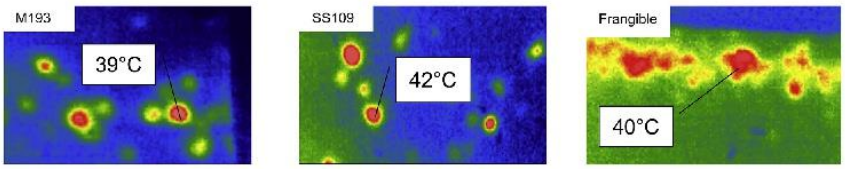

Fig. 16. Under the angle of 20°, the fragmentation spread increases for all projectiles investigated. The frangible projectile is under this angle entirely disintegrated.

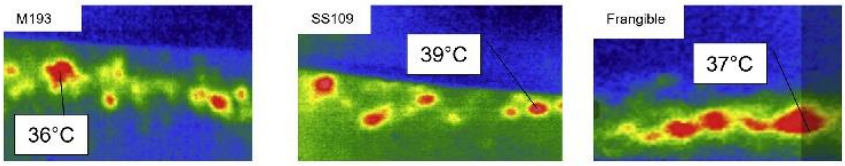

Fig. 17. Under the angle of 25°, all projectiles are entirely disintegrated and show a horizontal line pattern. This is because the projectiles are reflected under a similar angle, independent of the material and design of the projectile.

represent just a possible pattern. A problem was the temperature shift and the blurring out of the camera one can recognise this shift in the background of Figs. 13–17. Due to this fact, only the maximum temperature was indicated in the thermal images.

4. Discussion

In this ballistic experiment, positioning was performed manually by visual investigation. The results of the frangible projectile ricochets, small particles, showed that the rubber layer does not influence the test results. Even these small particles penetrate the layer easily, and the velocity is not affected by the rubber layer. In future, exact positioning with thermal imaging should be done using an algorithm-based approach.

It was not possible to conclude from the thermal signature direct to the impact strength or the shape of the ricochet. However, with a more in-depth investigation and using a camera capable of several hundred frames per second, which is more suitable for general ballistic analysis, this would be possible as part of the future work plans. Concerning the camera, there is an additional drawback that involves the temperature shift over time and the blurring of the temperature pattern, especially the background. This was the reason why only the maximal temperature was indicated. This drawback can be resolved by using a camera featuring an accurate temperature shift filter.

The momentum measurement was performed with accelerometers and a calibration step using different ammunition types. It is possible to augment the precision of the momentum measurement with precisely defined metal balls shot on the measurement plates using accurately defined acceleration machines like gas guns.

Please cite this article as: Muster M et al., Ricochet quantification using a multiple sensor approach, Defence Technology, https://doi.org/10.1016/j.dt.2020.02.017

The ricochet measurement device was in this publication used to investigate 5.56 mm projectiles and 9 mm projectiles. It is also possible to use this device to investigate all small-calibre types and all different projectile types like armour-piercing projectiles with a tungsten core or solid projectiles made of brass or copper.

5. Conclusion

The goal of this work was to assess the performance and trustworthiness of a novel ricochet measurement device with ammunition types of interest. The ballistic study showed that it is possible to quantify complicated and fast-flying structures like projectiles or its ricochets with regular signal processing approaches.

A Measurement system is proposed for ballistic impact investigations, which is suitable to measure ricochet velocities and impact momentums in the typical small-calibre range.

For ballistic momentum measurements, strain gauges are less suitable than accelerometers because the signal drifts strongly in the investigated time domain. However, AT detection is possible using both strain gauges and accelerometers. For multiple impact positioning of projectile fragments, the used thermovision device is appropriate to investigate the impact pattern. However, a more precise camera with an image-processing unit would enhance the performance of this sensor approach. The momentum measured using accelerometers is a valuable property for ballistic investigations like the estimation of danger potentials of specific projectile types and their fragments.

The transmitted momentum is further connected to the range safety. A large momentum loss after a deflection on an oblique plate indicates a projectile, which has good properties for a reduced ricochet danger.

Three different ammunition types showed that the basic design of the projectiles has a significant influence on the deflection process and with this on the range danger area. The results presented here are plausible. The acquired results can be used to estimate the danger potential of the different investigated ammunition types. The investigations also confirmed that a slight deflection of regular projectile types could lead to ricochets, which are still dangerous.

The main message is that quantifying of ricochets is possible using cost-effective and straightforward devices. The concept itself can also be applied to larger or smaller calibres to support the projectile design and development process.

Acknowledgement

Special thanks go to Donald Meyer and Dr. Peter Spatz who made these measurements possible. The authors would like to thank RUAG Ammotec AG Switzerland for the provision of the test facilities and equipment. The use of measurement devices would not have been possible without the great help of Markus Gruenig and Roland Niederhaeuser.

References

[1] Kusano H, Aoki Y, Hirano Y, Kondo Y, Nagao Y. High-speed imaging on static tensile test for unidirectional CFRP. Proc *SPIE* 2009;7126.
[2] Chou P, Toland R. Experimental study of multiple interior impacts. 1976. p. 201–2.
[3] Yan XL, et al. Characterization of a double Time-Of-Flight detector system for accurate velocity measurement in a storage ring using laser beams. Nucl Instruments Methods Phys Res Sect A Accel Spectrometers, Detect Assoc Equip 2019;931(March):52–9.
[4] Courtney M. Acoustic methods for measuring bullet velocity. Appl Acoust 2008;69:925–8.
[5] Espinosa HD. Low-velocity impact testing, vol. 8; 2000. p. 539–59.
[6] Espinosa HD, Raiser G, Clifton RJ, Ortiz M. Performance of the star-shaped flyer in the study of brittle materials: three dimensional computer simulations and experimental observations. J Appl Phys 1992;72(8):3451–7.
[7] Morsy R, Marzouk H, Haddara M, Gu X. Multi-channel random decrement smart sensing system for concrete bridge girders damage location identification. Eng Struct 2017;143:469–76.
[8] Dahlen U, Ryden N, Jakobsson A. Damage identification in concrete using impact non-linear reverberation spectroscopy. NDT E Int 2015;75:15–25.
[9] Allaeys F, Luyckx G, Van Paepegem W, Degrieck J. Development and validation of a set-up to measure the transferred multi-axial impact momentum of a bird strike on a booster vane. Int J Impact Eng 2017;99:102–10.
[10] Hammetter CI, Jones RL, Stauffacher HL, Schoenherr TF. Measurement and modeling of supersonic hailstone impacts. Int J Impact Eng 2017;99:48–57.
[11] Agnello A, Dosch J, Metz R, Sill R, Walter P. Acceleration sensing technologies for severe mechanical shock. Sound Vib 2014;48(2):8–U20.
[12] T H, O C, G D, C J, S R, Touzé C. Wave turbulence in vibrating plates: the effect of damping. EPL (Europhys Lett) 2013;102(3):30002.
[13] Zhao G, Hu H, Li S, Liu L, Li K. Localization of impact on composite plates based on integrated wavelet transform and hybrid minimization algorithm. Compos Struct 2;176:234–43.
[14] Perelli A, De Marchi L, Marzani A, Speciale N. Frequency warped cross-wavelet multiresolution analysis of guided waves for impact localization. Signal Process 2014;96(PART A):51–62.
[15] Musicki D, Kaune R, Koch W. Mobile emitter geolocation and tracking using TDOA and FDOA measurements. IEEE Trans Signal Process 2010;58(3 PART 2):1863–74.
[16] Gustafsson F, Gunnarsson F. Positioning using time-difference of arrival measurements. In: IEEE international conference on acoustics, speech, and signal processing, vol. 6; 2003. p. 553–6. vol. 6.
[17] Liu M, Yang J, Cao Y, Fu W, Cao Y. A new method for arrival time determination of impact signal based on HHT and AIC. Mech Syst Signal Process 2017;86(April 2016):177–87.
[18] Krylov VV, Tilman FJBS. "Acoustic 'black holes' for flexural waves as effective vibration dampers. J Sound Vib 2004;274(3–5):605–19.
[19] Krylov VV, Winward RETB. Experimental investigation of the acoustic black hole effect for flexural waves in tapered plates. J Sound Vib 2007;300(1–2):43–9.
[20] Bowyer E, Krylov V. Acoustic black hole manufacturing for practical applications and the effect of geometrical and material imperfections. 2016. p. 2411–21. no. 4.
[21] Howard A. Morphological control of censile release in ceramic penetration. Cranfield University; 2014.
[22] Muster M, Hameed A, Wood D, Appleby-Thomas G, Wasmer K. Damping of post-impact vibrations. Appl Acoust 2019;156:427–33.
[23] Manrad P. SYSTEMAND method for calculating ROJECTILE impact COORONATES. 2008.
[24] Johnston JP, Pereira JM, Ruggeri CR, Roberts GD. High-speed infrared thermal imaging during ballistic impact of triaxially braided composites. J Compos Mater 2018;52(25):3549–62.
[25] Domun N, et al. Ballistic impact behaviour of glass fibre reinforced polymer composite with 1D/2D nanomodified epoxy matrices. Compos B Eng 2019;167:497–506.
[26] Swiderski W, Hlosta P. Non-destructive evaluation of impacted CFRP by IR thermography. Materials 2019;12(6):956.
[27] Gopalakrishnan S, Senthil V. Failure analysis of ballistic material. Int Conf Adv Mater Eng 2011;15:95–100.
[28] Duan Y, et al. Reliability assessment of pulsed thermography and ultrasonic testing for impact damage of CFRP panels. NDT E Int 2019;102:77–83.
[29] Hwang S, An YK, Sohn H. Continuous line laser thermography for damage imaging of rotating wind turbine blades. Procedia Eng 2017;188:225–32.
[30] Spiridonakos MD, Fassois SD. Vibration based fault detection in a time-varying link structure via non-stationary FS-VTAR models. In: Proceedings of the International Operational Modal Analysis Conference (IOMAC), Ancona, Italy; 2009. p. 315–22.
[31] PCB, High shock ICP ® accelerometer.
[32] Komenda J, et al. Forensic and clinical issues in the use of frangible projectile. J Forensic Leg Med 2013;20(6):697–702.
[33] Martrille L, Artuso A, Cattaneo C, Baccino E. A deceptive case of gunshot entry wounds - beware of frangible bullets. J Forensic Leg Med 2007;14(3):161–4.
[34] Horsfall I, Crewther IR. Proc 19th international symposium on ballistics. In: Glass ceramic armour systems for light armour applications; 2001.
[35] Vanichayangkuranont T, Maneeratana K, Chollacoop N. Numerical Simulations of level 3A ballistic impact on ceramic/steel armor. 2006. p. 2–7. no. October.
[36] Arvidsson PG. Is there a problem with the lethality of the 5.56 NATO caliber. 2009.
[37] States U, Arms R. 5.56×45mm NATO. 1963.
[38] Ragsdale B, Sohn S. Comparison of the terminal ballistics of Full metal Jacket 7.62-mm M80 (NATO) and 5.56-mm M193 military bullets: a study in ornance gelatin BT. 1988.
[39] Sturtevant B. Shock wave effects in biomechanics. Sadhana 1998;23(5):579–96.
[40] Rottenberger I. Abprallverhalten von Jagdmunition. 2011. p. 105.
[41] Mattijssen EJAT, Kerkhoff W. Bullet trajectory reconstruction - methods, accuracy and precision. Forensic Sci Int 2016;262:204–11.
[42] AEP-97, *Multi calibre manual of proof and inspection (M-C MOPI) for 5.56 mm, 7.62 mm, 9 mm and 12.7 mm ammunition*, vol. vol. 23, no. December 2013.

Please cite this article as: Muster M et al., Ricochet quantification using a multiple sensor approach, Defence Technology, https://doi.org/10.1016/j.dt.2020.02.017

2014.
[43] Dudziński W, Konat Ł, Pękalski G. Structural and strength characteristics of wear-resistant martensitic steels. Arch Foundry Eng 2008;8(2):21–6.
[44] Hub J, Komenda J. Ballistic resistance of steel plate hardox upon impact of non-penetrating projectiles. Adv Mil Technol 2009;4(2):79–91.
[45] Muster M, Hameed A, Wood D. Dynamic qualitative bolt force measurements for investigating influence factors on the pushout effect of small calibre ammunition. AIP Adv 2019;9(6):065020.
[46] Mates SP, Rhorer R, Banovic S, Whitenton E, Fields R. Tensile strength measurements of frangible bullets using the diametral compression test. Int J Impact Eng 2008;35(6):511–20.

Please cite this article as: Muster M et al., Ricochet quantification using a multiple sensor approach, Defence Technology, https://doi.org/10.1016/j.dt.2020.02.017

Appendix II – Sensor Data Sheets

Model Number	ICP® FORCE SENSOR	Revision: G
204C		ECN #: 48681

Performance	ENGLISH	SI	
Sensitivity(± 15 %)	0.12 mV/lb	27.0 mV/kN	
Measurement Range(Compression)	40,000 lb	177.92 kN	
Maximum Static Force(Compression)	50,000 lb	222.4 kN	
Broadband Resolution(1 to 10,000 Hz)	0.80 lb-rms	3.6 N-rms	[1]
Low Frequency Response(-5 %)	0.0003 Hz	0.0003 Hz	[2]
Upper Frequency Limit	55 kHz	55 kHz	[3]
Non-Linearity	≤ 1.5 % FS	≤ 1.5 % FS	[4]
Environmental			
Temperature Range	-65 to +250 °F	-54 to +121 °C	
Temperature Coefficient of Sensitivity	≤ 0.08 %/°F	≤ 0.14 %/°C	
Electrical			
Discharge Time Constant(at room temp)	≥ 2000 sec	≥ 2000 sec	
Excitation Voltage	20 to 30 VDC	20 to 30 VDC	
Constant Current Excitation	2 to 20 mA	2 to 20 mA	
Output Impedance	≤ 100 Ohm	≤ 100 Ohm	
Output Bias Voltage	8 to 14 VDC	8 to 14 VDC	
Spectral Noise(1 Hz)	0.088 lb/√Hz	0.39 N/√Hz	[1]
Spectral Noise(10 Hz)	0.025 lb/√Hz	0.11 N/√Hz	[1]
Spectral Noise(100 Hz)	0.0060 lb/√Hz	0.0266 N/√Hz	[1]
Spectral Noise(1 kHz)	0.0016 lb/√Hz	0.00719 N/√Hz	[1]
Output Polarity(Compression)	Positive	Positive	
Physical			
Preload	8000 lb	35.585 kN	
Stiffness	29 lb/µin	5 kN/µm	[1]
Size (Diameter x Height x Bolt Diameter x Sensing Surface)	1.34 in x 0.47 in x 0.625 in x 1.10 in	34 mm x 12 mm x 16 mm x 28 mm	
Size (ID)(Hole Diameter)	0.660 in	16.76 mm	
Size (OD)(Sensor)	1.340 in	34 mm	
Weight	2.0 oz	57 gm	
Housing Material	Stainless Steel	Stainless Steel	
Sealing	Hermetic	Hermetic	
Electrical Connector	10-32 Coaxial Jack	10-32 Coaxial Jack	
Electrical Connection Position	Side	Side	

CE [5]

All specifications are at room temperature unless otherwise specified.
In the interest of constant product improvement, we reserve the right to change specifications without notice.

ICP® is a registered trademark of PCB Group, Inc.

OPTIONAL VERSIONS

Optional versions have identical specifications and accessories as listed for the standard model except where noted below. More than one option may be used.

M - Metric Mount
Supplied Accessory : Model M081A14 Mounting Stud, M14 x 1.25 x 1.400, BeCu (1)
Supplied Accessory : Model M083B04 Pilot Bushing (1)

N - Negative Output Polarity

Output Polarity(Compression)	Negative	Negative

W - Water Resistant Cable

Electrical Connector	Sealed Cable	Sealed Cable
Electrical Connection Position	Side	Side

NOTES:
[1] Typical.
[2] Calculated from discharge time constant.
[3] Estimated using rigid body dynamics calculations.
[4] Zero-based, least-squares, straight line method.
[5] See PCB Declaration of Conformance PS023 for details.

SUPPLIED ACCESSORIES:
Model 080A82 Assembly Lubricant (1)
Model 081A14 Mounting Stud,1/2-20 x 1.400, BeCu (1)
Model 082B04 Anti-friction washer (for Models 204C and 214B) (1)
Model 083B04 Pilot bushing (for Models 204C and 214B) (1)

Entered: LK	Engineer: RPF	Sales: KK	Approved: RPF	Spec Number:
Date: 9/19/2018	Date: 9/19/2018	Date: 9/19/2018	Date: 9/19/2018	5874

PCB PIEZOTRONICS
3425 Walden Avenue, Depew, NY 14043
Phone: 716-684-0001
Fax: 716-684-0987
E-Mail: info@pcb.com

APPLICATION		
NEXT ASS'Y	USED ON	VAR

REVISIONS				
REV	DESCRIPTION	ECN	DATE	APP'D

5608

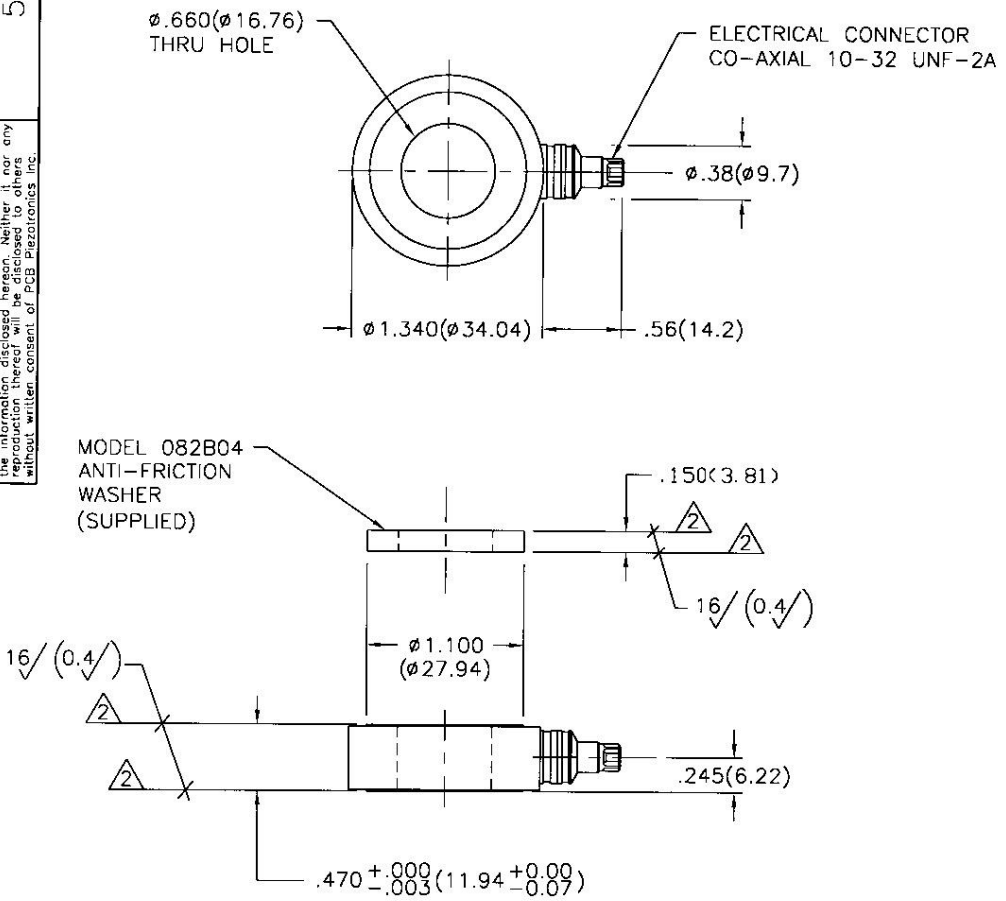

2 THESE SURFACES TO BE FLAT AND PARALLEL TO WITHIN .001(0.03) TIR.

1.) SEE SHEET TWO FOR MOUNTING INSTRUCTIONS.

UNLESS SPECIFIED TOLERANCES	
DIMENSIONS IN INCHES	DIMENSIONS IN MILLIMETERS (IN PARENTHESIS)
DECIMALS XX ±.01 XXX ±.005 ANGLES ±2 DEGREES	DECIMALS XX ±0.3 XXX ±0.13 ANGLES ±2 DEGREES
FILLETS AND RADII .003 - .005	FILLETS AND RADII (0.07 - 0.13)
DD011 REV. A 05/26/95	

DRAWN			MFG	RJP	11/6/97
CHK'D	DM	11/6/97	ENGR		
APP'D		11/6/97			11/6/97

TITLE: INSTALLATION DRAWING
MODEL 204C
FORCE RING

PCB PIEZOTRONICS, INC.
3425 WALDEN AVE. DEPEW, NEW YORK 14043
PHONE: (716) 684-0001

CODE IDENT. NO.	DWG. NO.
52681	5608
SCALE: FULL	SHEET 1 OF 2

KISTLER
measure. analyze. innovate.

Technical Data

Type*			9001A	9011A	9021A	9031A	9041A	9051A	9061A	9071A
Measuring range		kN	0 ... 7,5	0 ... 15	0 ... 35	0 ... 60	0 ... 90	0 ... 120	0 ... 200	0 ... 400
Calibrated ranges										
100 %		kN	0 ... 7,5	0 ... 15	0 ... 35	0 ... 60	0 ... 90	0 ... 120	0 ... 200	0 ... 400
10 %		kN	0 ... 0,75	0 ... 1,5	0 ... 3,5	0 ... 6	0 ... 9	0 ... 12	0 ... 20	0 ... 40
Overload		kN	9	18	42	72	108	144	240	480
Max. bending moment $M_{x,y}$***		N·m	≤±5	≤±15	≤±60	≤±130	≤±240	≤±370	≤±830	≤±2 500
Rigidity		kN/µm	≈1	≈1,8	≈3,5	≈6	≈7,5	≈9	≈14	≈26
Capacity		pF	≈8	≈23	≈37	≈54	≈65	≈64	≈148	≈203
Dimensions										
Internal diameter	d	mm	4,1	6,5	10,5	13	17	21	26,5	40,5
External diameter	D	mm	10,3	14,5	22,5	28,5	34,5	40,5	52,5	75,5
Height	H	mm	6,5	8	10	11	12	13	15	17
Weight		g	3	7	20	36	70	80	157	370

General Data		
Sensitivity**	pC/N	≈–4,3
Threshold	N	≤0,01
Operating temperature range	°C	–196 ... 200
Linearity typ., preloaded***	%FSO	±0,4
Hysteresis typ., preloaded***	%FSO	0,2
Insulation resistance	Ω	$\geq 1 \cdot 10^{14}$
Temperature coefficient	%/°C	–0,02
Natural frequency		depends on additional mass

* further Types see data sheet quartz load washers (9081A_000-106)

** applies only to sensor **without** preloading nut (see page 3, mounting)

*** Preload F_v = 0,5 · measuring range F_z = 0

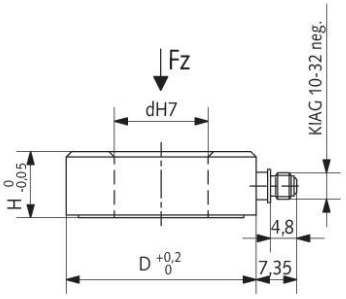

Fig. 1: Dimensions load washers

9001A_000-105e-08.07

SPECIFICATIONS		
Model Number	**740B02**	**740M04**
Performance		
Sensitivity (±20%)	50 mV/με	5 mV/με
Sensitivity (±20%)	50 mV/με	5 mV/με
Measurement Range	100 pk με	900 pk με
Frequency Range	0.5-100000 Hz	0.5-100000 Hz
Broadband Resolution	0.6 nε	5.0 nε
Non-Linearity	≤1 %	≤1.5 %
Transverse Sensitivity	≤5 %	≤5 %
Environmental		
Overload Limit (Shock)	±10000 g pk	±10000 g pk
	±98000 m/s² pk	±98000 m/s² pk
Temperature Range	-65 to +250 °F	-65 to +250 °F
	-53 to +121 °C	-53 to +121 °C
Acceleration Sensitivity	0.001 με/g	0.001 με/g
Electrical		
Excitation Voltage	20-30 VDC	20-30 VDC
Constant Current Excitation	2-20 mA	2-20 mA
Output Impedance	<100 Ohm	<100 Ohm
Output Bias Voltage	8-14 VDC	8-14 VDC
Discharge Time Constant	1-3 sec	1-3 sec
Spectral Noise (1 Hz)	210 pε/√Hz	1900 pε/√Hz
Spectral Noise (10 Hz)	70 pε/√Hz	600 pε/√Hz
Spectral Noise (100 Hz)	20 pε/√Hz	200 pε/√Hz
Spectral Noise (1 kHz)	5 pε/√Hz	60 pε/√Hz
Spectral Noise (10 kHz)	1 pε/√Hz	15 pε/√Hz
Physical		
Sensing Element	Quartz	Quartz
Housing Material	Titanium	Titanium
Sealing	Epoxy	Epoxy
Size - W x L x H	0.2 x 0.6 x 0.07 in	0.2 x 0.6 x 0.07 in
Weight	0.5 gm	0.5 gm
Electrical Connector	10-32 Plug	10-32 Plug
Electrical Connection Position	Side	Side
Mounting	Adhesive	Adhesive
Cable Length	10 ft	10 ft
	3 m	3 m
Cable Type	030 Coaxial	030 Coaxial
Accessories		
Removal Tool	039A07 (Supplied)	039A07
Quick Bonding Gel	080A90 (Supplied)	080A90
Piezoelectric Strain Sensor Calibration Certificate	ACS-15 (Supplied)	ACS-15

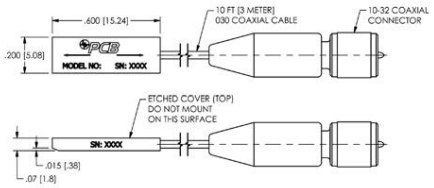

Model 039A07
Removable Tool

PCB PIEZOTRONICS
MTS SYSTEMS CORPORATION
3425 Walden Avenue, Depew, NY 14043-2495 USA
Toll-Free in the USA: 800 828 8840
Phone: 1 716 684 0001 | Email: info@pcb.com

PCB Piezotronics, Inc. is a designer and manufacturer of microphones, vibration, pressure, force, torque, load, and strain sensors, as well as the pioneer of ICP® technology used by design engineers and predictive maintenance professionals worldwide for test, measurement, monitoring, and control requirements in automotive, aerospace, industrial, R&D, military, educational, commercial, OEM applications, and more. With a worldwide customer support team, 24-hour SensorLine℠, and a global distribution network, PCB® is committed to Total Customer Satisfaction. Visit www.pcb.com for more information. PCB Piezotronics, Inc. is a wholly owned subsidiary of MTS Systems Corporation. Additional information on MTS can be found at www.mts.com.

AD-Series740-0419

MTS SENSORS

MTS Sensors, a division of MTS Systems Corporation (NASDAQ: MTSC), vastly expanded its range of products and solutions after MTS acquired PCB Piezotronics, Inc. in July, 2016. PCB Piezotronics, Inc. is a wholly owned subsidiary of MTS Systems Corp.; IMI Sensors and Larson Davis are divisions of PCB Piezotronics, Inc.; Accumetrics, Inc. and The Modal Shop, Inc. are subsidiaries of PCB Piezotronics, Inc.

Model Number	SHEAR ICP® SHOCK ACCELEROMETER	Revision: F
350B01		ECN #: 48057

Performance	ENGLISH	SI	
Sensitivity(± 30 %)	0.05 mV/g	0.005 mV/(m/s²)	
Measurement Range	± 100,000 g pk	± 981,000 m/s² pk	
Frequency Range(± 1 dB)	4 to 10,000 Hz	4 to 10,000 Hz	
Frequency Range(-3 dB)	2 to 25,000 Hz	2 to 25,000 Hz	[3]
Electrical Filter Corner Frequency(-3 dB)	21 kHz	21 kHz	[1][4]
Mechanical Filter Resonant Frequency	35 kHz	35 kHz	[1][5]
Resonant Frequency	≥ 100 kHz	≥ 100 kHz	
Broadband Resolution(1 to 10,000 Hz)	0.5 g rms	4.9 m/s² rms	[1]
Non-Linearity(per 10,000 g (98,100 m/s²))	≤ 2.5 %	≤ 2.5 %	
Transverse Sensitivity	≤ 7 %	≤ 7 %	
Environmental			
Overload Limit(Shock)	± 150,000 g pk	± 1,471,500 m/s² pk	
Temperature Range(Operating)	-10 to +150 °F	-23 to +66 °C	
Temperature Range(Storage)	-40 to +200 °F	-40 to +93 °C	
Temperature Response	See Graph	See Graph	[1][2]
Electrical			
Excitation Voltage	20 to 30 VDC	20 to 30 VDC	
Constant Current Excitation	2 to 20 mA	2 to 20 mA	
Output Impedance	≤ 200 Ohm	≤ 200 Ohm	
Output Bias Voltage	8 to 14 VDC	8 to 14 VDC	
Discharge Time Constant	0.10 sec	0.10 sec	[1]
Settling Time(within 10% of bias)	<1 sec	<1 sec	
Electrical Isolation(Case)	>1,000,000 Ohm	>1,000,000 Ohm	
Physical			
Sensing Element	Ceramic	Ceramic	
Sensing Geometry	Shear	Shear	
Housing Material	Titanium	Titanium	
Sealing	Hermetic	Hermetic	
Size (Hex x Height)	0.375 in x 1.04 in	9.5 mm x 26.5 mm	
Weight(without cable)	0.20 oz	5.5 gm	[1]
Electrical Connector	Integral Cable	Integral Cable	
Cable Length	10 ft	3.05 m	
Cable Type	031 Twisted Pair	031 Twisted Pair	
Mounting Thread	1/4-28 Male	1/4-28 Male	

CE[6]

Typical Sensitivity Deviation vs Temperature

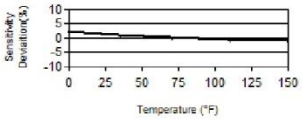

All specifications are at room temperature unless otherwise specified.
In the interest of constant product improvement, we reserve the right to change specifications without notice.

ICP® is a registered trademark of PCB Group, Inc.

OPTIONAL VERSIONS

Optional versions have identical specifications and accessories as listed for the standard model except where noted below. More than one option may be used.

M - Metric Mount

Mounting Thread	M6 x 0.75 Male	M6 x 0.75 Male

NOTES:
[1] Typical.
[2] Test conducted on shaker at 100Hz.
[3] Typical corner frequency for coupled electrical and mechanical filters.
[4] Electrical filter is a second order filter.
[5] Amplitude at resonance is +9 dB.
[6] See PCB Declaration of Conformance PS135 for details.

SUPPLIED ACCESSORIES:
Model ACS-14 High G shock accelerometer calibration using Hopkinson bar. (1)
Model ACS-22 NIST Traceable frequency response (100Hz to ±1 dB point) (1)

Entered: LK	Engineer: RB	Sales: RWM	Approved: BAM	Spec Number:
Date: 4/3/2018	Date: 4/3/2018	Date: 4/3/2018	Date: 4/3/2018	52263

PCB PIEZOTRONICS
3425 Walden Avenue, Depew, NY 14043
Phone: 716-684-0001
Fax: 716-684-0987
E-Mail: info@pcb.com

Appendix III - Drawings

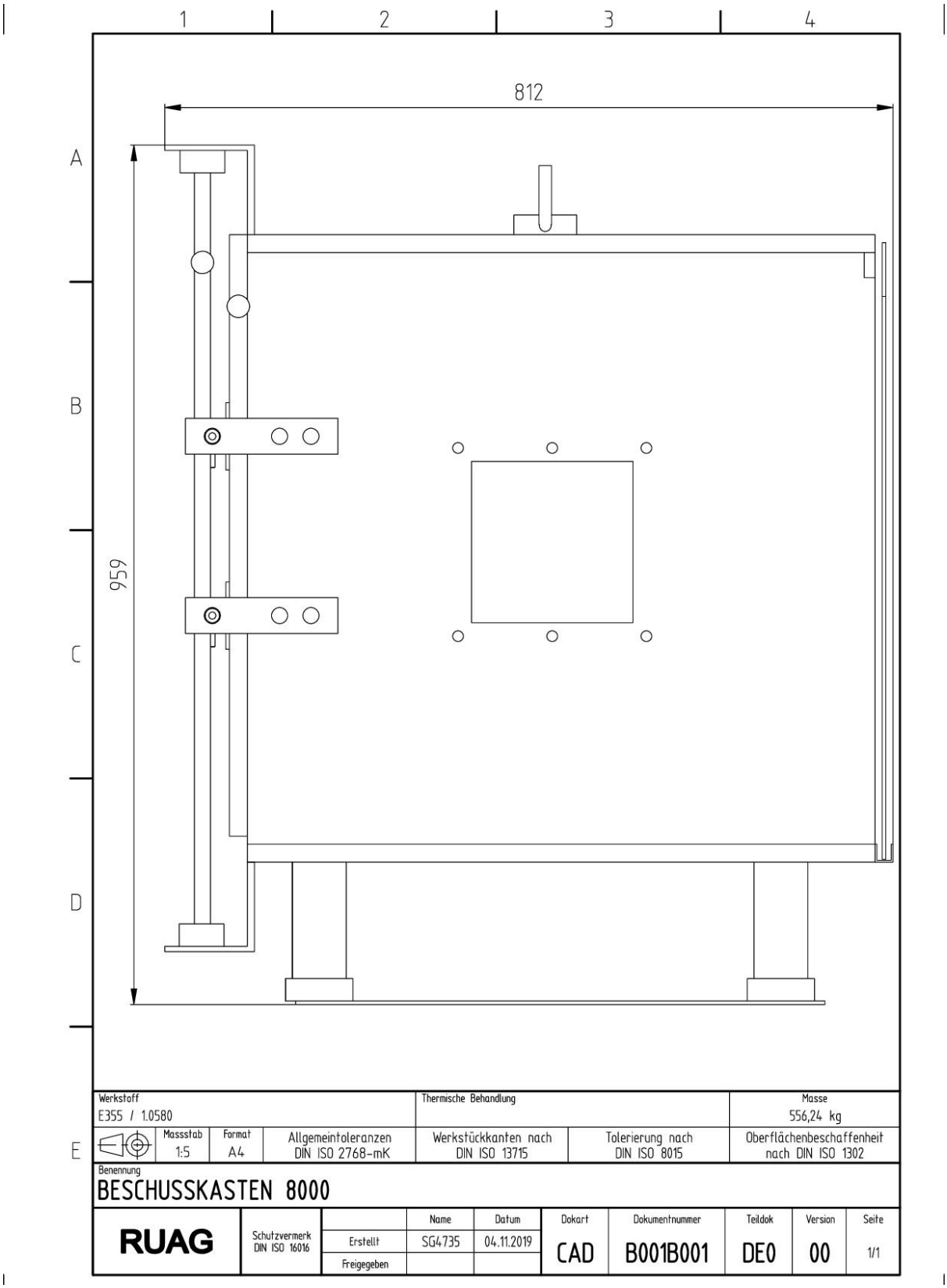

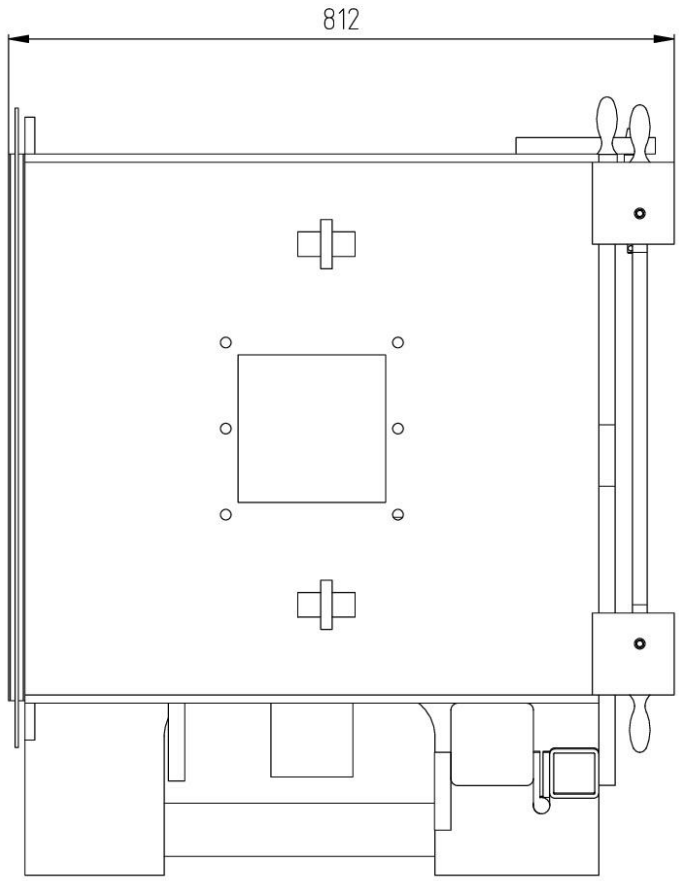

Werkstoff				Thermische Behandlung		Masse
E355 / 1.0580						556,24 kg
	Massstab	Format	Allgemeintoleranzen	Werkstückkanten nach	Tolerierung nach	Oberflächenbeschaffenheit
	1:5	A4	DIN ISO 2768-mK	DIN ISO 13715	DIN ISO 8015	nach DIN ISO 1302

Benennung

BESCHUSSKASTEN 8000

RUAG	Schutzvermerk DIN ISO 16016		Name	Datum	Dokart	Dokumentnummer	Teildok	Version	Seite
		Erstellt	SG4735	04.11.2019	CAD	B001B001	DE0	00	1/1
		Freigegeben							

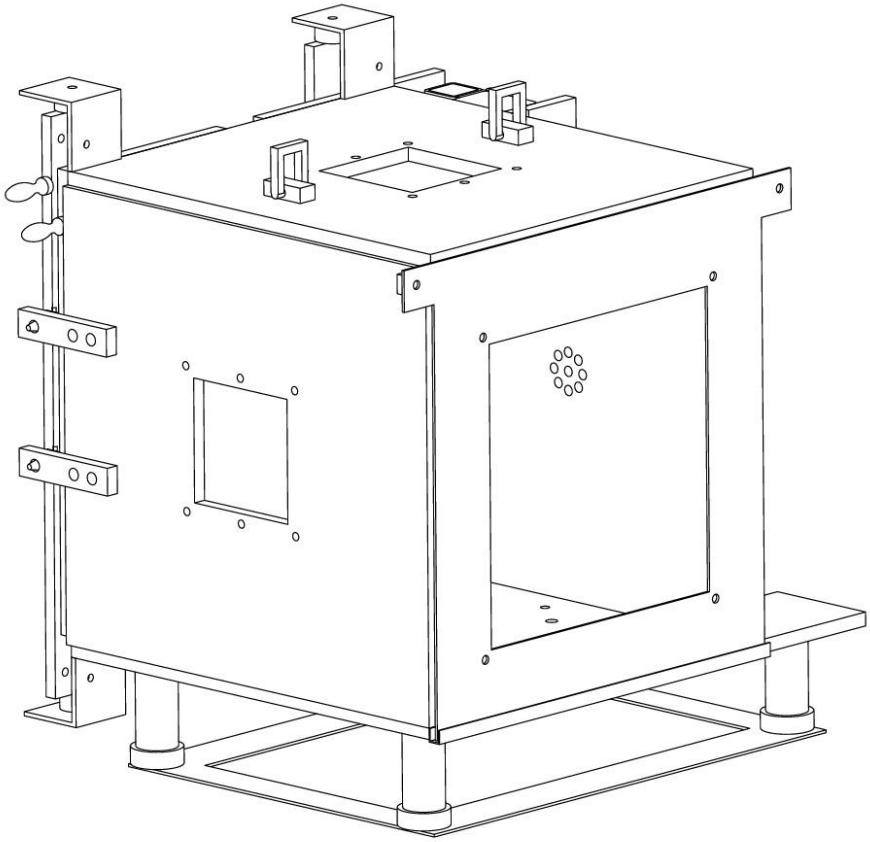

Werkstoff				Thermische Behandlung		Masse
E355 / 1.0580						556,24 kg
	Massstab	Format	Allgemeintoleranzen	Werkstückkanten nach	Tolerierung nach	Oberflächenbeschaffenheit
	1:5	A4	DIN ISO 2768-mK	DIN ISO 13715	DIN ISO 8015	nach DIN ISO 1302

Benennung

BESCHUSSKASTEN 8000

RUAG	Schutzvermerk DIN ISO 16016		Name	Datum	Dokart	Dokumentnummer	Teildok	Version	Seite
		Erstellt	SG4735	04.11.2019	CAD	B001B001	DE0	00	1/1
		Freigegeben							

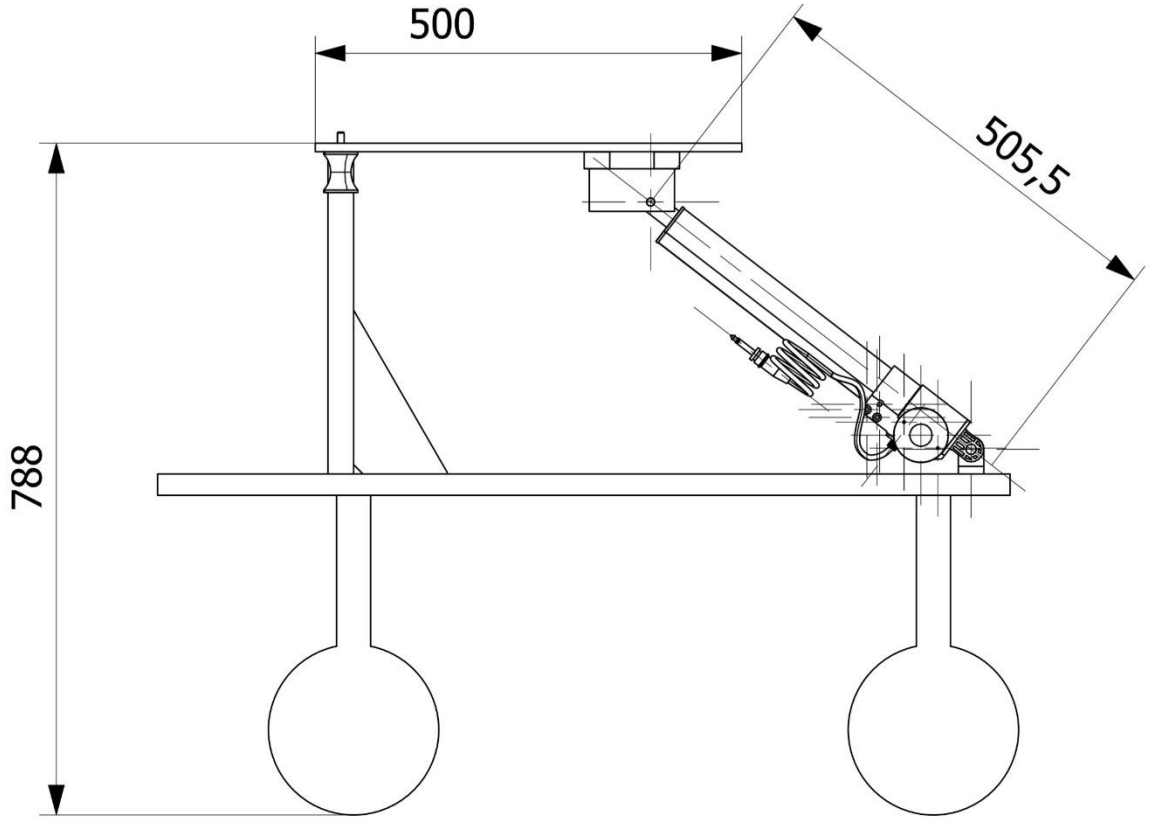
500
505,5
788

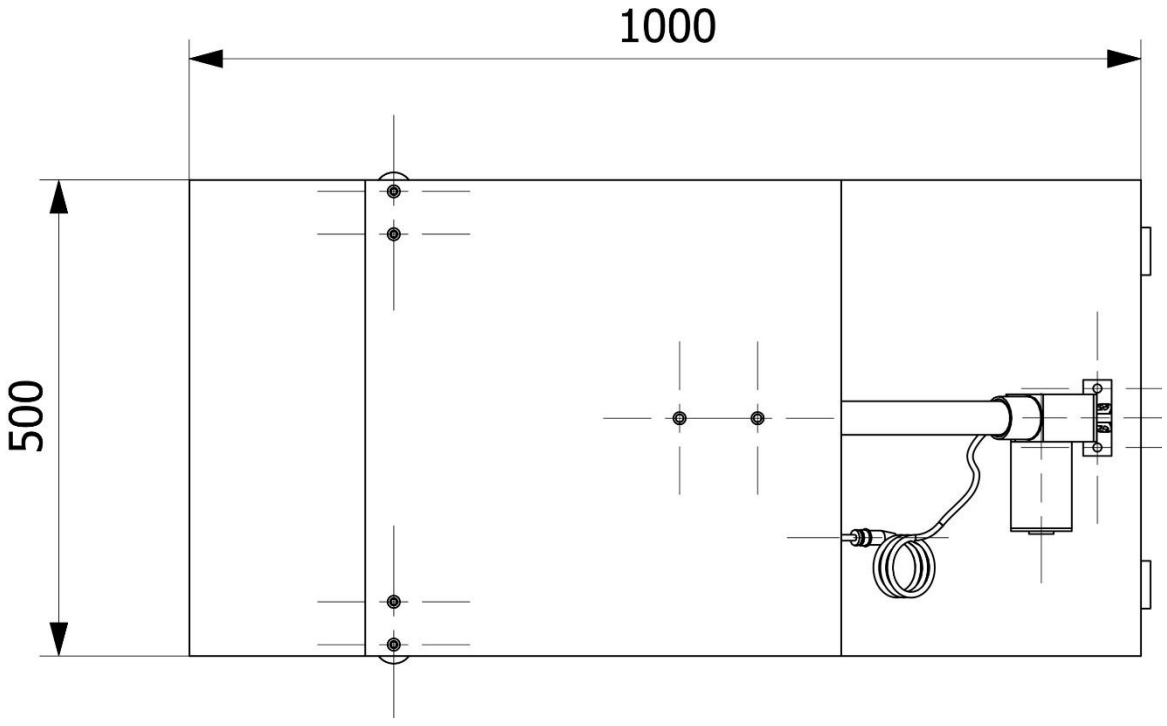
1000
500

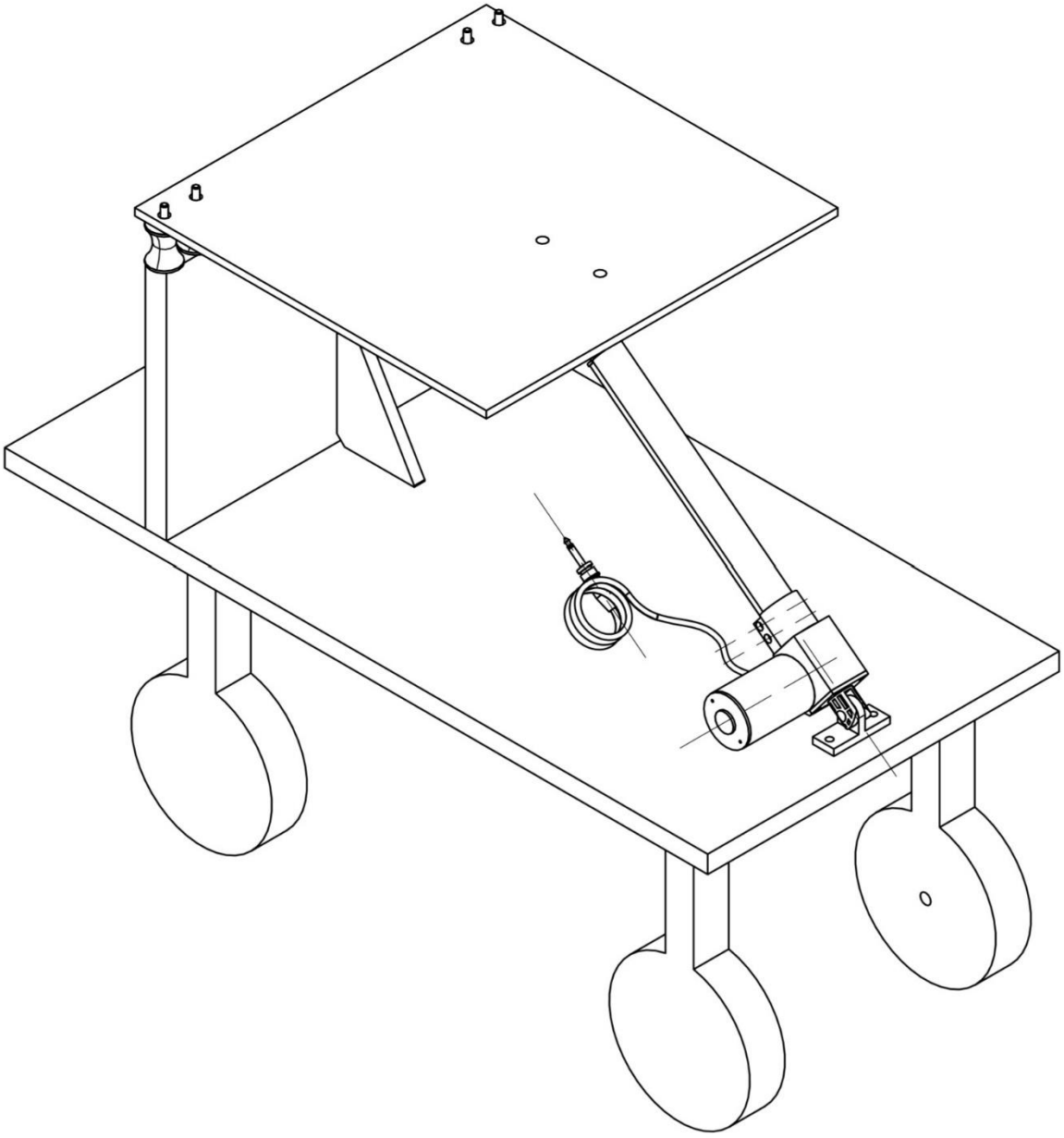

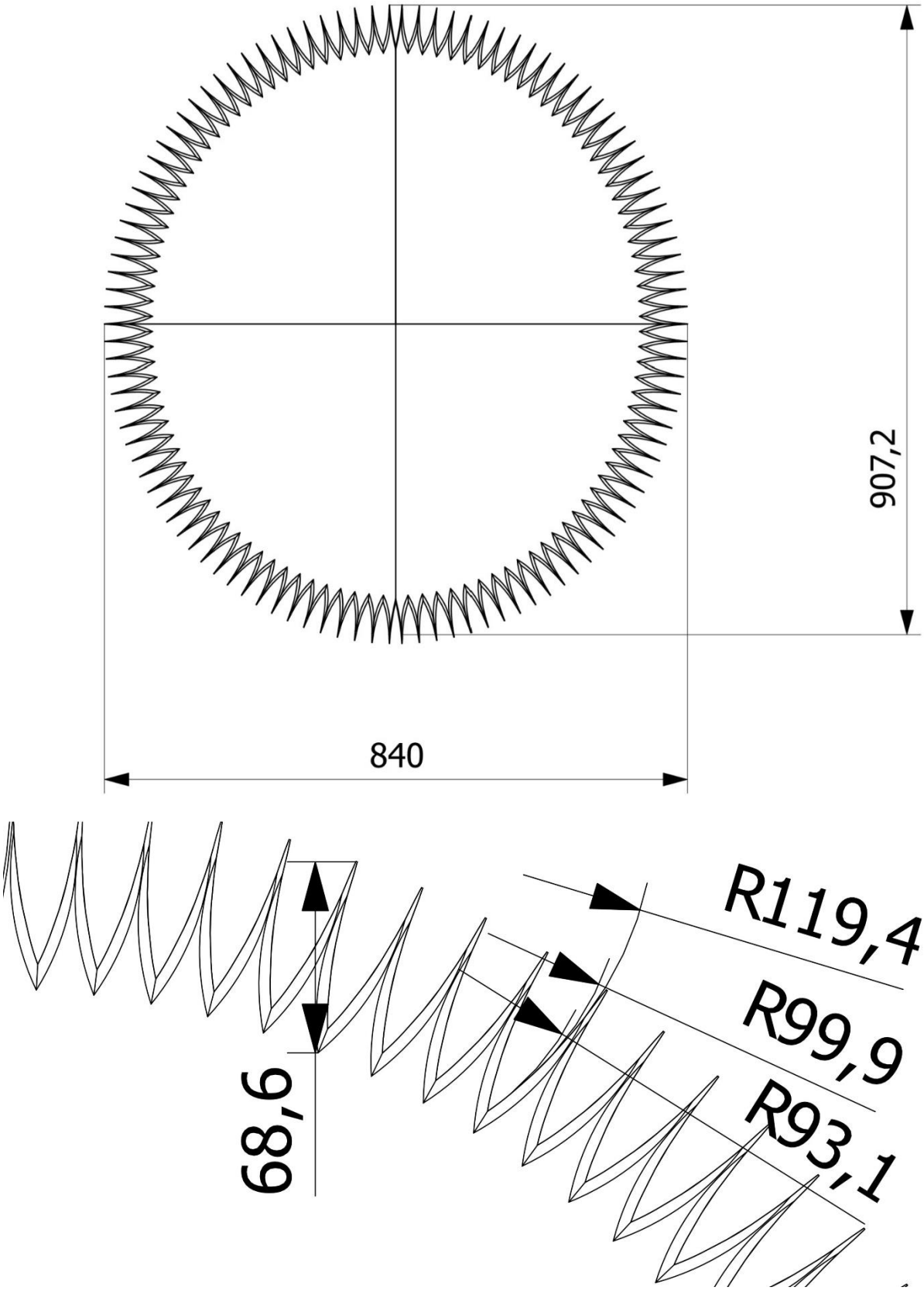
907,2
840
R119,4
R99,9
R93,1
68,6

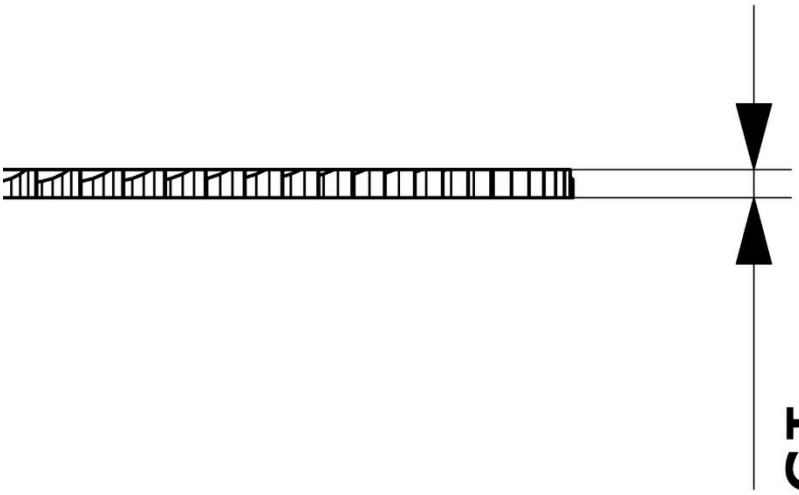
15